The Physico-chemical Characterisation of Bioactive Glass Air-abrasion on Human Enamel

Milly, Hussam

Awarding institution:
King's College London

The Physico-chemical Characterisation of Bioactive Glass Air-abrasion on Human Enamel

Thesis submitted for the degree of Doctor of Philosophy

Hussam Mahmoud Milly

King's College London
United Kingdom - London

2014

Abstract

Objectives: This research aimed to characterise the physico-chemical interaction of bioactive glass 45S5 (BAG) air-abrasion with human enamel including the controlled and selective removal of substrates and the remineralisation of enamel white spot lesions (WSLs).

Materials and methods: The effect of six operating parameters on air-abrasion dynamic cutting efficiency / patterns was assessed using an enamel analogue material (Macor^{TM}) and white light profilometry. Standardised resin composite restorations created within Macor^{TM} blocks, were removed in simulated clinical conditions and scanned using triangulation laser profilometry to investigate the effect of operating parameters on the selective resin composite removal using BAG air-abrasion. The remineralisation of artificial enamel WSLs treated using BAG mixtures were evaluated using Raman micro-spectroscopy, microhardness and scanning electron microscopy (SEM) coupled with energy dispersive X-ray spectrometry (EDX). The physical and optical changes in WSLs pre-conditioned using air-abrasion with BAG-polyacrylic acid (PAA-BAG) powder were detected using non-contact profilometry and optical coherence tomography (OCT). All comparisons were considered statistically significant if $p<0.05$.

Results: Significant differences in air-abrasion cutting efficiency / pattern were observed according to the tested parameters. BAG air-abrasion removed resin composite more selectively than conventional alumina air-abrasion and the effect of altering the unit's operating parameters was significant. Enamel WSLs treated with BAG mixtures exhibited a significantly higher Knoop microhardness compared to the negative control. Raman micro-spectroscopy detected significantly higher phosphate content and the SEM images revealed mineral depositions on the surface of treated lesions. Pre-conditioning WSL surfaces with PAA-BAG air-abrasion increased WSL surface area. This pre-treatment increased Knoop microhardness and the mineral content of remineralised WSLs.

Conclusions: The ultraconservative clinical applications of BAG air-abrasion can be improved by altering the operating parameters. BAG and PAA-BAG can remineralise enamel WSLs. Pre-conditioning the lesion surface with PAA-BAG air-abrasion modifies the lesion surface physically and consequently enhances remineralisation using BAG 45S5 therapy.

Table of Contents

Figure Legends

Table Legends

List of abbreviations

ACP: amorphous calcium phosphate.

AF: autofluorescence.

AFM: atomic force microscopy.

BAG: bioactive glass.

BisGMA: Bisphenol A-glycidyl methacrylate.

CCD: charge-coupled device.

CLSM: confocal laser scanning microscopy.

CMR: contact microradiographs.

CPP-ACFP: casein phosphopeptide - amorphous calcium fluoride phosphate.

CPP-ACP: casein phosphopeptide - amorphous calcium phosphate.

Ea: activation energy.

EDJ: enamel-dentine junction.

EDX: energy dispersive X-ray spectroscopy.

ERMI: endosseous ridge maintenance implant.

FA: fluorapatite.

FDA: food and drug administration.

FTIR: Fourier transform infrared spectroscopy.

HA: hydroxyapatite.

HCA: hydroxycarbonate apatite.

I_B: bioactivity index.

KHN: Knoop hardness number.

MI: minimally intervention.

MID: minimally invasive dentistry.

OCT: optical coherence tomography.

PAA: polyacrylic acid.

PBS: phosphate buffered solution.

PFR: powder flow rate.

ppm: parts per million.

QLF: quantitative light-induced fluorescence.

RMGICs: resin modified glass ionomer cements.

Sa: average surface roughness.

SBF: simulated body fluid.

SEM: scanning electron microscopy.

THAM: Tris-hydroxy methyl amino methane.

TL: triangulation laser.

TMR: transverse microradiography.

TSM: tandem scanning confocal microscopy.

VHN: Vickers hardness number.

WL: white light.

WSL: white spot lesion.

Acknowledgements

I would like to express my gratitude and deepest thanks to:

Professor Avijit Banerjee, my first supervisor, for his excellent supervision, intellectual guidance and continuous encouragement throughout the entire period of my research. I am grateful to him for being always available for help and advice throughout my PhD studies.

Dr Ian Thompson, my second supervisor, for his advice, expertise and precious help, for which I am extremely grateful. I appreciate his encouragement and support.

Dr Abigail Tucker, my coordinator, for her advice in keeping my progress on schedule.

Dr Frederic Festy, for his valuable help in the Raman and OCT analyses and Professor Timothy Watson for his suggestions for the progression of this work.

Mr Peter Pilecki and Mr Richard Mallet for their help and assistance in the lab.

Mr Manoharan Andiappan, for his kind assistance with the statistical analyses.

Damascus University, Syria for their financial grant throughout my study at King's College London.

My parents, for their tremendous encouragement, understanding and patience that supported me throughout my study; I will be always indebted to them.

And finally my dear wife, who shared with me all the difficult and pleasant times to finish my studying years.

I dedicate this work to my lovely daughters

Dana and Sana

Introduction

The improved understanding of dental caries activity with the advances in adhesive restorative material science has paved the way for the introduction of minimally invasive dentistry (MID) (Tyas et al., 2000; Peters and McLean, 2001a). Thereby, the traditional philosophy of caries management using conventional operative intervention, established by Black (1920), has been replaced by a minimal intervention approach that extols the “prevention of extension” concept (Burke, 2003). The clinical translation of MID includes the use of remineralisation strategies to reverse the demineralisation process non-operatively (Mount, 2007; Featherstone, 2009), and the excavation of irreparable carious tissues with maximum tissue preservation (Banerjee, 2013). Different operative technologies have been proposed for less invasive and more selective tooth preparation, including air-abrasion.

This thesis aims to characterise the physico-chemical interaction of bioactive glass (BAG) air-abrasion with human enamel to enhance the use of this technology as an operative technique in minimally invasive dentistry. Figure i-1 outlines the overall structure of this study in term of the relation to the MID concepts. The experiments were divided into two main sections. The first section was dedicated to the study of the cutting characteristics of BAG air-abrasion. This was initiated by calibrating the air-abrasion system including the characterisation of the abrasive powders and the validation of the unit’s operating parameters (Chapter 2). The effect of six air-abrasion operating parameters on the cutting efficiency / pattern was assessed in Chapter 3 in a dynamic cutting mode in order to mimic the clinical situation. Another study was conducted in Chapter 4 to assess the effect of three clinically adjustable air-abrasion operating parameters on the selective removal of resin composite restorative material, an important clinical procedure in Restorative Dentistry.

The second section of this thesis focuses on the remineralisation of artificial enamel white spot lesions using BAG 45S5 technology. Therefore, a study was conducted in Chapter 5 to assess the effect of BAG 45S5 mixtures on enamel WSL remineralisation through chemical, mechanical and ultra-structural assessments. The last experiment chapter, Chapter 6, evaluated the effect of

pre-conditioning enamel white spot lesion surfaces using BAG air-abrasion technology on the subsequent remineralisation therapy. In Chapter 7, the findings of the both experimental sections were considered, generally discussed and concluded with a suggested future work for potential areas of research continuation. Figure i-2 represents the experiments accomplished in this project with the analytical methods employed.

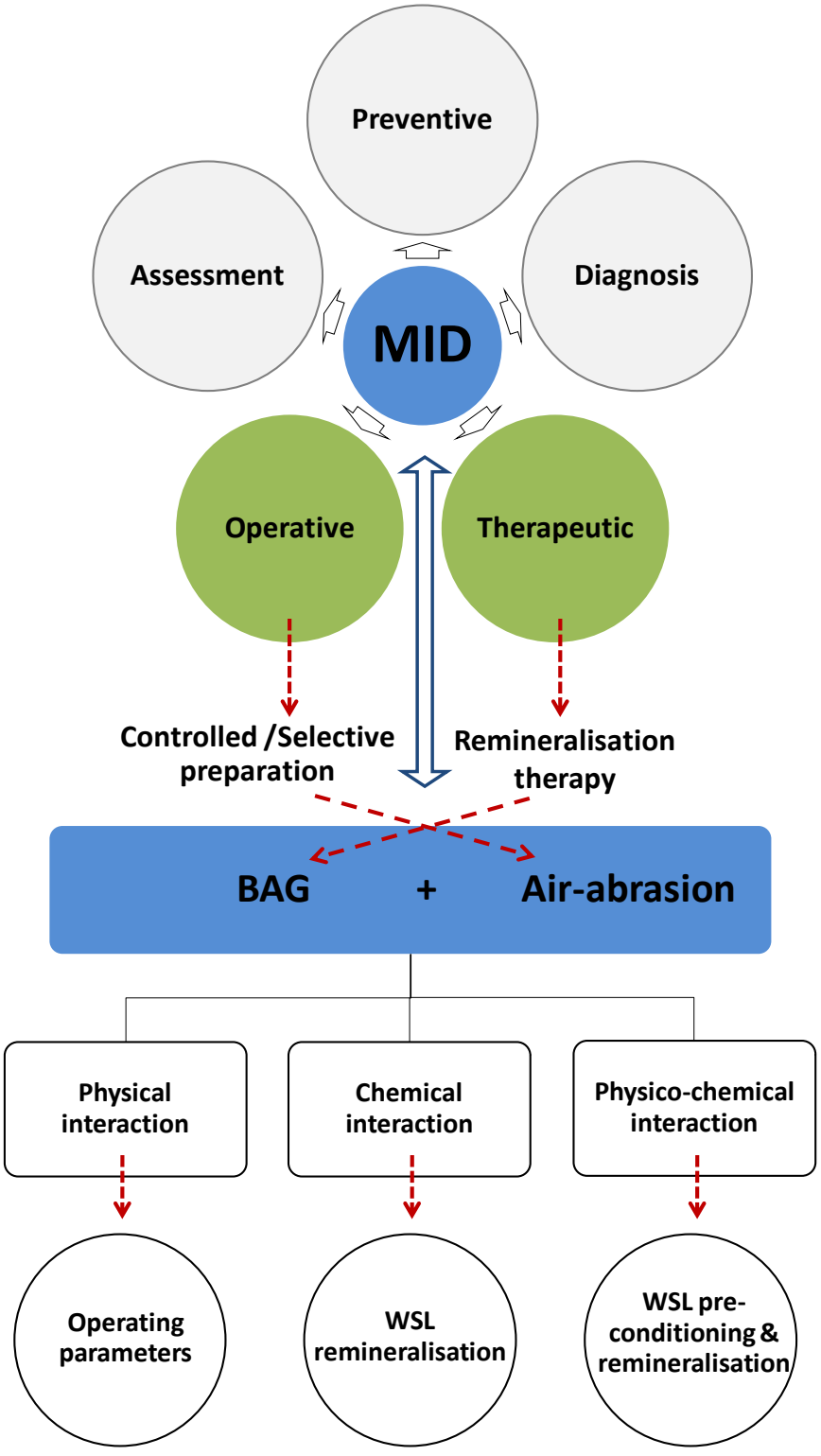

Figure i-1: Organisational flowchart of the overall structure of this thesis in relation to minimally invasive dentistry (MID).

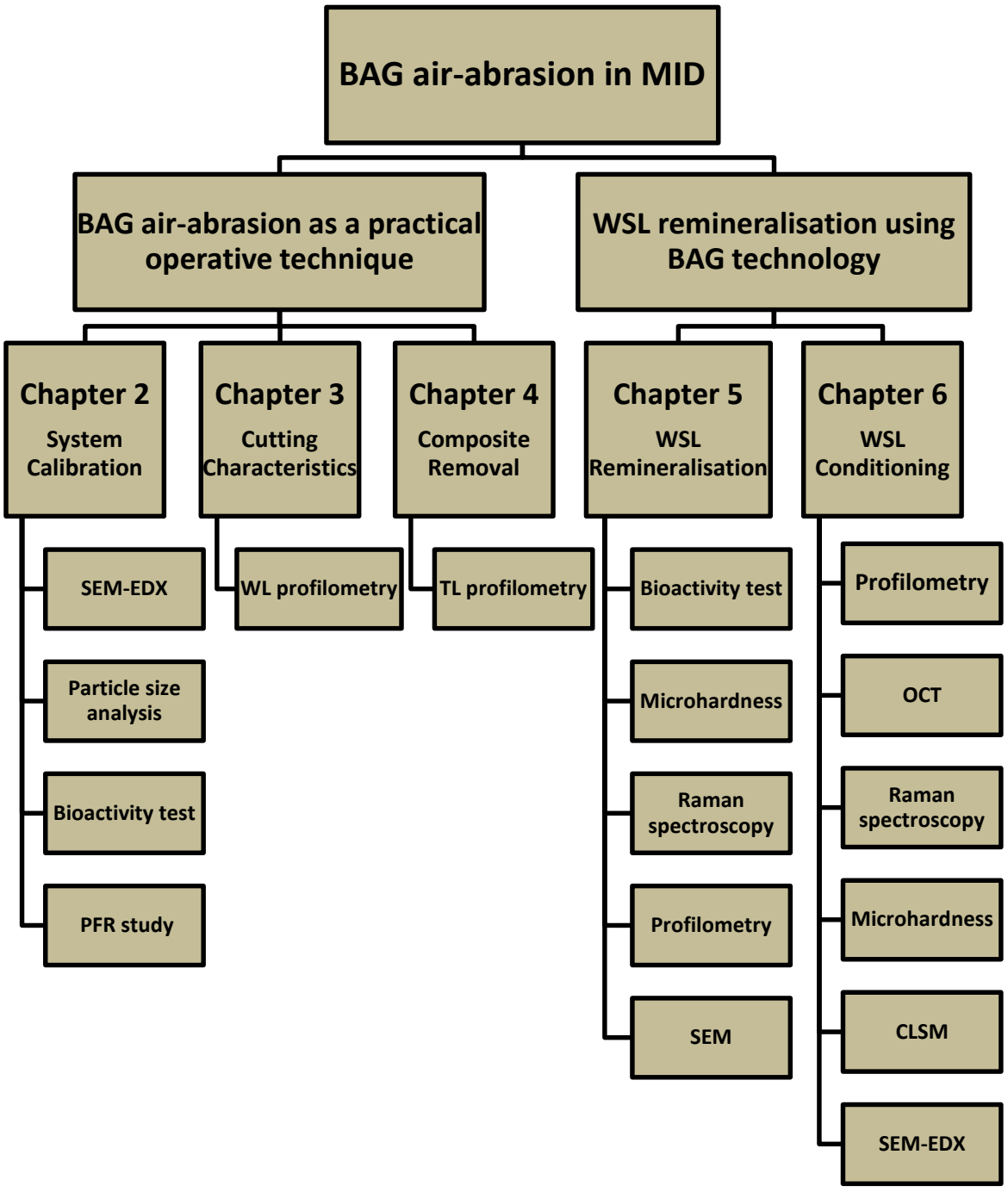

Figure i-2: Organisational flowchart of the experiments accomplished in this study with the analytical methods employed.

Chapter 1 Literature Review

1.1 BAG Air-abrasion system

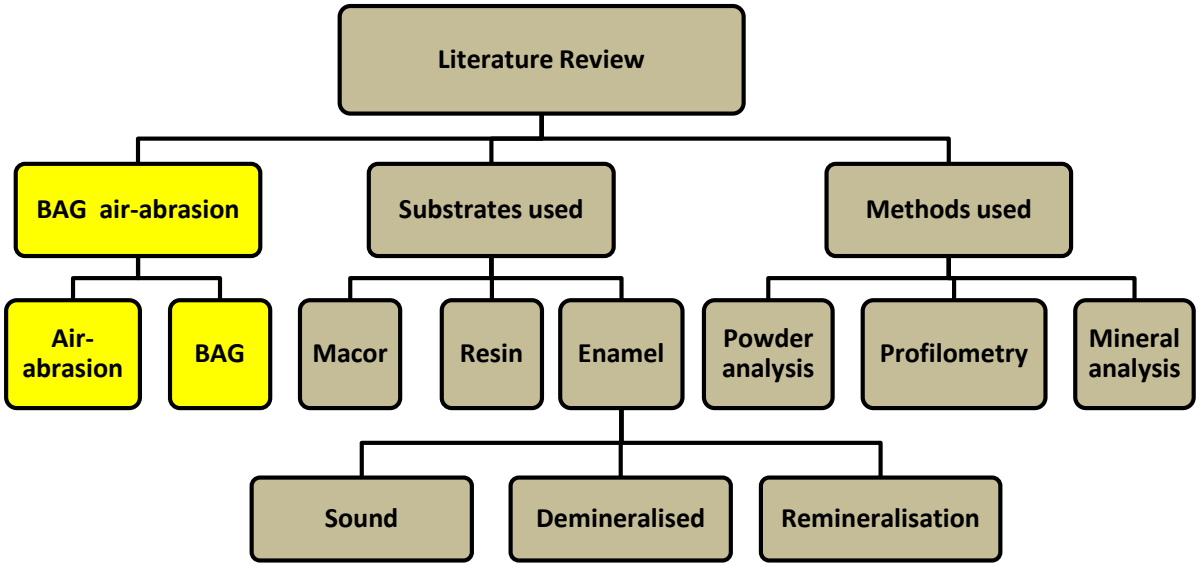

Flowchart of the literature review structure in this thesis.

1.1.1 Air-abrasion

Minimally invasive dentistry (MID) advocates the maximum preservation of intact and reparable dental tissues by minimising the unnecessary cutting of sound tooth structure (Peters and McLean, 2001a). This has stimulated new approaches for cavity design and tooth-cutting concepts. In order to meet MID concepts and to overcome the limitations of conventional rotary instrumentation, several technologies have been suggested to be used in clinical restorative dentistry, including air-abrasion. Table 1-1 outlines the clinical operative technologies available with their main features.

Air-abrasion is a non-mechanical method of cutting tooth tissue which employs the use of kinetics to micro-chip away the surface of hard tissues. This technology was developed by Black in 1945 to find an alternative method to the conventional slow-speed handpiece (Black, 1945). The use of air-abrasion then declined at that time due to three factors. Firstly, it could not produce cavities with clear surfaces and sharp internal line angles required for classical amalgam restorations. Secondly, the high-speed air turbine handpiece was introduced and

gained popularity rapidly, and finally high velocity suction had not yet been invented (White and Eakle, 2000).

This technology has recently gained renewed interest and reassessment due to three main factors (Banerjee and Watson, 2002):

1. The potential of newly developed powders to selectively remove diseased dental hard tissues and thus enhance the preservation of healthy tooth tissues during tooth preparation.
2. The widespread use of aesthetic restorations which rely on adhesive techniques and suitable cavity margin conditioning for their retention.
3. The advance in technologies designed to reduce the overspill and spread of aerosolised powder in the dental surgery.

In an air-abrasion system, the mechanical energy of the equipment is converted into kinetic energy, so charging the abrasive particles as they are emitted from the nozzle. Thus, the mechanical energy is not applied directly to the targeted surface (as in conventional instrumentation), but is firstly converted into kinetic energy. The abrasive particles are too small to create a sufficient impact that can be easily detected by the patient (Black, 1950). The term Kinetic energy was coined by Lord Kelvin and is defined mathematically by the following equation; (E_K=1/2 MV^2; M: the mass, V: the speed of particles) (Laurell and Hess, 1995). The transfer of kinetic energy of particles at the surface causes chipping rather than grinding of the target substrate (Horiguchi et al., 1997).

Table 1-1: The operative techniques available in-vivo for cutting tooth tissues / excavating caries:

Technique	Category	Advantages	Disadvantages	References
burs	Mechanical, rotary	1. Defines precise cavity shape, margins and angles. 2. Widely available at low cost.	1. Generates pressure against the tooth surface. 2. Bone-conducting vibration. 3. Noise from air-turbine. 4. High temperatures at the cutting surface. 5. Ineffective in the self-selective removal of carious tissues. 6. Forms smear layer on prepared surfaces.	(Peters and McLean, 2001b) (Antunes et al., 2008)
Air-abrasion	Kinetic	1. Eliminating of pressure applied against the tooth surface, bone vibration and rise in temperature. 2. Considered a pain-free technique. 3. Effective diagnostic and therapeutic use for management of early fissure.	1. Risk of over-preparation. 2. Scattering of the powder. 3. Technique dependent upon inter-related operating parameters. 4. Ineffective in removing some restorative materials such as amalgam. 5. The use of intraoral mirror is difficult.	(Yip and Samaranayake, 1998) (Banerjee et al., 2000b) (White and Eakle, 2000) (Rafique et al., 2003) (Paolinelis et al., 2009) (Banerjee et al., 2011b)
Hand excavators	Mechanical, non-rotary	1. Useful for domiciliary treatment of mentally or physically handicapped patients. 2. Offers best tactile control. 3. No temperature generation.	1. Limitation in providing access to cavity to manage the carious lesion. 2. The cavity access significantly affects the efficacy of caries removal. 3. Over-preparation. 4. Slower than other methods.	Peters and McLean, 2001b) (Flückiger et al., 2005) (Celiberti et al., 2006) (Navarro et al., 2008) (Molina et al., 2009)

Caridex *Carisolv* *Papacarie®*	Chemo-mechanical	1. Differential removal of the outer irreparable layer of dentine (infected tissue) caries leaving the reparable inner layers (affected tissue). 2. Minimal cavity preparation is required. 3. Reduced smear layer created. 4. Good option in treating deep lesions in an attempt to minimise pulp exposure. 5. Offers an efficient tool for the removal of root caries.	1. Relatively long procedure. 2. Other preparation methods are still required to provide access to carious dentine.	(Yip and Samaranayake, 1998) (Banerjee et al., 2000b) (Fure et al., 2000) Peters and McLean, 2001b) (Hosoya et al., 2005)
Ultrasonics & sono-abrasion	Mechanical, non-rotary	1. Minimises noise, heat and pressure compared to rotary instrumentation. 2. Better preparation of marginal bevels compared to hand instruments. 3. Less damage to the dental pulp tissue in comparison to the high-speed air-turbine bur.	1. Poor visibility. 2. Ineffective in removing some restorative materials such as amalgam. 3. More evaluation and clinical trials are still required. 4. Cracks may occur due to the vibration.	(Oman and Applebaum, 1955) (Lee et al., 2013) (Tassery et al., 2013) (Decup and Lasfargues, 2014)
Laser	Photo-ablation	1. Sterilises as it ablates. 2. Sealing dentine tubules reducing the possibility of postoperative sensitivity. 3. Less pain throughout the procedure was documented.	1. High-cost which limits its use in general dental practice. 2. Its cutting efficiency depends on different factors such as wavelength, intensity, pulse and duration. 3. A large amount of unexcavated decayed tissues reported. 4. Low caries removal effectiveness, with highly variable results. 5. More evaluation and clinical trials are still required.	(Midda and Renton-Harper, 1991) (Burns et al., 1995) (Myers and Myers, 1985) (Yip and Samaranayake, 1998) (Celiberti et al., 2006) (Neves et al., 2011)

The use of air-abrasion as an operative technique in Restorative Dentistry reduces the pressure applied against the tooth surface, the bone vibration and the rise in tissue temperature and consequently, reduces the unpleasant characteristics associated with the use of conventional rotary instruments (Black, 1950). Early data obtained by preparing 1,914 cavities on 1,141 patients showed that when air-abrasion was used in cavity preparation, 50.3% of the patients reported no pain, 40.6% reported mild pain and 9.1% suffered from severe pain (Myers, 1954). Another clinical trial, using the Modified Dental Anxiety Scale to assess patients' anxiety levels, showed that 75% of the patients were satisfied with using air-abrasion whilst 91% expressed some level of anxiety at the prospect of using conventional rotary instruments (Rafique et al., 2003).

Laurell and Hess (1995) described the characteristics of cavities prepared using air-abrasion and examined using scanning electron microscopy (SEM); three main features were recognised including rounded cavo-surface margins and internal line angles, a halo of abraded enamel surrounding the cavity outlines and a microscopic roughness of the treated enamel. These features provide the typical contours and surface finish required for modern dental adhesive materials. Banerjee et al. (2000a) characterised the surface finish of carious dentine excavated using air-abrasion and reported a featureless, stippled surface resulting from the retention of abrasive particles of different sizes, onto the abraded surface. The use of air-abrasion does not produce a smear layer that consists of debris remaining on the surface after cavity preparation and requires further removal prior to restoration placement (Los and Barkmeier, 1994).

Air-abrasion is a sensitive technique dependent upon parameters different from those affecting conventional rotary cutting. Several inter-related operating parameters have been reported in the literature (Bailey and Phillips, 1950; Myers, 1954; Laurell and Hess, 1995; Cook et al., 2001; Santos-Pinto et al., 2001; Peruchi et al., 2002; Paolinelis et al., 2009). In order to simplify and organise these parameters, a ternary powder-operator-unit parameters diagram is included (Figure 1-1). The parameters controlled by the operator include the nozzle angle, nozzle-substrate distance and nozzle movement speed. The second group of parameters are the built-in physics and mechanics of the equipment which includes the powder-air admix mechanism, powder flow rate

(PFR), powder volume reservoir, nozzle output pressure and water shrouding the powder stream. The third group of parameters is related to the abrasive powders used.

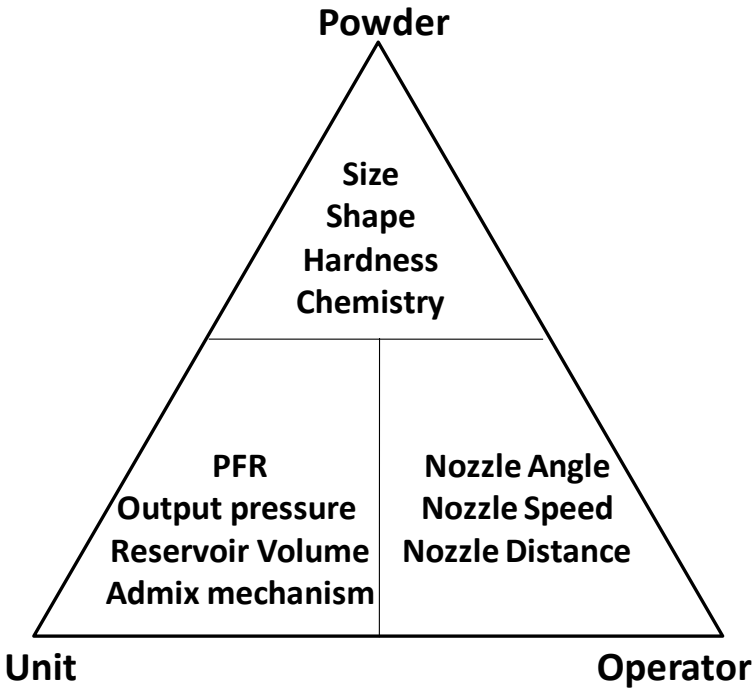

Figure 1-1: Schematic figure explains the main three categories of air-abrasion clinical operating parameters. The first group is related to the operator, the second is correlated to the air-abrasion unit and the third category is designed around the powder.

For the optimal use of this technology in minimally invasive dentistry (MID), the abrasive powder should be harder than carious dental tissues and at the same time softer than intact healthy tissues (Horiguchi et al., 1997). Alumina powder introduced by Black (1945) is still the most commonly used abrasive powder due to its favourable characteristics including chemical stability, low cost, a neutral colour and most importantly, that it's freely flowable. On the other hand, the fundamental limitation of using alumina air-abrasion is that the cutting rate of sound enamel and dentine is much faster than the cutting rate of carious enamel or dentine (Epstein, 1951). This early observation was supported by further studies using more advanced assessment methods. Cook et al. (2001) used real-time confocal imaging to observe air-abrasion cutting characteristics using 27 µm alumina particles. Here, it was reported that the deeper sound dentine was cut faster than the decayed tissues, even when further from the nozzle orifice. This cutting property of alumina leads to undesirable over-preparation of healthy tooth tissues. Motisuki et al. (2006) stated that the insufficiency of alumina air-abrasion

in cutting carious dental tissues may be due to the penetration of the heavy particles into the soft carious surface, so losing their kinetic energy.

In order to improve air-abrasion cutting efficiency with respect to caries removal, alternative powders were introduced such as dolomite, chalk, glass beads, crushed glass powder, crushed polycarbonate resin and 45S5 bioactive glass (BAG) (Bailey and Phillips, 1950; Black, 1955; Horiguchi et al., 1997; Paolinelis et al., 2008). The use of BAG air-abrasive powder may exhibit the following benefits:

1. Its potential to remove selectively more softened diseased or damaged tooth structure due to its reduced hardness (458 VHN; Vicker's hardness number) (Hench and Wilson, 1993), compared to that of alumina (2100 VHN) (Banerjee et al., 2011a).
2. Its potential to enhance the remineralisation of carious tissues as a consequence of its reactivity process which forms a hydroxycarbonate apatite (HCA) layer grown on the surfaces of reacted BAG particles (see Section 1.1.2.2; p: 34).
3. Its potential for antibacterial effects against certain oral bacteria species, including those associated with caries and periodontal diseases such as *Streptococcus sanguis*, *Streptococcus mutans* and *Actinomyces viscosus* (Stoor et al., 1998; Allan et al., 2001).

It has been shown that using 45S5 BAG as an air-abrasive powder resulted in more conservative cutting characteristics compared to the alumina, but still removed a quantity healthy dental tissues (Banerjee et al., 2008a; Paolinelis et al., 2008). Therefore, using bioactive glass powder with different particle hardness, size and formulation were suggested to promote the use of this system in MID. Substituting Na_2O for CaO in (SiO_2–P_2O_5–CaO–CaF_2–Na_2O) bioactive glass system caused a pronounced decrease in glass hardness, resulting in a considerably longer cutting time by air-abrasion (Farooq et al., 2013). Using bioactive glass powder containing PAA (15 wt.% or 40 wt.%) to treat dentine using air-abrasion technology reduced the micropermeability between the dentine and the adhesive layer in-vitro, and might be a suitable strategy to enhance bond durability (Sauro et al., 2012b). The concentrations of PAA powder were selected to modulate the cutting efficiency of bioactive glass air-abrasion

systems. Adding PAA to the system increases the presence of carboxyl acid groups at the resin-adhesive interface, which in turn may bind the water preventing water sorption into adhesive layer improving the microtensile bond strength after a prolonged storage in phosphate buffered solution (PBS) (Sauro et al., 2012b; Sauro et al., 2012c). In fact, adding PAA to bioactive glass powder for use in air-abrasion technology, not only modulates the cutting efficiency of the system and improves the prolonged bond performance of modern self-etching adhesives, but also may interact in the remineralisation process of demineralised dental tissue. This is due to PAA mimicking the non-collagenous matrix protein-1 (DMP1) function in binding calcium phosphate, and its use with bioactive Portland cement (Dentsply Tulsa, Tulsa, OK, USA) formed amorphous calcium phosphate mineral precipitations small enough to penetrate the collagen matrix enhancing the remineralisation of lesion depth (Tay and Pashley, 2008).

1.1.2 Bioactive glass

1.1.2.1 Bioactive glass compositions

A “bioactive material” was defined by Hench and co-workers as one “that elicits a specific biological response at the interface of the material which results in the formation of a bond between the tissue and material” (Hench, 1991). The first bioactive glass (BAG) was termed “45S5 Bioglass®” with a chemical composition: 45 wt.% SiO_2, 24.5 wt.% Na_2O, 24.5 wt.% CaO and 6 wt.% P_2O_5 (Hench et al., 1971). Thereafter, a series of glasses of this four-component system have been studied. Figure 1-2 represents a ternary SiO_2-Na_2O-CaO diagram, with a constant six weight percentage of P_2O_5, establishing the bioactive-bonding-boundary of compositions. Glasses with silica content up to 52 wt.% bond with both bone and soft tissues, whilst those with silica content between 52 and 58 wt.% bond only with the bone (region A). When the silica content extends past 60 wt.%, the glasses behave as nearly-inert materials due the increased number of bridging oxygen ions which reduce the network dissolution rate (region B). The compositions with a silica content of less than 40 wt.% are not technically practical and have not been implanted (region D) (Hench and Wilson, 1993).

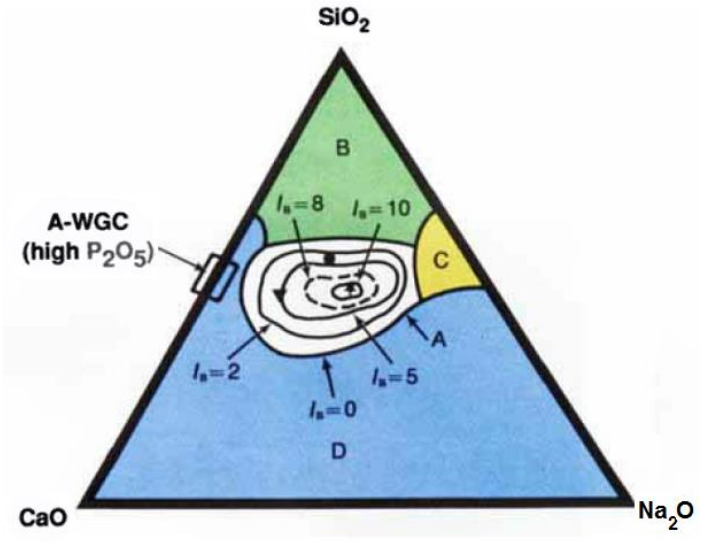

Figure 1-2: Compositional dependence (in weight percent) of bone and soft tissue bonding of bioactive glasses and glass-ceramics. All compositions in region A have a constant 6 wt.% content of P_2O_5. The area inside the dashed line where I_B >8 exhibits soft tissue bonding. (*) 45S5 Bioglass®, (▼) Ceravital® and (•) 55S4.3 Bioglass® [taken from Hench (1991)].

The role of phosphate in BAG composition is not necessary to form a hydroxycarbonate apatite (HCA) layer and the glass surface absorbs phosphate ions from the surrounding solution. P_2O_5-free CaO-SiO_2 glasses form surface apatite layer and bond to living bone (Kokubo, 1990). Bioactive glasses exhibit an amorphous two-dimensional network, whereby the SiO_2 acts as a network former and the CaO, Na_2O as network modifiers (Figure 1-3).

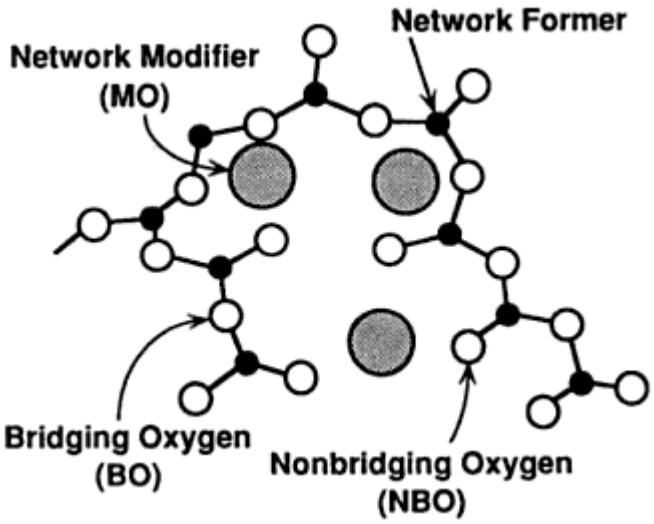

Figure 1-3: Schematic structure of a random glass network composed of network formers (SiO_2) [taken from Hench & Wilson (1993)].

1.1.2.2 Reaction kinetics

The chemical reactivity of BAG in the presence of aqueous solutions lead to the formation of a HCA layer to which bone and soft tissues can bond (Hench et al., 1977; Wilson et al., 1981). The interface between the bioactive implant and bone tissue is similar to that between bone and tendons / ligament whereby the collagen fibrils produced by osteoblasts are incorporated within polycrystalline agglomerates during the reactive process (Hench and Paschall, 1974).

The process of the apatite layer formation involves the following fives reaction stages (Hench and Wilson, 1993):

1. Rapid exchange of Na^+ or K^+ with H^+ or H_3O^+ of the solution:

$$\mathrm{Si-O-Na^+ + H^+ + OH^- \rightarrow Si-OH^+ + Na^+(solution) + OH^-}$$

This is a rapid stage as the exchanged cations are part of network modifiers rather than network formers. The cation exchange causes an increase in the interfacial pH to values >7.4.

2. Loss of soluble silica in the form of $Si(OH)_4$ to the solution, resulting in breaking of Si-O-Si bonds and formation of Si-OH (silanols) at the glass-solution interface:

$$\mathrm{Si-O-Si} + \mathrm{H_2O} \rightarrow \mathrm{Si-OH} + \mathrm{OH-Si}$$

3. Condensation and rearrangement of Si-OH to form the silica-rich layer on the glass surface:

$$\begin{array}{ccccc} \mathrm{O} & & \mathrm{O} & \mathrm{O} & \mathrm{O} \\ | & & | & | & | \\ \mathrm{O-Si-OH} & + & \mathrm{OH-Si-O} & \rightarrow & \mathrm{O-Si-O-Si-O} + \mathrm{H_2O} \\ | & & | & | & | \\ \mathrm{O} & & \mathrm{O} & \mathrm{O} & \mathrm{O} \end{array}$$

The silica-rich layer acts as a template for calcium and phosphorous precipitation and supplies the correct atomic distance required by crystal structure of bone apatite. In addition, this layer acts as a barrier to further cation exchange (Hench, 1988). The role of this layer is very important in the bioactivity process and it has been shown that a pure hydrated silica gel induced apatite formation on its surface in a simulated body fluid (SBF) (Li et al., 1994).

4. Migration of Ca^{2+} and PO_4^{3-} groups, released from the glass with those of the solution to precipitate at the top of the SiO_2-rich layer forming a CaO-P_2O_5 -rich layer.

5. Crystallization of the amorphous CaO-P_2O_5 layer by incorporation of OH^-, CO_3^{2-}, or F^- anions from solution to form a mixed hydroxyl, carbonate, fluorapatite layer.

The kinetics of reaction stages 1-5 do not depend on the presence of tissues, but on the glass and on the solution compositions and therefore, the formation of a HCA layer can be detected in distilled water, Tris buffer solution and simulated body fluid (SBF) (Hench and Wilson, 1993). Hench et al. introduced a quantitative method to rank the bioactivity, known as the Index of Bioactivity (I_B) and defined as “the time required for more than 50% of the interface to be bonded”; I_B= 100 / (time taken to achieve 50% of interface bonding) (Hench, 1988). Table 1-2 represents the bioactivity index value of some bioactive ceramic materials.

Table 1-2: I_B values for various bioceramics (Hench, 1988):

Bioactive material	**Index of Bioactivity (I_B)**
45S5 BAG	12.5
55S4.3 BAG	3.7
A/W glass-ceramic	5.6
HA	3.1

1.1.2.3 Bioactive glass processing

Bioactive glass processing includes melting and sol-gel methods. The sol-gel method presents the advantages of low processing temperatures and ease of control of the textural properties (Hench and West, 1990). Sol-gel-derived glasses exhibit higher surface area and porosity compared to the melt-derived glasses (Sepulveda et al., 2001). On the other hand, melting is a simple, low-cost technique, where the raw materials are melted at 1300-1450^o C for 4 hours using a platinum crucible. The melt is then quenched in water producing a frit which in turn, is ground into powder using air collision techniques, and sieved using ISO-standard sieves to get the required particle size (Hench and Wilson, 1993). The surface area and thus the dissolution rate of melt-derived particles can be controlled by changing the particle size range (Sepulveda et al., 2001).

Following BAG processing, different features should be characterised such as the chemical composition, the microstructure, the size / shape of particles and the phase state to assure that the product is amorphous. The most important procedure following BAG processing is the bioactivity test which is conducted to detect whether glass bioactivity is not affected adversely by processing procedures (Hench, 2013b). A standard bioactivity test has been long established in the literature to validate this property using Fourier transform infrared spectroscopy (FTIR). The tested material is immersed in a Tris (hydroxymethyl) aminomethan buffered solution for 20 hours at 37^o C (Warren et al., 1989). This test measures the ratio between the sample's silicon-oxygen-silicon peak at 475 cm^{-1} to the newly formed HA peak at 560 cm^{-1} which appears if the sample is bioactive. The ratio measurement is compared with a known standard value and the powder is accepted or rejected according to specific criteria, addressed in Figure 1-4, Table 1-3 and Table 1-4 (Warren et al., 1989).

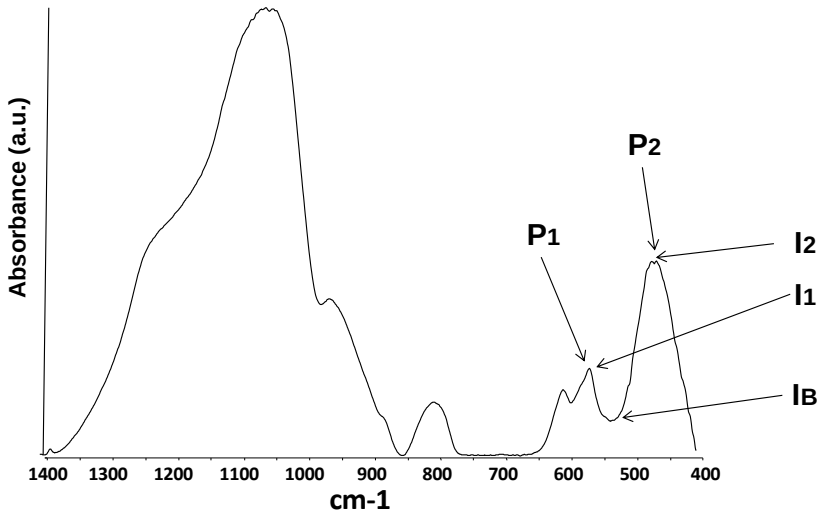

Figure 1-4: FTIR spectrum of BAG 45S5 immersed in Tris buffer solution for 20 hours. (I_1): the intensity of HA peak (P_1). (I_2): the intensity of silicon peak (P_1). (I_B): the minimum intensity between P_1 and P_2.

Table 1-3: Definitions for quality assurance criteria for BAG:

Notation	Definition
P_1	Peak maxima of FTIR signal between wave numbers 580 cm^{-1} and 535 cm^{-1}
P_2	Peak maxima of FTIR signal between wave numbers 490 cm^{-1} and 425 cm^{-1}
I_1	Intensity of P1
I_2	Intensity of P2
I_B	The minimum intensity between 650 cm^{-1} and 425 cm^{-1}
$(I_2-I_B)/(I_1-I_B)$	R1
R1/0.1074	Q1

Table 1-4: Quality assurance criteria for BAG:

Accept	Reject
$532<P_1<580$	$P_1>580$ or $P_1<535$
AND Q1≤5	OR Q1≥5

Cation release energy and structural density measurements can also help in evaluating the bioactivity of SiO_2-based glasses (Arcos et al., 2003). The activation energy (Ea) of soluble $Si(OH)_4$ is measured from the slope of the curve that represents the silicon concentrations as a function of soaking time, whilst the structural density of the tested sample is measured from the FTIR spectrum depending on the Si-O-Si stretch peak shift (Arcos et al., 2003).

1.1.2.4 Bioactive glasses: clinical applications in dentistry

Glass ceramic materials have been used in dentistry to regain masticatory function and improve aesthetic appearance (Hench, 2013b). These materials are able to match the aesthetic and mechanical properties of natural teeth and fulfil the dental restorative requirements of patients (Hench, 2010). The above applications do not require materials to be bioactive on the contrary to other clinical application, whereby the bioactive property of glasses is essential. Table 1-5 outlines the main application of BAG in dentistry. The use of BAG in enamel remineralisation has been discussed in more details in Chapter 5; p: 116 and Chapter 6; p: 149 of this thesis.

Table 1-5: The clinical applications of bioactive glasses in dentistry:

Field	Form	Outlines	References
Oral surgery	Endosseous ridge maintenance implant (*ERMI)*	- Cones of 45S4 Bioglass® used to fill the defect in the jaw following the extraction of the teeth to reduce the continuous resorption of the lingual and buccal alveolar plates. - Special burs matching the dimensions of the cones can be used to prepare the bone bed for implant. - Cleared by the Food and Drug Administration (FDA) in 1988	(Wilson et al., 1992) (Hench and Wilson, 1993)
	Particulate 45S5 BAG	- Bone grafts to be used in tooth extraction sites. - Bone grafts to be used in alveolar ridge augmentation. - Cleared by the FDA in 1996	(Hench, 2013a)
Periodontology	Particulate 45S5 BAG	- Particulate form of 45S5 Bioglass® (90-710µm) offers regenerative options for osseous treatment of periodontal disease without the biological complications associated with implanting auto- and xeno- grafts. - The ionic dissolution products of reacted bioactive glasses activate the cells to produce additional growth factors enhancing the tissue regeneration of bone. - It is recommended to use both a membrane and BAG particles to replace the lost bone with the soft tissue connections. - Cleared by the FDA in 1993	(Wilson and Low, 1992) (Robinson, 2013)

Dentine hypersensitivity treatment	Toothpaste containing 45S5 BAG particles	- The role of BAG in the treatment includes: 1. Physically filing the open dentine tubules. 2. BAG particles bind to the exposed dentine due to strong attraction between the bioactive glass particles and dentine collagenous matrix ; type I collagen fibres (remnant particles exhibit long term effect) 3. The HCA structures grown on remnant particles provides a protective layer attached to the dentine surface. - Cleared by the FDA in 2004	(Burwell et al., 2009b) (Greenspan and Hench, 2013)
Minimally invasive dentistry (MID)	Air-abrasive powder (BAG 45S5 particles)	- BAG abrasive powder has a potential to remove selectively more softened diseased or damaged tooth structure due to its reduced hardness compared to that of alumina, the most commonly used clinical abrasive powder. - The remnant particles on enamel / dentine surface may enhance the remineralisation.	(Paolinelis et al., 2008) (Banerjee et al., 2011b)
	Enamel remineralisation (Toothpaste-Slurry)	- BAG treatment increases the Knoop microhardness of enamel. - BAG treatment forms a protective deposit layer covering the surface of treated carious lesion.	(Alauddin et al., 2005) (Burwell et al., 2009b) (Gjorgievska et al., 2013)
	Bonding system (BAG 45S5 particles)	- BAG containing adhesive may enhance the durability of the resin-dentine bonds. - This approach may reduce the micro-permeability between the dentine and adhesive layer, and prevent the demineralisation within dentine surface.	(Sauro et al., 2012a) (Profeta et al., 2012) (Sauro et al., 2012b)

1.2 Substrates used in this thesis

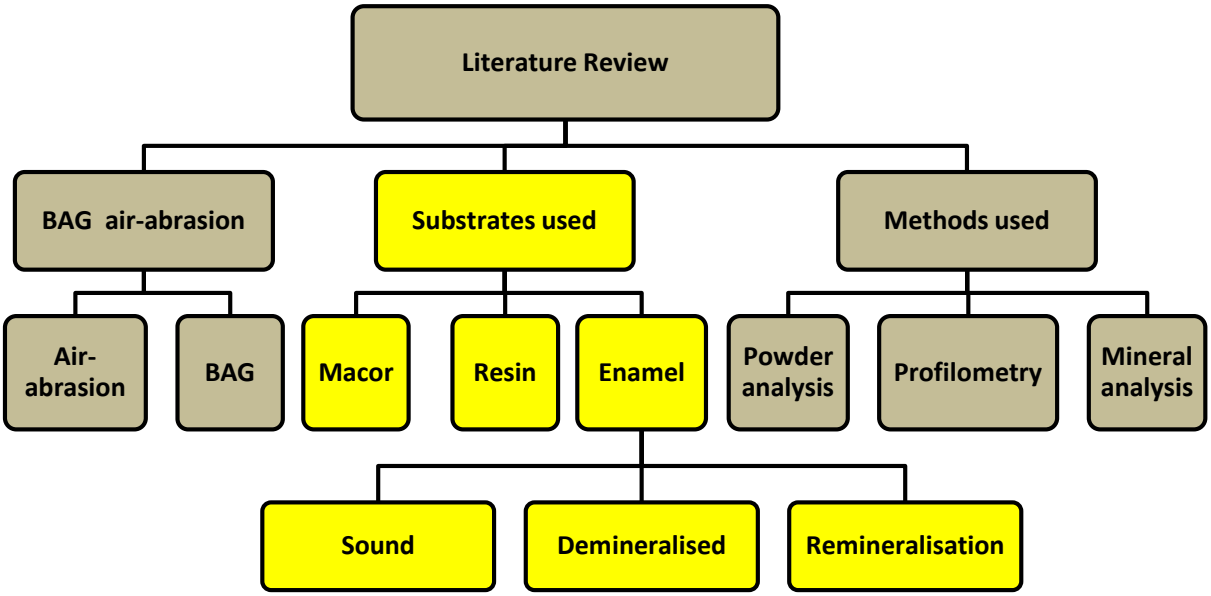

Flowchart of the literature review structure in this thesis.

1.2.1 Macor™

Macor™ is a glass-ceramic material used in this study as an enamel analogue to evaluate the operating parameters of BAG air-abrasion as well as the selective removal of resin composite restorative material. Its microstructure consists of an interlocked array of plate-like mica crystals (55 vol.% fluorophlogopite) dispersed within a glassy matrix (45 vol.% borosilicate glass). The chemical composition of Macor™ is 47.2 wt.% SiO_2, 14.5 wt.% MgO, 16.7 wt.% Al_2O_3, 9.5 wt.% K_2O, 8.5 wt.% B_2O_3 and 3.6 wt.% F (Holand and Beall, 2012). This material exhibits similar mechanical proprieties to those of human dental enamel, compared and addressed in Table 1-6. Taira et al. (1990) evaluated the cutting behaviour of Macor™ using dental diamond burs and concluded, after assessing both the cutting speed and the cutting volume that this material represents a good enamel analogue compared to other materials such as apatite-containing glass ceramics or resin composites.

Table 1-6: The mechanical properties of Macor™ compared to human dental enamel:

	Macor™	**Human dental enamel**
Density	2.52 g cm^{-3} (Carter and Norton, 2007)	3.15 g cm^{-3} (Elliott et al., 1998)
Hardness	250 Knoop (Holand and Beall, 2012)	250 - 290 Knoop (Meredith et al., 1996)
Porosity	0% (Holand and Beall, 2012)	1 - 2% (Robinson et al., 2000)
Compressive strength	50,000 psi (Holand and Beall, 2012)	53,900 - 55.700 psi (Craig et al., 1961)

In the dental literature, Macor™ was used to assess the cutting rate / efficiency of different operative technologies, and was considered a reliable substitute for enamel, in this regard, since it behaves similarly to human dental enamel during the cutting process (Wilwerding and Aiello, 1990; Gureckis et al., 1991; Siegel and von Fraunhofer, 2000; Ercoli et al., 2009; Paolinelis et al., 2009; Cristofaro et al., 2013; Bae et al., 2014). The use of Macor™ provides consistent hardness throughout air-abrasion cutting assessment, a critical factor in studying the cutting rate of operative techniques. The hardness of biological enamel samples varies from person to person and is a depth-dependent within the same tooth due to histological heterogeneity (Meredith et al., 1996; Maupomé et al., 1998; Wongkhantee et al., 2006). Using Macor™ blocks also provides a reliable, flat surface as a target substrate for air-abrasion cutting and subsequent objective analysis using optical surface profilometry, a “gold standard” method in assessing tissue surface loss (Field et al., 2010). The maximum sensitivity and accuracy of profilometry can only be achieved using flattened, polished samples (Schlueter et al., 2011).

1.2.2 Resin composite

Dental resin composites were introduced to provide an aesthetic adhesive direct restorative material suitable for restoring anterior teeth (Bowen, 1962). Significant changes and developments have occurred to improve the mechanical and aesthetic properties of the resin composites further, promoting their clinical performance (Ferracane, 2011). Generally, dental resin composites are composed of three main components, addressed with the chemical compositions highlighted in Table 1-7. Dental resin composites can be classified according to the fillers used into macrofill (10-50 µm), microfill (40-50 nm), nanofill (5-100 nm),

microhybrid (10-50 µm+40 nm), midifill (1-10 µm+40 nm) and minifill (0.6-1 µm+40 nm) composites (Ferracane, 2011).

Table 1-7: Typical composition of dental resin composite:

	Component		Chemical composition
1	Resin matrix	Monomer	BisGMA (bisphenol A-glycidyl methacrylate) (Peutzfeldt, 1997)
		Initiator	Photopolymerization: Camphorquinone Chemically cured: benzoyl peroxide-amine (Stansbury, 2000)
		Stabiliser	Hydroquinone monomethyl ether (García et al., 2006)
2	Inorganic fillers		Radiopaque glass, quartz and zirconia (Klapdohr and Moszner, 2005)
3	Coupling agent		Silane (Ferracane, 2011)

1.2.3 Enamel

1.2.3.1 Enamel structure

Enamel is an acellular tissue which does not retain its formative cells in the role of cell maintenance (Berkovitz et al., 2002). Equally, it may still be considered a dynamic tissue since it exhibits a physicochemical reactivity and ion exchange with the saliva and surrounding fluids (Osborn, 1981). It consists of 80-90 vol.% biological HA crystals and 10-20 vol.% water and organic components. The hydroxyapatite (HA) crystals are more dense than the other constituents and therefore, enamel is comprised of 96 wt.% HA minerals and 4 wt.% remaining components (Robinson et al., 2000). The HA crystal exhibits a flattened hexagonal cross-section, 40 nm wide, 25 nm thick and 150 µm long (Berkovitz et al., 2002). Approximately one thousand HA crystals are closely packed to form an enamel prism or rods (Figure 1-5). Each prism, approximately 5 µm wide, is surrounded by an irregular crystal-free area, 0.1 µm wide, known as a prism sheath (Meckel et al., 1965). The enamel prisms meet the outer surface at 90 degrees just above the cervical margin of the tooth, at 60 degrees on the smooth surface and 20 degrees in fissures of the occlusal surface (Berkovitz et al., 2002). A cluster of approximately 10 prisms run in the same direction to the outer surface with a different orientation to those of surrounding clusters producing a banding pattern detectable using optical microscopy of ground sections, known as Hunter-Schreger bands (Poole and Brooks, 1961).

Figure 1-5: Scanning electron micrograph of fractured etched enamel exhibits enamel prisms consisting of HA crystals [Silverstone et al. (1981)].

Two structureless, aprismatic enamel zones can be recognised; the outer surface layer and the area near the enamel-dentine junction. The appearance of a structureless region near the enamel-dentine junction is correlated to the irregular arrangement of HA crystals in this area, whist the absence of Tomes processes on the ameloblasts during the final stage of enamel deposition together with the increased mineralisation level may explain the appearance of aprismatic enamel at the outer enamel surface (Berkovitz et al., 2002). The highly organised microstructure and crystal packing density (2.85-3 g/cm^3) within enamel significantly improve its physical properties (Fan et al., 2009). The physical properties of enamel compared to that of dentine are addressed in Table 1-8. Enamel and dentine are mutually supportive as enamel's high degree of hardness protects the dentine from the abrasive effects of mastication, while the higher elasticity of dentine counterbalances the brittleness of enamel (Osborn, 1981).

Table 1-8: Ename physical properties compared to dentine (Osborn, 1981):
(MN= N x 10^6) (GN= N x 10^9)

Substrate	**Hardness (Knoop)**	**Tensile strength (MN m^{-2})**	**Young's modulus (GN m^{-2})**	**Compressive Strength (MN m^{-2})**
Enamel	250-290	30-35	131	76
Dentine	63	29-65	12	262

Variations in enamel mineral content can be recognised according to the anatomical site based on the fact that different histological zones exhibit less dense enamel prisms and greater spaces for organic material. The flatter surfaces with fewer complex histological features contain greater mineral concentrations compared to those reported within the fissure regions, cervical margins and cuspal enamel (Robinson et al., 1995).

Hydroxyapatite (HA) crystal structure

The molecular arrangement of each unit cell of HA is shown in Figure 1-6. It consists of a central hydroxyl ion column surrounded by a triangle of three calcium ions (Ca II), which in turn is surrounded by another triangle of three similarly spaced phosphate ions. These ions are enclosed by six calcium ions (Ca I) in a uniform hexagonal shape (Robinson et al., 1995). The calcium ions of the outer hexagon are shared between three adjacent similar hexagons. The entire crystal consists of this arrangement of hexagonal planes stacked one on top of another, but each turns by 60 degrees (Berkovitz et al., 2002).

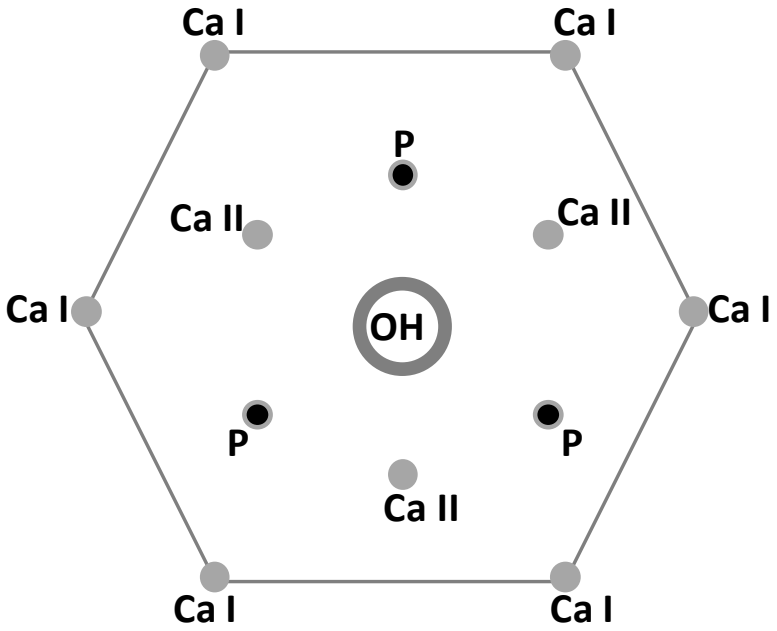

Figure 1-6: Crystal structure of HA: the overall planner hexagonal natural of the arrangement of calcium and phosphate ions around the central hydroxyl column [adapted from Robinson et al., (1995)].

The above hexagonal ion arrangement alone is not a crystallographic unit cell, which is parallelepiped. The crystallographic unit (parallelepiped) such as $Ca_{10}(PO_4)_6OH_2$ is made as follows: 4 columnar calcium ions (Ca II), 6 screw axis calcium ions (Ca I) and 6 phosphate ions located around the hydroxyls (Robinson et al., 1995). The HA in enamel is impure with different ions, such as carbonate, fluoride, sodium and magnesium, incorporated (Featherstone, 2000). The carbonate content presents 3-4 wt.% in enamel with 90% type B substitution (carbonate substituting phosphate ions) and 10% type A substitution (carbonate substituting hydroxide ions) (Penel et al., 1998; Spizzirri et al., 2012). The B-type substitution is believed to involve sodium for calcium exchange and therefore, the concentration of sodium may reflect that of carbonate in the enamel (Robinson et al., 2000). Fluoride incorporation in the HA occurs via a fluoride-hydroxyl exchange producing fluorapatite $Ca_{10}(PO_4)_6F_2$. The high charge density of fluoride ion stabilises the crystal structure reducing its solubilty (Featherstone, 2000). Magnesium may be also incorporated in the HA by displacing calcium ions, limited to approximately 0.3 %. The concentration of fluoride decreases from the outer enamel surface to the enamel-dentine junction (EDJ) in contrast to the carbonate and magnesium concentrations (Robinson et al., 2000).

Enamel protiens and organic components

The enamel organic component consists of original developing matrix remnants such as amelogenins and enamelins proteins (Acil et al., 2005). Amelogenins are secreted by ameloblasts and form 90% of the enamel matrix (Mangum et al., 2010). These can be detected near the enamel-dentine junction (EDJ) and in the fissures and the cuspal areas. The proportion of enamel proteins is negatively correlated with the mineralisation and maturation degree (Farah et al., 2010). The presence of collagen within enamel's organic component is controversial and there is a debate whether it is completely or partially degraded during the enamel mineralisation / maturation process (Acil et al., 2005). The presence of collagen in mature mineralised human enamel has been detected, but with considerably lower concentration to that in the dentine (Farah et al., 2010). It has been suggested that the collagen fibres from the EDJ may penetrate into enamel (Lin et al., 1993). The detected collagen in enamel is type I, whilst collagen type II and V, found within dentine and bone, are not present in enamel matrix (Acil et al., 2005). Finally, the organic component is affected by the integrity of the enamel,

and more proteins can be observed in the enamel of hypomineralised lesions (Farah et al., 2010; Mangum et al., 2010). However, the proteins detected here are not amelogenins, but are normally isolated from saliva fluid (Mangum et al., 2010).

1.2.3.2 Enamel demieralisation

Dental caries is a multi-factorial disease process involving the biofilm which can be controlled by a combination of strategies addressing its aetiological factors (Pitts and Wefel, 2009). The process of this complex lifestyle-related disease can be simplified as follows: (Featherstone, 2004)

1. Acidogenic oral plaque bacteria ferment carbohydrate producing organic acids such as lactic, formic, acetic, and propionic acid.
2. These acids diffuse into the enamel dissolving the minerals.
3. Minerals diffuse out of the enamel leading to cavitation if the demineralisation process continues.

The demineralisation process is counterbalanced by the remineralisation process numerous times daily and therefore, this disease is determined by the dynamic balance between the de- and remineralisation of dental hard tissues (ten Cate, 2001). The aetiology of dental caries is associated with four main factors including the bacteria, susceptible tooth surface, fermentable carbohydrate and the time for the plaque biofilm to dissolve the minerals at the teeth surface (Banerjee et al., 2001). The acidogenic bacteria, which produce organic acids, and the aciduric bacteria, which survive preferentially under acidic conditions, occupy no more than 1% of the total flora in normal dental plaque biofilm, but increase in number at the expense of the other benign bacteria throughout the caries process (Featherstone, 2004). *Streptococcus mutans* are believed to be the primary associative bacterial species and are used as microbiological markers for dental caries (Van Houte, 1993). *Lactobacillus and Bifidobacteria* are also found in the carious lesion, particularly in the advanced stages of the disease (Aas et al., 2008).

The susceptible tooth surfaces, upon which the dental plaque biofilm accumulates undisturbed for longer periods of time, mainly include the fissures of occlusal surfaces, the approximal surfaces cervical to the contact points of adjacent teeth, the surfaces adjacent to the gingival margin and finally, the margins of restorations (Banerjee and Watson, 2011). The critical pH for dissolution of enamel in oral fluids is 5.5; however, this value slightly varies depending on the concentrations of calcium and phosphate ions in the saliva and plaque fluid (Dawes, 2003). Other factors also influence the magnitude of the pH fluctuations, such as the fluoride ion concentration and the salivary secreting rate, reflecting the complexity of the dental cariogenic environment (Kidd and Fejerskov, 2004).

The acidic challenges affecting the enamel integrity in-vivo can be divided into those produced by acidogenic and aciduric bacteria which cause a dissolution of minerals from beneath the surface producing subsurface carious lesions, and those of extrinsic acid sources (food and beverages) which cause the removal of the minerals from the surface resulting in enamel erosion (Tung and Eichmiller, 2004). The first step in the enamel caries process is protein degradation followed by the loss of inorganic ions in specified histological areas which are belived to be interprismatic and intercrystalline regions (Darling, 1961; Robinson et al., 2000).

The enamel white spot lesion has been described as “the picture of enamel caries obtained before the attack has reached the enamel-dentine junction” (Gustafson, 1957). Initial demineralisation develops after 1 week of cariogenic challenge without clinical signs. The lesion exhibits a chalky and roughened appearance when the surface is air-dried after 2-3 weeks of cariogenic challenge and eventually after 4 weeks the lesion develops a white opaque area observed even before air-drying (Holmen et al., 1985). The correlation between the WSL appearance and air-drying is related to the refractive index of the media occuping the lesion pores which in turn, accentuates the difference in the refractivity between the enamel (1.63), water (1.33) and the air (1.0). Thus, when the lesion surface is air-dried, the pores become occupied by air rather than water making the lesion clearer and more distinguishable (Kidd and Fejerskov, 2004). The enamel caries lesion is divided histologically into four zones including the

translucent zone at the advancing edge of the lesion, the dark zone, the body of the lesion and the surface zone (Figure 1-7). Nanostructural examination of the enamel carious lesion has shown that the crystal orientation is preserved within the four zones resembling the sound enamel, and indicates that the orientation of crystals is independent of the degree of demineralisation (Deyhle et al., 2014).

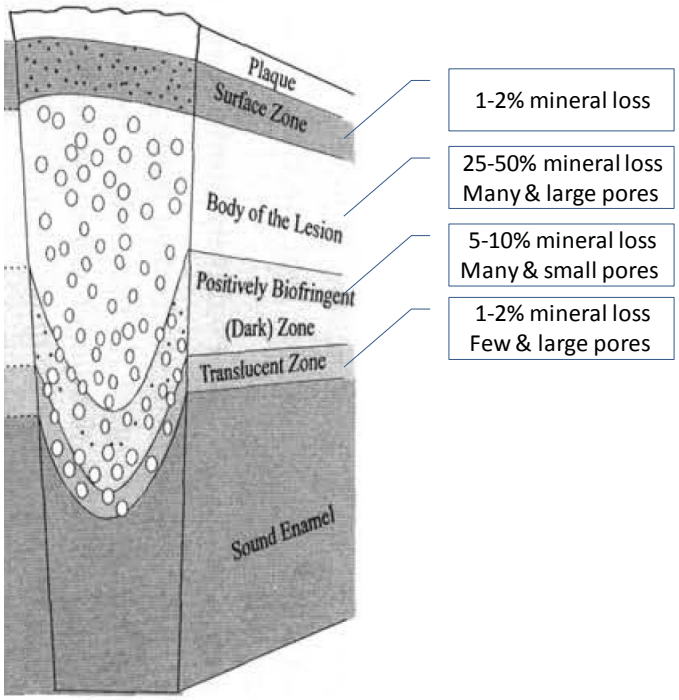

Figure 1-7: The four histological zones of enamel caries lesion [adapted from Robinson et al., (2000)].

1.2.3.3 Artificial enamel lesions:

In order to avoid the inherent biological variations in populations of natural WSLs, artificial lesions have been created for use in in-vitro remineralisation studies. The first artificial WSL was produced by von Bartheld in 1958 using an acidified charged gel (van Dijk et al., 1979). Different methods were thereafter introduced to induce artificial carious enamel lesions, which can be divided into four main categories addressed in Table 1-9.

Table 1-9: The main protocols used to create artificial enamel WSLs:

Protocol	Composition	Lesion features	Comments
Organic acids	Lactic acid alone (van Dijk et al., 1979)	The lesion is an acid-etched type and does not exhibit WSLs zones	The caries attack is a top-down approach
Methyl cellulose gel	6% methyl cellulose gel buffered using 0.1 mM lactic acid (Ingram and Silverstone, 1981)	The lesion has the structures of the WSL without the dark zone	The lesions exhibit a reduced depth (Magalhaes et al., 2009)
Hydroxyethyl cellulose gel	Mixtures of hydroxyethyl cellulose and acid (Gray, 1966)	The lesion has features of the WSL without the dark zone	Rapid surface attack (Silverstone, 1967)
pH-cycling models	Demineralisation and remineralisation solutions in simulating pH cycles (ten Cate and Duijsters, 1982)	The lesion depth and surface layer thickness vary according to the degree of saturation	Valuable in assessing the remineralisation of fluoride products (ten Cate, 1990)

In gel-based systems, lactic acid was selected as an acidic buffer to mimic the clinical environment as this organic acid is one of the bacterial metabolic products that are monitored regularly during the dental caries process (Gray, 1966). Different theories have been proposed in the literature to explain the formation of WSLs induced using gel-based systems. Some authors suggested that WSLs were produced due to the effect of diffusion-limiting of the gel (Ingram and Silverstone, 1981), which slows the attack of lactic acid and alters the rate of dissolution in a manner so that it becomes slower at the enamel surface and higher at the subsurface level (Gray, 1966; Silverstone, 1967; Holly and Gray, 1968; van Dijk et al., 1979). Gray in 1966 evaluated the kinetics of enamel dissolution during the formation of WSLs and suggested that the organic polymer gel may be absorbed by the enamel surface forming a protective coating similar to the biofilm that covers the enamel surface in-vivo and controls the diffusion rate during caries progression (Gray, 1966). Another explanation for WSL formation using gel-based systems is the calcium-binding activity of methyl cellulose gel which enhances the mineral re-deposition on the surface layer (Magalhaes et al., 2009).

1.2.3.3 Enamel remineralisation

Dental caries is a complex lifestyle-related disease determined by the dynamic balance between demineralisation and remineralisation within dental hard tissues (ten Cate, 1990; Featherstone, 1999). In the MID philosophy, the optimal purpose is to “heal” the incipient carious enamel lesion by reversing the demineralisation process, preventing any further mineral loss and enhancing remineralisation. Enamel remineralisation is the process whereby calcium and phosphate ions are supplied from a source external to the tooth to promote ion deposition into crystals voids of demineralised enamel to produce net mineral gain (Cochrane et al., 2010). The remineralisation process may include a new crystal growth, existing crystal repair and external mineral deposition (Silverstone, 1967; Briner et al., 1974; White et al., 1988; Preston et al., 2008).

The role of saliva in controlling the equilibrium between the de- and remineralisation processes of dental hard tissues has been long established resulting from its buffering power, clearance effect and saturation of ions (Edgar et al., 1994; Lagerlöf, 1994; Dowd, 1999). Salivary minerals can assist enamel remineralisation, but within a limited range due to pH fluctuations *in vivo* (Eisenburger et al., 2001; Huang et al., 2013). Therefore, external ion sources can be introduced to accelerate the remineralisation process before any further deterioration within the lesion structure occurs. The key approach in enamel remineralisation is to apply materials that contain essential ions required to form minerals similar to those of enamel (Tung and Eichmiller, 2004).

Enamel remineralisation systems

- ***Fluoride***

The role of fluoride in enamel de- and remineralisation has been extensively evaluated in the literature. This role includes three mechanisms of action; inhibiting bacterial metabolism, inhibiting demineralisation and enhancing the remineralisation (Featherstone, 2000). The role of fluoride in inhibiting enamel demineralisation is well-investigated and documented (ten Cate, 2004). However, its role in enhancing the remineralisation of enamel WSL has been discussed with different theories outlined in the literature. Bader et al. (2001) stated after a review of 1435 articles, that there was not sufficient in-vivo evidence supporting the role of fluoride in reversing the demineralisation of WSLs. In fact, there is

uncertainty about the ability of fluoride-containing products to deliver the sufficient fluoride concentration required in the remineralisation process, and the compliance of the patients in this regard affects significantly the remineralisation outcome (Geiger et al., 1988; ten Cate, 2013). Other aspects to be considered in WSL remineralisation are fluoride kinetics which are correlated to different factors including saliva characteristics / flowability, application volume / period and delivery mode (Newbrun, 2001). These also determine the bioavailability of fluoride in-vivo, which decreases rapidly to reach the baseline level (0.02-0.15 ppm F^-) only after 2 hours of fluoride application (Naumova et al., 2012). Indeed, most in-vitro studies ignored fluoride bioavailability and applied static fluoride concentrations throughout the experimental protocols. Even though constant fluoride concentrations were used to remineralise WSLs, the remineralisation has been shown to be a slow process due to fluoride's low solubility. In addition, fluoride's rapid precipitation at the lesion surface layer fills the porosities preventing further ions diffusing and resulting in an undesirable aesthetic appearance (Robinson et al., 1990; Bishara and Ostby, 2008; Beerens et al., 2010).

In order to promote the efficiency of fluoride in WSL remineralisation, it has been suggested to apply a combination of fluoride with calcium phosphate. However, the introduction of a singular vehicle containing the soluble calcium and fluoride in-vivo is challenging as separating fluoride from calcium is essential to prevent the formation of CaF_2 that inhibits the formation of fluorapatite (FA) restricting the remineralisation process (Karlinsey and Mackey, 2009). Another widespread approach to accelerate WSL remineralisation is applying a high concentration of fluoride, which has been shown to increase the WSL's initial remineralisation, but results in undesirable aesthetic consequences due to the incomplete remineralisation occurrence (Bishara and Ostby, 2008). The frequent use of high concentration fluoride may cause erosion and a degree of demineralisation due to the reduced pH 4.5 of the fluoride vehicle (Zero, 1996). In addition, it has been shown that increasing the fluoride concentration did not exhibit an increased cariostatic benefits and might affect negatively the enamel structural integrity due to the formation of CaF_2 which in turn, reduces the available Ca^{2+} ions required for remineralisation (Mohammed et al., 2014).

The formation of one unit cell of FA ($Ca_{10}(PO_4)_6F_2$) requires two fluoride ions, 10 calcium ions and six phosphate ions implying that the role of fluoride in enamel remineralisation is limited by the bioavailability of calcium and phosphate (Whitford et al., 2005; Vogel et al., 2008). From this perspective, two factors should be considered in-vivo including the low concentration of calcium and phosphate ions in saliva and the role of salivary proteins in particular, statherin groups in binding calcium and phosphate ions preventing any further ion diffusion into the enamel subsurface (Cochrane et al., 2010). Therefore, it can be concluded from the above discussion that applying fluoride is more useful and efficient in inhibiting demineralisation rather than enhancing remineralisation. Hence, calcium phosphate-based remineralisation systems were introduced to provide external calcium and phosphate ions with the intention of promoting and accelerating enamel remineralisation *in vivo*.

- ***Amorphous calcium phosphate (ACP)***

This macromolecule is prepared by a low-temperature process, where other elements such as zirconia and silica could be incorporated to increase the stability of ACP toward HA conversion (Skrtic et al., 2002). It is applied clinically as two systems; firstly, in a single phase whereby the water is not included to avoid the early reaction between the components. An example of this delivery mode is an ACP-containing chewing gum. Secondly, in a two-phase system to separate the calcium from the phosphate, e.g. toothpaste and mouth rinse (Tung and Eichmiller, 2004). The main limitation of this system is the low solubility of its components which reduces the remineralisation process while promoting calculus formation (Cochrane et al., 2010). To overcome this limitation, carbonate was added to reduce the pH and consequently increase its solubility (Tung and Eichmiller, 1998). Overall, ACP is an un-stabilised system containing high calcium and phosphate components without sufficient atomic arrangement and thereby, the stability of ACP in dental products is questionable (Walsh, 2009).

- ***Casein phosphopeptide - amorphous calcium phosphate (CPP- ACP)***

CPP-ACP was developed by Reynolds and co-workers at the University of Melbourne, and has incorporated into chewing gum, tooth cream and topical gels (Reynolds, 1987). The solubility of the ACP system is controlled by a milk protein, casein phosphopeptide (CPP), added to regulate the ACP solubility and to inhibit its early transformation into crystalline form (Reynolds et al., 1995). It is believed that CPP mimics the functional role of salivary proteins in controlling and regulating the solubility of calcium and phosphate providing an ion reservoir within dental plaque and at the same time preventing calculus formation, by the means of CPP negative charge which binds the calcium under neutral and alkaline conditions (Reynolds et al., 2003; Cross et al., 2005; Reynolds, 2008). CPP-ACP consists of 144 calcium ions, 96 phosphate ions and 6 peptides of CPP. Fluoride (900 ppm) has been added into some products (CPP-ACFP) since the Ser(P)-Ser(P)-Ser(P)-Glu-Glu sequence of CPP can also stabilise fluoride ions (Ferrazzano et al., 2011).

The results obtained using CPP-ACP products have shown inconsistent outcomes and the role of this system in WSL remineralisation has not been proven according to some researchers (Sudjalim et al., 2006; Azarpazhooh and Limeback, 2008). Rehder Neto et al. (2009) compared the in-vitro effect of CPP-ACP in controlling enamel carious lesions and concluded that the fluoride products exhibited better results to those of CPP-ACP products. Also, Beerens et al. (2010) in a double-blind prospective randomised clinical trial of 65 patients, showed that there were no differences in the effect of CPP-ACP paste and fluoride-free control paste on WSL remineralisation after a 3-month follow up. Another randomised control clinical trial with two parallel groups reported that the improvement of WSLs after 4 weeks of daily CPP-ACP application was not superior to that induced by fluoride toothpaste (Brochner et al., 2011). The same findings were reported in a recent in-vivo study conducted by Huang et al. (2013). The review of 642 articles concluded that there is a lack of evidence to support the effectiveness of CPP-ACP in WSL remineralisation *in vivo* (Chen et al., 2013).

On the other hand, it has been shown that the use of CPP-ACP offered a significant benefit in enamel WSL remineralisation since the lesions treated with CPP-ACP paste exhibited an increased HA crystals size, a decreased surface roughness and an increased hardness and elastic modulus compared to that of the control group (Elkassas and Arafa, 2014; Zhou et al., 2014). The use of CPP-ACP may inhibit enamel demineralisation and reduce the adherence of *Streptococcus sobrinus* and *Streptococcus mutans* bacteria at the tooth surface (Schupbach et al., 1996). An in-situ study showed that the use of a chewing gum containing CPP-ACP improved the mineral precipitation of eroded enamel (Prestes et al., 2013). This is in agreement with the results of a 24-month clinical trial evaluating the effect of chewing gum containing CPP-ACP on the regression of approximal caries (Morgan et al., 2008). Other than fluoride, CPP-ACP is one of the most extensively researched remineralisation technologies with sufficient evidence to support its role in enamel remineralisation *in vitro* (Walsh, 2009). However, more evaluation is still required to evaluate this role *in situ* and *in vivo*.

- ***Bioactive glass 45S5 (BAG)***

The composition and reactivity process of this system has been addressed in Sections 1.1.2.1; p: 33 and 1.1.2.2; p: 34. Even though it has been long established that BAG particles form HCA structures when interact with aqueous solutions such as saliva (Hench et al., 1971), few studies have been reported in the dental literature to evaluate the role of this system in enamel remineralisation compared to those of fluoride and CPP-ACP. This fact has been highlighted by different authors; Reynolds (2008) and Cochrane et al. (2010) stated that there were no published studies supporting the role of this system in WSL remineralisation *in vitro* and *in situ*, implying that this approach is at a very early stage of development. Walsh (2009) also noted that he could not find published information from refereed journals at the time of writing to support the role of BAG 45S5 in enamel remineralisation and the only available sources of information in this regard were unpublished data provided by manufacturers. In contrast, the role of BAG in dentine hypersensitivity treatment has been well investigated *in vitro* and *in vivo* (Efflandt et al., 2002; Du Min et al., 2008; Burwell et al., 2009a; Pradeep and Sharma, 2010). The affinity of dentine collagen to the glass surface promotes the physical occlusion of open dentine tubules, whilst the ionic release

of the retained particles leads to apatite formation at the dentine surface (Greenspan and Hench, 2013).

An in-vitro study using confocal laser scanning microscopy (CLSM) showed that treating enamel surfaces with BAG paste during pH-cycling exhibited a degree of remineralisation when compared to the negative control (Alauddin et al., 2005). Burwell et al. (2009) and Rehder Neto et al. (2009) reported an increase in the surface microhardness of artificial WSLs created within bovine enamel slabs and treated with BAG 45S5-containing pastes. Evaluation of the ultra-structural changes of WSLs treated with BAG-containing toothpaste and scanned using scanning electron microscopy (SEM) showed a protective layer of deposits covering the treated lesion surface (Gjorgievska et al., 2013). The use of BAG 45S5 has been shown to enhance the remineralisation of enamel surfaces etched with 0.25% citric acid and treated with BAG 45S5 slurry, assessed by SEM and nano-indentation (Dong et al., 2011). The SEM observation of sound enamel surfaces submitted to pH-cycling or to bleaching procedure and treated with BAG paste revealed mineral precipitations attached to the surfaces (Gjorgievska and Nicholson, 2010; Gjorgievska and Nicholson, 2011). Treating the surface of bovine enamel with BAG 45S5 during bleaching procedures reduced the microhardness loss and the ultra-structural changes of the bleached surface (Deng et al., 2013). In addition, the application of 45S5 BAG paste significantly improved the microhardness of the sub-surface of the eroded enamel surface (Bakry et al., 2014a). In another in-vitro study, the use of toothpaste containing BAG 45S5 exhibited no significant remineralisation effect on eroded enamel surfaces when compared to the control group, assessed using nanohardness (Wang et al., 2011a). Overall, the previous investigations explored the potential role of BAG in enamel remineralisation and presented promising results. However, bovine enamel substrate exhibits a markedly different microstructure to that of human dental tissue (Oesterle et al., 1998), which may affect the remineralisation outcomes. In addition, etched and eroded enamel do not exhibit the subsurface demineralisation characteristic of enamel WSLs and therefore, the results of some reported studies may not representative of WSL remineralisation. Finally, the assessment of chemical changes and the study of WSL depth changes following to the remineralisation therapy using 45S5 BAG are still outstanding.

Pre-conditioning WSL surfaces

Enamel WSL remineralisation has been acknowledged to be a difficult and slow process in-vivo and in-vitro, with incomplete remineralisation of the deeper aspects of the lesion (White et al., 1988; Larsen and Pearce, 1992). Larsen et al. (1992) evaluated the penetration of ions into WSLs and reported that the solution inside lesion pores is saturated with respect to calcium / phosphate ions since it is in contact with enamel HA and is almost sealed off from the external environment implying that the remineralisation of interior lesion structures may only occur when the intact outer surface of the lesion is broken or removed. It has been proposed that pre-conditioning the enamel surface with phosphoric acid prior to remineralisation treatment creates porosities required for mineral penetration, increases the total surface area and removes the superficial aprismatic layer exposing reactive enamel prisms (Aasenden et al., 1968). This approach might enhance WSL remineralisation and reduce the lesion depth assessed by the resultant improved lesion hardness, more fluorescence gain and increased mineral density compared to non-etched lesions (Collys et al., 1991; Flaitz and Hicks, 1993; Al-Khateeb et al., 2000; Al-Khateeb et al., 2014).

Pre-conditioning WSL surfaces with 30% phosphoric acid for 30 seconds increases the roughness of the surface and dissolves prism cores at the lesion surface and prism peripheries at the interior lesion structure (Hicks and Silverstone, 1984b). This treatment causes the loss of 3-6 µm depth of surface layer and increases the subsurface porosity to 21 µm in depth, detected using polarised light microscopy (Hicks and Silverstone, 1984a). Microradiography assessment showed that acid etching of a WSL resulted in the dissolution of a layer of lesion tissue, but did not cause an excessive mineral loss within the lesion body (Van Dorp et al., 1990). The remineralisation therapy of pre-conditioned lesions produced a thicker mineral layer at the surface compared to that of a non-etched group (Flaitz and Hicks, 1993), but with less mineral content according to microradiography assessment (Al-Khateeb et al., 2000). This reduction in mineral content at the outer layer of the lesion maybe due to the demineralisation effect caused by phosphoric acid used to modify the lesion surface prior to the remineralisation treatment.

1.3 Analysis methods used in this thesis

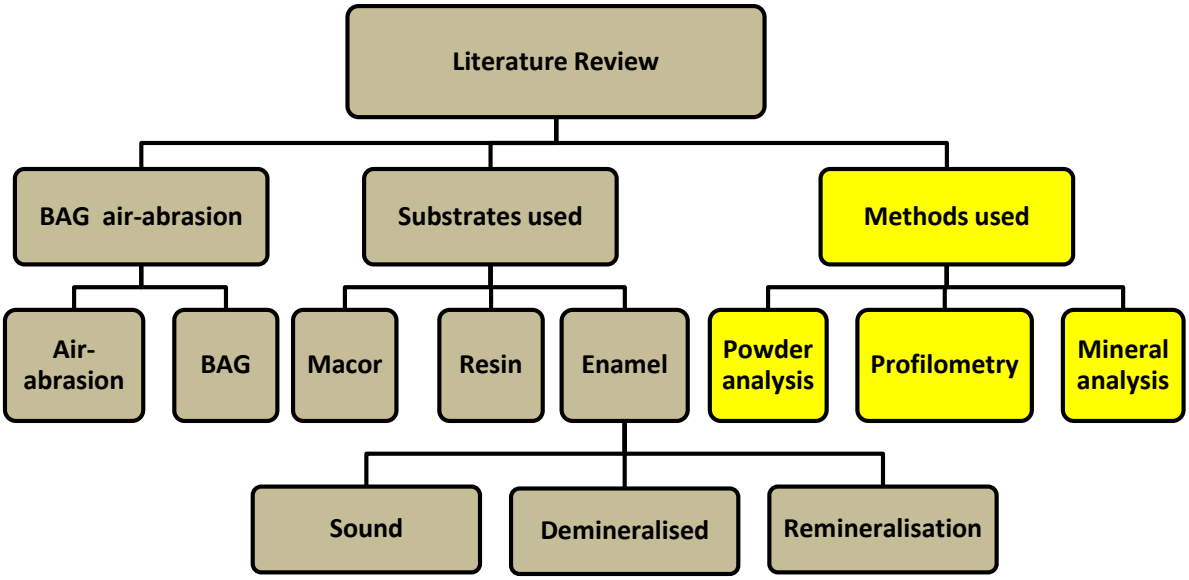

Flowchart of the literature review structure in this thesis.

1.3.1 Characterisation of abrasive powder

Particle shape analysis

The morphological characteristics of an abrasive powder affect its bulk density, flowability and surface area (Mikli et al., 2001), which all in turn, determine its technological applications. In air-abrasion, the powder's particle shape affects the cutting efficiency; angular particles exhibit increased abrasive properties compared to these of rounded particles (Stachowiak, 2000). The shape or out-line profile of an abrasive powder is assessed using microscopy techniques according to the visual appearance: rounded, cubic, semi-angular or angular based on (a) the diameter of the particle projection area, (b) the length-to-width ratio (L/W) and (c) the roundness factor which describes the closeness of the particle perimeter to the circular shape (Umeda et al., 1998).

Particle size distribution analysis

The particle size of an abrasive powder affects the cutting efficiency of an air-abrasion system (Horiguchi et al., 1997). This parameter is determined using different methods, divided into three main categories; imaging (microscopic techniques), physical techniques (sieving) and light scattering methods (laser diffraction particle analyser) (Lee Black et al., 1996). In order to aid obtaining representative powder samples, the powder should be sampled after motion, withdrawn from different regions and then reduced into smaller sub-samples (Jillavenkatesa et al., 2001).

Microscopy techniques measure the diameter which divides the particle into two equal projected areas (Merkus, 2009). The main limitation of this approach is that only a small portion of particles is analysed as a representative of the whole sample (Kissa, 1999). Sieving is the simplest approach which depends on weighing the different fractions after powder sieving. However, this method is affected by different parameters such as the particle shape, the sieve pore shape, the brittleness of the particles and the sieve loading (Beuselinck et al., 1998; Kissa, 1999; Eshel et al., 2004). Alternatively, laser diffraction particle analysis can be used to obtain accurate information about the particle size distribution. In this system, the particle size is defined depending on diffraction measurement of a laser beam transilluminating through a viewing cell containing particles in suspension (Masuda et al., 2006). It is a quick method with a good reproducibility, and a single measurement represents objectively a wide range of particle size since the motion of the particles through the fluid media is random (Beuselinck et al., 1998).

Bioactivity test of bioactive glass powders

Bioactivity tests of BAG air-abrasive powders have been conducted in this thesis using Fourier transform infrared spectroscopy (FTIR) according to a standard bioactivity test introduced by Warren et al. (1989). Fourier transform infrared spectroscopy detects the changes in dipole moment during molecular vibration which is induced by an incident infrared radiation to investigate functional groups, bonding types and molecular conformation within the tested material. It is a non-destructive measurement technique with a high scanning speed and sensitivity. Two main FTIR scan techniques can be used, the transmittance method where

the light passes through a sample, and the reflectance method which can be performed using an attenuated total reflectance cell in contact with the sample (Kuptsov and Zhizhin, 1998).

1.3.2 Surface topography measurement

Assessment methods available to analyse enamel surface topographic changes are divided into quantitative and qualitative techniques (Schlueter et al., 2011), summarised and addressed in Figure 1-8. Among these methods, surface profilometry is one of the most established approaches to measure topographical surface change (Field et al., 2010). It depends on quantifying the loss of a substrate in relation to non-treated surface areas (Barbour and Rees, 2004).

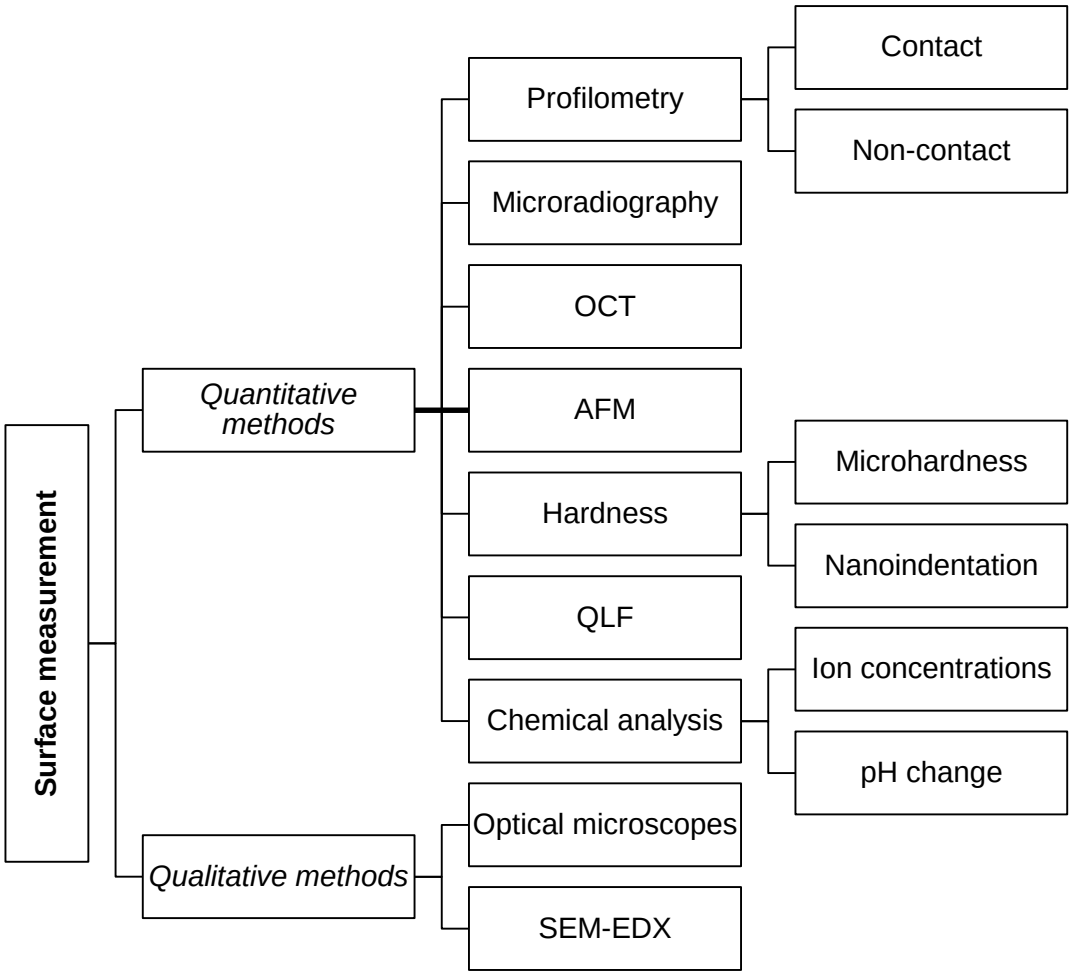

Figure 1-8: Flowchart of surface topography measurement methods [summarised from Barbour and Rees (2004) and Schlueter et al. (2011)]. (OCT): Optical Coherence Tomography, (QLF): Quantitative Light-induced Fluorescence, (SEM-EDX): Scanning Electron Microscopy - Energy Dispersive X-ray Spectroscopy and (AFM): Atomic Force Microscopy.

Surface profilometry

Surface profilometry creates a digital map of a surface in the form of a point cloud, which presents the 3D coordinates in the X, Y and Z planes of the digitised surface (Ireland et al., 2008). This can be obtained using either contact or non-contact measuring devices. The first use of this technology in dental research was in 1972 to assess the effect of different toothpastes on a tooth surface (Ashmore et al., 1972). This non-destructive assessment method has been calibrated and described as a "gold standard" for enamel surface loss assessment (Hall et al., 1997; Ganss et al., 2005). It can be used to measure dental surface loss resulting from erosive mineral loss, dental restoration removal and carious tissue excavation (Ganss et al., 2005; Paolinelis et al., 2006; Kim et al., 2007).

- ***Contact profilometry***

Contact profilometry relies on moving a diamond-tip stylus (steel, ruby, and tungsten carbide) over a surface and converting the movement into electrical data by the means of a provided transducer (Field et al., 2010). The resolution as well as the accuracy of the measurement is determined by the size of stylus (Ren et al., 2009). The limitations of this technology are (Jost-Brinkmann, 1998; Ireland et al., 2008; Leach, 2010):

1. It can be used only to scan hard surfaces.
2. The stylus cannot fully penetrate narrow fissures and grooves.
3. The stylus force may cause a surface deformation.
4. The stylus lateral deflection and skid can deteriorate results.
5. Significantly more time is required to complete the surface scan compared to that in non-contact profilometry.

- ***Non-contact profilometry***

Non-contact profilometry depends on optical techniques to scan the surface without any physical contact with the targeted surface (Ireland et al., 2008). In this thesis, two optical techniques have been used included laser triangulation and white light confocal systems. Laser triangulation profilometry employs optical triangulation principles by employing a twin detector configuration (Chen et al., 2000). It is important to note that a potential reflection of the laser beam on a polished surface may produce an "overshot" and results in artefacts. Therefore,

it is not recommended to use this technique to scan a polished, mirror-like enamel surface (Whitehead et al., 1999). The main advantage of this system is that it exhibits a large gauge range permitting an effective measurement of surfaces with a large variance between the highest and lowest points (Leach, 2010). White light profilometry uses distance measuring sensors, whereby the light passes through a dispersive medium into different wavelengths focused at different distances from the surface. In this technique, only one point is measured at a time achieved by the means of two pinholes; one in front of the light source and the other in front of the detector (Leach, 2010). The reflected light is analysed by a spectrometer depending on wavelength peak values. The measurement error of this system has been shown to be ±0.06 µm for enamel and 0.09 µm for dentine (Steiner-Oliveira et al., 2010).

1.3.3 Assessment methods for studies of mineral content of enamel WSL

1.3.3.1 Raman micro-spectroscopy

Micro-Raman spectroscopy provides details about the chemical composition and the molecular interaction of both biological and synthetic materials (Choo-Smith et al., 2002). It is a non-destructive assessment method where samples require no physical preparation prior to analysis that may affect the structure and therefore the interruption of results. Raman micro-spectroscopy analyses the chemical content of tissues by detecting their characteristic molecular vibrational energy signatures. The difference in energy between the incident and the inelastic scattered photons corresponds to the energy of the molecular vibration (Figure 1-9) (Bertoluzza et al., 1992; Petry et al., 2003).

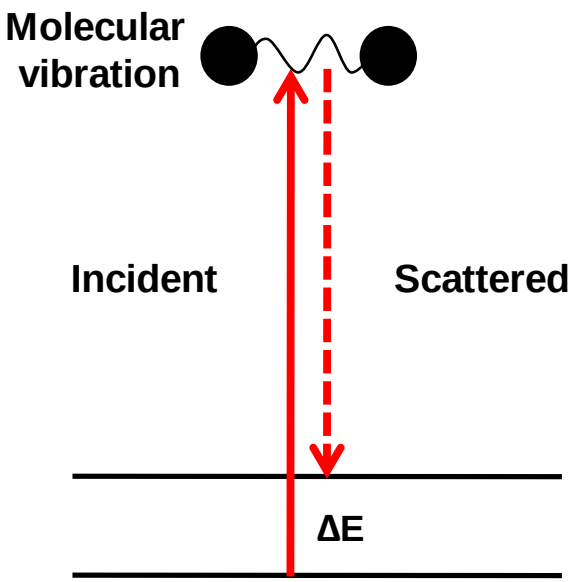

Figure 1-9: The energy-level diagram of Raman scattering; the molecular vibration energy (ΔE), caused by an incident photon, calculated as the energy difference between the incident and scattered photons [Adapted from Bertoluzza et al. (1992].

The main limitation of using Raman is that the observation of Raman scattering in some biological systems may be obscured by intrinsic fluorescent excitation (Petry et al., 2003). Human dental enamel contains little organic component and therefore, the excitation of fluorescence has no significant impact on the resultant spectra (Tsuda and Arends, 1997). The Raman spectrum of sound enamel exhibits peaks representing phosphate and carbonate within enamel crystals, with their corresponding assignment in Figure 1-10 (Salehi et al., 2012; Spizzirri et al., 2012). The four phosphate (PO_4^{3-}) peaks are assigned to the internal vibrational modes of the phosphate groups as described in Table 1-10.

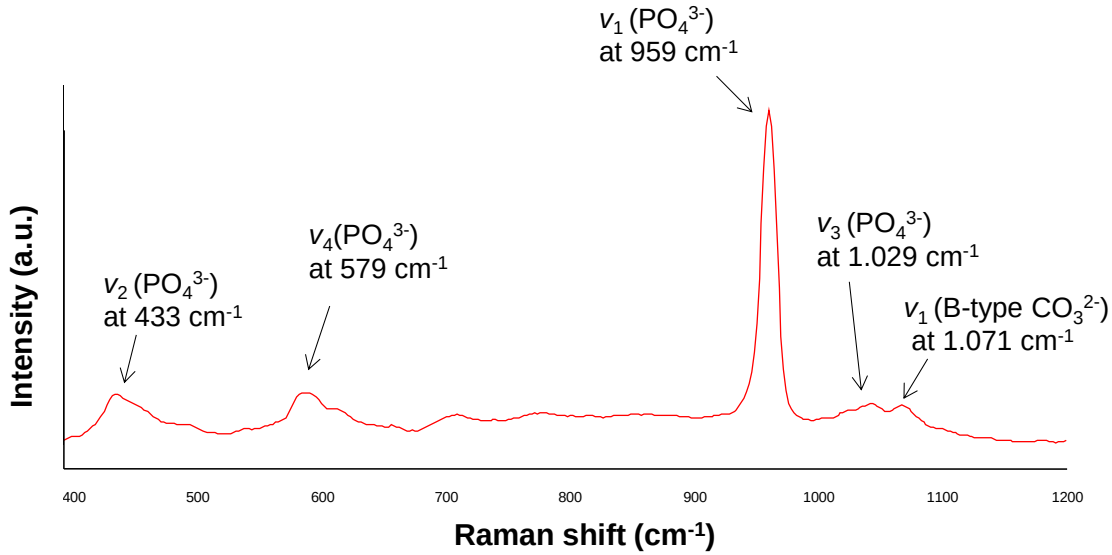

Figure 1-10: Representative Raman spectrum of sound human enamel including the observed peak positions and their assignments.

Table 1-10: Raman shift assignment for HA (Koutsopoulos, 2002):

(PO_4^{3-}) peak	**Vibratioal mode**
1,029 cm^{-1} (Weak)	Asymmetric stretching mode (*v*3) of (PO_4^{3-}); (P−O bond)
959 cm^{-1} (Very strong)	Symmetric stretching mode (*v*1) of the tetrahedral (PO_4^{3-}); (P−O bond)
579cm^{-1} (Medium)	Asymmetric bending mode (*v*4) of (PO_4^{3-}); (O−P−O bond)
433 cm^{-1} (Medium)	Symmetric bending mode (*v*2) of (PO_4^{3-}); (O−P−O bond)

Quantitative information about the mineral concentration of materials can be obtained using Raman micro-spectroscopy since the peak intensity is proportional to the number of molecules within the volume of the scanned area (Penel et al., 1998; Tramini et al., 2000). Hence, the measurement of phosphate peak intensity can be employed to assess the concentration of phosphate within the dental tissues; Mohanty et al. (2012) measured the intensity of the phosphate peaks along the cross-sectional view of an artificial enamel white spot lesion and showed that this technique was able to characterise the chemical content of the lesion. The intensity of phosphate peaks within the lesion body dropped by >40% compared to the deeper healthy sound enamel (Mohanty et al., 2012). Mapping the enamel of pits and fissure caries showed a considerable reduction in the intensity of phosphate peak, approximately three times less than that of the intact surrounding enamel (Kinoshita et al., 2008). In addition, evaluating the effect of lactic acid and bleaching agents on enamel by measuring phosphate peak

intensity at 959 cm^{-1} showed that Raman micro-spectroscopy was able to detect the chemical dynamic changes of enamel minerals at different points of time (Tramini et al., 2000; Santini et al., 2008). The phosphate peak at 956 cm^{-1} has been employed to detect the apatite mineral forming at the early stage of mineralisation within cartilage tissue, and the observation of its intensity introduces information about the dynamic mineral changes within this tissue (Sauer et al., 1994).

Regarding BAG 45S5, the Raman modes of HCA grown on a BAG 45S5 surface have been shown to be similar to those of HAC in the bone (San Miguel et al., 2010). The peak positions of the grown HCA are v_1 (PO_4^{3-}) at (959 cm^{-1}), v_3 (PO_4^{3-}) at (1,077 cm^{-1}), v_4 (PO_4^{3-}) at (595 cm^{-1}) and (CO_3^{2-}) at (1,085 and 711 cm^{-1}) (Rehman et al., 1994; Notingher et al., 2003). It has been suggested that the amount of HCA grown on the BAG 45S5 surface can be estimated by measuring the intensity of P-O peaks at 959 cm^{-1} since this intensity is correlated to the thickness of the formed HCA layer (Notingher et al., 2002; San Miguel et al., 2010). In addition, the C-O Raman peak at 1085 cm^{-1} is sharp and can be detected within the formed HCA layer (Rehman et al., 1994).

1.3.3.2 Microhardness

Hardness is a measure of a material's resistance to permanent deformation (Sirdeshmukh et al., 2006). Microhardness uses a low load of < 200 g to create an indentation in a substrate surface using a diamond tip of known geometrical dimensions. Microhardness is a commonly used method in dental research to assess enamel hardness producing quantitative data about the tested tissue (Attin, 2006). Featherstone et al. (1983) reported a linear relationship between the hardness and the mineral content of WSLs assessed by comparing the microhardness data with that of microradiography. It can be used to monitor the mineral gain and loss throughout de- and remineralisation dynamic processes (Featherstone et al., 1983; Lippert and Lynch, 2014). A strong relationship has been also documented between the mineral content of an in situ-induced WSL and microhardness implying that this technique can be considered as a reliable method for the indirect measurement of WSL's mineral content *in vitro* and *in situ* (Kielbassa et al., 1999).

Two indenters; Knoop or Vickers indenters penetrate the tested surface by approximately 1.5 µm and 5 µm respectively (Figure 1-11) (Schlueter et al., 2011). Using magnification, the length of the indention is measured to obtain a hardness value using the following equation (Purdell-Lewis et al., 1976; Gong et al., 1999):

For Vickers hardness number: VHN (kg/mm^2) = (1.85 x K) / D^2

For Knoop hardness number: KHN (kg/mm^2) = (14.23x K) / L^2

K: the applied force (kg), L: the length of the indentation (mm) and D: the diameter of the indenter (mm).

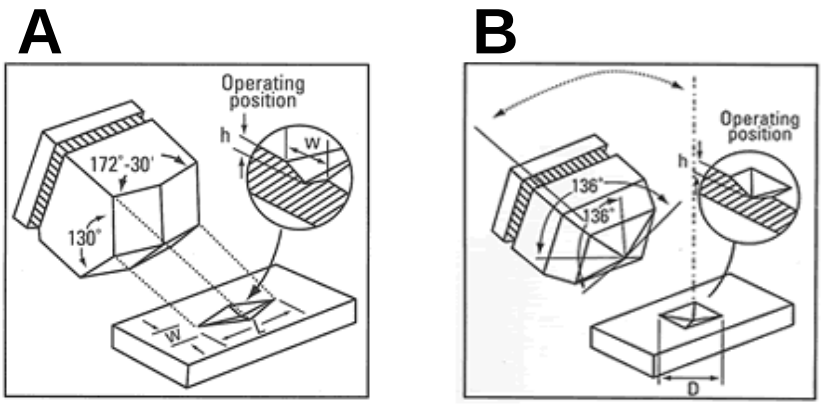

Figure 1-11: A diagram representing the shape of Knoop (A) and Vickers (B) indenters. (W): indentation width, (L): indentation length and (D): diameter of indentation [From the manufacturer's provided booklet].

In the dental literature, microhardness testing has been used to detect enamel WSL remineralisation using different remineralisation agents such as fluoride, CPP-ACP, and BAG. It has been suggested that the improvement of hardness reflects better crystalline and denser apatite substrate structures (ten Cate et al., 1988; Rehder Neto et al., 2009; Wang et al., 2011b; Amaechi et al., 2013). However, microhardness testing is a destructive method where the indentations not only affect the immediate contact areas, but also surfaces at a distance of approximately 10 times the dimensions of the indenter. Therefore, a sufficient distance between adjacent indentations should be allowed (de Jong et al., 1987; Barbour and Rees, 2004). In addition, this measurement develops inaccuracies when used on an anatomical, curved substrate surface (Schlueter et al., 2011). Magalhaes et al. (2009) showed that microhardness testing introduced information about the mineral content of WSLs, but this varied according to the experimental conditions, the area of indentation and the depth of the WSLs.

1.3.3.3 Nano-indentation

Nano-indentation depends on measuring the depth of the surface indentation rather than its length and the hardness is calculated according to the load-displacement curve of the indenter (Doerner and Nix, 1986; Mahoney et al., 2000). This sensitive method uses a small indentation (<1 μm) to measure the hardness at the depth of less than 100 nm (Finke et al., 2001). Huang et al. (2010) mapped natural WSLs using this technique and reported that both the body and the surface layer of the lesion have been distinguished with values similar to those described in the dental literature using microhardness testing. The nano-mechanical map of artificial WSLs exhibited a positive correlation with the calcium content of the lesion particularly at a subsurface level (Dickinson et al., 2007). Nano-indentation was able to detect the mineral gain following effective remineralisation treatments (Lippert et al., 2004; Dong et al., 2011; Zhou et al., 2014). The main limitation of this method, however, is the potential bias of small sampling area (Radhakrishnan and Mao, 2004). In addition, the results of nano-indentation have been shown to be affected by different variables including sample preparation, lesion pores volume / number and the inherent crystal growth (Habelitz et al., 2001; Alauddin, 2004).

1.3.3.4 Scanning electron microscopy (SEM)

Scanning electron microscopy (SEM) is a qualitative analytical method which produces images at high resolution (at a nanometre scale) (Boyde and Lester, 1967). The use of SEM micrographs permitted not only to observe the ultrastructural changes within the WSL tissue, but also to detect the shape and the size of newly formed crystals which in turn, have an important impact on enhancing the remineralisation through the whole lesion depth (Onuma et al., 2005; Fan et al., 2009). Coating the sample surface with a metal such as gold or carbon is essential prior to SEM imaging in order to increase the surface conductivity to prevent the surface charging that deteriorates micrographs (Lyman, 1990). This coating prevents any further use of the sample in order to detect any dynamic changes within it, an important aspect in the de- and remineralisation of WSLs.

1.3.3.5 Energy dispersive X-ray spectroscopy (EDX)

Energy dispersive X-ray spectroscopy (EDX) is an analytical technique used for the chemical characterisation of both biological and synthetic materials (Barbour and Rees, 2004). The spectroscope is incorporated into an SEM system whereby, the elements of a sample emit a characteristic X-ray pattern when excited by electrons of sufficient energy. In the dental literature, EDX has been used to measure the concentrations of calcium, phosphorous and fluoride in sound enamel submitted to repeated demineralisation challenges, as well as to measure these concentrations within new mineral depositions formed during the remineralisation treatment of WSLs (Naumova et al., 2012; Amaechi et al., 2013; Gjorgievska et al., 2013). The accuracy of this system in obtaining quantitative information is questionable as changing the beam voltage affects the intensity of the peaks within the EDX spectrum, and the overlapping of some peaks may interrupt the results. In addition, the resolution of EDX has been shown to be insufficient to detect some elements, as well as the density of the tested material affects the degree of electron beam penetration within the sample (Canli, 2010). For the above reasons, EDX tends to introduce valuable and accurate information when used as a qualitative approach to determine the chemical composition of the material.

1.3.3.6 Optical coherence tomography (OCT)

Optical coherence tomography (OCT) is a non-invasive imaging technique which enables cross-sectional imaging of internal biological structures by differentiating between incident and reflected photons using a near-infrared light source at a micron resolution (Hariri et al., 2012). In this technology, OCT images are constructed depending on the wave interference occurring when coupling a backscattered light with a reference one (Shimada et al., 2013). OCT images exhibit high lateral and vertical resolutions in the order of 10 μm (Baumgartner et al., 2000). Optical coherence tomography has been used in de- and remineralisation assessment in-vitro and in-vivo as it images non-destructively the interior structure of WSLs by measuring light scattering which in turn, correlates reversely to the mineral content of the lesion (Baumgartner et al., 2000; Can et al., 2008; Wilder-Smith et al., 2009; Mandurah et al., 2013). This depends upon light scattering which increases in porous demineralised enamel (Kang et al., 2012).

Mandurah et al. (2013) reported a positive correlation between the OCT and nano-indentation measurements of WSLs treated using a remineralisation solution for 14 days. The compositional changes of enamel crystals throughout WSL remineralisation treatment have been detected using OCT measurements which showed results consistent with those of microradiography (Hariri et al., 2013). The advantages of using OCT over radiographic methods in enamel de- and remineralisation assessment are it employs near-infrared light rather than hazardous ionizing radiation, it exhibits a better resolution compared to other clinical radiographic techniques, and it is a rapid procedure which requires no physical sample preparation (Baumgartner et al., 2000; Kang et al., 2010; Mandurah et al., 2013). However, the limitations of this technology are that enamel surface hydration considerably affects OCT signal intensity (Baumgartner et al., 2000; Mandurah et al., 2013; Nazari et al., 2013).

1.3.3.7 Transverse microradiography (TMR)

Transversal microradiography (TMR) is one of the most documented methods in assessing the mineral content of WSLs (Fontana et al., 1996). It was developed in 1963 to measure the mineral content in a small volume of dental tissue (Angmar et al., 1963). This technique depends on measuring the absorption of monochromatic X-rays by a tooth substrate in comparison with a standard alumina stepwedge involved in the imaging, with a resolution of approximately 6 µm (ten Bosch and Angmar-Månsson, 1991; Damen et al., 1997; Lo et al., 2010). It is a time-consuming technique which demands a preparation of thin sample slices of the order of 100 µm (Fontana et al., 1996). Moreover, these slices must be homogenous over their thickness (ten Bosch and Angmar-Månsson, 1991). Preparing such thin slices of enamel containing WSLs is difficult due to the brittle property of enamel (Can et al., 2008). Another drawback of using this method is the potential for misalignment when specimens with curved outlines, such as anatomical tooth surfaces, are analysed (Meyer-Lueckel et al., 2007). Finally, TMR is a destructive method, unsuitable for sequential measurements, an important aspect in de- and remineralisation studies.

1.3.3.8 Quantitative light-induced fluorescence (QLF)

Quantitative light-induced fluorescence measures the intensity of the fluorescence resulting from the interaction between dental tissues and a light induced by a near ultraviolent radiation (Koenig and Schneckenburger, 1994; Angmar-Mansson and Bosch, 2001). An enamel WSL exhibits a reduced QLF measurement compared to that of healthy sound enamel since the pores in the WSL are assumed to increase the scattering of the light and consequently, reduce its absorption (Al-Khateeb et al., 1998). Another explanation for the QLF measurement reduction in the WSL is that the scattering of the light within the lesion forms a barrier to the fluorescence light emitted from dentine (Angmar-Mansson and Bosch, 2001).

The remineralisation of WSLs has been shown to cause a fluorescence gain within the treated carious lesion; reported in a number of studies supporting the role of QLF as a method to assess the dynamic mineral changes within WSLs *in vitro* and *in vivo* (Al-Khateeb et al., 2000; Fujikawa et al., 2007; Sano et al., 2007; Alammari et al., 2013; Tahmassebi et al., 2014). It is important to point out that the presence of dentine within the tested sample affects the fluorescence output and therefore, a layer of dentine beneath the enamel substrate is required to study WSL *in vitro* (Gomez et al., 2014). Although the use of QLF has been reported widely in the dental literature to evaluate WSLs, the theoretical basis in this regard has not been determined precisely. Additionally, the determination of the remineralised tissue is unmeasurable using this method (Tranaeus et al., 2001). The QLF measurement is affected significantly by different variables including the tooth size, the curvature and the staining of the outer enamel surface (Adeyemi et al., 2006).

1.3.3.9 Optical microscopic techniques

Polarised light microscopy has been used to investigate the mineral content of enamel WSLs in-vitro, measuring enamel birefringence by the means of different media, including water and quinoline (Silverstone, 1973; Hicks and Silverstone, 1984a). Quantifying the information obtained using this method showed inconsistent results compared to those of microradiography; and therefore, it was recommended that this method be used only for the histological examination of enamel WSLs (Carlström and Glas, 1963; Theuns et al., 1993).

Confocal laser scanning microscopy (CLSM) improves the contrast of the optical image by using an aperture in the conjugate focal plane of an objective lens, in both the illumination and imaging pathways of the microscope (Watson et al., 2008). It has been shown that there is a correlation between the autofluorescence of carious dentine detected using CLSM and the mineral content of the tissue (Banerjee and Boyde, 1998). In order to study enamel WSLs, a method has been developed depending on staining the WSL with a fluorescent dye to analyse quantitatively a representative length from the lesion (Fontana et al., 1996). It has been suggested that this approach may be used as an alternative to TMR in measuring the mineral content of WSLs during the de- and remineralisation since the CLSM showed a positive correlation with TMR when used to assess enamel WSLs (Fontana et al., 1996; González-Cabezas et al., 1998). However, the use of light microscopy for quantitative assessment is questionable as there is no available way to ascertain if the liquid has filled all the pores of the WSL. Therefore, only qualitative information about the structure of WSLs can be obtained using optical microscopes (Angmar et al., 1963; Lo et al., 2010).

1.3.3.10 Considerations for choosing a method

The selection of an assessment method to study mineral changes of enamel WSLs depends upon different factors including: the study design (e.g. single measurement vs. repeated measurements), the resources (e.g. available expertise, availability of equipment, the cost and the required time) and the specification of quantitative or qualitative accuracy (ten Bosch and Angmar-Månsson, 1991). As there is no one method that can evaluate the entire range of aspects of enamel WSLs alone, it appears that a combination of different methods is preferable in order to detect the ultra-structural, mechanical and chemical changes within treated WSLs. Table 1-11 outlines the methods used to assess mineral changes of WSLs, indicating those used in this thesis.

Table 1-11: A summary of the methods used to assess the mineral changes of enamel WSLs:

Assessment method	**Output**	**Type**	**Analysis principle**	**Resolution**	**Used in this thesis**
Micro-Raman spectroscopy	Qualitative/Quantitative	Non-destructive	Chemical	Up to 2.7 µm	Yes
Energy dispersive X-ray spectroscopy	Qualitative/Quantitative	Destructive	Chemical	According to the accelerating voltage (few microns)	Yes
Microhardness	Quantitative	Destructive	Mechanical	-	Yes
Nanoindentation	Quantitative	Destructive	Mechanical	-	No
Scanning electron microscopy	Qualitative	Destructive	Morphological	(few nanometres)	Yes
Optical microscopy	Qualitative/Quantitative	Destructive/ Non-destructive	Morphological	According to the objective and system	Yes
Transversal Microradiography	Quantitative	Destructive	X-ray absorption	6 µm	No
Quantitative light-induced fluorescence	Qualitative/Quantitative	Non-destructive	Light fluorescence	-	No
Optical coherence tomography	Qualitative/Quantitative	Non-destructive	Light scattering	6 µm	Yes

Overall aims of Chapters 2, 3, 4, 5 and 6

The overall aim of this project was to develop the use of BAG air-abrasion as an operative technique in minimally invasive dentistry (MID) for the controlled and selective removal of substrates and for enhancing the remineralisation of enamel white spot lesions (WSLs) using BAG 45S5 technology.

Objectives

1. To calibrate the air-abrasion system including the characterisation of the abrasive powders and the validation of the unit's operating parameters.
2. To evaluate the effect of six operating parameters: air pressure, powder flow rate, nozzle-substrate distance, nozzle angle, shrouding the air stream with a curtain of water and the abrasive powder itself, on the cutting efficiency / pattern of BAG air-abrasion using alumina air-abrasion as a positive control.
3. To assess the effect of three clinically adjustable air-abrasion operating parameters on the selective removal of resin composite, and to determine the required time taken to carry out the procedure.
4. To evaluate the effect of BAG 45S5 and PAA-BAG powders on artificial enamel WSL remineralisation through chemical, mechanical, optical and ultra-structural assessments.
5. To assess the physical modification of enamel white spot lesion pre-conditioning using BAG air-abrasion technology and to study the impact of this modification on the overall remineralisation.

Chapter 2 Bioactive glass air-abrasion system calibration.

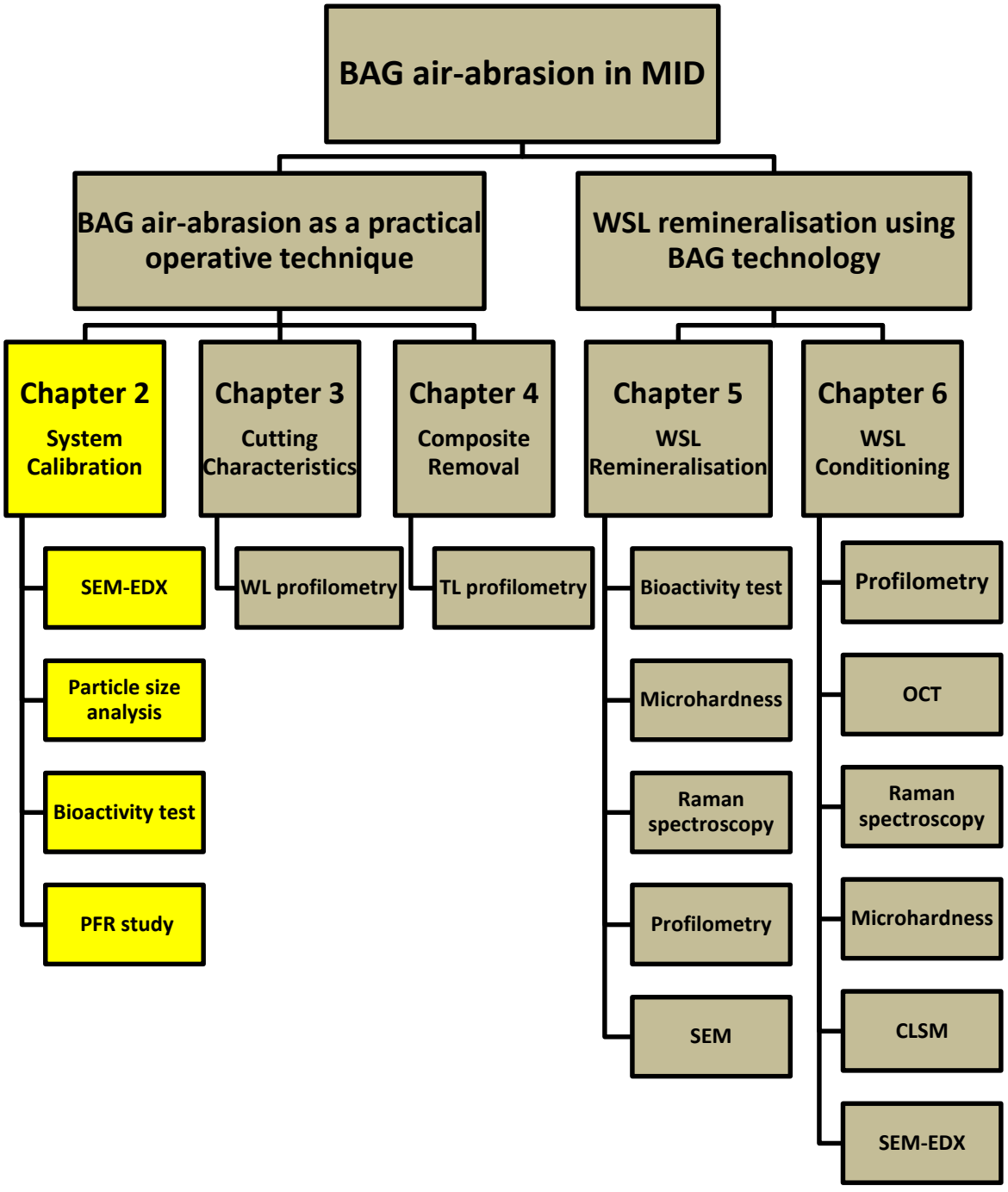

Organisational flowchart of the experiments accomplished in this study.

2.1 Introduction

Air-abrasion is an operative tooth cutting technique whose efficacy is dependent upon several factors including the physical mechanics of the equipment such as air pressure, powder flow rate (PFR) and the powder-air admix mechanism (Jost-Brinkmann, 1998; Cook et al., 2001; Paolinelis et al., 2009), as well as those related to the abrasive powders used including the shape, size and chemistry of the particles (Horiguchi et al., 1997; Motisuki et al., 2006). The results from investigations concerning air-abrasion vary widely which may be in part due to the cutting ability of a particular air-abrasion unit being correlated to the amount of expelled powder which in turn, varies according to the specific unit used (Jost-Brinkmann, 1998; Honda et al., 2008). Indeed, there are a large number of commercial air-abrasion units and each can be used at various settings with different mechanisms used to mix the abrasive particles with the propellant air stream. Therefore, in order to improve the comparability of air-abrasion studies, it is important to establish the factors which have an effect on PFR.

BAG 4SS5 has the potential to enhance remineralisation of dental hard tissues by developing hydroxycarbonate apatite (HCA) structures when it interacts with aqueous solutions (Burwell et al., 2009b; Gjorgievska et al., 2013). The effect of BAG air-abrasion technology on enamel remineralisation has been evaluated later in Chapter 5 and Chapter 6. The BAG abrasive powder used was sourced from an external supplier (Denfotex Ltd, UK). Therefore, the bioactivity of this material was validated prior to experimental further use based on the standard bioactivity test introduced by Warren et al. (1989).

The aims of this study were:

1. To characterise the morphology, the chemistry and the particles size distribution of alumina and BAG abrasive powders.
2. To validate the bioactivity of BAG abrasive powder.
3. To calibrate air-abrasion system by studying the effect of air pressure on the emitted PFR of two dental air-abrasion units.
4. To measure the ranges of PFR (g/min) for alumina and BAG abrasive powders calibrated to PFR instrument settings.

The null hypotheses investigated in this study were that the used BAG air-abrasive powder does not develop HCA structures when soaked in Tris-buffer solution, and that there is no effect of air pressure on the emitted PFR in both an Aquacut™ and Air-Flow Master® air-abrasion units.

2.2 Materials and methods

2.2.1 Abrasive powders' shape and elemental composition

Characterization of the abrasive powders' surface topography and elemental composition were determined using scanning electron microscopy (SEM) (FEI Co. Ltd., Cambridge, UK) coupled to energy dispersive X-ray spectroscopy (EDX) (EDAX Inc., 91 McKee Drive, Mahwah, NJ 07430 USA). The abrasive particles were mounted on alumina stubs using double-sided adhesive tab, and carbon sputter-coated (Emitech K550, UK). The operating parameters used throughout the experiments were an accelerating voltage of 10 kV and a working distance of 10 mm.

2.2.2 Particle size distribution

The particle size analysis was carried out using a CILAS 1180 laser diffraction particle analyser (Cilas, Orleans; France) operating at an 830 nm central wavelength and 7 mW energy power. The measurement was conducted by introducing approximately 200 mg of the tested powder into the tank of the analysing unit. The analysis was conducted in an aqueous medium. The powders were sonicated (frequency 38 KHz for 60 sec) to aid dispersion in the media prior to the analysis. The system was cleaned and a background control reading was taken prior to each actual measurement. The results were analysed using the standard operating parameters by the means of a provided software package (Particle Size Expert, Cilas, Orleans; France). The results were expressed numerically for the median particle size (d_{50}), the 10^{th} percentile particle size (d_{10}) and the 90^{th} percentile size (d_{90}). In addition, a histogram was provided containing the bars of particle size distribution as well as the curve of cumulative percentage.

2.2.3 Bioactivity test of bioactive glass abrasive powder

The bioactivity of BAG abrasive powder was validated by soaking the powder in a Tris-buffer solution then analysing the glass in an FTIR to determine if the HCA layer has been formed (Warren et al., 1989). The Tris-hydroxy methyl amino methane (THAM) buffer solution was prepared as follows:

- THAM powder (30.18 g) was added to 2000ml de-ionised water and stirred until completely dissolved.
- 88.4 ml of 2N HCl was added gradually to the solution with stirring.
- The flask was filled up to 4000 ml with de-ionised water.
- The solution was mixed well and warmed using a water bath to 37^{o}C.
- The pH was measured (Oakton® pH meter, Gresham, OR, USA) and adjusted to 7.25±0.1using 2N HCl.

The tested powder (0.3 g) was soaked in a 200 ml Tris-buffer solution, with continuous stirring (stirring rate: 175 rpm) at 37^{o}C for 20 hours (n=3). At the end of the soaking time, the powder was separated from the solution using a filter paper (Whatman Limited, UK), rinsed with acetone to halt any further surface reaction and air dried for 15 min. Potassium bromide (KBr) pellets were prepared by mixing 0.003 g of the reacted powder with 0.3 g KBr (ratio 1:100) (Saravanapavan et al., 2003). The mixture was compressed using an INSTRON model 5569A mechanical strength machine using a pellet former (Figure 2-1). FTIR spectroscopy (Perkin-Elmer, Beaconsfield, UK) was used to collect the absorbance spectra with a diffuse reflectance accessory in the frequency range of 400-1400 cm^{-1}. The resultant spectra were linearised, smoothed and normalised to peak at ~1070 cm^{-1} in order to compare the relative peak intensities (Cerruti et al., 2005).

Figure 2-1: The pellet former used in this study to produce the KBr pellets.

2.2.4 Powder flow rate study

The nozzle output air pressure of each air-abrasion unit was measured using a digital pressure indicator (DPI 705, Druck, UK) attached to the output nozzle. The internal nozzle diameter was validated using a digital measurement device (Quadra-Check 300). Periodic calibration of both output pressure and the nozzle diameter was conducted throughout all experiments to ensure consistency and standardisation under all experimental conditions.

Comparing the weight of a collecting container, including a layer of sponge and a paper filter, before and after 1 min of active air-abrasion, permitted the study of powder flow rate (PFR) (Figure 2-2). The included sponge layer acted as a pre-filter to gather the powder allowing the air stream to pass preventing a build-up of pressure inside the container. The internal pressure of the container was kept consistent (0.12 psi), and monitored throughout the air-abrasion exposure using a manometer attached to the collecting cylinder since any increase in the container pressure could affect the overall PFR. Both the sponge layer and the paper filter were replaced after 5 exposures to prevent the build-up of the pressure inside the container according to results from an earlier pilot study which investigated this. The weight of the container was recorded, using an electronic scale (Sartorius-Werke GmbH, Gijttingen, Germany).

In order to investigate the effect of air pressure on PFR on both Aquacut™ (Velopex, Harlesden, UK) and Air-Flow Master® (EMS, Nyon, Switzerland) air-abrasion units, the PFR dial was fixed at the middle setting (3) and the air pressure was adjusted into 40, 60 and 80 psi, on both units. Ten measurements were conducted within each experimental group using BAG powder in a dry air-abrasion mode. The powder reservoir was refilled with the abrasive powder to a pre-determined line consistently after three measurements (Banerjee et al., 2008b), and the powder was manually stirred prior to use before each abrasion procedure.

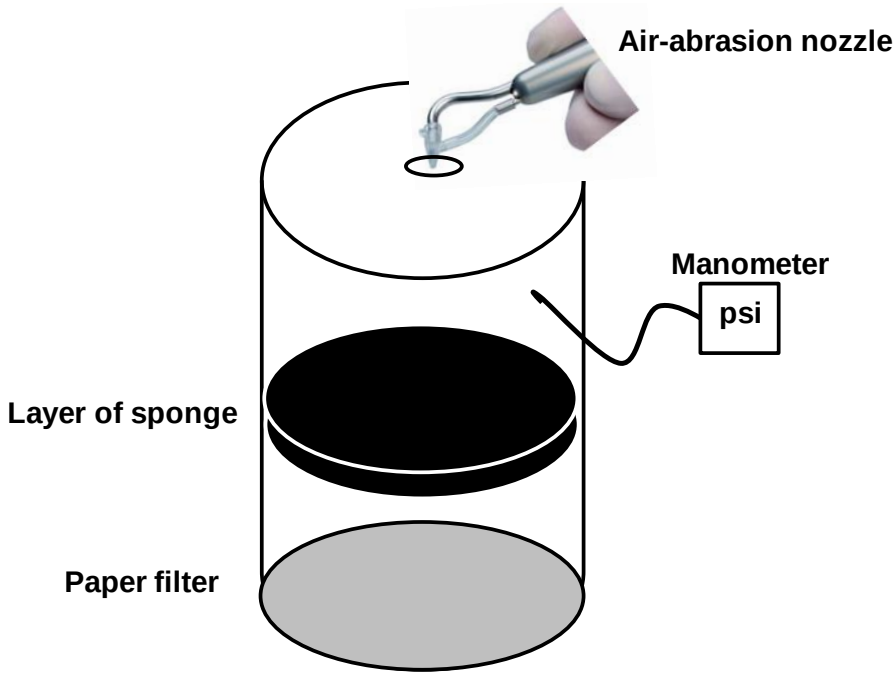

Figure 2-2: A diagram representing the apparatus used to study the PFR.

Since the Aquacut™ air-abrasion unit (Velopex, Harlesden, UK) with a rounded cross sectional nozzle (internal diameter 600 µm) was chosen for cutting efficiency / pattern assessment experiments, the previous method was employed to determine PFR ranges of the PFR dial settings. For the determination, air pressure was fixed at 60 psi and the powder flow rate dial was adjusted to 1, 3 and 5 values representing the minimum, middle and maximum settings respectively. Ten measurements were conducted in each group to calculate the PFR ranges for alumina and BAG powders.

2.2.5 Statistical Analysis

The statistical analysis was conducted using SPSS statistical package (version 19, SPSS Inc/IBM, Chicago, IL). The data was tested for normality using Histogram/Q-Q plots/Shapiro-Wilk tests. Two-way analysis of variance (ANOVA) followed by a Bonferroni post-hoc test evaluated the statistical significance of PFR data (p=0.05).

2.3 Results

2.3.1 Abrasive powders' shape and elemental composition

SEM micrographs showed that the alumina particles had an angular shape, shard-like. BAG 45S5 powder exhibited rounded outline profiles surrounded by a submicron dust but with an irregular surface roughness (Figure 2-3). The chemical compositions of the tested powder were determined as peaks within the EDX spectrum (Figure 2-3).

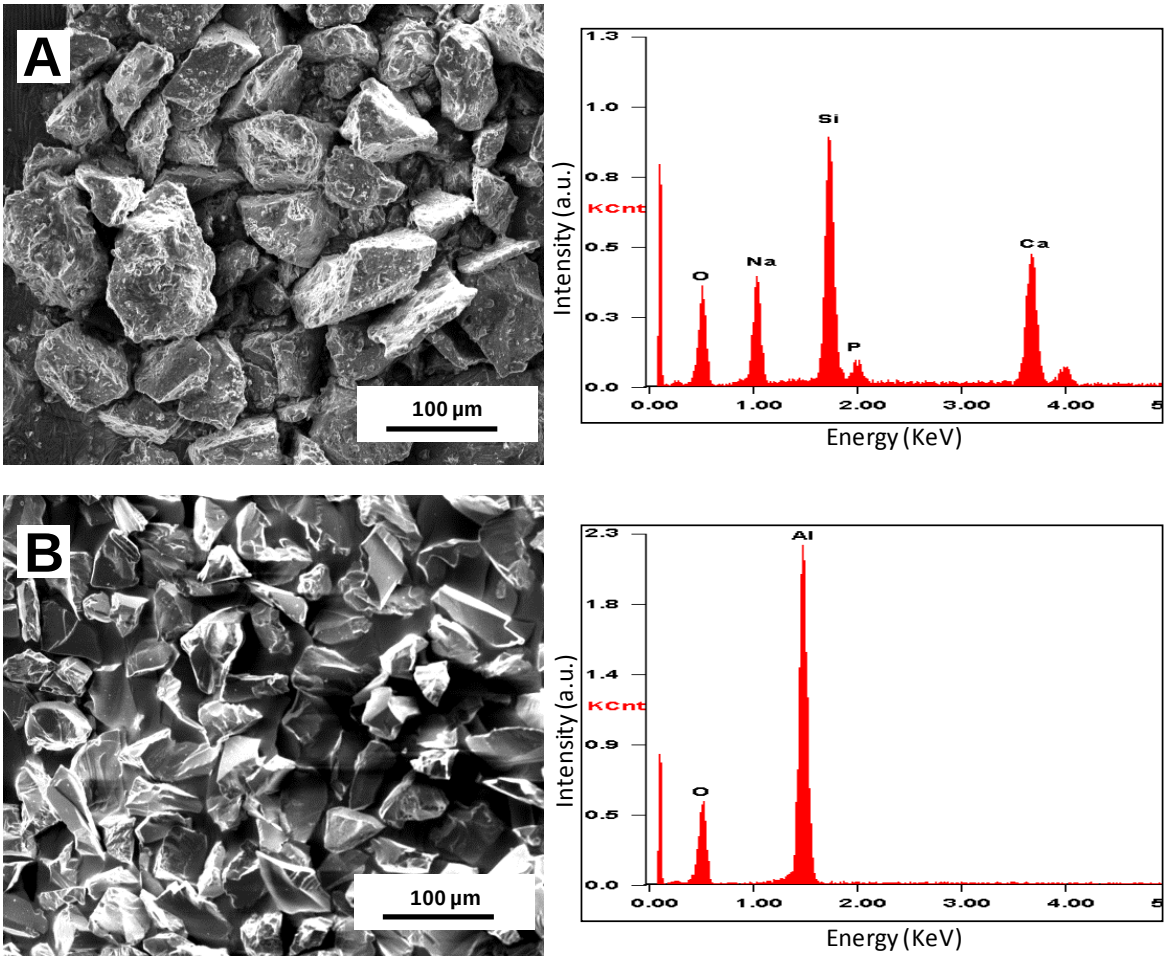

Figure 2-3: SEM-EDX for BAG (1-A) reveals the particles' aspect ratio of 1:1, with rounded outline profile surrounded by a submicron dust. They contained silicon, calcium, phosphorus and sodium oxides. The particles within the alumina powder (1-B) exhibit an angular shape and consist of alumina. (Accelerating voltage: 10 kV, working distance: 10 mm and magnification: 800x).

2.3.2 Particle size distribution

The particle size distribution percentiles (10, 50 and 90 %) of BAG powder and alumina powder are presented in Table 2-1, whilst the histogram of particle size distribution and the cumulative percentage of the data are shown in Figure 2-4 and Figure 2-5. Narrow distribution characterised both tested powders, slightly narrower for alumina. The histograms of the tested powders exhibited a normal distribution.

Table 2-1: Particle size distribution of BAG and alumina abrasive powders as percentile classes:

	d10 (µm)	**d50 (µm)**	**d90 (µm)**
Particle size distribution BAG	29.40	60.26	92.58
Particle size distribution Alumina	16.61	34.69	51.87

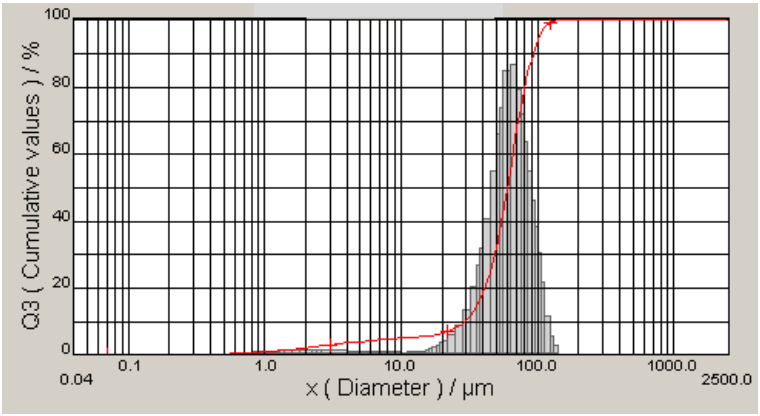

Figure 2-4: The particle size distribution of BAG air-abrasive powder in cumulative percentage (red line) and in frequency percentage (bars).

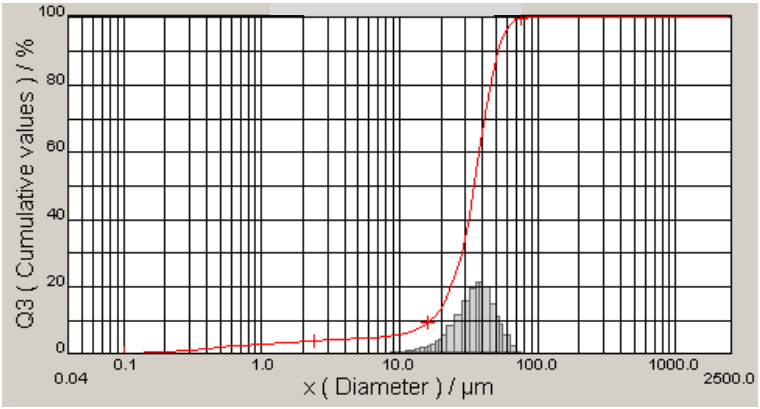

Figure 2-5: The particle size distribution of alumina air-abrasive powder in cumulative percentage (red line) and in frequency percentage (bars).

2.3.3 Bioactivity test of bioactive glass abrasive powder

Representative FTIR spectra of BAG powder before and after soaking in Tris-buffer are presented in Figure 2-6. The spectrum of non-reacted powder (Figure 2-6-A) shows a prominent peak assigned to Si-O-Si stretching mode at 1040 cm^{-1} with a shoulder at 910 cm^{-1} related to the non-bridging oxygen Si-O-NBO (Cerruti et al., 2005; Aina et al., 2009). A notable peak assigned to Si-O-Si bending vibrational mode at 520 cm^{-1} can be also observed (Hench and Wilson, 1993).

Following the powder soaking in Tris-buffer, the frequency (wavenumber) of the Si-O-Si binding peak decreased to be observed at 460 cm^{-1}, and the non-bridging oxygen Si-O-NBO disappeared due to the loss of soluble silica (Figure 2-6-B). A new shoulder appeared at 1220 cm^{-1} associated with the surface component of the Si–O–Si vibration of a newly formed silica phase (Aina et al., 2009). Here, double peaks at 560 and 600 cm^{-1} related to the P-O bending vibrational mode of PO_4^{3-} in crystalline calcium phosphate layer can be observed (Warren et al., 1989; Hench and Wilson, 1993). In addition, the spectrum shows a peak at 1350 cm^{-1} related to the P=O stretching vibrational mode (Peitl Filho et al., 1996).

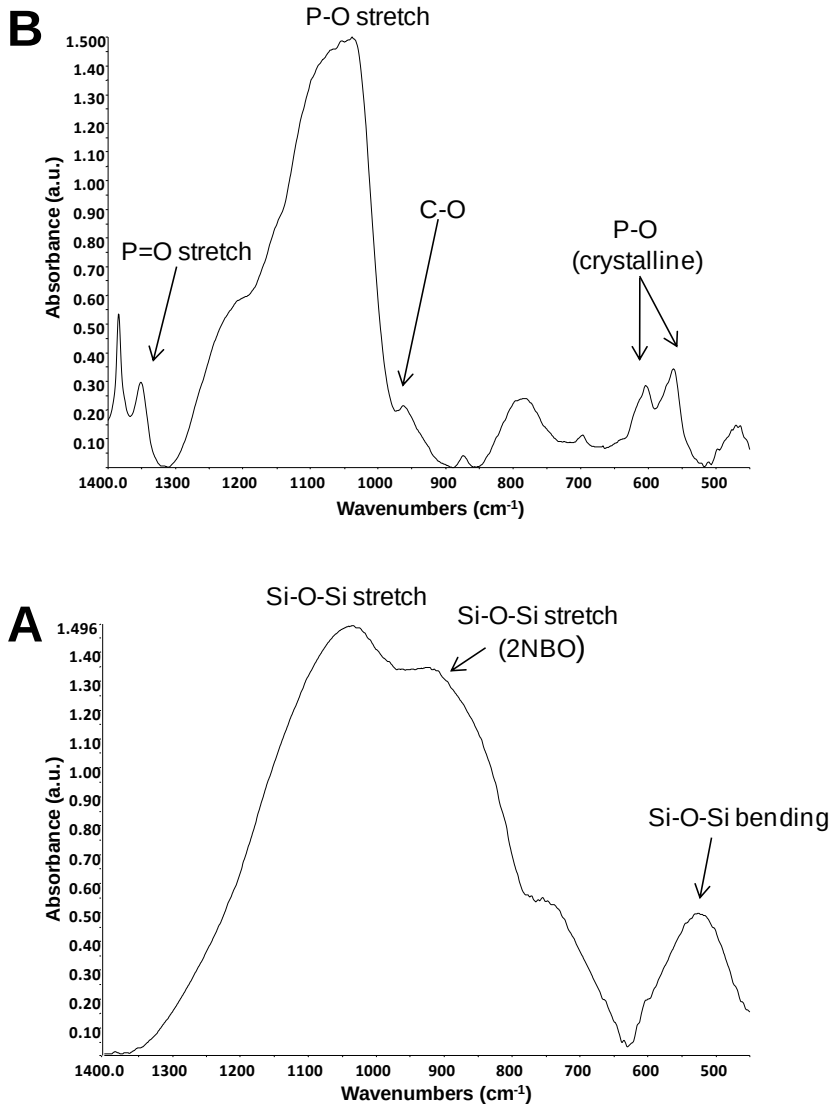

Figure 2-6: FTIR spectra of BAG air-abrasive powder before (A) and after soaking in Tris-buffer solution for 20 hours (B). The baseline spectrum presented prominent peaks assigned to Si-O-Si vibrational modes, whilst the spectrum of reacted powder presents double peaks assigned to the P-O bending vibrations of PO_4^{3-} in crystalline calcium phosphate layer.

2.3.4 Powder flow rate study

The means and their standard errors (g/min) of PFR according to the air pressure are presented in Figure 2-7. There was a statistically significant difference in PFR values between the two air-abrasion units (p<0.05). Air pressure had no effect on the PFR in the Aquacut™ unit which showed constant PFR for all air pressure values (p>0.05). However, in the Air-Flow Master® unit, the PFR at 40 psi (2.6±0.2 mean±SE g/min) and at 60 psi (3±0.1 g/min) were significantly less than that at 80 psi (3.9±0.1 g/min) (p<0.05).

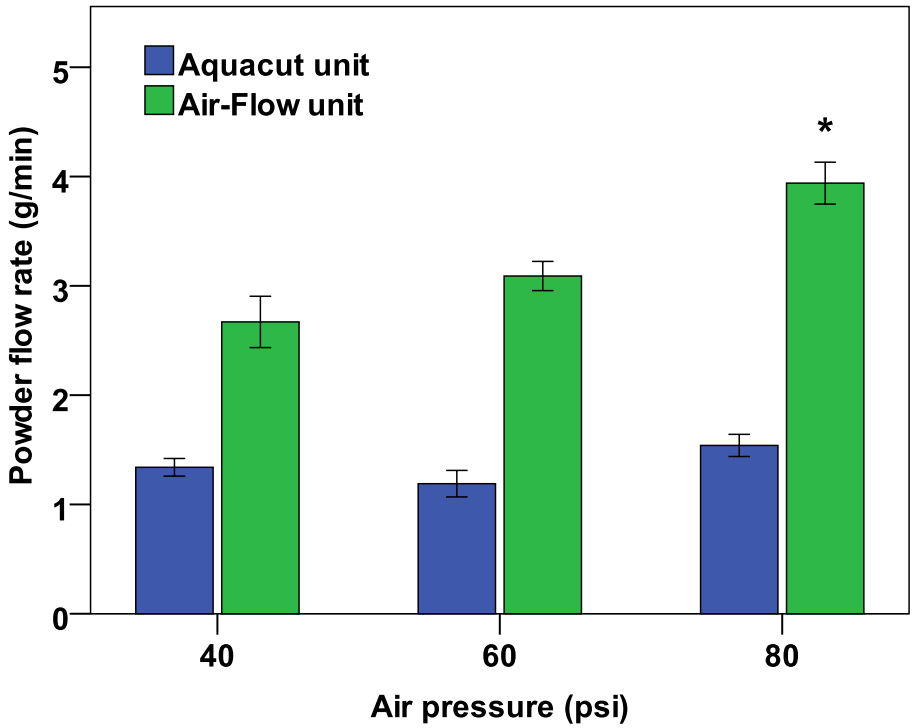

Figure 2-7: Powder flow rate (PFR) mean±SE (g/min) according to the air pressures. (*) indicates statistically significant differences in PFR measurements between air pressure 40/60 and 80 psi in Air-Flow® unit.

PFR ranges for the Aquacut unit settings for both powders are shown in Figure 2-8. There was a statistically significant difference in PFR between alumina and BAG for the same settings ($p<0.05$). The PFR increased significantly when the powder flow rate was adjusted from minimum to maximum value within BAG powder groups ($p<0.05$).

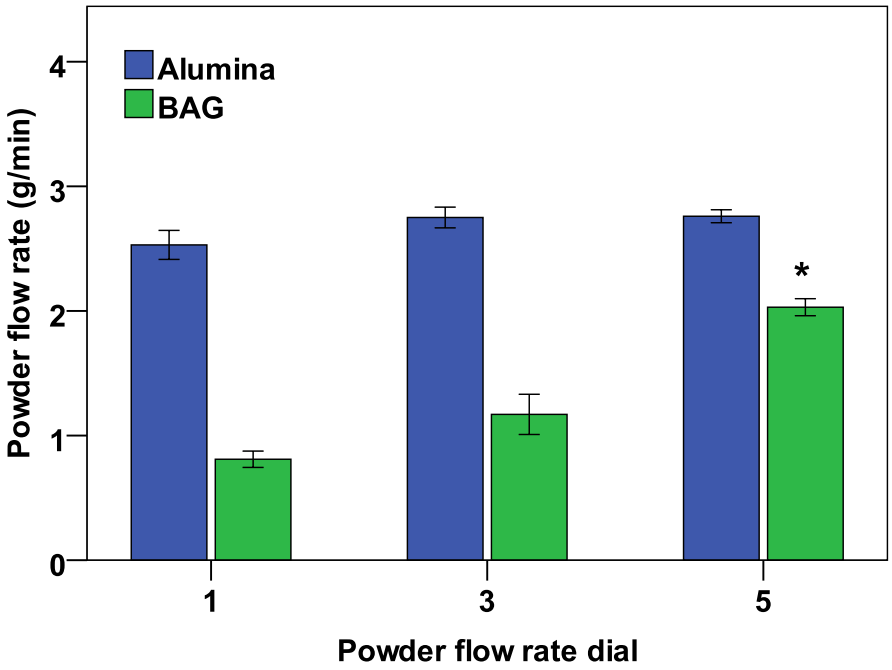

Figure 2-8: PFR mean values ± SE (g/min) for alumina and BAG powders correlated with variable powder flow rate settings (air pressure fixed at 60 psi). (*) indicates statistically significant differences between powder flow rate dial 1 and 5 within the BAG powder group.

2.4 Discussion

BAG particles have rounded outline profiles, while alumina particles have sharper, angular edges so potentially increasing alumina's physical abrasiveness. The EDX observations revealed the chemical composition of the powders, showing that the powders have not been contaminated during the manufacturing and storage conditions. The bioactivity of BAG 45S5 powder has been long established in the literature (Warren et al., 1989). The BAG abrasive powder used was provided by an external supplier. Therefore, it was felt that the bioactivity of this material should be validated prior to any further use since the experiments in this thesis considered both the cutting efficacy as well as the remineralisation effect of the BAG air-abrasion system. In addition, the bioactivity test of BAG particles prepared for use in dental air-abrasion systems has not been reported in the dental literature using the standard protocol introduced by Warren et al. (1989). FTIR spectra shown in Figure 2-6 confirm the bioactivity of BAG abrasive powder by revealing the two characteristic phosphate peaks that correspond to the P-O bending vibrations of PO_4^{3-} in the crystalline calcium phosphate layer formed on the particles surface (Warren et al., 1989). A previous study showed that BAG particles are retained on the dental surface following BAG air-abrasion procedure (Paolinelis et al., 2008). Hence, the ability of BAG

abrasive particles to develop HCA structures similar to that of dental hard tissue may prove an advantage in minimally invasive, reparative dentistry by enhancing the remineralisation potential of dental tissues treated using BAG air-abrasion.

The variety between the alumina and BAG particles with respect to the shape and the size of particles may explain the differences in PFR measurements observed between the two powders. In addition, BAG powder exhibits different bulk density and atmospheric moisture uptake when compared to alumina. The submicron dust surrounding the BAG particles, observed in SEM micrographs, may influence and reduce the flow of the glass powder. Therefore, it is advised that BAG powder should be manually stirred in the reservoir prior to the abrasion procedure to help prevent the formation of agglomerates which will affect the flow rate and therefore, cutting efficiency.

In the majority of air-abrasion units both PFR and air pressure can be controlled using the unit's pre-set dials. Powder flow rate has a significant effect on air-abrasion cutting efficiency and pattern (Jost-Brinkmann, 1998). For this reason, it is preferable to employ a constant PFR during the abrasion procedure. A previous study has shown that the emitted PFR was affected significantly by the amount of the powder in the powder reservoir of air-abrasion system (Banerjee et al., 2008b). This study evaluated the effect of air pressure on the PFR using two clinical air-abrasion units. These units use different mechanisms to admix the abrasive powder with the air propellant stream. The Aquacut™ unit depends upon a vibration mechanism to admix the abrasive particles with the air stream and this explains why a constant PFR was recorded regardless of the air pressure values. However, in the Air-flow Master® unit where an air vortex is created inside the powder chamber, air pressure not only modifies the particles velocity, but also alters the amount of expelled powder from the air-abrasion nozzle. These findings are valuable for researchers and clinical users as the PFR cannot be separately controlled without considering the air pressure settings in some air-abrasion systems.

Powder flow rate measurement in air-abrasion systems demands the use of specialist equipment such as an electrostatic mass flow meter and heat transfer mass flow meter (Yan, 1996; Huang et al., 2002). The technique used in this study based on a simple, reproducible method to study the PFR ranges for the parameters tested. Powder flow rate measurement (g/min) for the powder flow dial values makes the results obtained using a specific air-abrasion unit comparable and reproducible using different air-abrasion units when the PFR is equilibrated to the same ranges.

2.5 Conclusions

The two null hypotheses were rejected. BAG abrasive powder formed an HCA layer when immersed in a simple Tris-buffer solution. Using air-abrasion should be preceded by system calibration to identify the factors affecting the abrasive powder propulsion as they differ according to each unit's design. Vibration admix units exhibited a constant powder flow rate regardless of air pressure. However, it is advisable to check the BAG powder condition within the powder chamber before the abrasion procedures to obtain a consistent powder flow rate. Manufacturers need to take note and provide this information clearly to clinicians. This information should include the powder-air stream admix mechanism, the relationship between the set air pressure and the PFR, the ranges of PFR in g/min and the optimal volume of the powder in the reservoir. Those can help in understanding the factors that control the cutting efficiency promoting the ultra-conservative applications of air-abrasion technology in minimally invasive dentistry (MID).

Chapter 3 In-vitro effect of air-abrasion operating parameters on the dynamic cutting characteristics of alumina and bioactive glass powders.

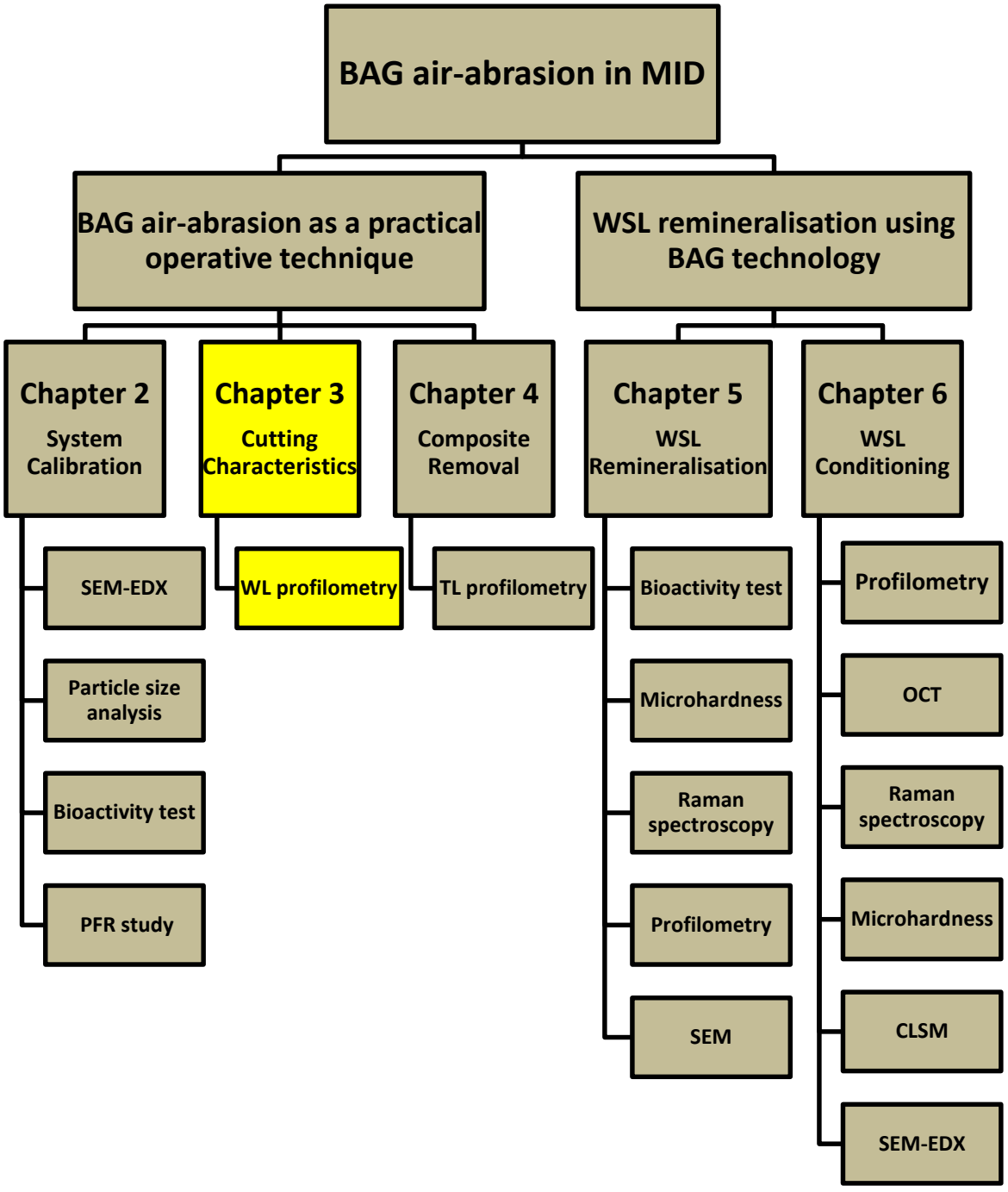

Organisational flowchart of the experiments accomplished in this study.

3.1 Introduction

Minimally invasive dentistry (MID) encourages the maintenance of as much repairable tooth tissue as possible and relying on adhesion techniques to achieve the retention and seal of the overlying restorative materials (Mount, 2007). Air-abrasion cuts tooth tissue employing the use of kinetic energy to blast away surface hard tissues (Black, 1950). Using this technology in MID has the potential to remove irreparable carious dental tissues selectively and consequently enhances the preservation of healthy tooth tissues during cavity preparation (Banerjee and Watson, 2002; Murdoch-Kinch and McLean, 2003). Air-abrasion is a sensitive technique dependent upon parameters different from those of conventional rotary cutting (see Figure 1-1; p: 30). Therefore, it is essential to understand and control the system's inter-related operating parameters for the optimal use of this technology in minimally invasive restorative dentistry.

Using alumina abrasive powder can lead to undesirable clinical over-preparation of dental hard tissues (Horiguchi et al., 1997; Motisuki et al., 2006). Alternatively, BAG 45S5 powder has been introduced for this purpose to benefit from its antibacterial and remineralisation properties and its potential to remove selectively more softened diseased or damaged tooth structure (Paolinelis et al., 2008). Previous studies showed that using BAG 45S5 as an abrasive powder exhibited more conservative cutting characteristics compared to that of alumina, but still removed some healthy dental tissue (Banerjee et al., 2008a; Banerjee et al., 2011b).

Air-abrasion cutting characteristics can be altered by using different abrasive powders since the particles' kinetic energy varies according to the shape, size, hardness and density of the abrasive powder (Bailey and Phillips, 1950; Laurell and Hess, 1995; Horiguchi et al., 1997). In the literature, there are no investigations assessing the effect of different air-abrasion parameters on the cutting efficiency / pattern when BAG 45S5 powder is employed as an abrasive powder. The present study evaluated the effect of operating parameters on BAG air-abrasion cutting efficiency / pattern for its development as a minimally invasive operative technique. This in-vitro evaluation was conducted using an enamel analogue, Macor™ to avoid the inclusion of confounding experimental variables including the variation found in the hardness of human enamel samples. This

evaluation was conducted under simulated clinical conditions fulfilled by establishing a controlled movement between the air-abrasion nozzle and the substrate. The dynamic cutting mimics more realistically the clinical situation whereby clinicians move the nozzle over the targeted substrate in a continuous sweeping motion. Non-contact white light profilometry was used in this study to measure the volume of Macor™ removed.

The aim of this study was to evaluate the effect of six operating parameters: air pressure, powder flow rate (PFR), nozzle-substrate distance, nozzle angle, shrouding the air stream with a curtain of water and the abrasive powder itself, on the cutting efficiency / pattern of air-abrasion.

The null hypotheses investigated in this study were:

1. Altering the operating parameters of air-abrasion system has no effect on the cutting efficiency / pattern.
2. Alumina and bioactive glass (BAG) abrasive powders exhibit the same cutting efficiency when used under standardised simulated clinical conditions.

3.2 Materials and methods

3.2.1 Air-abrasion dynamic cutting

An Aquacut™ air-abrasion unit (Velopex, Harlesden, UK) with a rounded nozzle (internal diameter 600 µm) was used throughout this study. The powder reservoir was refilled to a pre-determined line consistently at the beginning of each experiment, and the nozzle was fixed using a micro-positioning device allowing the control of nozzle-substrate distance and angle according to the conditions of each experimental group. Periodic calibration of both output pressure and the nozzle diameter was conducted before each experimental session as explained in Section 2.2.4; p: 78. The dynamic cutting was performed in a plastic chamber attached to a high vacuum suction. A Macor™ sheet (Macor™, Corning, USA), 50 x 50 x 5 mm, was located on the stage attached to a moving coil actuator (SMAC, Crowley, UK). This actuator employs an attractive or repulsive magnetic force for its movement, whereby the position, range and speed of the produced linear movement are programmable. For this investigation, the SMAC was programmed for 10 mm linear movement at a velocity of 0.5 mm/sec, chosen as

this velocity was considered relatively similar to that applied by practitioners when the system is used for clinical enamel preparation.

The six air-abrasion operating parameters evaluated in this study are addressed in Table 3-1. When each variable was tested, the remaining parameters were fixed as follows: air pressure 60 psi, PFR dial: middle value (3), nozzle angle: 90 degrees and nozzle distance: 2 mm. Twenty experimental groups were evaluated by preparing ten troughs in the flat Macor™ substrate block within each group (n=10). Evaluation of the effect of the operating parameters was conducted in dry air-abrasion mode. However, to evaluate the influence on the cutting efficiency by shrouding the air-powder stream with a water curtain, a disposable plastic tip, used to mix the air stream with water, was attached to the tip of the nozzle.

Table 3-1: The operating parameters evaluated in this study with the tested values:

Operating parameters	**Parameter value tested**
Air pressure (psi)	20, 40 and 60
Powder flow rate (PFR) dial	Minimum (1), middle (3) and maximum (5)
Nozzle angle (degrees)	45 and 90
Nozzle distance (mm)	1, 2 and 5
Cutting mode	Dry and wet
Abrasive powder	- BAG: (29, 60 and 92 µm- particle size distribution) - Alumina: (16, 34 and 51 µm- particle size distribution)

3.2.2 Macor™ volume removal measurement

Using proprietary measurement control software (STAGES™, TaiCaan Technologies Ltd., Southampton, England), a standard scan area of 5x2 mm was chosen over the central region of each trough. This area included the prepared trough in the centre surrounded by intact Macor™ on each side, acting as a reference area for volume measurement. Non-contact white light confocal profilometry (Xyris™ 4000 WL, TaiCaan™ Technologies Ltd., Southampton, UK) was used to image the surface topography of the resulting 200 experimental troughs. The white light sensor has a 10 nm vertical resolution, a spot size of 7 µm and a gauge range of 350 µm. The scan was performed with a 10 µm step-over distance.

The resulting 3D topographic data-sets were analysed using MountainsMap® surface analysis software (Version 6.2.6332, SARL Digital Surf, Besançon, France) to obtain the volume of the troughs (mm^3). A MountainsMap® macro was written to read and analyse the 3D data automatically using the "measure volume of a hole" function provided by the analysis software. This identifies and delineates the abraded area and calculates the volume (mm^3) of included data points between the bottom of the abraded surface and all the points outside of the delimited abraded area which are used as a least squares reference plane (Figure 3-1). The entire trough was selected by placing four markers at the corner of the trough. This method is used when the outside area is sufficiently flat to be considered as the top of the hole by extrapolation, such as the flat Macor™ surface used in this study.

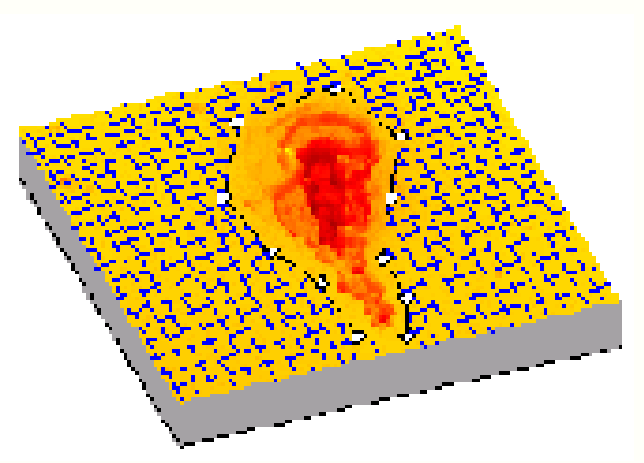

Figure 3-1: Schematic of the "measure volume of a hole" function in Mountains® surface analysis software used to measure the volume of abrasion troughs. The hole in the centre surrounded by the least squares plane acting as a reference level [adapted from the analysis software provided instructions]

Air-abrasion cutting efficiency was established by comparing the volume removed with the assumption that the settings were more efficient when air-abrasion removed a greater volume of Macor™. Representative 3D selected images from BAG air-abrasion groups were examined to characterise the cutting pattern.

3.2.3 Statistical analysis

The statistical analysis was conducted using SPSS statistical package (Version 19, SPSS Inc/IBM, Chicago, IL). Data were tested for normality using Histogram/Q-Q plots/Shapiro-Wilk tests. Repeated measures analysis of variance (ANOVA) and Bonferroni post-hoc tests were performed to analyse the cutting efficiency assessment data (p=0.05).

3.3 Results

An increase in air pressure resulted in an increase in Macor™ volume removal using BAG and alumina abrasive powders. In the alumina groups, the increase was not different statistically between the 40 and 60 psi values (p>0.05), while it was within BAG groups which showed statistical differences for all air pressures tested (p<0.05). The volume of material removed when the air pressure was fixed at 20 psi was 0.75±0.05 mm³ (mean±SE mm³) in the alumina group whereas a significantly less material was removed in BAG group 0.3±0.01 mm³ (p<0.05). However, the difference in the Macor™ volume removed between the two powders was not significant; 1.39±0.1 mm³ in the alumina group and 0.97±0.01 mm³ in the BAG group, when the overall air pressure was increased to 60 psi.

Analysis of box-and-whisker plots of the Macor™ volume removed according to the air pressure indicated that the BAG powder experimental groups exhibited a narrower range (whiskers) compared to those of the alumina powder groups (Figure 3-2), indicating that results obtained with BAG powder were more consistent than those of alumina. Concerning the troughs' cross-sectional outline shape, air pressure variations altered the trough depth, whereas the trough width was not affected (Figure 3-3).

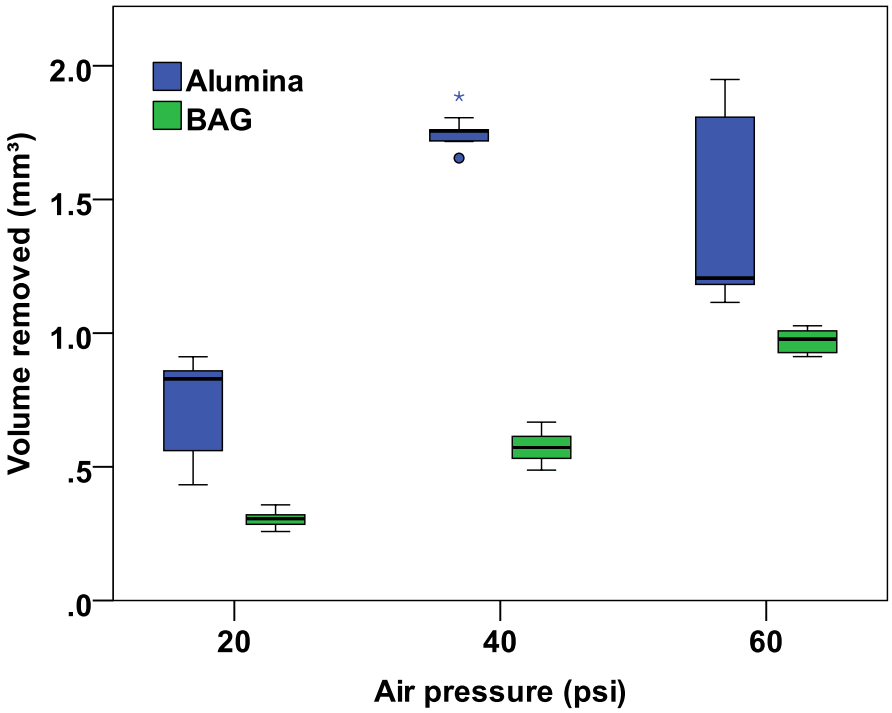

Figure 3-2: Box-and-whiskers plots showing Macor™ volume removed according to the air pressure for both powders (The star and the circle marks represent outlying values). BAG powder experimental groups exhibited a narrower range (whiskers) compared to those of the alumina powder groups.

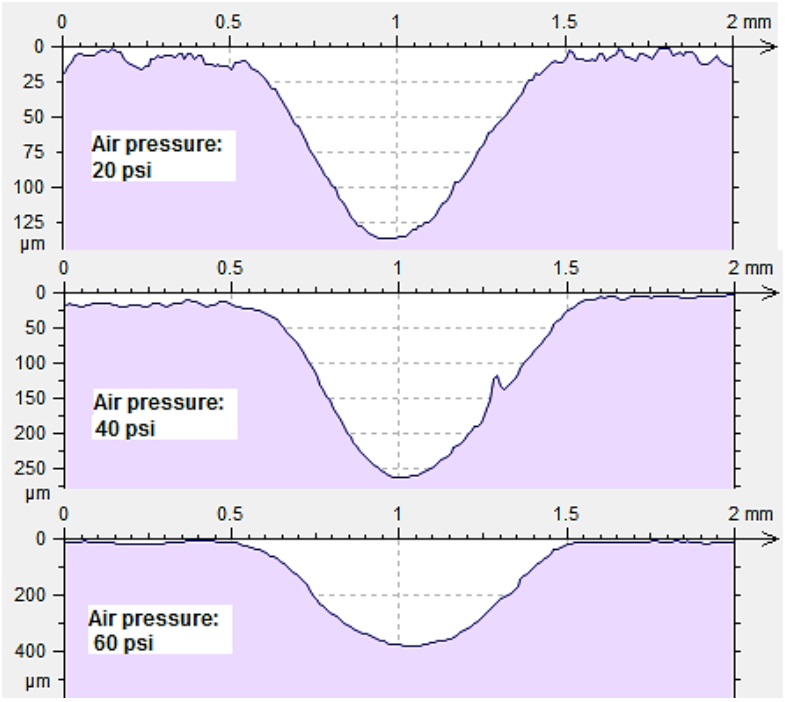

Figure 3-3: Trough's cross-sectional outline shape according to air pressure values within BAG air-abrasion. Air pressure variations altered the trough depth, while the trough width was not affected.

Adjusting the powder flow rate dial from a low (1) to high (5) value increased the cutting efficiency significantly within alumina and BAG powders (p<0.05). However, this increase was more pronounced in alumina powder groups as the volume of material removed increased from 1.64±0.04 mm³ to 2.94±0.03 mm³ (mean±SE mm³), while in BAG powder groups the increase was from 1.45±0.1 mm³ to 1.94±0.05 mm³ (Figure 3-4). Setting the PFR to the lowest value caused more pronounced fluctuation in the base of the trough along its length (Figure 3-5).

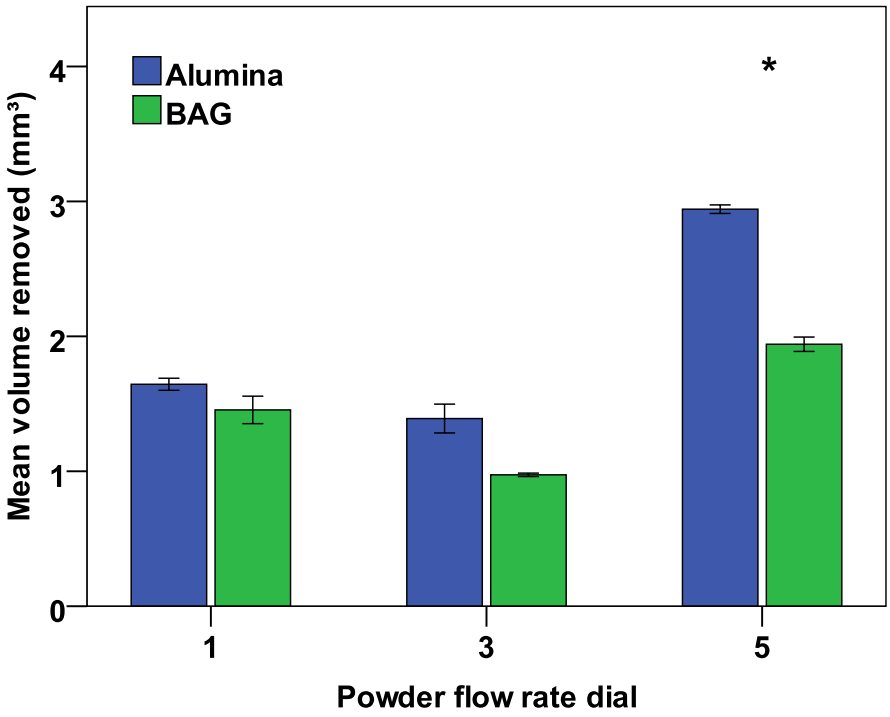

Figure 3-4: Macor™ volume removed mean±SE for alumina and BAG groups according to powder flow rate dial settings. (*) indicates statistically significant difference between powder flow rate dial 1/3 and 5 in alumina and BAG groups.

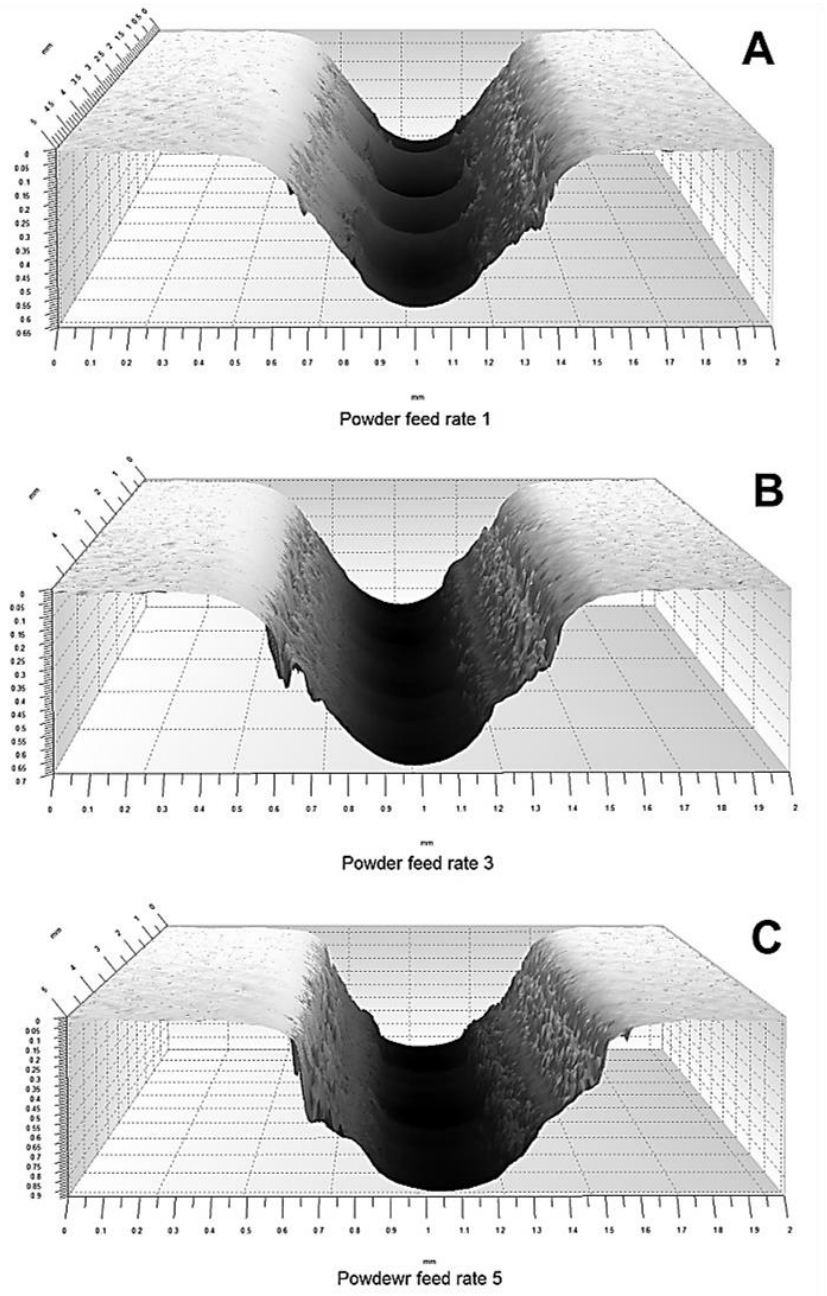

Figure 3-5: 3D views of selected, representative BAG air-abrasion troughs showing the fluctuation in the base of the trough when powder flow rate dial was set at 1 (A).

The means and their standard errors of Macor^{TM} volume removed according to the nozzle-substrate distance are presented in Figure 3-6. Cutting efficiency in BAG powder groups was affected statistically by all nozzle distances included in this experiment (p<0.05), whereas it was only increased when the distance was increased from 1 mm or 2 mm to 5 mm within the alumina powder groups (p<0.05). The nozzle distance of 5 mm produced more rounded trough margins compared to those produced with shorter distances (Figure 3-7).

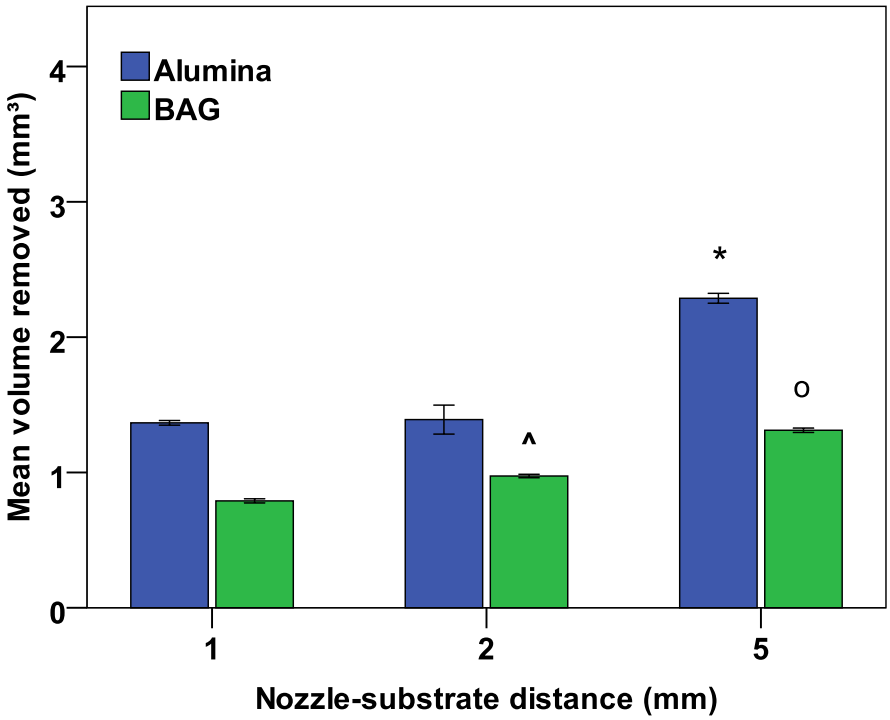

Figure 3-6: Macor™ volume removed mean±SE for alumina and BAG groups according to the nozzle-substrate distance. (*) statistically significant difference between distance 1/2 and 5 mm in alumina groups, (^) statistically significant difference between distance 1 and 2 mm in BAG groups, (°) statistically significant difference between distance 1/2 and 5 mm in BAG groups.

Significantly more Macor™ was removed when the air-abrasion nozzle was fixed at 45 degrees (2.52±0.04, 1.76±0.02 mm³ within alumina and BAG respectively) (mean±SE mm³) rather than 90 degrees (1.39±0.1, 0.97±0.01 mm³ within alumina and BAG respectively) (p<0.05). The shape of the troughs varied according to the nozzle angle; 45 degrees produced a trough with “V” cross-section, while 90 degrees presented troughs with a “U”-shaped cross-section (Figure 3-8).

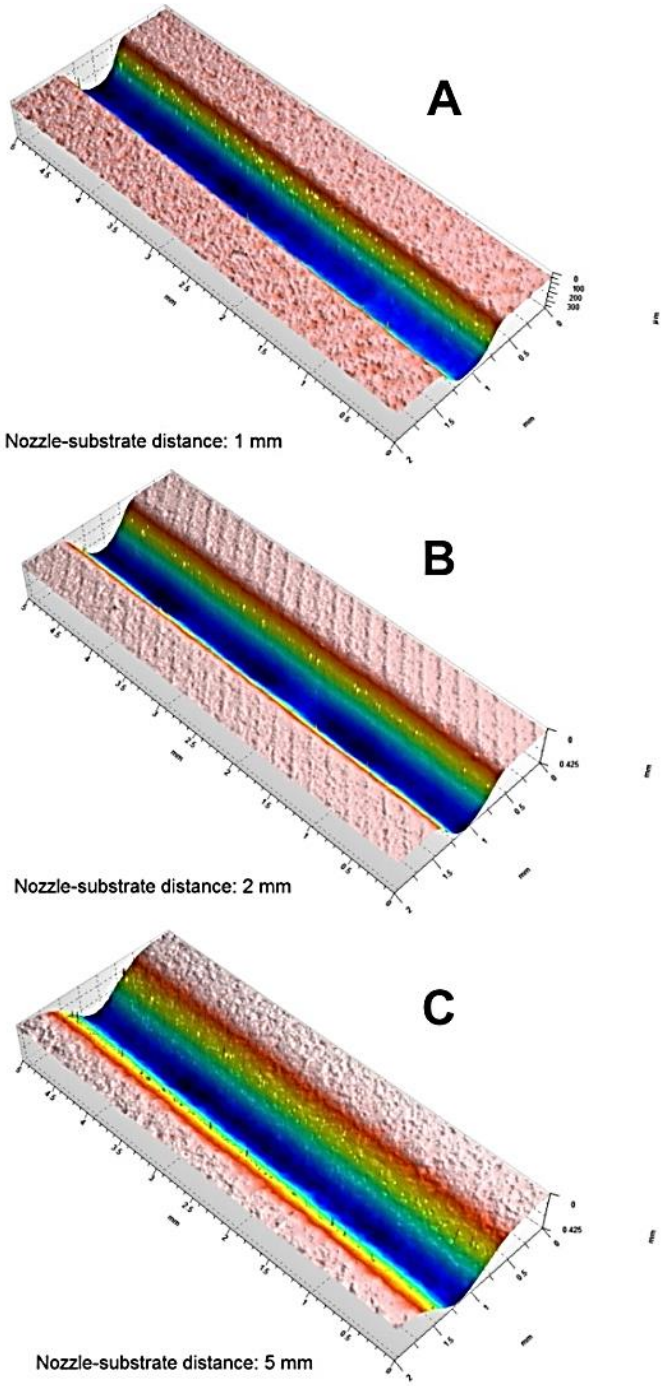

Figure 3-7: Trough margin variation according to the nozzle-substrate distance within BAG powder group (A: 1 mm, B: 2 mm, C: 5 mm). Nozzle-substrate distance of 5 mm results in a rounded, less well defined trough margin.

There was no significant difference in the cutting efficiency between dry and wet air abrasion systems for both powders. In alumina groups, dry air-abrasion removed 3.36±0.17 mm^3 (mean±SE mm^3) and wet air-abrasion removed 3.49±0.48 mm^3. The Macor™ volume removed in the BAG groups was 1.84±0.34 mm^3 and 1.93±0.61 mm^3 in dry and wet abrasion respectively, indicating that the water shroud inclusion had no statistically or clinically significant effect on the cutting efficiency of either abrasive powder.

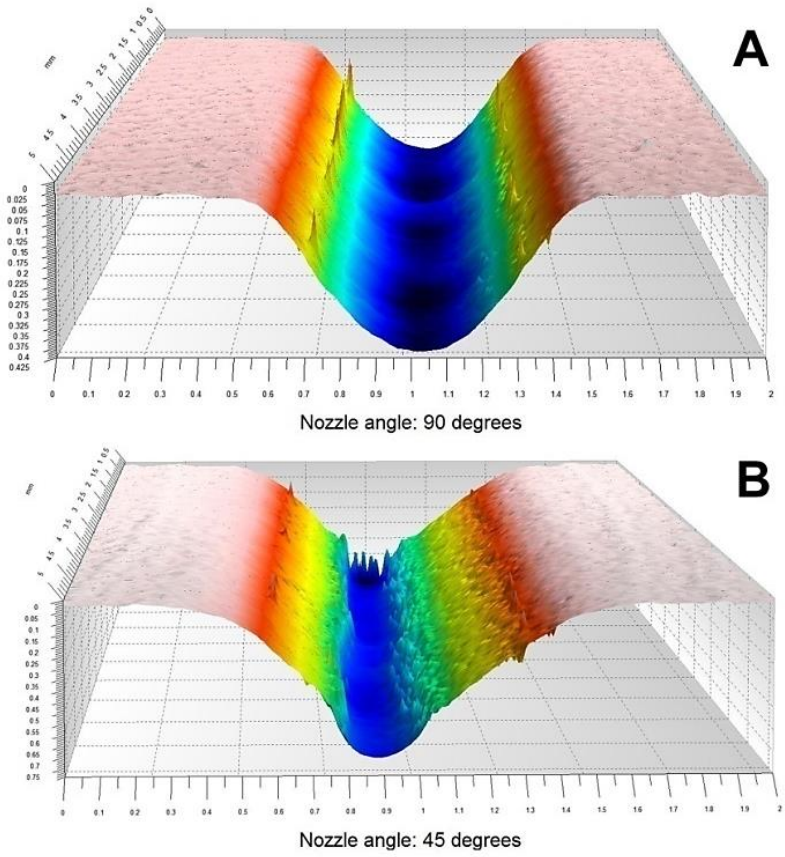

Figure 3-8: Representative scans revealed the cross-sectional trough shape differences between the 45 degrees nozzle angle (B) (trough with “V” cross-section) and 90 degrees nozzle angle (A) (trough with “U” cross-section) within BAG powder groups.

3.4 Discussion

Macor™ was used as the substrate in this in-vitro study for assessing the cutting rate and efficiency due to its consistent, uniform hardness which is not found in human enamel as natural enamel hardness varies from person to person according to the individual’s food consumption and is depth-dependent within the same tooth due to histological heterogeneity (Meredith et al., 1996; Maupomé et al., 1998; Wongkhantee et al., 2006; Cristofaro et al., 2013; Bae et al., 2014). It has been reported that Macor™ exhibits similar mechanical properties to those of enamel and behaves similarly during its cutting (Table 1-6; p: 42). Using Macor™ sheets also provided a reliable, flat surface as a target substrate for air-abrasion cutting and subsequent objective analysis using optical surface profilometry, a “gold standard” method in assessing the substrate surface loss. The maximum sensitivity and accuracy of the non-contact profilometry can only be achieved using flattened samples (Schlueter et al., 2011). In the present study, the nozzle-angle was fixed at 90 degrees when other operating parameters were

evaluated as this setting is achievable reliably in clinical practice, and the nozzle-substrate distance was set at 2 mm since the abrasive particles remain parallel and the scattering is minimal through this distance (Myers, 1954). Assessing the dynamic cutting efficiency has the advantage over static cutting as it mimics more realistically the clinical situation where the procedure is accomplished by moving the nozzle over the target substrate.

The results of this study suggest that there was an increase in the air-abrasion cutting efficiency for both powders when air pressure was increased. Since the increase in air pressure does not increase the PFR in this unit, calibrated in Section 2.3.4; p: 83, this finding may be explained as being dependent upon the increased kinetic energy of the particles whereby the particle velocity has increased due to the increase in propellant pressure, thus making them more destructive to the substrate, concurring with previous investigations (White and Eakle, 2000).

The finding concerning the effect of PFR on the cutting efficiency is inconsistent with a previous study which claimed that an increase in PFR without a concomitant increase in the air pressure is pointless (Cook et al., 2001). In the present study, employing both a dynamic cutting protocol and high vacuum suction reduced the surface choking of particles when excessive quantities of abrasive were applied. The undulating troughs resulting from using less powder may be caused by the irregular distribution of particles within the air stream. Most of the particles might be concentrated into a small portion of the stream's cross sectional area (Yan, 1996).

An inverse relationship between the distance and the cutting efficiency has been reported previously (Bailey and Phillips, 1950; Peruchi et al., 2002). When the nozzle-substrate distance was increased in the present study, the cutting efficiency improved significantly. The previous investigations' findings were based on measuring the cross-sectional aspects of the cut surfaces to assess the cutting efficiency, whereas in this experiment the whole volume removed from the trough was calculated from the 3D measurements, a more accurate assessment of air-abrasion cutting efficiency due to two factors. Firstly, air-abrasion removes material unevenly. Secondly, when the working distance is increased, the trough

width increases more than its depth (Figure 3-7; p: 98) and this can cause misleading cutting efficiency assessment when the depth measurement is employed as in such cases, the data obtained using surface profile line measurements are not similar to that gained when the volume is calculated using a 3D profilometer. The coning angle of the air stream at 5 mm is approximately 13 degrees (Black, 1950), and this would explain why more rounded trough margins were obtained at this distance.

When the nozzle was fixed at 45 degrees, the percentage of the air stream's peripheral portion, which presents a reduced concentration of particles with reduced velocity (Laurell and Hess, 1995), increased and that in turn, produced cross-sectional "V" shape troughs. The air-abrasion operating parameters controlling the nozzle position, affected significantly the cutting efficiency observed in both powder groups. This can be explained by the fact that increasing the distance and fixing the nozzle at 45 degrees reduced the surface choking of particles which is assumed to disturb negatively the propellant stream.

In order to reduce the abrasive particle scattering during air-abrasion, a technique of shrouding the powder stream with a curtain of water has been introduced in some air-abrasion units. This modification also helps in preventing the dehydration of treated tissues (Banerjee et al., 2011b). The current study showed that shrouding the powder stream with a curtain of water had no effect on air-abrasion cutting efficiency for both powders as the wet and dry air-abrasion groups resulted in similar data sets. This might be related to the fact that water is not involved in the powder / air admix mechanism and is only added thereafter.

One of the objectives in this study was to determine the difference in cutting efficiency between alumina and BAG powders. It is noticeable that alumina powder was more aggressive than BAG powder in all settings examined in this study. The abrasive particles in both powders exhibit different hardness (aluminium oxide: 2100 VHN, BAG: 458 VHN), sizes and shapes (see Sections 2.3.1; p: 80 and 2.3.2; p: 81). These factors contribute considerably to the cutting efficiency in an air-abrasion system (Horiguchi et al., 1997; Motisuki et al., 2006). BAG powder groups were more sensitive to slight differences in the operating parameters, whilst alumina powder groups demanded considerable

alterations in the parameters to exhibit statistically differences in cutting rate. It is important to be aware that when air pressure was applied at a low value (20 psi), the difference in air-abrasion cutting efficiency between the two powders more than doubled implying that at low air pressure settings, the cutting efficiency of air-abrasion depends mainly on the nature of the abrasive powder rather than on the physics of air-abrasion unit itself. This could be a useful finding for researchers when they test the cutting efficiency of different abrasive powders.

3.5 Conclusions

The two null hypotheses investigated were rejected. The results of this study permit the following conclusions:

1. All operating parameters involved in this study, except shrouding the powder stream with a curtain of water affected significantly the cutting efficiency of air-abrasion as well as its cutting pattern.
2. Alumina and BAG abrasive powders revealed statistically different cutting efficiencies.
3. Air-abrasion cutting efficiency is more conservative and controllable when BAG powder is used as an abrasive powder, encouraging its role in minimally invasive operative dentistry.

In order to use air-abrasion efficiently, the operating parameters have to be controlled precisely. Both dentists and researchers are advised to set the air pressure to low values and consider the effect of the operating parameters on cutting efficiency and pattern in order to benefit from the conservative characteristics of BAG air-abrasion in minimally invasive dentistry (MID).

Chapter 4 An in-vitro evaluation of the effect of operating parameters on selective resin composite removal using bioactive glass air-abrasion.

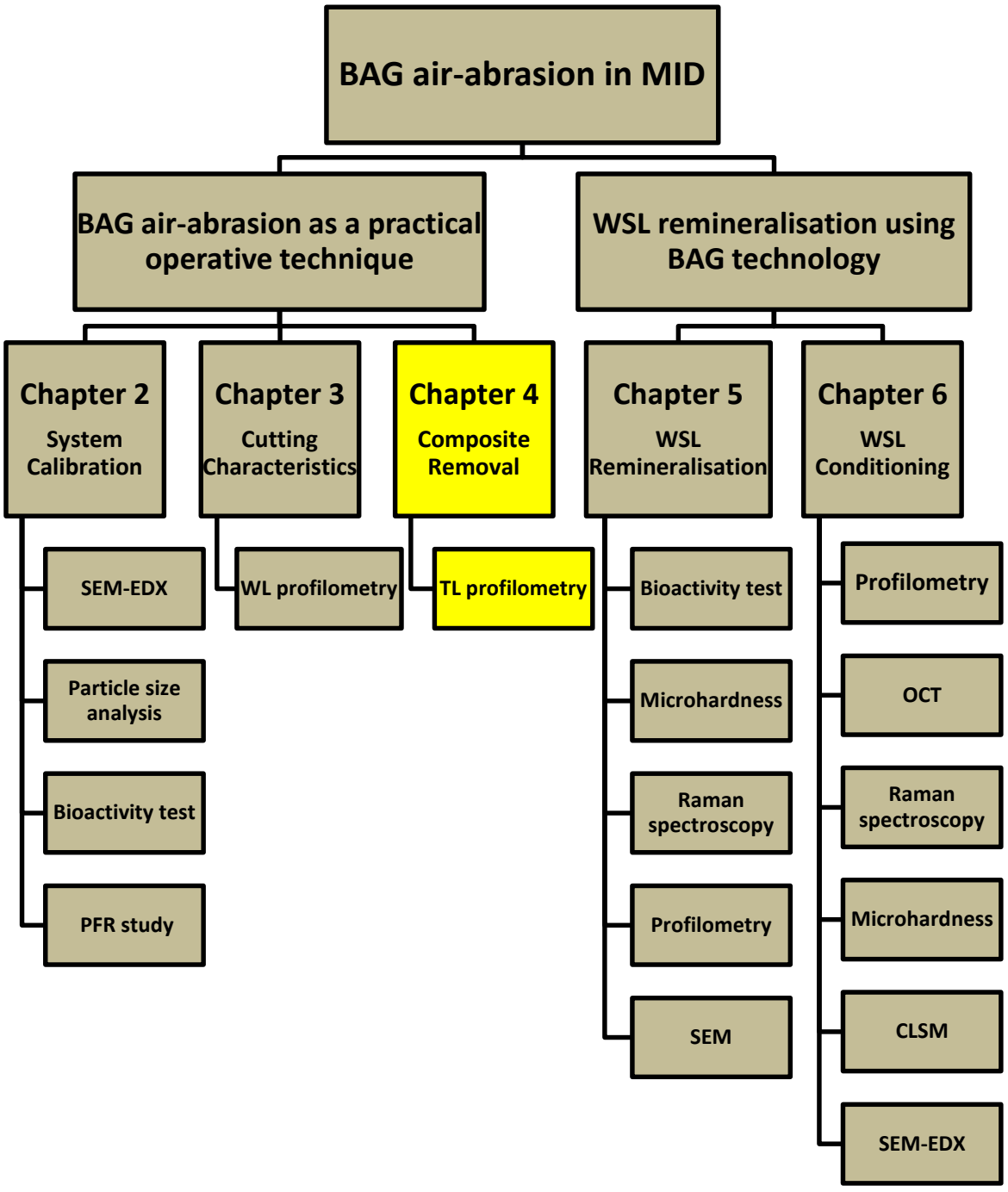

Organisational flowchart of the experiments accomplished in this study.

4.1 Introduction

Using rotary instruments to remove or repair aesthetically and biologically unsatisfactory resin composite restorations or resin luting cement remnants on tooth surfaces after de-bonding fixed orthodontic appliance brackets, can alter tooth surface topography resulting in enamel cracks, scarring and scratches (Eliades et al., 2004; Ozer et al., 2010; Pont et al., 2010; Bonetti et al., 2011). These aspects are incompatible with the tooth preserving minimally intervention (MI) dentistry philosophy which aims to preserve the quality and quantity of healthy dental tissues wherever possible (Ericson, 2003). Air-abrasion tooth cutting technology may be a useful alternative, employing the abrasive particulate kinetic energy to produce rounded cavity margins, ideal internal line angle contours and a surface finish optimised for the adhesion of contemporary dental materials (Myers, 1954; Banerjee and Watson, 2002; Kim et al., 2007). The observation of alumina air-abrasion cutting by means of real-time confocal imaging revealed that air-abrasion cutting of resin composite restorations was not suspended at the restoration / enamel interface (Cook et al., 2001). Consequently, this removed similar or greater amounts of enamel to that removed using a bur (Kim et al., 2007; Khosravanifard et al., 2011).

BAG air-abrasion has the potential to remove resin composite more selectively than conventional alumina air-abrasion. This has been concluded in-vitro when removing orthodontic adhesive cement remnants (Banerjee et al., 2008a). In the light of the results of Chapter 3 evaluating BAG air-abrasion cutting efficiency / patterns, it would seem logical to expect that altering air-abrasion operating parameters may affect its capacity to remove selectively resin composite and consequently preserve more intact enamel. Since there is no previous investigation published in the literature testing this hypothesis, the objectives of this study were to assess: (a) the effect of three clinically adjustable air-abrasion operating parameters, air pressure, powder flow rate (PFR) and the abrasive powder itself on the selective removal of resin composite and (b) the required clinical time taken to carry out the procedures. The selective removal measurement was accomplished by comparing the volume of standardised cavities created within an enamel analogue (Macor^{TM}) permitting an experimental standardisation of hardness and thermal properties, both similar to those of human dental enamel.

The three null hypotheses investigated in this study were:

1. Using BAG as an alternative to conventional alumina powder exhibits no difference in resin composite removal selectivity.
2. There is no effect of air pressure and PFR setting on resin composite removal selectivity within both abrasive powder groups.
3. The required clinical time taken is no different between alumina and BAG powders.

4.2 Materials and methods

4.2.1 Sample preparation

Ninety rounded cavities with standard dimensions (diameter; 3 mm, depth; 0.7 mm) were prepared within Macor™ blocks 50 x 50 x 5 mm (Macor™, Corning, USA) using a standardised drill bit. A flat reference area around each cavity was protected by placing an adhesive polyvinyl chloride tape with a standard 8 mm round aperture, onto the Macor™ surface over the cut cavity. Thus, each cavity was surrounded by a peripheral ring of flat Macor™ exposed to the air-abrasion stream and a taped, covered area which acted as a reference from which to analyse the profilometry data (Figure 4-1). All cavities were filled completely with Filtek™ Supreme Ultra (3M ESPE, St. Paul, MN, USA) resin composite restorative material, and light cured (Optilux 501, Kerr, USA) for 40 seconds according to the manufacturer's instructions.

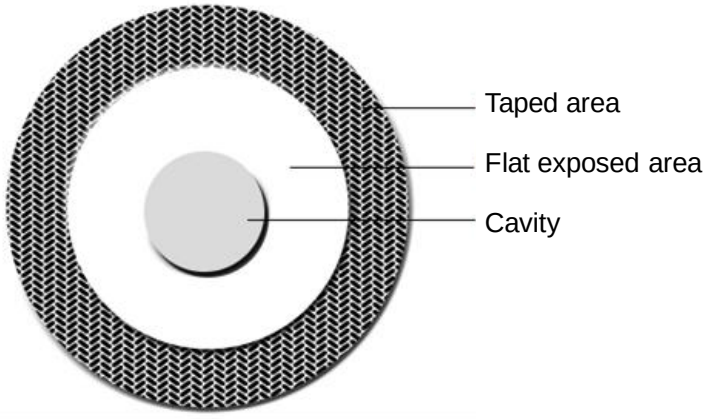

Figure 4-1: Schematic of the Macor™ surface sample design: the central circle is the cavity prepared and subsequently filled by the resin composite, the white middle ring presents the flat Macor™ surface exposed to air-abrasion throughout resin composite removal and the shaded peripheral ring shows the taped protected area which acted as an untouched reference level.

4.2.2 Resin composite removal

An Aquacut™ “wet” air-abrasion unit (Velopex, Harlesden, UK) with a circular cross-section nozzle (internal diameter 600 µm) was used throughout the study. This unit depends on a vibration mechanism to admix the abrasive powder with the propellant air stream and thus enables the operator to control both air pressure and powder flow rate (PFR) independently using pre-set dials on the unit’s fascia (see Section 2.3.4; p: 83). Periodic calibration of output pressure readings (40, 60 and 80 psi) was carried out before each experimental session using a digital pressure indicator (DPI 705, Druck, UK) attached to the output nozzle. The particle size distribution percentiles of alumina were (d_{10}=16, d_{50}=34 and d_{90}=51 µm) and those of BAG powder were (d_{10}=29, d_{50}=60 and d_{90}=92 µm).

In order to obtain a constant powder flow rate, the powder reservoir was refilled to a pre-determined line regularly throughout the experiment (Banerjee et al., 2008b). A disposable plastic tip was attached to the external aperture of the nozzle to mix the powder-air stream with de-ionised water, drawn up from the reservoir by the negative pressure created at the nozzle tip by the emitted air-powder stream. This reduced the powder scattering associated with the conventional dry abrasion procedure, but had no effect on air-abrasion cutting efficiency, as shown in Section 3.3. For each clinically adjustable air pressure value (40, 60 and 80 psi) three PFR dial settings (1, 3 and 5 representing the lowest, the middle and the highest values respectively on the unit) were tested, establishing nine experimental groups for each abrasive powder (Table 4-1; p: 110). The resin composite was removed according to the conditions of each group (n=5).

Complete resin composite removal was confirmed after rinsing and drying the cavity, by visual inspection using 2.5x magnification loupes (OrascopticHiRes; Sybron Dental Specialties, Orange, CA, USA) and a fibre-optic illuminator light (OSL1-EC, Thorlabs, USA) oriented into the operating field throughout the experiment. The resin composite shade (B2) was selected to present a different opacity to the white Macor™ background allowing the restoration in full to be visualised and checked for complete “clinical” removal. The total time for complete clinical removal of the resin composite was recorded in seconds. The

recorded time did not include the cavity examination periods throughout the experiment.

4.2.3 Macor™ volume measurement

The tape was removed to expose the protected reference areas. Using proprietary measurement software (STAGES™, TaiCaan Technologies Ltd., Southampton, England), a standard 10 mm circle containing the cavity in its centre was determined. Therefore, the scanned area included the exposed 8 mm area in its centre and the reference 2 mm area originally untouched and covered by tape. Non-contact laser profilometry (Xyris™ 4000 TL, TaiCaan™ Technologies Ltd., Southampton, UK) was used to scan the 90 cavities prior to placing the resin composite as baseline scans and then again after the completed air-abrasion procedure. This system employs a diode laser with 785 nm wavelength light source, a 0.25 µm vertical resolution, a spot size of 30 µm, and a gauge range of 2.5 mm. The scan was performed with a 30 µm step-over distance.

The resulting 3D cavity images were analysed using Boddies® surface analysis software (Boddies v2.09, TaiCaan Technologies Ltd., Southampton, UK) to obtain the cavity volume after levelling the reference areas of the 3D image to a best fit plane. Thus, the protected reference areas surrounding the abraded surface became a “zero” plane, and the volume of the cavity was calculated using a “volume calculation function” which calculates the volume (mm^3) below the set reference plane. The amount of intact, undesirable Macor™ volume loss was determined by comparing the volume of each cavity before and after resin composite removal. In this study, the less the Macor™ volume loss, the more optimal were the air-abrasion settings in as much as they led to an improved selectivity for resin composite removal.

4.2.4 Statistical analysis

Data was tested for normality using Histogram/Q-Q plots/Shapiro-Wilk tests. Multilevel linear modelling was performed to figure the significant factors using Stata statistical package (Stata-CorpLP v 11.2, Texas, USA). All comparisons were considered statistically significant if $p<0.05$.

4.3 Results

Representative 3D views and cross-sectional profiles of a cavity treated with BAG air-abrasion are shown in Figure 4-2 and Figure 4-3. There was an increase in the dimensions of cavities following resin composite removal. The cross-sectional profiles exhibited irregular outlines following the abrasion. Rounded cavo-surface and internal angles with micro-roughness were observed in the cross-sectional views of treated cavities. The means and standard errors of Macor™ volume loss using alumina air-abrasion are presented in Figure 4-4 and those using BAG air-abrasion in Figure 4-5. BAG air-abrasion removed significantly less Macor™ volume compared to alumina air-abrasion ($p<0.05$). The interaction between air pressure and PFR setting on Macor™ volume loss was statistically significant within both abrasive powders ($p<0.05$). This interaction affected the variability between the tested powders in removal selectivity. The treatment at PFR setting 1 and an air pressure of 60 psi removed 3.5± 0.5 mm³ and 3± 0.5 mm³ (mean ± SE) Macor™ volume within alumina and BAG groups respectively. Higher air pressure (80 psi) for the same PFR setting 1 abraded 5.3± 0.6 mm³ Macor™ with alumina and 3.7± 0.3 mm³ for BAG.

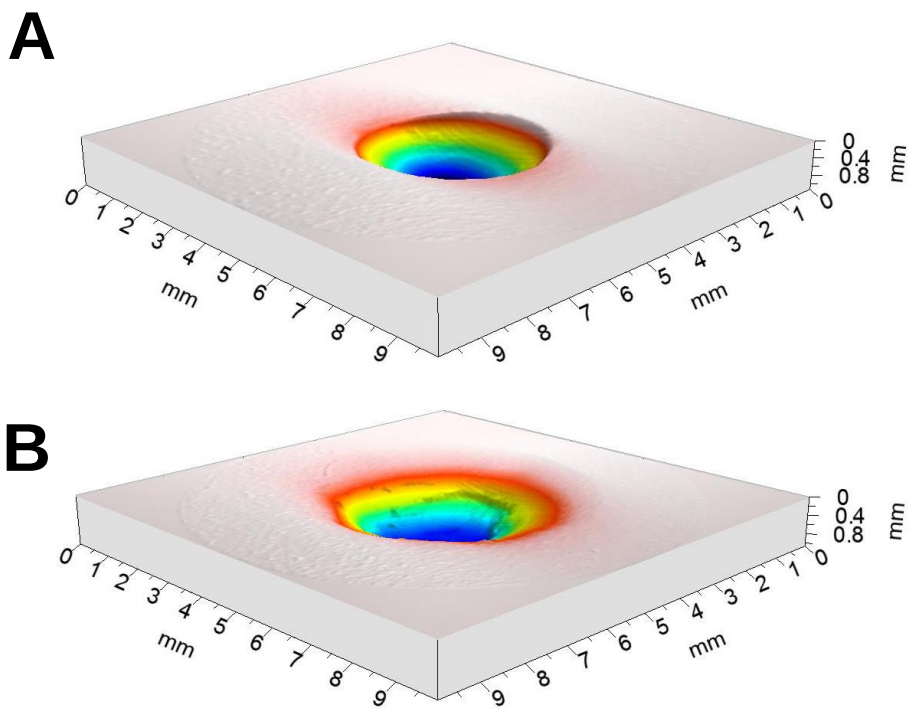

Figure 4-2: 3D views of selected, representative images of a cavity treated using BAG air-abrasion. (A): The cavity prior to restoring with resin composite which was then removed using BAG air-abrasion (B). There was a slight increase in the dimensions of the cavity due to undesirable Macor™ material removal.

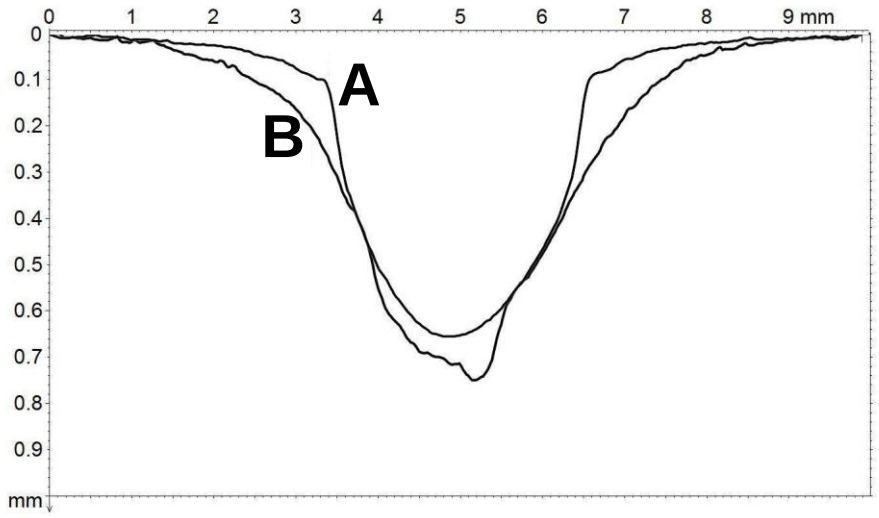

Figure 4-3: The cross-sectional views of the same cavities, presented in Figure 4-2. There was a slight increase in the dimensions of the cross-section (B) following the abrasion procedure when compared to the baseline view prior to restoring with composite (A). More rounded cavo-surface angles can be observed following the composite removal.

Further analysis of the interaction between PFR setting and air pressure revealed that the Macor™ volume removed within PFR setting groups differed significantly within the alumina groups at air pressure of 60 psi and within BAG at air pressure of 60 and 80 psi (p<0.05), whilst no statistical differences within PFR setting groups were observed at an air pressure of 40 psi for both abrasive powders. More Macor™ material was removed unnecessarily when the air pressure was raised to 80 psi at PFR setting 3 and 5 (p<0.05).

The air-abrasion parameters causing the largest undesirable removal of Macor™ volume with alumina were 80 psi air pressure and PFR setting 3: 7.1± 1.1 mm³, whilst for BAG, these settings were 80 psi air pressure and PFR setting 5: 6.7± 0.5 mm³ (mean ± SE). Alumina removed resin composite the fastest (p<0.05) (Table 4-1). The time range for alumina air-abrasion was 50-130 sec, and 65-170 sec using BAG air-abrasion. Analysis of the main effect showed there were no statically significantly differences in the required removal time between alumina and BAG abrasive powders when the air pressure was adjusted to 80 psi (p>0.05) and the PFR set at 5 (p>0.05). The statistically significant differences between the two tested powders using equivalent parameters are presented in Table 4-1.

Table 4-1: Mean ±SE (sec) of the time required for resin composite removal according to conditions of each group, and the statistically significant differences between the two tested powders using equivalent parameters:

Group n=5	Powder	PFR	Air pressure (psi)	Required removal time (mean±SE sec)
*1**	Alumina	1	40	93 ±9.4
2			60	73.4±10.2
3			80	90.4±11.2
4		3	40	129±18.6
*5***			60	66.4±3.6
*6****			80	49.4±3.3
7		5	40	96.6±8
8			60	66.8±3.7
9			80	54.6±3.17
*10**	BAG	1	40	172±24.7
11			60	95.6±9.7
12			80	94.4±19.2
13		3	40	160.8±13.9
*14***			60	111.8±10.6
*15****			80	74.2±2.2
16		5	40	103.8±12.8
17			60	74.6±5.5
18			80	64.6±13.6

Significance: (1 vs. 10); (5 vs. 14); (6 vs. 15): *p<0.05*

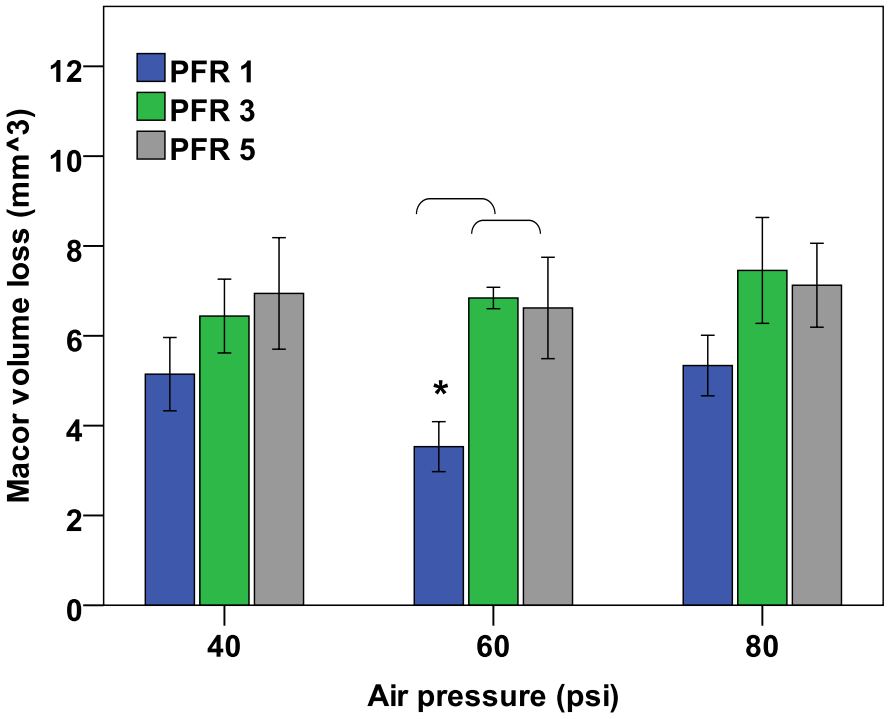

Figure 4-4: Mean±SE (mm³) of Macor™ volume loss using alumina air-abrasion. (*) indicates statistically significant differences between PFR 1 and 3/5 at air pressure of 60 psi.

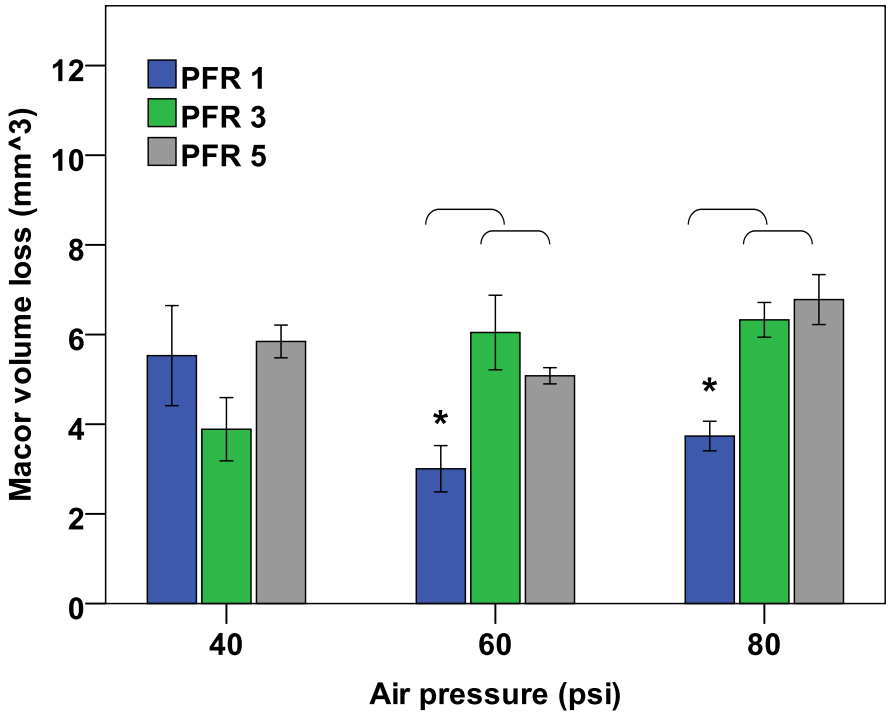

Figure 4-5: Mean±SE (mm³) of Macor™ volume loss using BAG air-abrasion. (*) indicates statistically significant differences between PFR 1 and 3/5 at air pressure of 60 and 80 psi.

4.4 Discussion

Optical scanning profilometry was used to assess the selective removal of resin composite restorations permitting an objective approach for volume loss quantification (Heintze et al., 2006; Ryf et al., 2012). Triangular laser profilometry was used for this purpose as there was a large variation between the highest and lowest points in 3-dimensional cavity depths (Leach, 2010). A specific area surrounding each cavity was taped to establish a reference level. This is a documented procedure in in-vitro investigations when 3D analysis has been used for bulk volume analysis (van Waes et al., 1997; Eliades et al., 2004; Schlueter et al., 2005; Kim et al., 2007).

The resin composite was placed in the prepared cavity without adhesive procedures to avoid resin composite remnants being retained on the surface. It has been revealed that even though the tooth surface appeared to be resin-free after removing resin remnants, many retained resin islands were observed using SEM analysis (Hong and Lew, 1995; Tufekci et al., 2004; Banerjee et al., 2008a; Pont et al., 2010). In addition, the chemical composition and the microstructure of Macor™ are different from those of human enamel and therefore, the composite bonding with Macor™ is not similar to that with enamel. As mentioned earlier, the hardness and thermal properties of Macor™ are similar to those of

human enamel (see Table 1-6; p: 42), and its use in the present study eliminated variables that might have been induced if biological and histologically heterogeneous human enamel samples had been used. This use also permitted standardisation of the cavity shape and size within all samples.

The clinical performance of dental resin composite is correlated positively to its mechanical properties, which in turn, are determined primarily by the filler content within the structure (Ferracane, 2011). The resin composite restorative material used in this study is a nanofilled composite containing 78.5 wt% fillers (SiO_2: 20 nm, ZrO_2: 4–11 nm, SiO_2/ZrO_2: 0.6–20 µm aggregates) and exhibited high Knoop hardness (69.87 MPa) and flexural modulus (12 GPa) (Passos et al., 2013; Thomaidis et al., 2013). These are deemed clinically suitable to permit its use as a restorative dental material for both anterior and posterior teeth.

Resin composite restorations can be removed clinically using different operative technologies including rotary burs, ultrasonic instruments, lasers and air-abrasion (Hong and Lew, 1995; Banerjee et al., 2008a; Bonetti et al., 2011; Cochrane et al., 2012b; Chan et al., 2014). No single technique has been approved as ideal in term of removing resin composite selectively without causing unnecessarily damage to the enamel surface (Ozer et al., 2010; Cochrane et al., 2012b). Using conventional rotary instruments in this regard may produce an irregular enamel surface and could cause pulp inflammation due to the heat generated and conducted within dental tissues (Correa-Afonso et al., 2010). Lasers are a high-cost technology and their use as a cutting tool has showed a highly variable cutting rate and therefore, laser use in restorative dentistry requires further investigation (Yip and Samaranayake, 1998; Neves et al., 2011). Cracks can develop using ultrasonic instruments when they are applied to a brittle enamel substrate (Tassery et al., 2013). In air-abrasion, the pressure applied against the tooth surface, the bone vibration and the rise in tissue temperature are negated, resulting in a relatively pain-free procedure (Black, 1955; Rafique et al., 2003). Using BAG abrasive powder and considering the air-abrasion operating parameters may promote the selectivity of resin composite removal using this technology. However, the clinical use of air-abrasion requires adequate training to avoid tooth over-preparation that may occur due to the lack of tactile feedback.

In the present study, air-abrasion was conducted by one operator as individual experience and technical skill can affect the outcome of the technique when removing resin composite restorations (Dorter et al., 2003). Some of the air-abrasion operating parameters, including nozzle-substrate distance, nozzle angle and nozzle-movement speed, were not fixed in order to mimic the variable clinical situation where these parameters would and could not be controlled effectively and are fully operator-dependent.

The cross-sectional views of cavities treated using air-abrasion exhibited rounded cavo-surface margins and internal line angles with micro-roughness. Those features are similar to those reported in human enamel and dentine using air-abrasion (Laurell and Hess, 1995). This cutting pattern provides ideal contours for dental adhesive restorative materials and increases the wettability of the treated surface promoting the adhesion to enamel. Repairing rather than replacing the defective restorations is advocated in minimally invasive dentistry (Sharif et al., 2010). The physical interaction between air-abrasion and resin composites may enhance the repair of aged biological restorations (Cho et al., 2013).

BAG air-abrasion was significantly more selective than alumina air-abrasion in removing resin composite. This could be explained as the BAG particles used exhibit rounded outline profiles, while alumina particles have sharper, angular edges so increasing the physical abrasiveness of alumina (see Figure 2-3; p: 80). Also, BAG particles' have a reduced Vicker's hardness (VHN 458) compared to that of alumina powder (VHN 2300) (Hench and Wilson, 1993; Banerjee et al., 2008a), which might reduce the removal rate of Macor™ using BAG air-abrasion. The results from this study are corroborated by those of a previous study where it was found that BAG powder was more efficient than alumina powder in removing selectively the orthodontic cement adhesive after bracket de-bonding (Banerjee et al., 2008a).

The findings of this study suggested that there was an increase in the Macor™ substrate removal when air pressure was increased. The rise in propellant pressure increases the velocity and the kinetic energy of the carried abrasive particles making them more destructive to the substrate (Horiguchi et al., 1997). Adjusting the powder flow rate dial to its highest value led to the removal of significantly more of the Macor™ substrate, indicating that using excessive quantities of either powder is not advised. However, when reduced quantities of both powders were used with a low air pressure, more Macor™ substrate was also removed. This could be explained as the operator felt compelled clinically to reduce the relative movement of the air-abrasion nozzle over a specific area of the restoration surface to compensate for the reduction of both powder flow rate and particle speed. This would have the ultimate clinical effect of increasing the risk of operator-induced “over-preparation” at particular sites as the nozzle may be held stationary over specific areas of the cavity for longer periods. Therefore, an extreme reduction in the volume of the abrasive stream to avoid cavity over-preparation is not recommended as the apparent benefit is nullified by the clinical variation of the operator.

Comparing the Macor™ volume removed and the required removal time between both abrasive powders showed that using higher air pressure and excessive amounts of both powders produced similar air-abrasion cutting performances in contrast to those produced using reduced settings. This implies that within the parameters of low air pressure and PFR settings, the cutting efficiency of clinical air-abrasion depends primarily on the nature of the abrasive powder rather than on the operating physics of the unit itself. Cavity shape / size standardisation throughout the experimental groups allowed time evaluation due to the similarity of resin composite restoration volume within all samples. BAG powder required statistically significantly more time than alumina powder to remove the restoration fully. However, this difference was not significant clinically and deemed acceptable in-vivo, particularly if more healthy intact tissues will be preserved as an outcome.

4.5 Conclusions

The three null hypotheses were rejected. Within the limitations of this in-vitro study, the following conclusions can be drawn:

1. BAG powder is more efficient than alumina in the selective removal of resin composite.
2. The interaction effect between air pressure and PFR on resin composite removal was significant.
3. Using moderate air pressure value with reduced PFR enhanced the selective removal of resin composite.
4. The time required for resin composite removal was deemed acceptable clinically.

Bioactive glass air-abrasion promoted the selective removal of resin composite and therefore, may be recommended clinically for the purpose of removing resin composite restorations under the auspices of minimally invasive operative / reparative tooth preserving dentistry.

Chapter 5 An in-vitro evaluation of enamel white spot lesion remineralisation using bioactive glass and polyacrylic acid-modified bioactive glass powders.

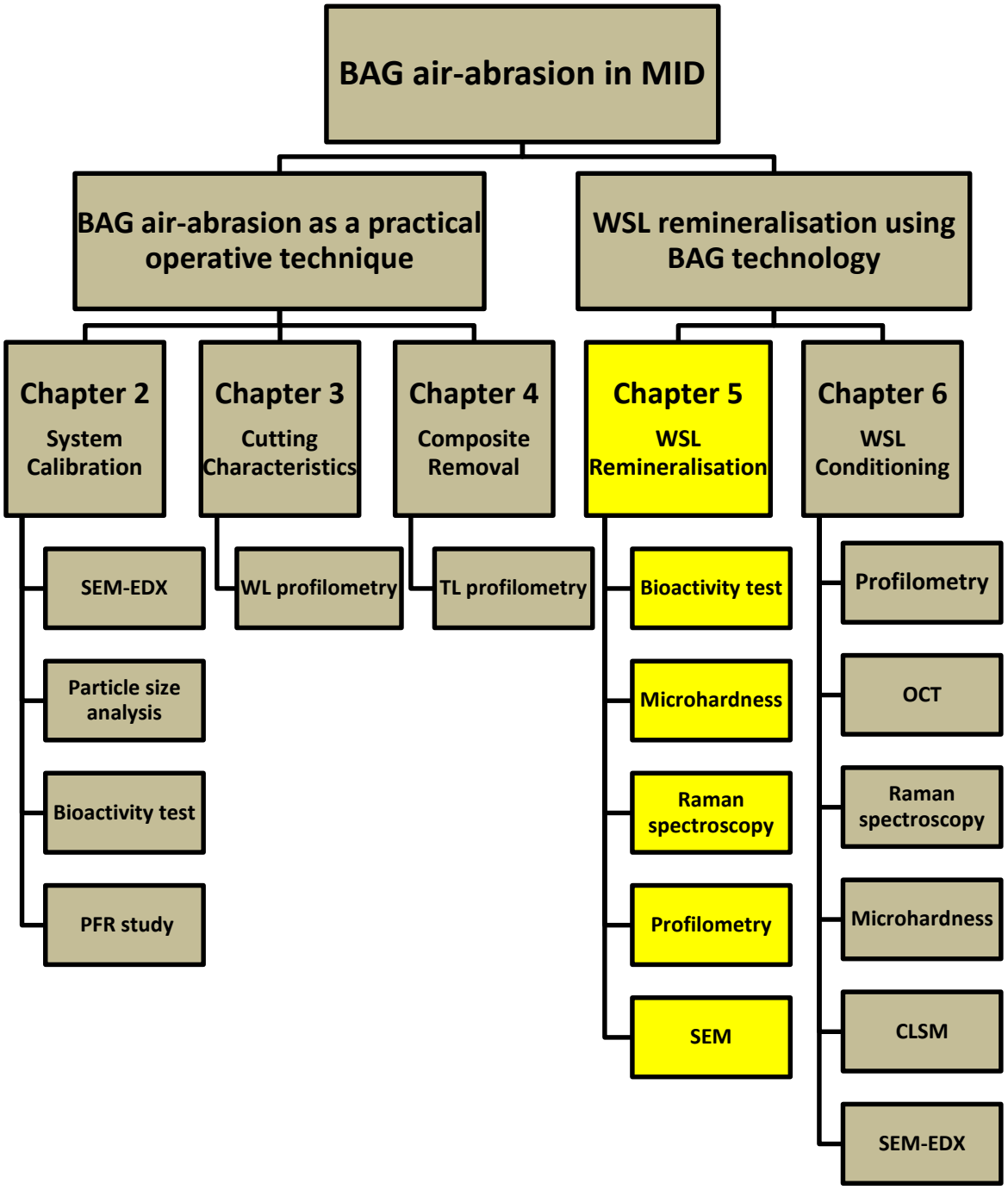

Organisational flowchart of the experiments accomplished in this study.

5.1 Introduction

The subsurface porosity of an enamel white spot lesion (WSL) is the earliest clinical manifestation of caries caused by an imbalance between the dynamic biological processes of de- and remineralisation (Kidd and Fejerskov, 2004). In minimally invasive dentistry (MID), incipient carious enamel lesions should not be managed with surgical intervention, but with non-invasive preventive remineralisation strategies aiming to “heal” them by reversing the demineralisation process, preventing any further mineral loss and enhancing remineralisation (Featherstone, 2009). The key factore in enamel WSL remineralisation is to use dissolvable materials containing those ions required to deposit minerals similar to those of enamel and at the same time which have the ability to diffuse into the lesion depths (see Section 1.2.3.3; p: 51) (Tung and Eichmiller, 2004; Cochrane et al., 2010).

Bioactive glass (BAG) 45S5 can act as a source of a large amount of CaO with some P_2O_5 in a Na_2O-SiO_2 matrix (Hench, 2006) and therefore, it has the potential to remineralise WSLs. The use of BAG 45S4 in enamel remineralisation, however, is relatively new when compared to other well-documented remineralisation systems such as fluoride and casein phosphopeptide-amorphous calcium phosphate (CPP-ACP) implying that more evaluation is still required to assess the interaction between the reacted BAG particles and enamel substrate (Reynolds, 2008; Walsh, 2009; Wefel, 2009; Cochrane et al., 2010; Li et al., 2014). Polyacrylic acid (PAA) powder has been introduced into BAG abrasive powder in order to modulate and reduce the cutting efficiency of air-abrasion when operatively managing dentine carious tissues (Sauro et al., 2012b). Using BAG powder containing 40 wt% PAA might also be used to enhance the bond durability of self-etch adhesive systems to dentine (Sauro et al., 2012b). PAA may mimic the functional role of non-collagenous proteins in binding the calcium and phosphate ions to form nano-precursors, small enough to penetrate the carious lesion more effectively. (Tay and Pashley, 2008; Kim et al., 2010). The potential effect of PAA-BAG powder on enamel WSL remineralisation has not been reported in the literature to date.

Raman micro-spectroscopy is used as a quantitative chemical assessment methodology for biological samples since the Raman peak intensity is proportional to the number of molecules within the volume of the scanned area (Tsuda and Arends, 1997; Penel et al., 1998; Tramini et al., 2000). The Raman phosphate peak at 959 cm^{-1} characterises the tetrahedral PO_4 group, a P−O bond, within hydroxyapatite (HA) (see Figure 1-10; p: 64 and Table 1-10; p: 64). The present study measured the intensity of this peak to assess the potential chemical changes during enamel remineralisation. Depth profiles of phosphate peak intensity along the cross-sections of the samples were created and fitted using a double-step function.

Conventional point-by-point serial scanning mode requires long acquisition times, since increasing the speed of Raman imaging without compromising its inherent quality is unachievable in this system. This may explain why Raman micro-spectroscopy is not as widely used in dental research compared to other techniques such as confocal laser scanning microscopy. Alternatively, StreamLine™ scanning technology was used in this study. This technology is a novel Raman imaging technique from Renishaw plc (Wotton-under-Edge, UK) that permits faster, parallel and continuous spectral acquisition utilising the Raman microscope optics to illuminate a moving line across the sample to read the data continuously (Hedoux et al., 2011). As the sample is moved using a motorised stage with a definable step-over distance, the spectrum moves across the detector so reducing the dead time between sequential data points (Evans, 2008). To date, the use of Raman StreamLine™ scanning technology to map chemically dental enamel has not been reported in the literature.

The aim of the present study was to evaluate the effect of BAG 45S5 and PAA-BAG powders on artificial enamel WSL remineralisation through chemical, mechanical and morphological assessments using a “standard” remineralisation solution as a positive control and de-ionised water as a negative control. Microhardness measurement provides information about the mineral density and mechanical properties of hard tissue surfaces (White et al., 1988; Buchalla et al., 2008), and is a reliable objective method to study de- and remineralisation of enamel and dentine lesions (Section 1.3.3.2; p: 65). The ultra-structural changes of the lesion surface were assessed using non-contact white light confocal

profilometry and scanning electron microscopy (SEM). Prior to the remineralisation study, the structure of the artificial WSLs were characterised using tandem scanning confocal microscopy (TSM) and optical coherence tomography (OCT), and the bioactivity of tested powders was chemically analysed using a Fourier-transform infrared spectroscopy (FTIR).

The null hypothesis investigated was that enamel WSL treatment with BAG or PAA-BAG powders has no beneficial effect on enamel WSL remineralisation when compared to the positive and negative control solutions.

5.2 Materials and methods

5.2.1 Materials and Methods: sample preparation

Fifty-two caries-free human extracted molars were used in this study. The teeth were stored in refrigerated de-ionised water and used within a month of the extraction. A diamond wafering blade (XL 12205, Benetec Ltd., London, UK) was used to obtain one slab (4 x 4 x 2 mm) from the buccal surface of each tooth. The slabs' surface integrity was inspected using a confocal tandem scanning microscope (TSM) (Noran Instruments, Middleton, WI, USA), with a x20 air objective in reflection scanning mode. The samples were then included face down in acrylic resin (Oracryl, Bracon Limited, UK) using a hard-anodized aluminium and brass sample former (Syndicad Ingenieurbüro, München, Germany) (Figure 5-1).

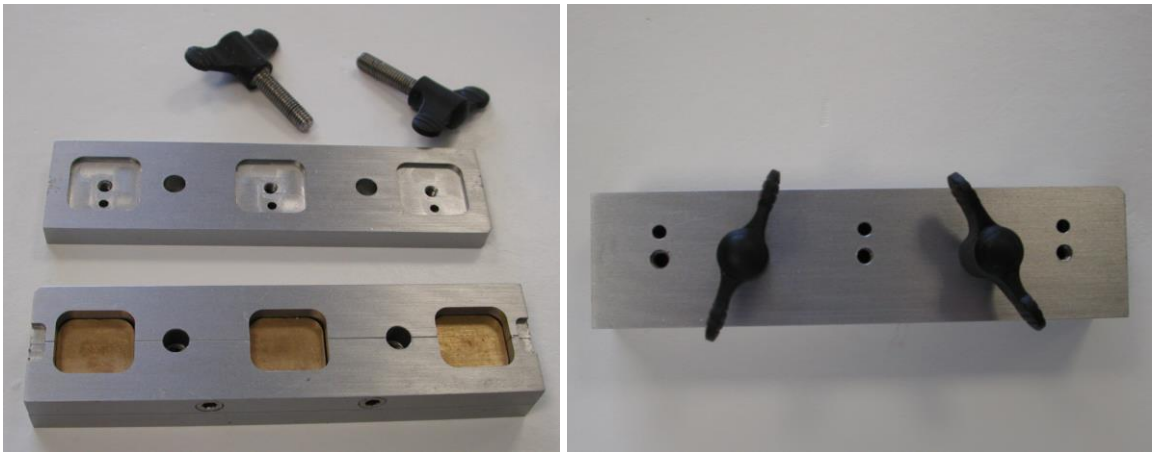

Figure 5-1: The hard-anodized aluminium and brass sample former used to include enamel slabs in acrylic resin.

The outer enamel layer was removed using a water-cooled rotating polishing machine (Meta-Serv 3000 Grinder-Polisher, Buehler, Lake Bluff, Illinois, USA) (Figure 5-2) using a sequential polishing protocol; 180-grit silica carbide disk (Versocit, Struers A/S, Copenhagen, Denmark) for 5 sec, 600-grit for 10 sec, 1200-grit for 20 sec, 2400-grit for 30 and 4000-grit for 45 sec, followed by 3 min of ultrasonication to remove the smear layer at the enamel surface. The polishing protocol helped create more consistent, reproducible artificial enamel lesions reducing the variation between the samples (ten Cate and Duijsters, 1982; White et al., 1988), and improved the reliability of the profilometry assessment (Austin et al., 2010).

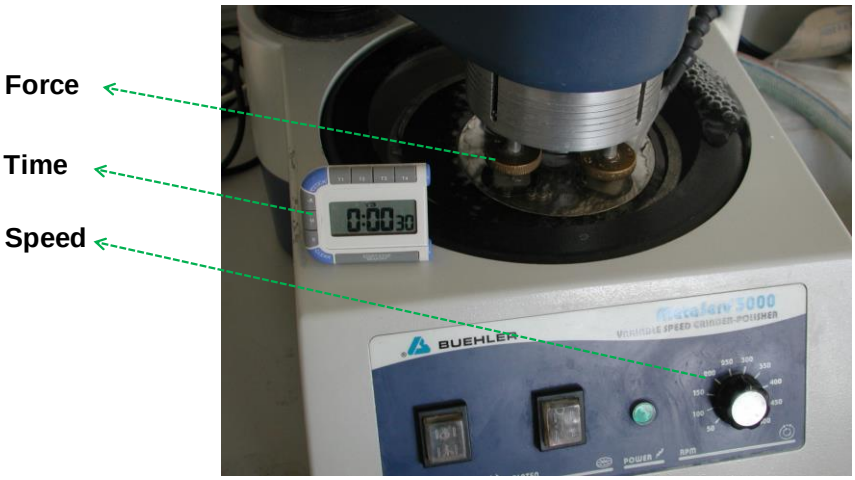

Figure 5-2: The polishing machine used in this study to remove the outer layer of enamel under copious water irrigation creating a flattened, polished surface. The speed of the polishing disk, the force of polishing head and the polishing periods were standardised throughout.

Dental wax was applied to protect part of the enamel leaving an exposed window of 3 x 1 mm in the central area. WSLs were created using a previously reported bi-layer demineralisation protocol of 8 % methyl cellulose gel buffered with a lactic acid layer (0.1 mol/L, pH 4.6) for 14 days at 37°C (Ingram and Silverstone, 1981; ten Cate et al., 2006), as explained in Figure 5-3. The structure of the enamel surface was examined in a pilot study after completing the polishing procedures. A confocal tandem scanning microscope (TSM) (Noran Instruments, Middleton, WI, USA), with a x100 oil-immersion objective in reflection scanning mode with a wavelength of 409 nm, was used to image the enamel prisms in the sound / demineralised enamel surfaces. In order to determine the lesion shape / depth, the samples were examined using optical coherence tomography (OCT) (VivoSight, Kent, UK) operating at a central wavelength of 1305 nm, 10 kHz rate

and 15 mW energy power. The set scan area (3 cm wide, 2 mm deep) included the lesion in the middle surrounded by sound enamel from each side.

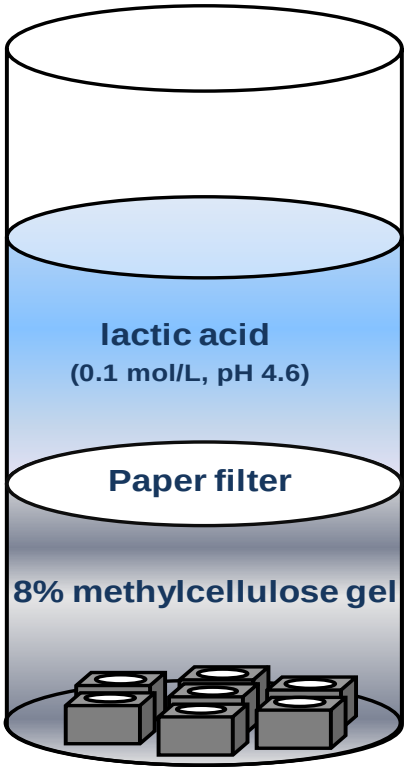

Figure 5-3: A schematic explaining the bi-layer demineralisation protocol used in this study to create artificial WSLs. Seven samples are placed at the bottom of a glass container and covered by a layer of 8% methyl cellulose gel (200 ml) which in turn is buffered by a layer of lactic acid solution (200 ml) at pH 4.6 for 14 days.

5.2.2 Materials and Methods: powder preparation and bioactivity testing

PAA-BAG powder was prepared by mixing 60 wt.% BAG 45S5 powder with 40 wt.% PAA powder (MW: 1800, Sigma Chemicals, Gillingham, Dorset, UK) for 5 min at 300 rpm. Prior to the mixing procedure, BAG and PAA powders were sieved for 120 min using a sieve (Fischer Brand, UK) with an automatic shaking unit (Endecott, London, UK) to break down any agglomerations that might have formed within the powder during the storage. The particle size of BAG and PAA-BAG powders was measured as explained in Section 2.2.2; p: 76. The homogeneity of the mixed powders was validated using FTIR spectroscopy (Perkin-Elmer, Beaconsfield, UK) to detect the vibration of C=O (PAA) at 1710 cm^{-1} and of Si-O-Si (BAG) at 1040 cm^{-1} (n=3).

The bioactivity tests of BAG and PAA-BAG were conducted as explained in section 2.2.3; p: 77. Briefly, 0.3 g of tested powder was added to 200 ml Tris (tris-hydroxymethyl amino methane) buffer solution adjusted to 7.25±0.1using 2N HCl. The bioactivity test was conducted with continuous stirring (stirring rate: 175 rpm) at 37^{o}C for 20 hours (n=3 for each tested powder). The powder was then filtered, acetone-washed and air-dried. Potassium bromide (KBr) pellets were prepared as mentioned in section 2.2.3 and scanned using FTIR spectroscopy to collect the absorbance spectra with a diffuse reflectance accessory in the frequency range of 400-1400 cm^{-1}.

5.2.3 Materials and Methods: remineralisation therapy

Samples were assigned randomly into four experimental groups, detailed in Table 5-1. Microhardness measurements of intact sound enamel in each sample were recorded to calculate any statistical difference between specimens in each group prior to any remineralisation therapy. The sound enamel areas around the WSL were taped over with polyvinyl chloride tape throughout the experimental procedures, and removed at the end of the remineralisation therapies. BAG and PAA-BAG were prepared as slurries using de-ionised water (L/P ratio of 1g m^{-1}) (Dong et al., 2011), and applied onto the lesion surface without any mechanical agitation. The remineralisation therapies were conducted for 7 days at 37° C and refreshed daily. At the end of the remineralisation therapies, the samples were rinsed with de-ionized water and assigned for microhardness and Raman analyses (n=8), and for profilometric and SEM (n=5) assessments (Figure 5-4).

Table 5-1: The experimental groups and composition of applied materials:

Group (n=13)	Remineralisation therapy	Composition
1	BAG slurry prepared with de-ionized water (L/P ratio of 1g ml^{-1})	45S5 BAG powder
2	PAA-BAG slurry prepared with de-ionized water (L/P ratio of 1g ml^{-1})	60 wt% 45S5 BAG powder 40 wt% Polyacrylic acid (PAA) powder MW: 1800 (Sauro et al., 2012b)
3	Positive control	Remineralisation solution (ten Cate et al., 2006): 20 mM Hepes 130 mM KCl, 1.5 mM $CaCl_2$ 0.9 mM KH_2PO_4 pH 7.0 with KOH
4	Negative control	De-ionised water - pH 6

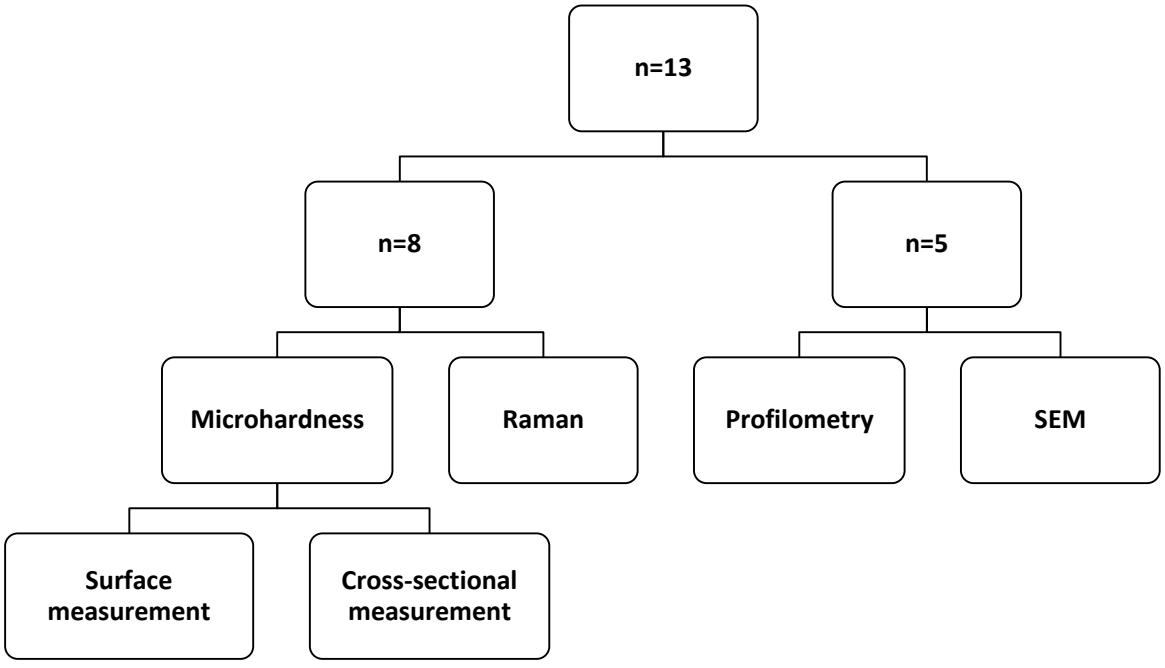

Figure 5-4: A schematic representing the number of specimens within each experiential group distributed according to the analytical tests.

5.2.4 Materials and Methods: surface and cross-sectional microhardness measurements

A Struers Duramin microhardness tester (Struers Ltd., Denmark) with a Knoop diamond indenter was used (25 g load applied for 10 sec). The indentations were imaged using a x40 air objective and the Knoop microhardness values (KHN) were calculated using the manufacturer's software supplied. Prior to each measuring session, the tester was calibrated (n=5) using a calibrated transfer-standard block (N 0441, UKAS calibration, UK). Five measurements, 200 µm apart, were recorded and then averaged to measure the lesion surface microhardness of each sample.

The samples were then hemi-sectioned using a diamond wafering blade. Each cross-sectioned surface was hand-polished up to 1200-grit to produce a flat surface. The integrity of the lesion and the flatness of the cross-sections were examined prior to any further experimental analyses using a confocal tandem scanning microscope (TSM) used in a reflection scanning mode using a x20 air objective and 409 nm wavelength. For cross-sectional microhardness testing, three measurements, 100 µm apart and 30 µm away from the outer lesion surface were recorded and averaged within each sample.

5.2.5 Materials and Methods: Raman micro-spectroscopy

A Renishaw inVia Raman microscope (Renishaw Plc, Wotton-under-Edge, UK) running in Streamline^{TM} scanning mode was used to scan the cross-sectioned surfaces using a 785 nm diode laser (100% laser power) focused using a x20 air objective. The signal was acquired using a 600 lines/mm diffraction grating centred at 800 cm^{-1} and a CCD exposure time of 2 sec. Raman spectra were displayed using Renishaw WiRE 3.2 software (Renishaw Plc, Wotton-under-Edge, UK). The microscope was calibrated using an internal silicon sample with a characteristic band at 520 cm^{-1} prior to each scan session.

The sample was positioned in focus, placing the air/lesion interface exactly parallel to the horizontal line of the crosshairs pointer. Using the charge-coupled device (CCD) supplied with the system, a stitched montage image was created at the middle part of the lesion for each sample composing of 1x2 images in the horizontal and vertical directions respectively. For each sample, a Raman map of

the air/lesion/enamel interface was recorded. The map was started at 125 µm on the outer side of the lesion (air) and extended to approximately 400 µm within the sound enamel, covering an area of 525 X 350 μm^2 and containing 1740 spectra acquired with a 2.7 µm resolution across the air/lesion/enamel interface.

Raman maps were exported into in-house curve-fitting software to fit the spectra and to generate grey-scale images (Figure 5-5-A) and depth profiles of phosphate peak intensity at 959 cm^{-1} (PO_4^{-3} v1) over the distance across the interface (Figure 5-5-C). The minimum and the central energy values of the phosphate peak were selected in the spectrum at 939 cm^{-1} and 959 cm^{-1} respectively, identified using a liner regression model provided by the software. The demineralised enamel produced a background autofluorescence (AF), as do most biological samples (Figure 5-5-B). To take this slowly varying background signal into consideration, the spectra were fitted by the means of in-house curve-fitting software with a linear combination of a Gaussian function and a first order polynomial.

The Raman analysis in the current study was based on peak ratio analysis, namely: the ratio between the mineral peak within the lesion and the mineral peak within healthy enamel. This ratio was analysed by fitting the depth profiles of phosphate peak intensity objectively using a double-step function, by the means of a custom-written software (Figure 5-5-C), to obtain the phosphate peak intensity percentage within the lesion compared to that of the deeper sound enamel (the distance between lesion and sound steps in the vertical direction), and the lesion depth (the distance between lesion and sound enamel steps in the horizontal direction).

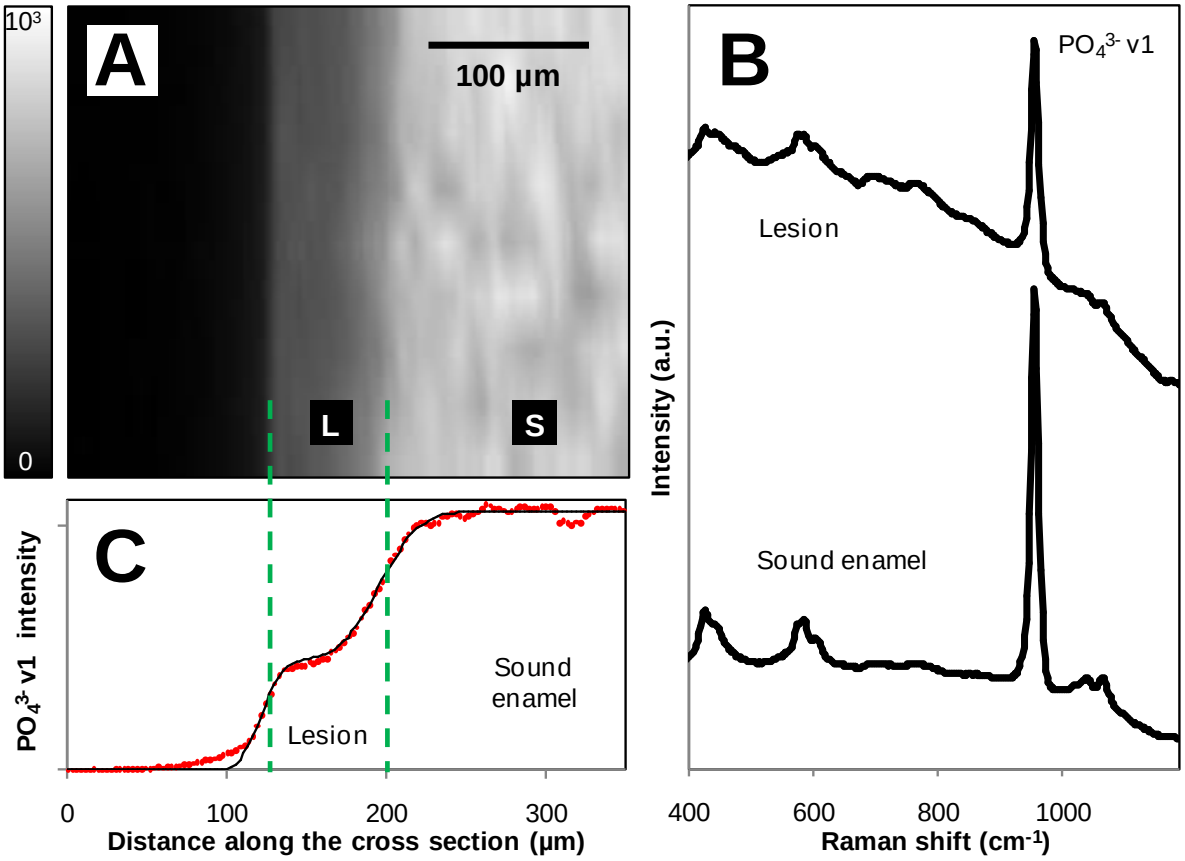

Figure 5-5: (A): representative grey-scale image of Raman phosphate peak intensity at 959 cm^{-1} including the lesion (L) and sound enamel (S) areas of the scanned map. (B): Raman spectra of the lesion and deep sound enamel areas within the same sample. (C): depth profile of phosphate peak intensity (broken red line) fitted using a double-step function (solid line).

5.2.6 Materials and Methods: profilometric analysis

A standard scan area of 3 x 2 mm was chosen over the WSL to include the lesion in the centre (1 mm) surrounded by flat sound enamel on each side (1 mm), acting as a reference area. The sample surface was scanned before and after remineralisation therapy using optical white light confocal profilometry (Xyris™ 4000 WL, TaiCaan™, Southampton, UK) with a 10 µm step-over distance and a 10 nm vertical resolution. The resulting 3D images were analysed by levelling the sound enamel areas to a best-fit. Thus, the protected reference sound enamel areas surrounding the WSL became a reference plane with an average "z" height value of "0". The step height measurement of the lesion surface in relation to the sound enamel level, which was protected by a tape throughout the remineralisation therapy, was obtained by averaging five measurements along the lesion within each sample using Boddies® surface analysis software (Boddies v2.09, TaiCaan Technologies Ltd., Southampton, UK).

5.2.7 Materials and Methods: SEM

A scanning electron microscope (FEI Co. Ltd., Cambridge, UK) was used to examine the ultra-structure of the lesion surface (accelerating voltage of 10 kV, working distance of 10 mm). The samples were gold sputter-coated before SEM analysis (Emitech K550, UK). A further two samples from the PAA-BAG and negative control groups were sectioned using a diamond wafering blade, gold sputter-coated and scanned using the same parameters. The scanned area included both the lesion cross-section and part of its surface.

5.2.8 Materials and Methods: statistical analysis

Statistical analysis was conducted using SPSS statistical software (version 20; SPSS Inc., IBM, Chicago, IL, USA). Data were tested for normality using Histogram/Q-Q plots/Shapiro-Wilk tests, and using one-way analysis of variance (ANOVA) and Tukey's HSD post-hoc tests to calculate the significant factors at p=0.05.

5.3 Results

5.3.1 Results: sample preparation

A photograph of one of the samples used in this study is presented in Figure 5-6 showing the artificial WSL in the centre surrounded by flattened, polished sound enamel acting as a reference area. The OCT images showed the cross-sectional view of the lesion in the centre (approximately 70-100 µm deep), with an increased signal intensity when compared to the surrounding sound enamel (Figure 5-6). The lesion surface layer was intact and at the same level of the adjoining sound enamel. Figure 5-7 shows representative TSM images of the polished enamel surface prior to (A) and post- (B) production of an artificial WSL. The cross-sectional views of enamel prisms were detected in both TSM images, with mineral dissolution in the interprismatic regions in the WSL surface (Figure 5-7-B).

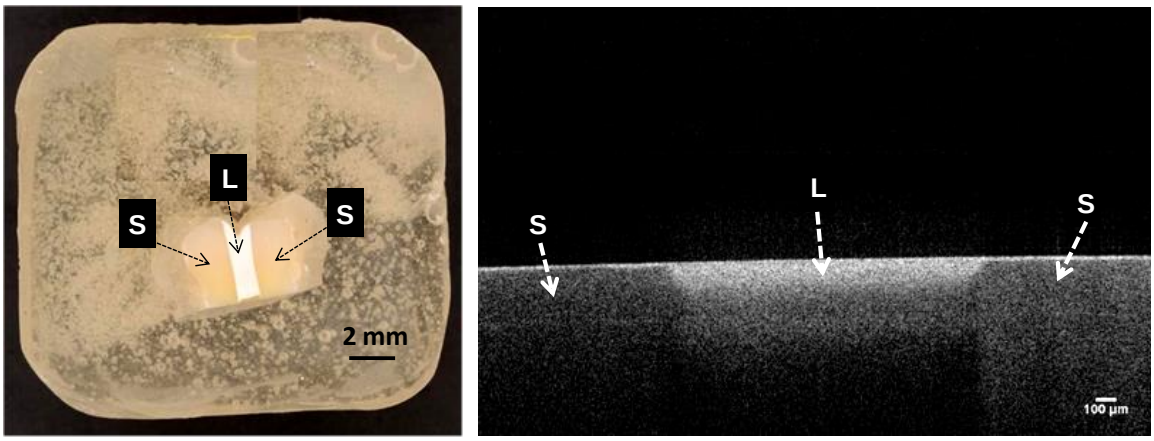

Figure 5-6: A photograph of one of the samples used in this study shows the WSL (L) in the centre of the enamel slab surrounded by an intact enamel area (S). The OCT image on the right side presents the cross-sectional view of the sample. The lesion in the centre exhibits an increased signal intensity compared to the surrounding sound enamel.

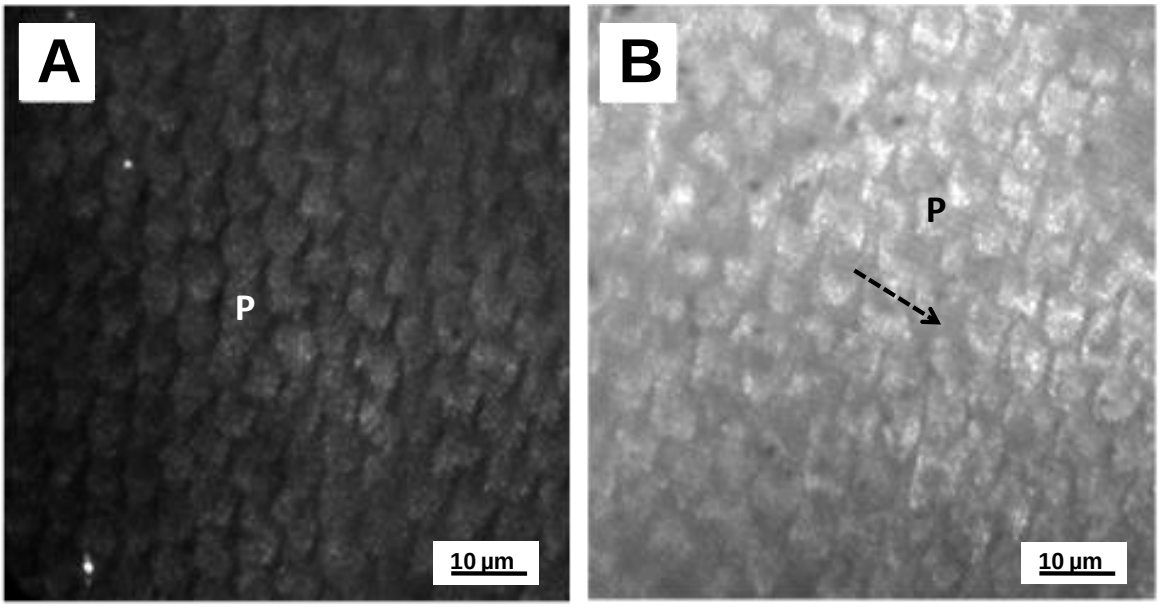

Figure 5-7: Confocal tandem scanning microscopy images of an enamel surface after the polishing procedure (A) and after the demineralisation process (B). The cross-sections of enamel prisms (P) can be detected in both images, with mineral dissolution in the interprismatic region (the arrow) in the lesion surface (B).

5.3.2 Results: powder preparation and bioactivity testing

The particle size distribution percentiles (10, 50 and 90 %) of BAG and PAA-BAG powders are presented in Table 5-2, whilst the histogram of particle size distribution and the cumulative percentage of the data are shown in Figure 5-8 and Figure 5-9.

Table 5-2: Particle size distribution of BAG and PAA-BAG powders as percentile classes:

	d10 (µm)	**d50 (µm)**	**d90 (µm)**
Particle size distribution BAG	1.98	10.88	20.84
Particle size distribution PAA-BAG	2.12	12.05	25.12

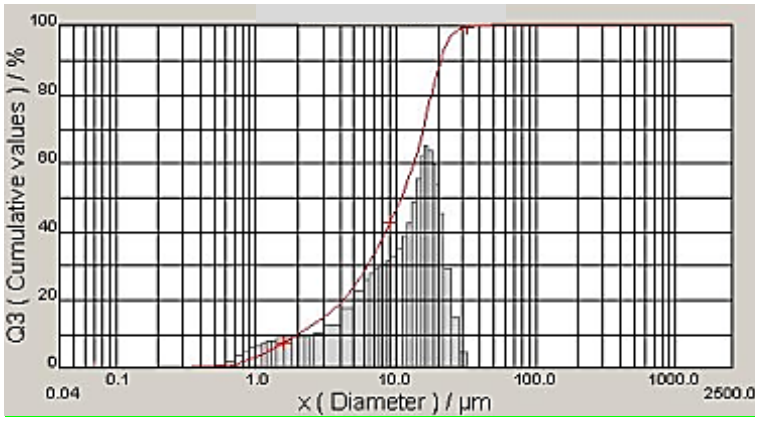

Figure 5-8: The particle size distribution of BAG powder in cumulative percentage (red line) and in frequency percentage (bars).

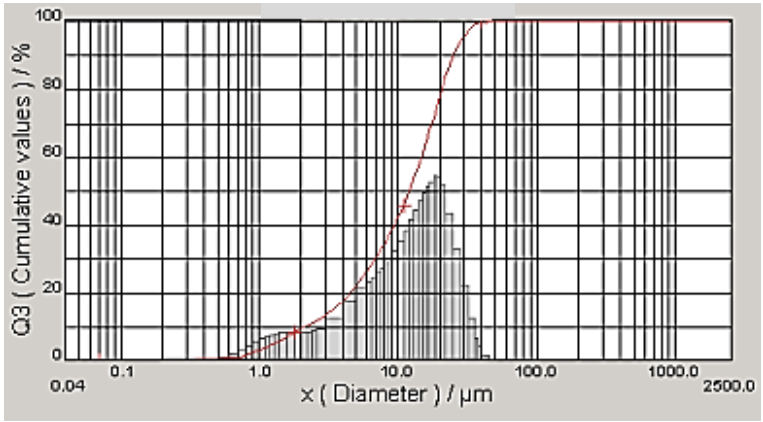

Figure 5-9: The particle size distribution of PAA-BAG powder in cumulative percentage (red line) and in frequency percentage (bars).

Representative FTIR spectra of PAA-BAG and BAG are shown in Figure 5-10. The spectrum of BAG presented high prominent peaks of Si-O-Si stretching mode at 1040 cm^{-1} and 910 cm^{-1} related to the non-bridging oxygen Si-O-NBO (Hench and Wilson, 1993; Aina et al., 2009). The band at 1450 cm^{-1} is assigned to a carbonate group which formed due to the reaction between the atmospheric CO_2 and some available Ca^{2+} surface ions (Cerruti et al., 2005). The FTIR spectrum of PAA-BAG exhibited the above peaks, but with an additional peak at 1710 cm^{-1} related to a carbonyl group (C=O) of PAA powder (Li et al., 2004), providing evidence of the powder's homogeneity.

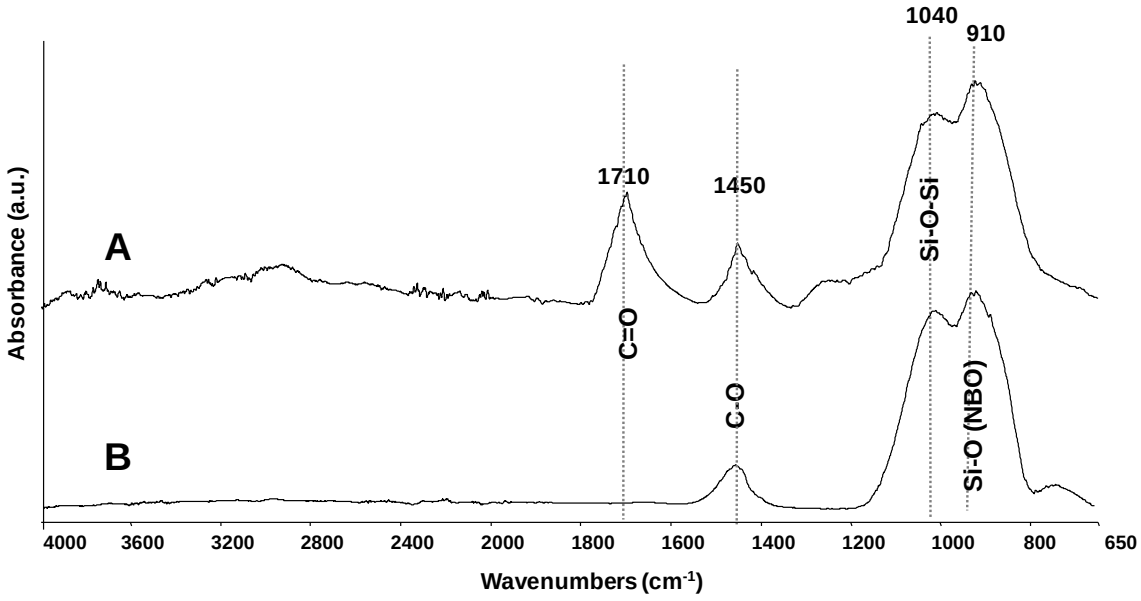

Figure 5-10: FTIR spectra of PAA-BAG (A) and BAG (B) powders showing the peaks assigned to Si-O-Si vibrational modes of BAG in both spectra. An additional peak at 1710 cm^{-1} assigned to the C=O of PAA appeared in (A).

The results of the bioactivity test of BAG and PAA-BAG powders are presented in Figure 5-11 and Figure 5-12 respectively. A shift in the main peak was monitored in both powders as a result of growing phosphate component (Cerruti et al., 2005; Aina et al., 2009). The non-bridging oxygen Si-O-NBO disappeared due to the loss of soluble silica within BAG and PAA-BAG powders (Peitl Filho et al., 1996). Double peaks at 570 and 600 cm^{-1} related to a P-O bending vibrational mode within the crystalline hydroxyapatite layer could be recognized in BAG powder (Figure 5-11-B) (Hench and Wilson, 1993). However, those double peaks did not appear in PAA-BAG, but were replaced with one peak at 570 cm^{-1} (Figure 5-12-B). The intensity of this peak was lower than those of the double peaks observed in the BAG spectra.

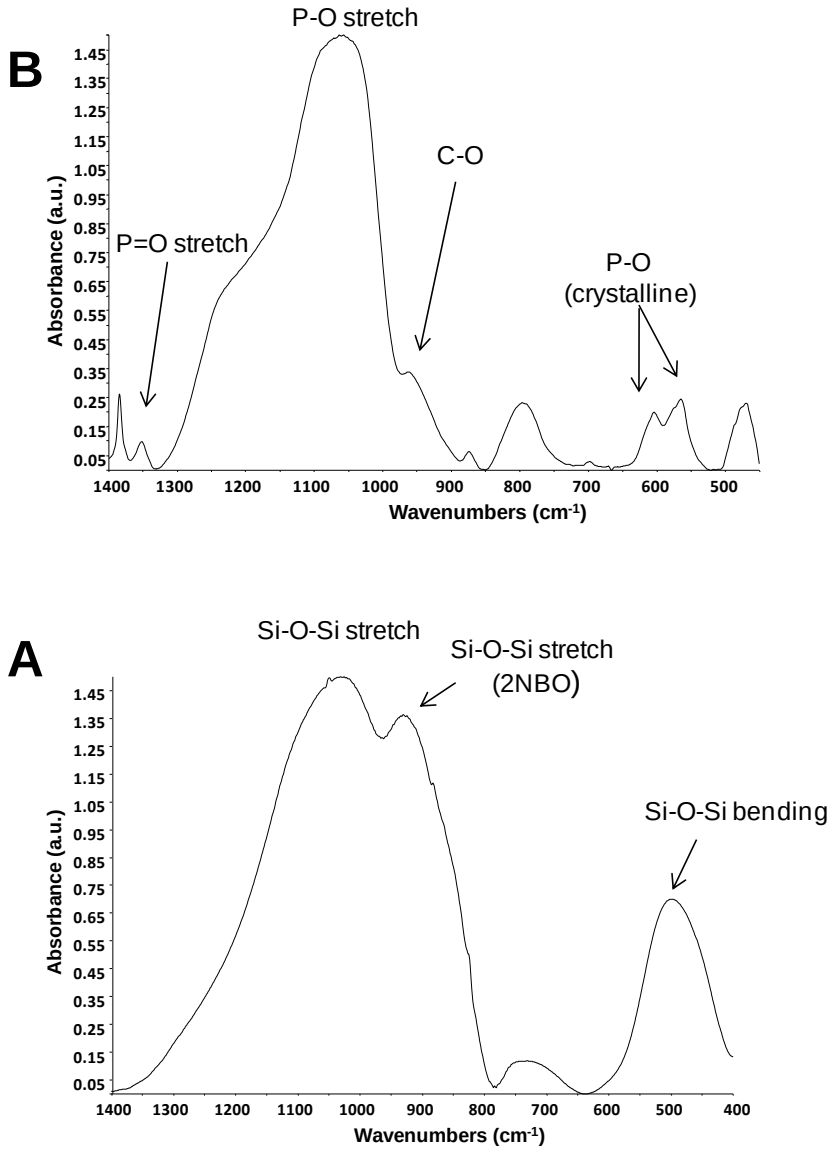

Figure 5-11: FTIR spectra of BAG powder (d_{10}=1.98, d_{50}= 10.88, d_{90}=20.84 µm) before (A) and after soaking in Tris-buffer solution for 20 hours (B). The baseline spectrum presented prominent peaks assigned to Si-O-Si vibrational modes, whilst the spectrum of reacted powder presents double peaks assigned to the P-O bending vibrations of PO_4^{3-} in crystalline calcium phosphate layer.

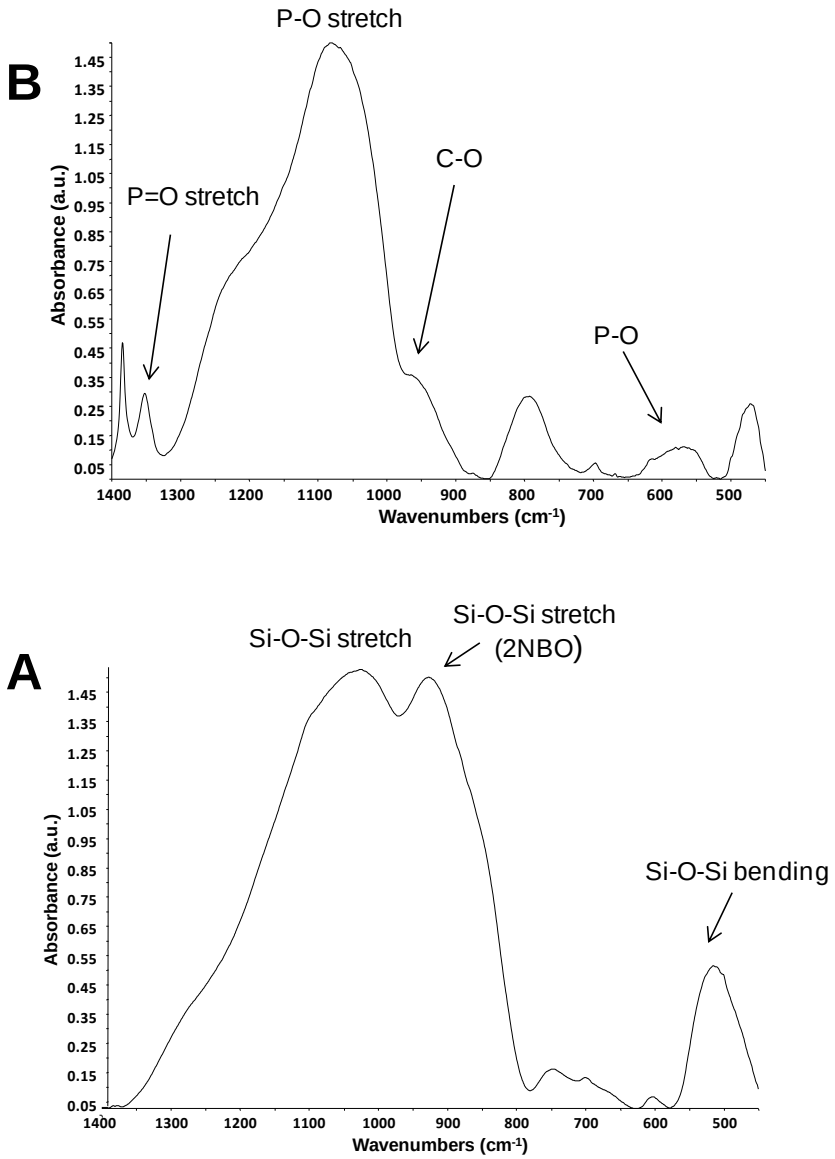

Figure 5-12: FTIR spectra of PAA-BAG powder before (A) and after soaking in Tris-buffer solution for 20 hours (B). The baseline spectrum presented prominent peaks assigned to Si-O-Si vibrational modes, whilst the spectrum of reacted powder presents one peak at 570 cm^{-1}.

5.3.3 Results: surface and cross-sectional microhardness measurements

Knoop microhardness measurements of sound enamel showed consistent values (p>0.05) within the experimental groups prior to commencing the remineralisation therapies. The sound enamel Knoop microhardness was 329.5±23.1 KHN (mean±SE) within the BAG group, 307.5±20.9 KHN in the PAA-BAG group, 299.9±22.0 KHN in the remineralisation solution group and 326.1±21.4 KHN for the negative control group.

The means and the standard errors of lesion microhardness measurements are shown in Figure 5-13. The treated enamel lesions using BAG slurry, PAA-BAG slurry and standard remineralisation solution exhibited significantly higher (p<0.05) surface microhardness when compared to the negative control group. The BAG group exhibited the highest surface Knoop microhardness (138.3±4.7) KHN, but with no statistically significant differences compared to PAA-BAG (114.8±4.5 KHN) and remineralisation solution (131±16.4 KHN) groups (p>0.05). The cross-sectional Knoop microhardness in the negative control group was significantly less (p<0.05) than those in the BAG, PAA-BAG and remineralisation solution groups. The highest cross-sectional Knoop microhardness was found within the remineralisation solution group (77.3±10.6 KHN), but with no statistically significant differences (p>0.05) to BAG (64.2±2.7 KHN) and PAA-BAG (62.2±5.1 KHN) groups.

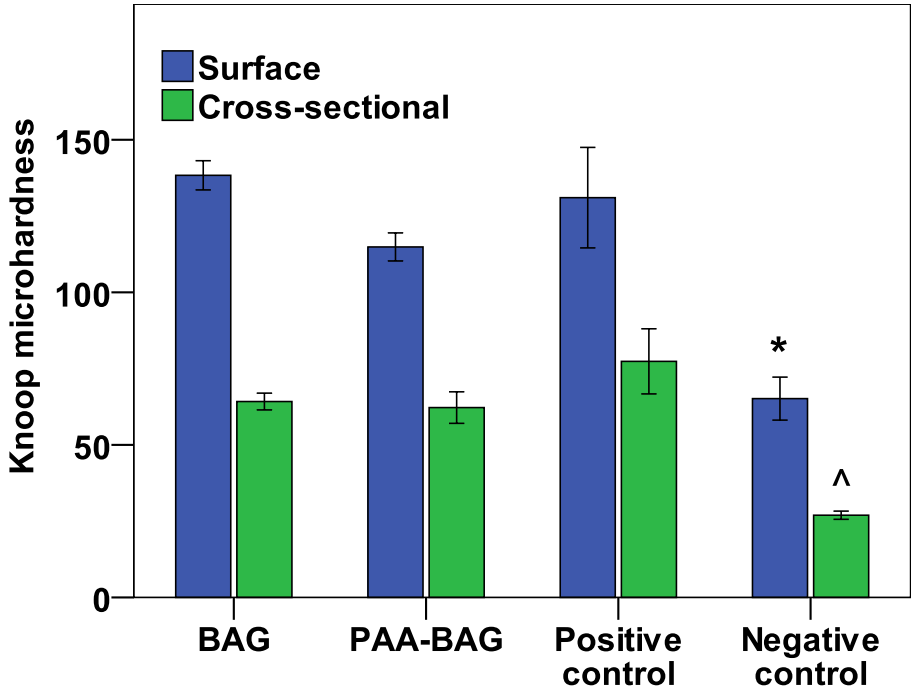

Figure 5-13: Mean±SE of surface and cross-sectional Knoop microhardness according to the remineralisation therapy. (*) indicates statistically significant difference in the surface Knoop microhardness between the negative control and the remaining groups. (^) indicates statistically significant difference in the cross-sectional Knoop microhardness between the negative control and the remaining groups.

5.3.4 Results: Raman micro-spectroscopy

Representative Raman spectra of sound and demineralised enamel within the same sample are presented in Figure 5-5-B; p: 126. The four internal vibration modes of phosphate (PO_4^{3-}) within the enamel were observed as peaks at 433 cm^{-1} (symmetric bending vibrational mode - PO_4^{3-} v_2), 579 cm^{-1} (asymmetric bending vibrational mode - PO_4^{3-} v_4), 959 cm^{-1} (symmetric stretching vibrational mode - PO_4^{3-} v_1) and 1029 cm^{-1} (asymmetric stretching vibrational mode - PO_4^{3-} v_3). All those peaks were observed within sound and demineralised enamel spectra with no difference in their positions, but with a considerable reduction in the peaks' intensity within the demineralised enamel compared to the sound. The strongest peak along sound and demineralised enamel spectra was that of v_1 PO_4^{3-} at 959 cm^{-1}.

The percentage of phosphate peak intensity within the lesion varied significantly according to the remineralisation therapies (p<0.05). The means and the standard errors of lesion phosphate peak intensity percentage are presented in Figure 5-14. The phosphate peak intensity percentage within the lesion compared to that of the deeper sound enamel in the negative control group was 38.18±1.7% (mean±SE), significantly less (p<0.05) than that of BAG group (48.93±2.7%), PAA-BAG (49.1±2.6%) and remineralisation solution (50.19±3.5%). However, the treatment did not reduce the lesion depth significantly (p>0.05) compared to that of the negative control group. The lesion depth was 81.4±3.2 µm (mean±SE) within the negative control group, 66.7±3 µm in the BAG group, 75.1±6.5.1 µm in the PAA-BAG group and 67.6±4.8 µm for the remineralisation group.

Representative grey-scale images and depth profiles of PO_4^{3-} v_1 peak intensity are presented in Figure 5-15. Overall, there was a considerable drop in the depth profile in all groups within the lesion area (125 – 200 µm) compared to the deep sound enamel area (≥200 µm) which in turn, presented similar intensity profiles within all the samples tested. The depth profiles within the negative control group exhibited larger distances between the lesion and deeper sound enamel steps, in the vertical direction, compared to the other groups implying that less phosphate content was present within the lesion. The depth profiles of BAG and the remineralisation solution showed a sharp peak within the lesion step, whilst

within PAA-BAG depth profiles the phosphate peak intensity increased along the whole lesion depth.

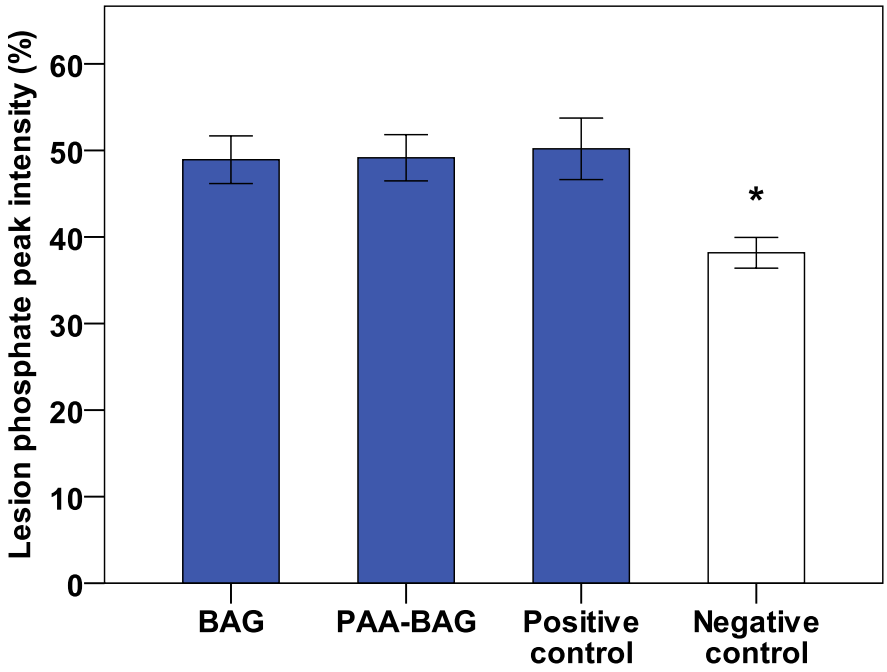

Figure 5-14: Mean±SE of phosphate peak intensity percentage within the lesion according to the remineralisation therapy. (*) indicates statistically significant difference between the negative control and the remaining groups.

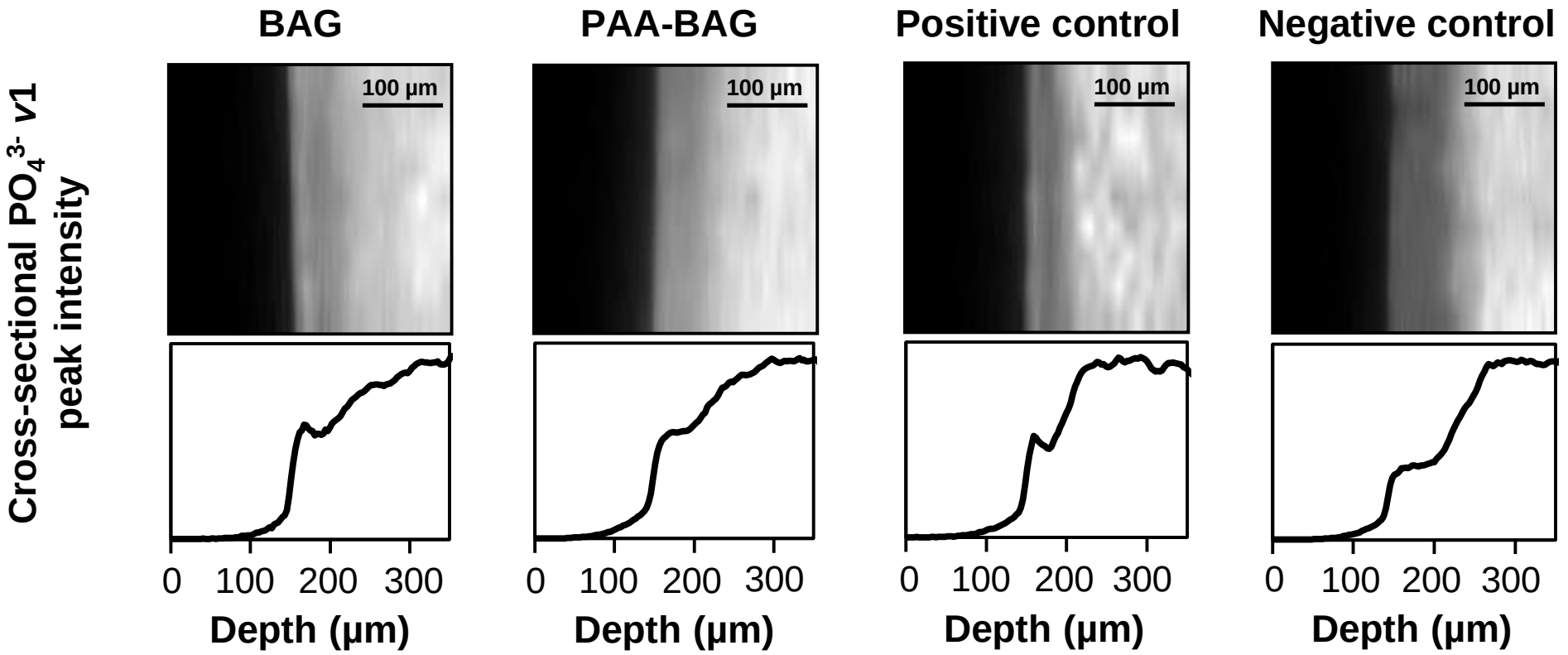

Figure 5-15: Representative grey-scale images and depth profiles of phosphate peak intensity according to the treatment. A variance in the height / shape of the lesion step, within the depth profile, can be detected between the experimental groups.

5.3.5 Results: profilometric analysis

A representative 3D view of the sample surface showing the lesion in the centre surrounded by sound reference enamel is presented in Figure 5-16. Using BAG and PAA-BAG as a slurry did not damage the surface layer of the lesion as the profilometry step height difference measurement of lesion surface before and after treatment showed no statistically significant difference (p>0.05) within all experimental groups; (0.64±0.29 µm) (mean±SE) in the BAG group, (0.78±0.24 µm) for the PAA-BAG group, (0.56±0.24 µm) within remineralisation solution group and (0.46±0.20 µm) in the negative control group.

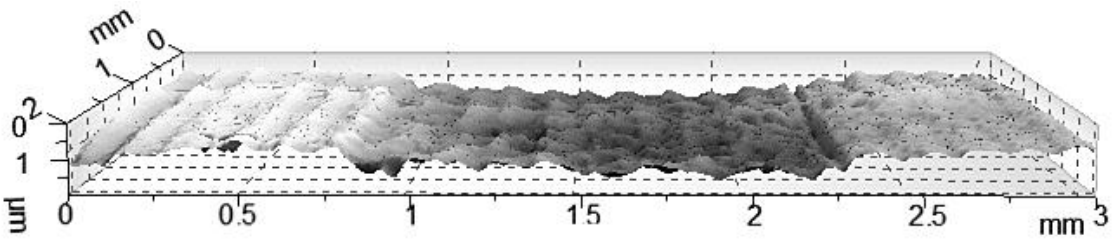

Figure 5-16: Representative 3D profilometry image of the surface shows the lesion in the centre surrounded by sound enamel acting as a reference level for step height measurements.

5.3.6 Results: SEM

Representative SEM images of samples from each of the four experimental groups are shown in Figure 5-17. Variance was detected between the negative control and the remaining experimental groups. The lesion surface in the negative control exhibited porosity resulting from the demineralisation process, with no evidence of mineral deposition (Figure 5-17-A). SEM images of BAG exhibited mineral depositions with large plate-like structures and small cubic structures (Figure 5-17-B). The mineral precipitations were smaller within the PAA-BAG compared to the BAG group with small flake-like structures blocking completely the porous lesion surface (Figure 5-17-C). Small rounded particles covering the lesion surface were observed in the remineralisation solution group (Figure 5-17-D).

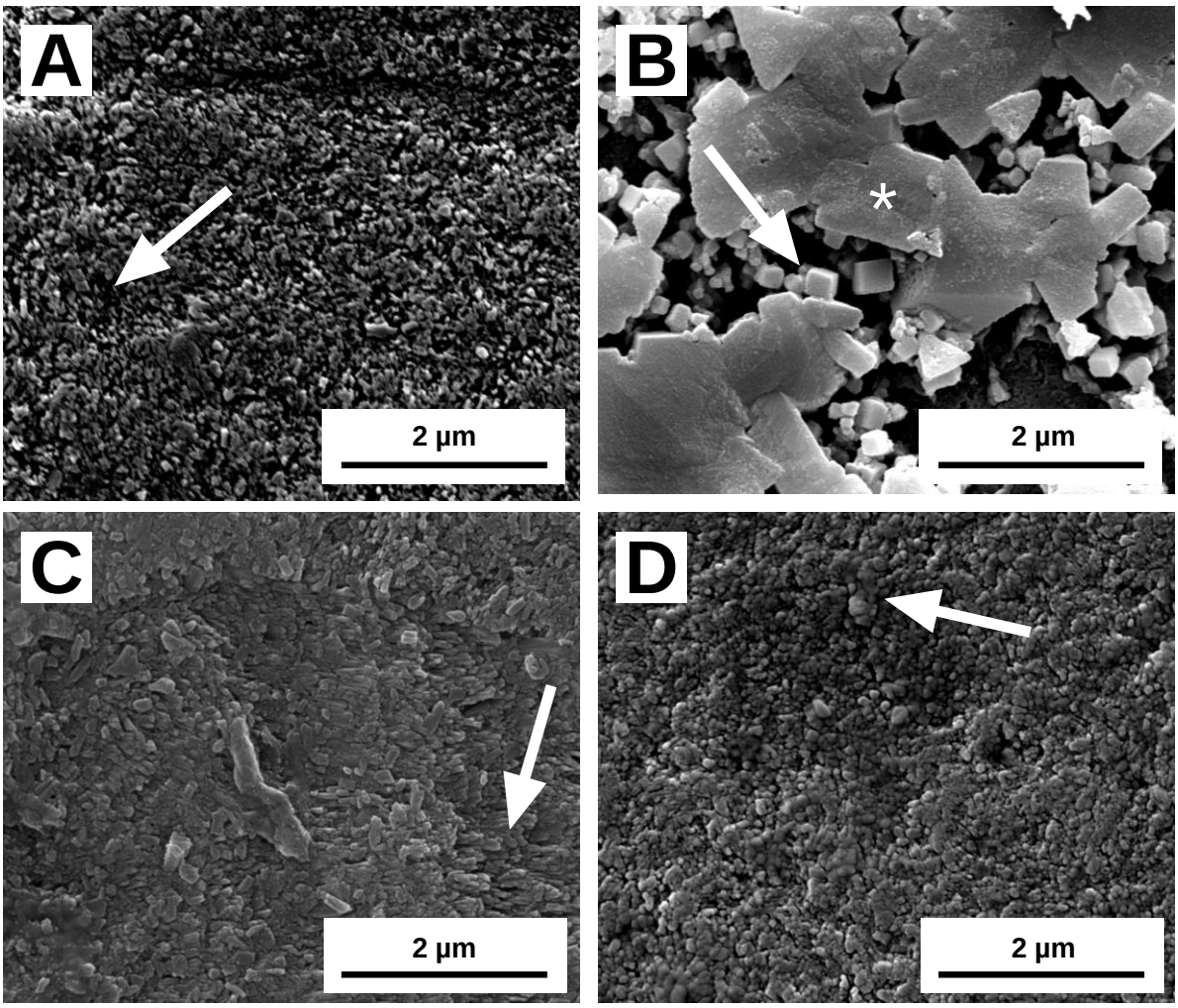

Figure 5-17: Representative SEM images of lesion surface according to the treatment (at 50,000x magnification). (A): lesion surface within the negative control group exhibits porosity (arrow) with no mineral depositions. (B): mineral precipitations with large plate-shape (star) and small cubic-shape (arrow) structures in BAG group. (C): small flake-like structures covered and blocked the surface porosity in PAA-BAG group (arrow). (D): small rounded particles (arrow) within the positive control group.

The cross-sectional views of PAA-BAG (Figure 5-18-B) showed a layer of mineral covering the lesion surface, whilst no evidence of remineralisation was detected within the negative control group (Figure 5-18-A). The high magnification images of the cross-sections showed flake-like structures attached and embedded to the lesion surface within the PAA-BAG group (Figure 5-18-B).

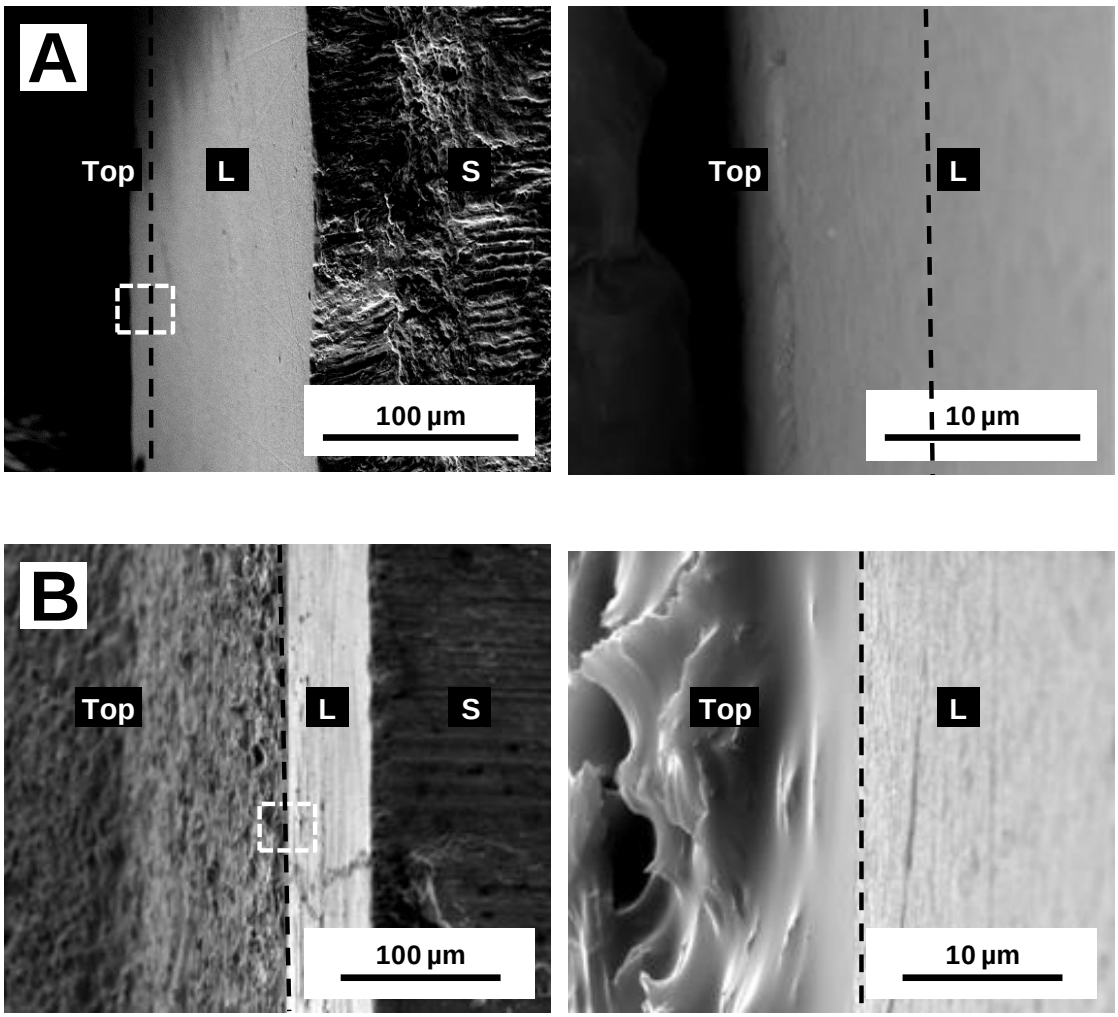

Figure 5-18: SEM images of cross-sections within the negative control and PAA-BAG groups at 800x (left) and 10,000x (right) magnifications. The broken line determines the border between the cross-sectional view and the lesion surface (top). The lesion surface within PAA-BAG (B) is covered with a layer of flake-like structures in contrast to that of the negative control which showed no mineral precipitations (A). Higher magnification of the outer edge of the lesion showed the mineral structures attached to the lesion surface within PAA-BAG.

5.4 Discussion

5.4.1 Sample preparation

Natural enamel WSLs exhibit a wide variety in shape, size and mineral content (Huang et al., 2007; Cochrane et al., 2012a). These variations have a marked influence on the effect of remineralisation therapy since the absolute amount of mineral gain is negatively correlated to the baseline mineral content of the lesion (Strang et al., 1987; White et al., 1988; Lynch et al., 2007). A study conducted by Silverstone et al. (1981), to compare the remineralisation between natural and artificial WSLs in human dental enamel, revealed large differences in remineralisation outcomes of natural lesions compared to those of artificial lesions which followed a similar trend in reminerlistion rate. In order to avoid the inherent biological variations in populations of natural WSLs, artificial lesions have been created for use in in-vitro remineralisation studies. Different methods have been described in the dental literature to create artificial enamel carious lesions (see Table 1-9; p: 50).

The protocol used in this study to produce WSLs is based on using a thick methyl cellulose gel layer over the enamel surface (Figure 5-3; p: 121) to slow the attack of lactic acid, thus altering the rate of dissolution in a manner so that it becomes slower at the enamel surface and higher at the subsurface level (Gray, 1966; Silverstone, 1967; Holly and Gray, 1968; van Dijk et al., 1979). The lesion created using this protocol has been described as a subsurface enamel carious lesion as it exhibits an intact outer surface and a reduced depth when compared to those created using other protocols (Magalhaes et al., 2009). The OCT images revealed that the lesions exhibited an intact surface layer and extended approximately to 70-100 µm. Those features are similar to those of natural enamel white spot lesions.

After tooth eruption, changes occur in the outermost enamel layer as it is hyper-mineralised by fluoride and salivary ions during the dynamic balance of de- and remineralisation processes in the oral environment (Weatherell et al., 1972; Wilson and Beynon, 1989). Removing the outermost layer prior to creating artificial WSLs is a well-documented procedure that helps in creating more consistent, reproducible enamel lesions and reduces the variation between the biological samples (ten Cate and Duijsters, 1982; White et al., 1988; Weir et al.,

2012). The TSM micrographs showed the removal of the aprismatic layer and the exposure of enamel prisms in the polished sound and demineralised enamel surfaces.

5.4.2 Powder preparation, bioactivity testing and remineralisation therapy

The further purpose of this study was to use the tested powders in air-abrasion technology to treat and pre-condition carious tissues using bioactive materials so potentially enhancing the following remineralisation therapies (see Chapter 6). A pilot study showed that using BAG (d_{10}=24, d_{50}=60 and d_{90}=92 μm) as an abrasive powder was inefficient in pre-conditioning the WSL surface rather than cutting it and therefore, significantly a smaller BAG 45S5 powder (d_{10}=1.98, d_{50}= 10.88 and d_{90}=20.84 μm) was selected for this purpose. The use of BAG 45S5 in enamel remineralisation is at an early stage of development compared to other well-investigated and documented remineralisation systems such as fluoride or CPP-ACP implying that further evaluations are still required (Zero, 2006; Reynolds, 2008; Rehder Neto et al., 2009; Walsh, 2009; Cochrane et al., 2010; Li et al., 2014). In the present study, the chemical, mechanical and ultra-structural changes within enamel WSLs remineralised using BAG or PAA-BAG slurry were evaluated using positive and negative controls permitting accurate comparisons throughout.

PAA powder has been introduced into BAG 45S5 powder in order to modulate the cutting efficiency of air-abrasion and to reduce the micropermeability between the dentine and the adhesive layer so enhancing the bond durability (Sauro et al., 2012b). The incorporation of PAA into bioactive materials interacts in the nucleation / growth of HA crystals (Kamitakahara et al., 2001; Yli-Urpo et al., 2005; Liu et al., 2011; Niu et al., 2014). It has been assumed that the (–COOH) functional group of PAA mimics the carboxyl terminal regions of non-collagenous proteins in binding the calcium and phosphate ions to form nano-precursors small enough to penetrate the carious lesion more effectively (Tay and Pashley, 2008; Qi et al., 2012). The FTIR spectra of reacted PAA-BAG did not show the double peaks of the crystalline calcium phosphate layer at 570 cm^{-1} and 600 cm^{-1} which appeared in the FTIR spectra of reacted BAG. Alternatively, a single peak was observed in the spectrum at this region indicating that the addition of PAA to the BAG particles affected the rate at which the glasses' calcium phosphate

crystallises. Adding PAA to BAG, however, did not inhibit the dissolution of the glass and the growing of the phosphate component since the FTIR spectra of reacted PAA-BAG exhibited:

1. a shift in the main peak from 1030 cm^{-1} to 1070 cm^{-1} representing the growing phosphate component (Cerruti et al., 2005),
2. a dissolution of non-bridging oxygen Si-O-NBO due to the loss of soluble silica (Peitl Filho et al., 1996),
3. the presence of C-O vibrational peak, associated with the incorporation of carbonate anions in the apatite crystals (Hench and Wilson, 1993),
4. a peak at 13050 cm^{-1} assigned to the P=O vibrational mode (Peitl et al., 2001).

In the present study, PAA was not included in BAG processing and therefore, it was not released from BAG particles, but interacted with reacted BAG agglomerates. The concentration of PAA was selected depending on an earlier pilot study which considered using PAA-BAG as an air-abrasive to pre-condition enamel WSLs. Both the flowability as well as the abrasiveness of the PAA-BAG composition, used in this study, were deemed suitable to pre-condition enamel WSLs prior to the following remineralisation therapy.

5.4.3 Surface and cross-sectional microhardness measurements

The mineral content change of remineralised carious lesions does not reflect necessarily a functional mechanical recovery (Bertassoni et al., 2009). Therefore, the biomechanical properties of remineralised lesions should be evaluated to assess the tissue integrity. From a clinical perspective, hardness is one of the main methods used by practitioners to assess carious lesions (White et al., 1988; Banerjee et al., 2010). Microhardness measurement introduces indirect, quantitative information about the de- and remineralisation of enamel WSLs (Section 1.3.3.2; p: 65). The cross-sectional measurement in the present study was conducted 30 µm away from the outer lesion surface due to the size of the Knoop indenter and to the reduced depth of the lesion itself which did not allow accurate measurement other subsurface levels. The results indicated that the lesion surface microhardness was considerably higher than the equivalent cross-sectional measurement within all experimental groups. In the negative control group, this could be explained as the WSLs exhibit increased porosity and

demineralisation at the subsurface level (Robinson et al., 2000). Raman micro-spectroscopy analysis showed that much of the “new” minerals were formed and deposited at the superficial part of the lesion rather than the lesion body, which in turn can explain the increased surface microhardness compared to cross-sectional measurement within the remineralisation groups.

BAG, PAA-BAG and the positive control groups exhibited higher surface and cross-sectional Knoop microhardness values compared to the negative control group. A previous study showed that WSLs created within bovine enamel slabs and treated using BAG paste had significantly higher surface microhardness than the untreated lesions (Burwell et al., 2009b). Sound enamel surface submitted to acid solutions and treated with BAG 45S5 particles also presented higher surface and cross-sectional hardness when compared to the negative control group (Dong et al., 2011; Deng et al., 2013). This mechanical improvement might reflect the “new” mineral deposition within the lesion, resulting from BAG 45S5 bioactivity process that forms HCA structures.

5.4.4 Raman micro-spectroscopy

Raman micro-spectroscopy is a non-destructive sample preparation technique, with a linear response to chemical concentration and label-free analytical method (Tsuda and Arends, 1997). This method was used in this study to measure the phosphate content along the cross-sections of enamel WSLs. The use of the StreamLine™ technique in the present study permitted the acquirement of 1740 spectrum per sample in a relatively short time (approximately 15 min). The StreamLine™ mapping technique has been shown to be 3-7 times faster than conventional point-by-point serial scanning (Hutchings et al., 2008; Hedoux et al., 2011). In this system, the sample is stepped along an illuminated laser line synchronously with the data read out, thus reducing the dead time between sequential data points (Hutchings et al., 2009).

Increasing the number of spectra exhibits an advantage in obtaining a more representative dataset of the scanned sample. The Raman charge-coupled device (CCD) records the back scattered beam from each point and projects it as a Raman spectrum for each designated point to produce a Raman chemical image whereby, every point is represented by its own Raman spectrum that

indicates the chemical composition of the sample at that point (see Figure 5-5-A; p: 126). The number of Raman spectra acquired in this study for each sample (1740) is considerably higher than those reported in previous studies evaluating enamel carious lesions, Ko et al. (2005) acquired 81 spectra, Gilchrist et al. (2007) recorded 9 spectra, Mohanty et al. (2012) measured 50 spectra and Spizzirri et al. (2012) scanned 10 spectra per sample.

The phosphate Raman peaks were observed within Raman spectra at the same positions detected in the literature (Tsuda and Arends, 1997; Awonusi et al., 2007). Peak intensity evaluation has been reported as a suitable parameter to detect a difference between sound and demineralised enamel regions (Ko et al., 2005). In the present study, the phosphate peak intensity within the demineralised enamel was compared to that of the deeper sound enamel within the same sample, acting as a reference area. The lesion presented 40% phosphate peak intensity compared to the deeper sound enamel in the control group. This drop in the depth profile extended to approximately 80 µm depth. These depth profile features, of phosphate peak intensity within artificial enamel white spot lesions, are consistent with those described in a previous study (Mohanty et al., 2012).

Scanning the demineralised enamel lesion produced a small amount of autofluorescence. In order to consider the background fluorescence in each Raman spectrum, the PO peak was fitted by the means of in-house software using a Gaussian function and a first order polynomial. Fitting the spectrum peaks is a well-documented procedure in Raman analysis prior to any further measurement (Awonusi et al., 2007; Atmeh et al., 2012; Salehi et al., 2012; Jegova et al., 2013; Toledano et al., 2014). In the present study, the combination of high spatial resolution (2.7 µm), rapid map acquisition with an efficient curve fitting and data analysis software provided a unique analytical technique to characterise the mineral changes in the treated WSLs.

The measurement of Raman phosphate peak intensity at 959 cm^{-1} has been used previously to assess the demineralisation degree in enamel and dentine caries (Tsuda and Arends, 1997; Tramini et al., 2000; Kinoshita et al., 2008; Almahdy et al., 2012). This study translated this measurement to detect the phosphate increase in WSLs following the remineralisation therapy. The statistical analysis,

the grey-scale images and depth profiles of PO_4^{3-} v_1 peak intensity measurement showed that the remineralisation therapies increased significantly the phosphate content within the lesion when compared to the negative control group. A previous study has reported the appearance of the PO_4^{3-} v_1 peak at the early stage of the remineralisation process within cartilage tissue (Sauer et al., 1994). The appearance of this peak was also used to detect the formation of HA on the calcium silicate pill after treatment in phosphate buffer at pH 7 (Parker et al., 2014). The spectral characteristic of the HCA layer formed on the reacted BAG 45S5 presented a peak at 959 cm^{-1} within the Raman spectrum assigned to P-O symmetric vibration of the PO_4^{3-} groups (Rehman et al., 1994; Notingher et al., 2002). The amount of the formed HAC can be estimated by evaluating the intensity of this peak (Rehman et al., 1994).

Treating BAG particles with an aqueous solution causes a leaching and exchanging of BAG ions with those in the solution and that in turn increases the interfacial pH followed by breaking Si-O-Si bonds and forming a $Si(OH)_4$ layer. Calcium and phosphate ions are released from BAG, at this stage, to form an amorphous CaP layer, which is crystallised to HCA (Hench and Wilson, 1993). Raman phosphate peak intensity percentages were significantly higher within BAG and PAA-BAG groups compared to that of the negative control group implying that more phosphate ions were presented as a result of remineralisation therapy. The bioactive process of BAG and the precipitation of minerals at the lesion surface, observed in SEM images, can explain the higher Raman phosphate peak intensity monitored in the present study.

5.4.5 Profilometry analysis

Protecting part of the sound enamel using an adhesive tape is a documented in-vitro procedure to establish a reference level when analysing the profilometry 3D images (Barbour and Rees, 2004; Kielbassa et al., 2005; Tostes et al., 2013). Profilometry is a “gold standard” method in assessing the surface loss providing objective quantitative information about the surface topography. BAG and PAA-BAG were applied as slurries, without mechanical agitation, to avoid any damage to the lesion structure, and this was confirmed by profilometric analysis. The profilometry results imply that the improvement in the mechanical and chemical measurements of the treated lesions occurred within the structure of the lesion

and not as a result of damaging histologically, the lesion morphology and exposing the deeper intact tissue. This also indicates that the reduction in the lesion depth reported in the Raman dataset has occurred within the lesion and not as a result of abrading the outer surface layer.

5.4.6 SEM

Even though the lesion surface was rinsed prior to SEM analysis, mineral deposits were detected in the SEM micrographs within the BAG, PAA-BAG and remineralisation solution groups implying that the observed structures attached to lesion surface. This attachment was also observed in the cross-sectional images, when minerals were observed to be embedded into the outer edge of the treated lesion. The development of a negative surface charge at the surface of BAG 45S5 particles during the reactivity process forms a strong attraction with the tooth surface (Greenspan and Hench, 2013), which may explain the retention of the minerals on treated WSL surfaces in spite of the post-treatment cleaning regimen.

Gjorgievska et al. (2013) reported that the SEM micrographs of artificial enamel WSLs remineralised using BAG 45S5 paste showed the bioactive glass deposits sealing the enamel irregularities. In another in-vitro study, applying BAG 45S5 during enamel bleaching with 35% hydrogen peroxide formed flower-like crystallites on the enamel surface (Deng et al., 2013). It has been recently demonstrated that treating erosive-like lesions with a suspension of BAG 45S5 and phosphoric acid formed densely packed crystalline structures on the enamel surface (Bakry et al., 2014b). Submitting this layer to a brushing-abrasion challenge (6000 cycles under a load of 250 g) mimicking the abrasion conditions in-vivo did not affect significantly the percentage of enamel coverage with this crystalline layer (Bakry et al., 2014b).

In the current study, the plate-like structures observed in the SEM images of the BAG group are comparable to the apatite crystal shapes induced by 45S5 BAG (Kokubo, 1990; Li et al., 1993; Wen et al., 1999; Zhong et al., 2002). When the WSLs were treated with the remineralisation solution, rounded structures were observed in the SEM micrographs, in agreement with a previous study reporting the same mineral shape using this remineralisation solution (Collys et al., 1991).

The mineral precipitations formed within the PAA-BAG group were significantly smaller than those of the BAG group. When PAA was used with Portland cement to remineralise acid-etched dentine slabs, smaller structures were also observed (Tay and Pashley, 2008). Theoretically, the smaller minerals have a potential to penetrate the lesion surface enhancing the remineralisation along the whole lesion depth. As mentioned earlier, PAA may interact in the growth / nucleation of HA, and the formation of the small structures might be explained depending on non-classical crystallisation pathway concepts whereby, the Ca and P ions are sequestered by the –COOH of PAA to form amorphous calcium phosphate nano-precursors transformed into small crystalline apatite minerals (Niu et al., 2014). The question of how PAA could modify the shape of the minerals within PAA-BAG composition still needs to be answered. A possible answer could be related to the nucleation sites, mineral extending along its' axes or forming a different mineral phase.

Using BAG, PAA-BAG and a remineralisation solution in the present study did not reduce significantly the lesion depth. This result may be explained as the calcium and phosphate ions' diffusion / precipitation may be restricted to the superficial area of the lesion inhibiting whole lesion remineralisation. This feature has been reported in the literature when different remineralisation agents were applied to treat enamel carious lesions (Beerens et al., 2010; Ferrazzano et al., 2011; Pliska et al., 2012). To overcome this limitation, modifying / pre-conditioning the lesion surface to improve mineral diffusion may be required or even desirable as a clinical intervention before remineralisation therapy (Robinson et al., 1990; Al-Khateeb et al., 2000; Crombie et al., 2013).

5.5 Conclusions

The original null hypothesis was rejected. The results of this study lead to the following conclusions:

1. Treating enamel WSLs using BAG or PAA-BAG slurry improved the mechanical proprieties of the lesion.
2. These remineralisation therapies increased the phosphate content according to the Raman analysis.
3. Mineral depositions at the treated lesion surface were detected in SEM micrographs.
4. BAG and PAA-BAG remineralisation therapies showed similar mechanical and chemical outcomes.
5. Smaller particle precipitations were detected within PAA-BAG compared to the BAG.

The beneficial effect of using BAG and PAA-BAG powders in enamel white spot remineralisation paves the way for further investigation into the clinical application of such materials in the remineralisation of enamel under the auspices of minimally invasive dentistry (MID) which advocates the preservation of repairable enamel structure and the use of remineralisation strategies.

Chapter 6 Remineralisation of in-vitro enamel white spot lesions may be enhanced by their pre-conditioning using bioactive glass air-abrasion.

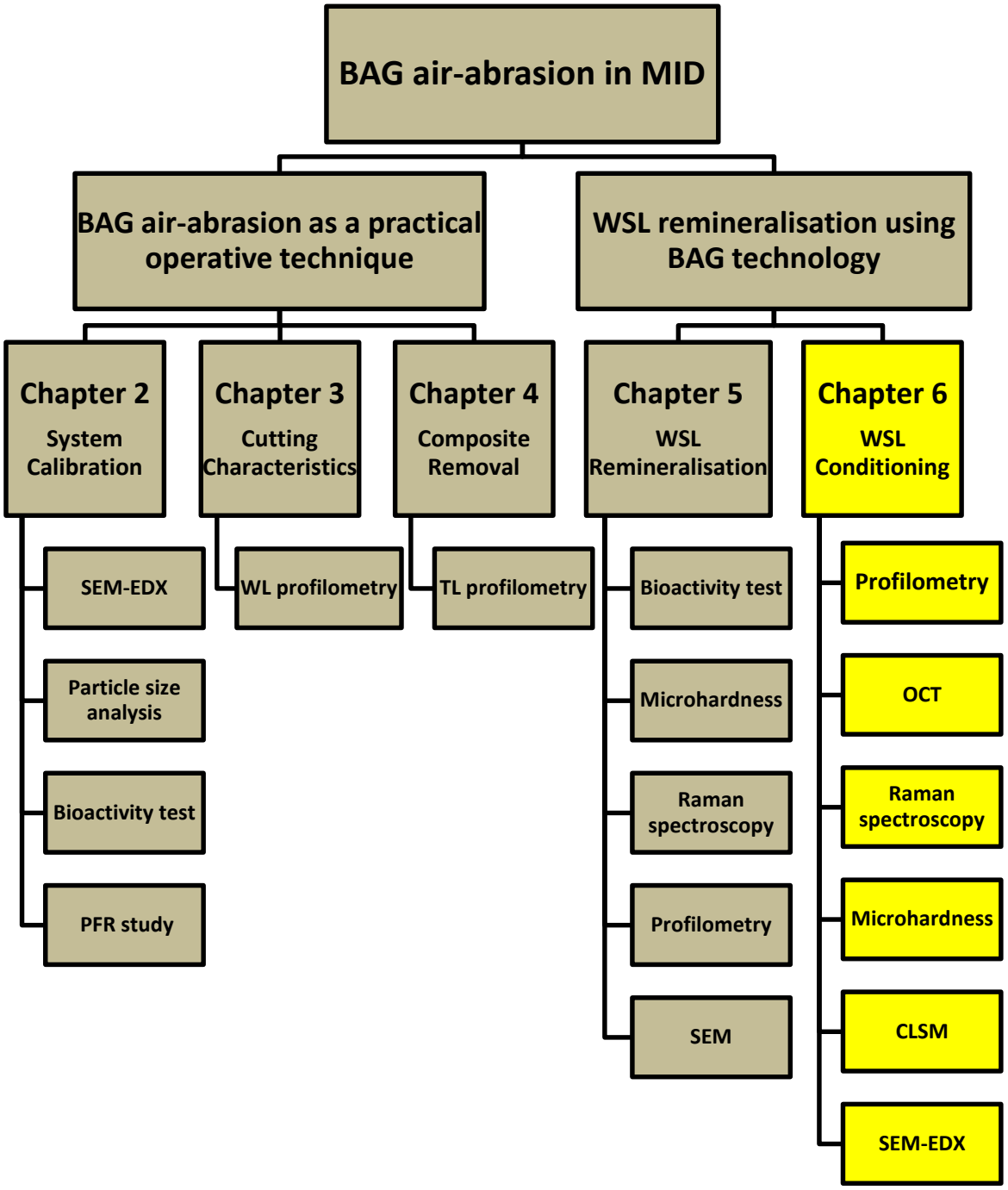

Organisational flowchart of the experiments accomplished in this study.

6.1 Introduction

The optimal goal of minimal invasive dental caries management is to heal the incipient lesion by inhibiting the demineralisation process and enhancing the remineralisation repair process (Featherstone, 2000). The enamel white spot lesion (WSL) results from the physical changes occurring in enamel due to the caries process before it has reached the enamel-dentine junction (EDJ) (Gustafson, 1957). Different protocols have been described to remineralise enamel WSLs including bioactive glass (BAG) 45S5 (see Section 1.2.3.3; p: 51). BAG 45S5 is an inorganic amorphous, calcium, sodium phosphosilicate material which interacts with aqueous solutions such as saliva to form a hydroxycarbonate apatite (HCA) layer, attached chemically to the treated surfaces (Hench, 2013a).

The remineralisation of an enamel WSL is a difficult and slow process both *in vivo* and *in vitro* (White et al., 1988; Larsen and Pearce, 1992). It is a complex physico-chemical process where the remaining mineral crystals are less reactive, covered by salivary proteins and the limited diffusion of ions lessens the net mineral gain within the lesion (ten Cate, 1990). In order to promote the WSL remineralisation process, an additional stage of pre-conditioning the lesion surface with phosphoric acid prior to the remineralisation therapy has been described in the dental literature and shown to increase the remineralisation of WSLs (Collys et al., 1991; Al-Khateeb et al., 2000).

However, there are some limitations with the acid-etching technique in this regard: (a) the demineralisation effect of phosphoric acid can further decalcify and deteriorate the integrity of the lesion structure (Van Dorp et al., 1990), (b) the potential retention of acid remnants following phosphoric acid application may negatively affect the lesion structure (Van Meerbeek et al., 2005), (c) the effect of the phosphoric acid on the WSL is not only limited to the surface layer, but extends to increase the subsurface porosity up to 21 µm (Hicks and Silverstone, 1984a) and (d) the phosphoric acid can affect the sound enamel surrounding the WSL increasing its porosity and thus making it more susceptible to caries (Lee et al., 1995). These factors might explain the infrequent reporting of the use of this procedure to promote the WSL remineralisation in the dental literature. Therefore, presenting an alternative method may be preferable if this can modify the lesion

surface and at the same time minimise the drawbacks outlined above created by the acid-etching technique.

In the present study, air-abrasion with PAA-BAG powder was used to pre-condition the lesion surface as opposed to cutting it, in order to promote remineralisation using different topical therapies including mixtures of BAG 45S5. The objectives of this study were to assess the physical interaction of this surface pre-conditioning and to study the impact of this modification on overall lesion remineralisation. Acid-etching using 37% phosphoric acid was selected as a positive control for the surface pre-conditioning variable. The physical changes were assessed using non-contact white light confocal profilometry and optical coherence tomography (OCT). The mineral content at the lesion surface following the application of the remineralisation therapies was evaluated using Raman micro-spectroscopy used in a StreamLine^{TM} scanning technique to map the lesion surface measuring the v-$(CO_3)^{2-}$/v_1-$(PO_4)^{3-}$ ratio of 2880 spectra per sample. The biomechanical properties of the WSLs were assessed using Knoop microhardness testing. Confocal laser scanning microscopy (CLSM), and SEM-EDX were used to study the ultra-structural changes within remineralised artificial WSLs created using bi-layer demineralisation protocol.

The two null hypotheses investigated in this study were:

1. Pre-conditioning the WSL using PAA-BAG air-abrasion has no effect on lesion surface characteristics.
2. Pre-conditioning the lesion surface with PAA-BAG air-abrasion has no effect on remineralisation therapy using BAG 45S5.

6.2 Materials and methods

6.2.1 Materials and methods: sample preparation

Caries-free human molars were stored in refrigerated de-ionised water and used within a month from the extraction to obtain one buccal enamel slab from each tooth using a diamond wafering blade (XL 12205, Benetec Ltd., London, UK). The slab's initial surface integrity was inspected using a confocal tandem scanning microscope (TSM) (Noran Instruments, Middleton, WI, USA), with a x20 air objective in reflection scanning mode. Ninety samples were included in this study. The samples were included face down in acrylic resin and polished to remove the

outermost layer of the enamel as explained in Section 5.2.1; p: 119 to create more consistent, reproducible artificial enamel lesions.

The flat, polished enamel surface was covered with dental wax to protect part of the enamel leaving an exposed window of 3 x 1 mm in the central area of the exposed enamel slab. The specimens were submitted to a bi-layer demineralisation protocol to create artificial WSLs with an average depth of 70-100 µm as illustrated in Figure 5-3; p: 121. The resultant sample consisted of an artificial WSL at its centre surrounded by sound enamel Figure 5-6; p: 128), which was covered with polyvinyl chloride tape throughout the experiments, and removed at the end of the remineralisation therapies. The samples were assigned to 9 experimental groups according to the surface pre-conditioning and remineralisation therapies tested in this study (n=10; Figure 6-1).

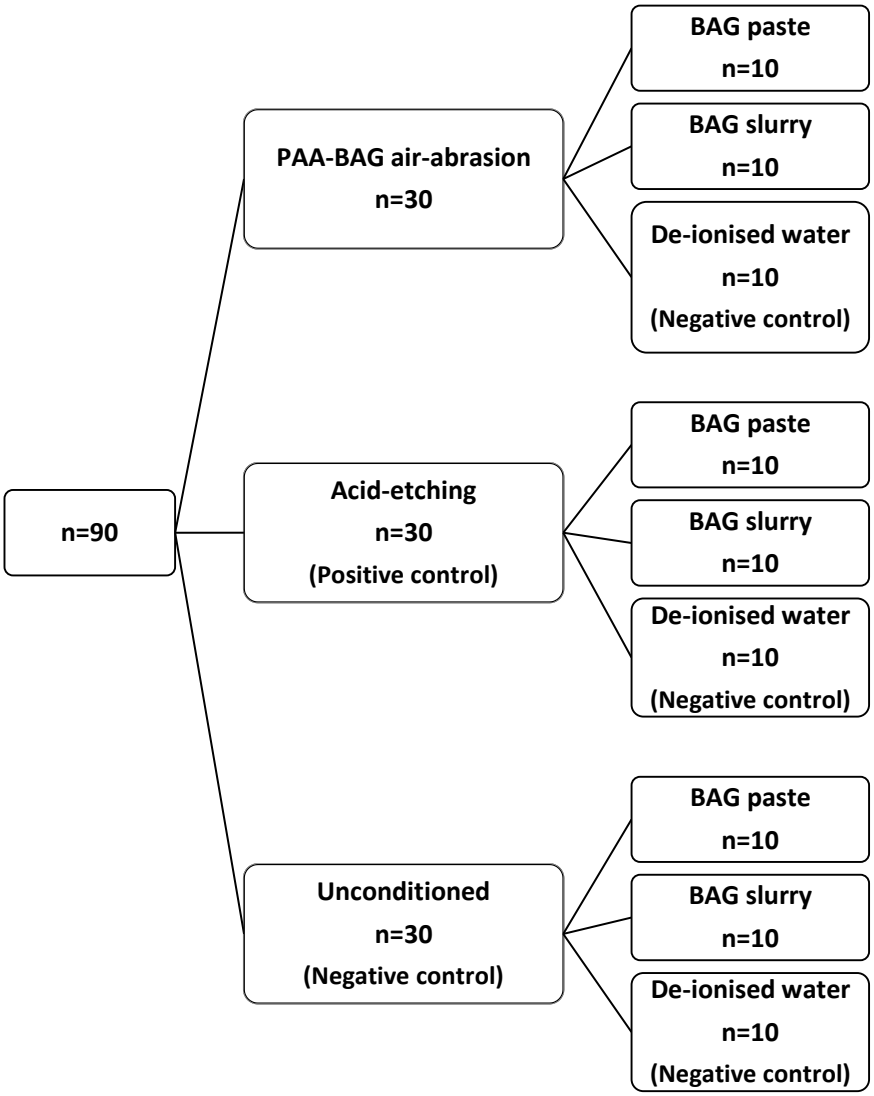

Figure 6-1: A schematic representing the experiential groups according to the experimental procedures.

6.2.2 Materials and methods: surface pre-conditioning

The surface pre-conditioning procedure was conducted once before initiating the remineralisation therapy. PAA-BAG abrasive powder (d_{10}=2.12, d_{50}= 12.05, d_{90}=25.12 µm) was prepared as mentioned in Section 5.2.2; p: 121. An Aquacut™ (Velopex, Harlesden, UK) dental air-abrasion unit was used to pre-condition the lesion surface. The operating parameters of air-abrasion are addressed in Table 6-1. For acid-etching treatment, 35% phosphoric acid gel (3M ESPE Dental Products, St Paul, MN, USA) was applied onto the lesion surface for 30 sec followed by 1 min rinsing with de-ionized water and 5 sec drying with a gentle oil-free air stream using the three in one syringe of a dental unit. The negative control

samples in the surface pre-conditioned groups remained untreated (n=30; Figure 6-1).

Table 6-1: The air-abrasion operating parameters used in this study:

Operating parameters	Parameter value
Air pressure (psi)	20
Powder flow rate (PFR) dial	5 (maximum)
Nozzle angle (degrees)	90
Nozzle-lesion distance (mm)	5
Internal nozzle diameter (µm)	900
Cutting mode	Wet with de-ionised water
Abrasion period (sec)	10

6.2.3 Materials and methods: post-conditioning remineralisation therapy

The remineralisation therapy included the application of a 45S5 BAG paste or a 45S5 BAG slurry (d_{10}=1.98, d_{50}= 10.88, d_{90}=20.84 µm) twice daily (5 min per application) for 21 days. The remineralisation agent was applied onto the exposed WSL surface using a microbrush with hand-agitation by a single operator blinded to the surface pre-conditioning procedure. Following each application, the samples were rinsed thoroughly with de-ionised water and incubated at 37^0C in de-ionised water, which was refreshed at each application for all of the nine experimental groups. The BAG slurry was prepared using de-ionised water (L/P ratio of 1g/ml) prior to the treatment as conducted in Chapter 5. The BAG paste was prepared using the following formula: 36 wt.% BAG 45S5 powder, 25.7 wt.% chalk ($CaCO_3$) and 38.3 wt.% glycerine and stabilisers. This paste did not include water in its composition to prevent any premature BAG chemical reaction. The de-ionised water was introduced into the paste at the lesion surface to initiate the reaction kinetics of BAG particles. At the end of the remineralisation therapies, the protecting tapes were removed and the samples were rinsed with de-ionized water. The negative control of the remineralisation agent was de-ionised water, whilst the positive control was a BAG slurry (100 wt.% BAG particles) relying upon the results of Chapter 5 whereby, this formula has shown to remineralise effectively enamel WSLs when compared to the remineralisation solution.

6.2.4 Materials and methods: profilometry analysis

The samples' surface topography was scanned three times: before surface pre-conditioning, after surface pre-conditioning and finally, post-remineralisation therapy, using non-contact optical white light confocal profilometry (Xyris™ 4000 WL, TaiCaan™ Technologies Ltd., Southampton, UK) with a 10 µm step-over distance and 10 nm vertical resolution. A standard scan area of (3 mm x 2 mm) was chosen over the centre of the surface using proprietary measurement control software (STAGES™, TaiCaan Technologies Ltd., Southampton, England), including the lesion in the middle surrounded by sound enamel from each side acting as internal sample reference levels. The step height of the lesion surface in relation to the sound enamel level was obtained as explained in Section 5.2.6; p: 126.

In order to obtain the average roughness (S_a) of the lesion surface, a further three areas of 250 µm x 250 µm were scanned individually within the lesion surface as shown in Figure 6-2. The scanned area was analysed using Boddies® surface analysis software (Boddies v2.09, TaiCaan Technologies Ltd., Southampton, UK), by levelling the surface into a best-fit plane. Three Sa values were calculated and averaged within each sample at three times as done for step height measurements.

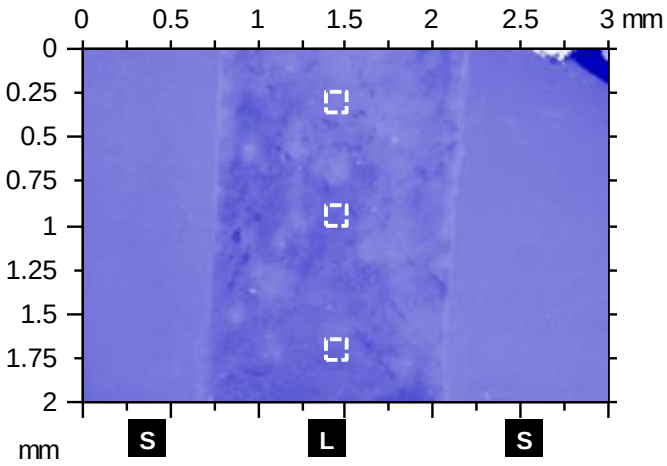

Figure 6-2: 2D view of the scanned area (2 mm x 3 mm) using non-contact profilometry showing the lesion in the centre surrounded by intact sound enamel form each side acting as a reference level for step height measurements. The three delineated areas in the lesion surface (250 µm x 250 µm) were scanned individually to measure the average lesion surface roughness (Sa).

6.2.5 Materials and methods: optical coherence tomography (OCT)

The specimens were scanned prior to surface pre-conditioning and again after remineralisation therapy was complete using OCT (VivoSight, Kent, UK) operating at a 1305 nm central wavelength, 10 kHz rate and 15 mW energy power. This system uses XY mirror sets with multi-beam Z technology in order to maintain the axial resolution over an extended range of depth (Ring et al., 2013; Wang et al., 2013). The lateral resolution is 7.5 µm and the axial resolution is 10 µm in air which corresponds to 6.1 µm in enamel assuming a refractive index (*n*) of 1.63. The OCT beam was oriented perpendicularly and set at a fixed distance over the sample surface by means of a moving stage. For each sample, 50 *b*-scan images were acquired at 5 µm intervals covering an area of (3000 µm x 250 µm) with a pixel size of 3.36 µm x 4.06 µm. The multi-beam scan creates a scan depth of approximately 2 mm.

The 16-bit Tagged Image File Format (TIFF) *b*-scan images were imported into a macro custom-written for the image processing software ImageJ (ImageJ, Maryland, USA) which analysed individual *b*-scans using a polynomial fitting function. Both the air/lesion interface reflection and the average subsurface scattering, up to 40 µm in depth, were recorded for each X and Y sample position (Figure 6-3).

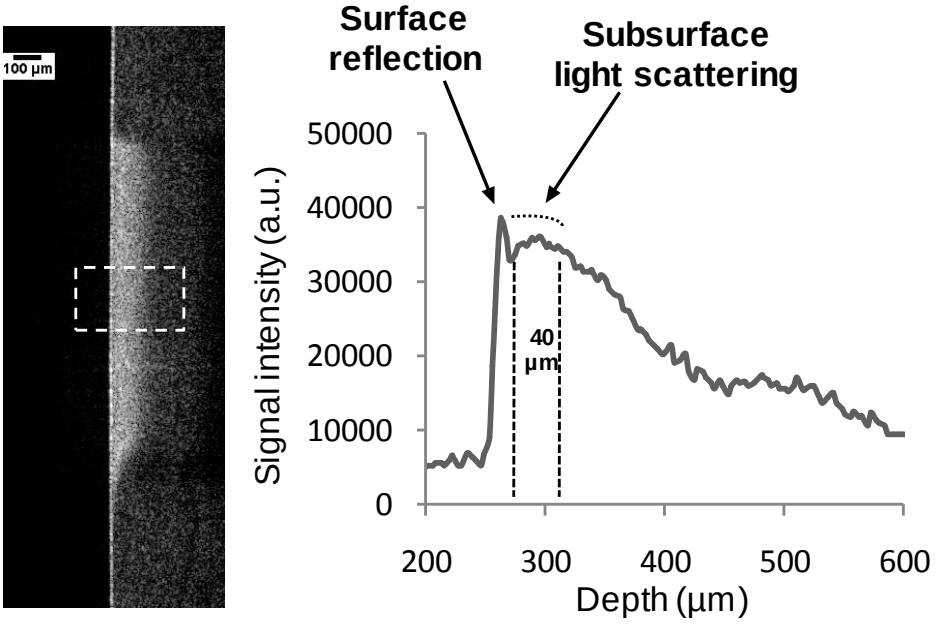

Figure 6-3: Representative OCT-image of WSL and the depth OCT-signal intensity showing the two parameters tested in this study (arrows).

The results of the OCT analysis were exported as 32-bit TIFF grey-scale images. The 32 bits value of each pixel corresponded to the intensity of the OCT signal at this position. The grey-scale images were opened using ImageJ and the average intensity of OCT signal in the WSL was measured from the corresponding image. The subsurface light scattering was normalised to the surface reflection within each sample to be analysed statistically, measuring the reduction percentage in the subsurface light scattering at the end of the remineralisation therapies in comparison with baseline scans.

6.2.6 Materials and methods: Raman micro-spectroscopy

The lesion surfaces were scanned using a Renishaw inVia Raman microscope (Renishaw Plc, Wotton-under-Edge, UK), running in StreamLine^{TM} scanning mode with the same scanning parameters addressed in Section 5.2.5; p: 124. Using the charge-coupled device (CCD) supplied with system, a stitched montage image was created at the middle part of the lesion surface for each sample composing of 2 x 2 images in the vertical and horizontal directions. For each sample, a Raman map was set at the centre of the lesion surface covering an area of 700 x 500 μm^2 and including 2880 spectra acquired with 2.7 µm resolution across the lesion. The demineralised enamel produced a slight background autofluorescence (AF) and therefore, the resultant spectra were exported into in-house curve-fitting software to fit the spectra using a Gaussian function and a first order polynomial.

The intensity of the phosphate peak at 959 cm^{-1} and that of the carbonate peak at 1085 cm^{-1} were measured by the means of in-house Raman analysis software. The results of the peak intensity measurements were exported as 32-bit TIFF grey-scale images. The 32 bits value of each pixel corresponded to the intensity of the peak at this position. For each sample, the grey-scale images of phosphate v_1-$(PO_4)^{3-}$ and carbonate peaks v-$(CO_3)^2$ were opened together using image processing software ImageJ (ImageJ, Maryland, USA) and a new grey-scale image representing the v-$(CO_3)^{2-}$/v_1-$(PO_4)^{3-}$ was generated using “image calculator” function. The mean of the peak ratio intensity was calculated to be analysed statistically.

6.2.7 Materials and methods: Knoop microhardness

A Struers Duramin microhardness tester (Struers Ltd., Denmark) with a Knoop diamond indenter (50 g load applied for 10 sec) produced elongated diamond-shaped indentations which were imaged with a x40 air objective and the Knoop values were calculated from measurements of each long-axis indentation, using the manufacturer's software supplied. Three measurements, 500 µm apart, were recorded and then averaged to measure the lesion surface microhardness of each sample at the end of remineralisation therapies. The instrument was calibrated prior to each measurement session as mentioned in Section 5.2.4; p: 124. Three measurements, 500 µm apart, were recorded and then averaged to measure the lesion surface microhardness of each sample.

6.2.8 Materials and methods: microscopy imaging

Imaging was conducted for three selected experimental groups including, air-abrasion + BAG paste, air-abrasion + BAG slurry and unconditioned + de-ionised water (negative control). For CLSM imaging, three samples from each experimental group were sectioned vertically across the lesion and ground with carborundum paper up to 1200-grit. The samples were soaked in a freshly prepared 0.1 mM Rhodamine-B solution (R6626-Sigma-Aldrich, Dorset, UK) for 24 hours, without further rinsing (Fontana et al., 1996). A confocal laser scanning microscope (CLSM) (Leica Microsystems, Heidelberg GmbH, Germany) was used to image the samples with a x63 oil objective lens in conjunction with a 568 nm excitation wavelength and 640 nm emission filter for the Rhodamine-B (Atmeh et al., 2012). Samples were scanned between 10 and 50 µm below the sectioned surface to avoid the smear layer, created during the cutting procedures (Fontana et al., 1996).

For SEM scanning, three samples from each group were fractured across the WSL to provide a sagittal view without surface grinding or polishing artefact, secured to aluminium stubs and sputter coated with gold (Emitech K550, UK). The fractured surfaces were imaged using an FEI Quanta 200F field emission scanning electron microscope (FEI Co. Ltd., Cambridge, UK), with an accelerating voltage of 10 kV and a working distance of 10 mm. For EDX analysis of the lesion top surface, a further three samples from each group were carbon sputter-coated and scanned using energy dispersive X-ray diffraction (EDAX Inc.,

91 McKee Drive, Mahwah, NJ 07430 USA) to map the emission lines of silicon, sodium, calcium and phosphorus (accelerating voltage of 10 kV, working distance of 12 mm).

6.2.9 Materials and methods: statistical analysis

Statistical analysis was carried out using Stata statistical software (Stata-CorpLP v 11.2, Texas, USA) at p=0.05 significance. Data were tested for normality, and the non-normal data were transformed into the normal using an appropriate transformation prior to further analysis. The profilometry data were tested using two-way analysis of variance (ANOVA) and Tukey's HSD as post-hoc including significant interactions, whilst those of Raman micro-spectroscopy, microhardness and OCT were analysed using linear modelling by including the interaction term for pre-conditioning and remineralisation therapy.

6.3 Results

6.3.1 Results: profilometry analysis

The means and standard errors of the step height measurements at three measurement points are shown in Figure 6-4, Figure 6-5 and Figure 6-7. The average surface roughness (Sa) is presented in Table 6-2. The baseline measurement showed no statistically significant differences in step height and roughness measurements between the nine experimental groups prior to commencing any experimental procedure (p>0.05) (Figure 6-4).

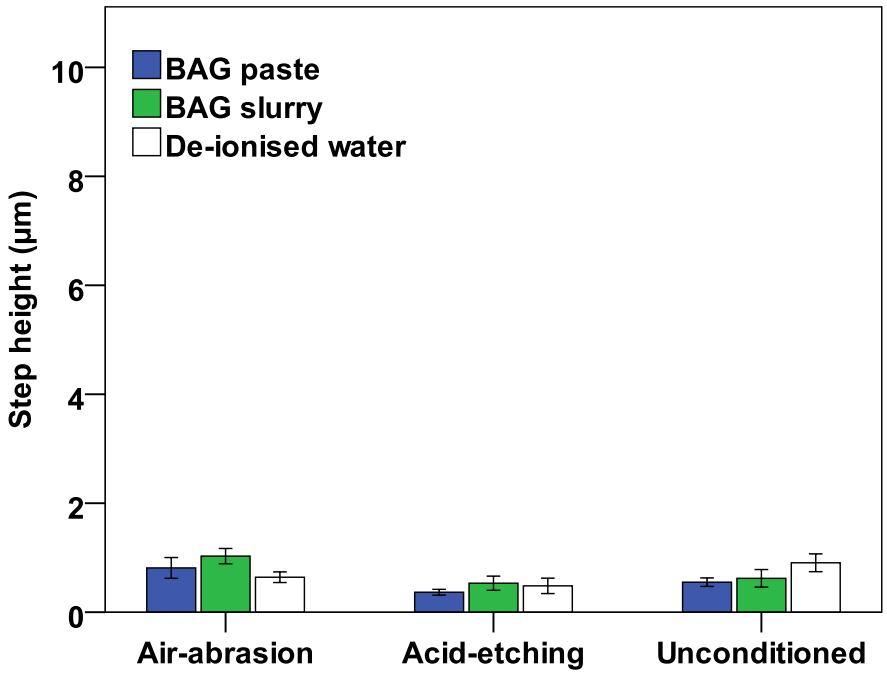

Figure 6-4: Mean±SE (µm) of step height measurements before surface pre-conditioning. There were no statistically significant differences between the experimental groups.

Pre-conditioning the lesion surface using air-abrasion and acid-etching significantly increased the surface roughness and the step height values compared to unconditioned control groups (p<0.05), but this difference was deemed not to be clinically significant. PAA-BAG air-abrasion removed significantly more substrate (5.1±0.6 µm, mean±SE) from the lesion surface compared to that removed by acid-etching (2.2±0.1 µm) (p<0.05) (Figure 6-5). The 3D views of the lesion surfaces (250 µm x 250 µm) exhibited an increase in roughness after pre-conditioning the lesion surface using PAA-BAG air-abrasion (Figure 6-6-A) or acid-etching (Figure 6-6-B). The pre-conditioned surfaces presented more sites for mineral deposition during the subsequent remineralisation therapy.

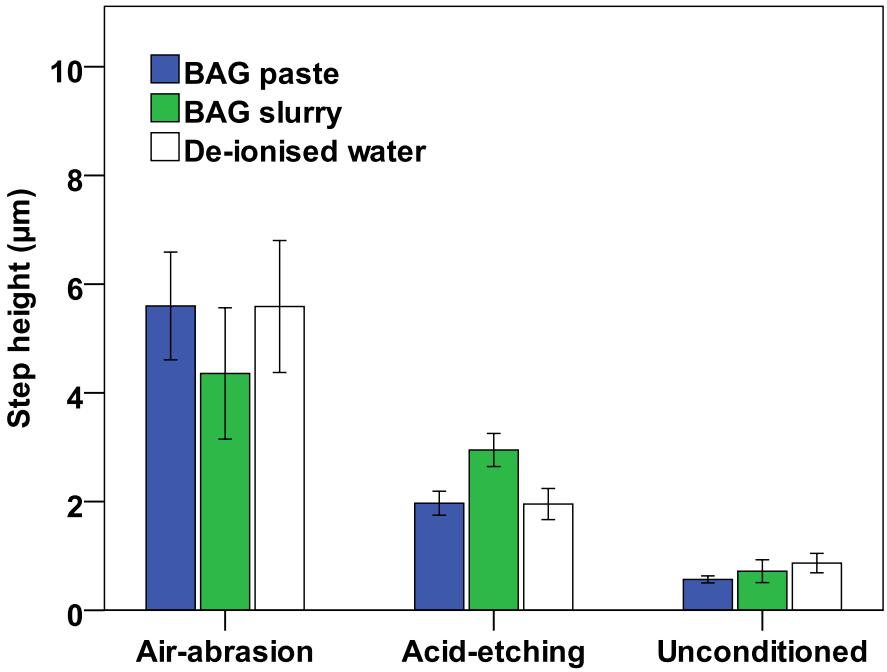

Figure 6-5: Mean±SE (µm) of step height measurements after surface pre-conditioning. There were statistically significant differences between the air-abrasion/acid etching *vs.* unconditioned groups and between air-abrasion *vs*. acid etching groups.

Table 6-2: The experimental groups according to the procedures (n=10), showing the means and their standard errors (µm) of average surface roughness (Sa):

Group n=10	Experimental procedures		Before surface pre-conditioning	After surface pre-conditioning	After remineralisation therapy
	Surface pre-conditioning*	Remineralisation therapy**			
1	PAA- BAG air-abrasion	BAG paste (36 wt.% BAG)	0.18±0.02	0.71±0.15	0.80±0.13
2	PAA- BAG air-abrasion	BAG slurry (100 wt.% BAG)	0.17±0.01	0.57±0.15	0.60±0.06
3	PAA- BAG air-abrasion	De-ionised water (-ve control)	0.16±0.01	0.49±0.09	0.59±0.08
4	Acid-etching (+ve control)	BAG paste (36 wt.% BAG)	0.19±0.01	0.90±0.07	1.14±0.10
5	Acid-etching (+ve control)	BAG slurry (100 wt.% BAG)	0.21±0.02	0.70±0.04	0.82±0.05
6	Acid-etching (+ve control)	De-ionised water (-ve control)	0.20±0.01	0.80±0.07	0.82±0.05
7	Unconditioned (-ve control)	BAG paste (36 wt.% BAG)	0.19±0.02	0.20±0.01	0.24±0.02
8	Unconditioned (-ve control)	BAG slurry (100 wt.% BAG)	0.29±0.07	0.25±0.04	0.31±0.06
9	Unconditioned (-ve control)	De-ionised water (-ve control)	0.16±0.15	0.20±0.02	0.25±0.03

* Applied once at the beginning of the experiment.
** Applied twice daily (5 min per application) for 21 days.
The underlined cells present the significant differences within the same experimental group (before) vs. (after) surface pre-conditioning.

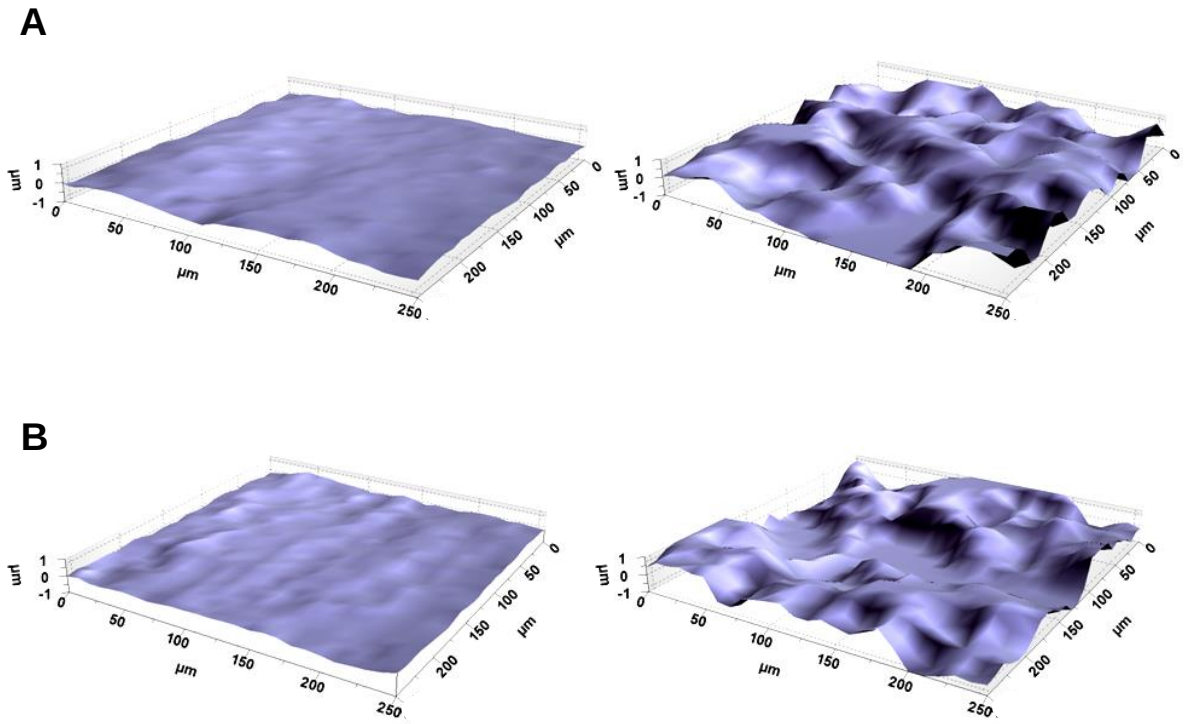

Figure 6-6: Representative 3D views of lesion surfaces (250 µm x 250 µm) before and after surface pre-conditioning using PAA-BAG air-abrasion (A) and acid-etching (B). The pre-conditioned surfaces exhibited an increased surface roughness when compared to the baseline scans.

The surface roughness measurements after remineralisation therapy were similar to those after surface pre-conditioning. However, there was a significant increase in the step height measurements within the acid-etch groups at this stage (p<0.05). The acid-etching groups in Figure 6-7 show that samples treated with BAG paste and slurry exhibited significantly higher step height values (5.4±0.4 µm and 5.8±0.3 µm respectively) (p<0.05) compared to those treated with de-ionised water (2.3±0.1 µm), the negative control of remineralisation therapy in acid-etching groups. Representative profiles showing the step height differences within the same samples according to the surface pre-conditioning procedures at three measurement points are presented in Figure 6-8.

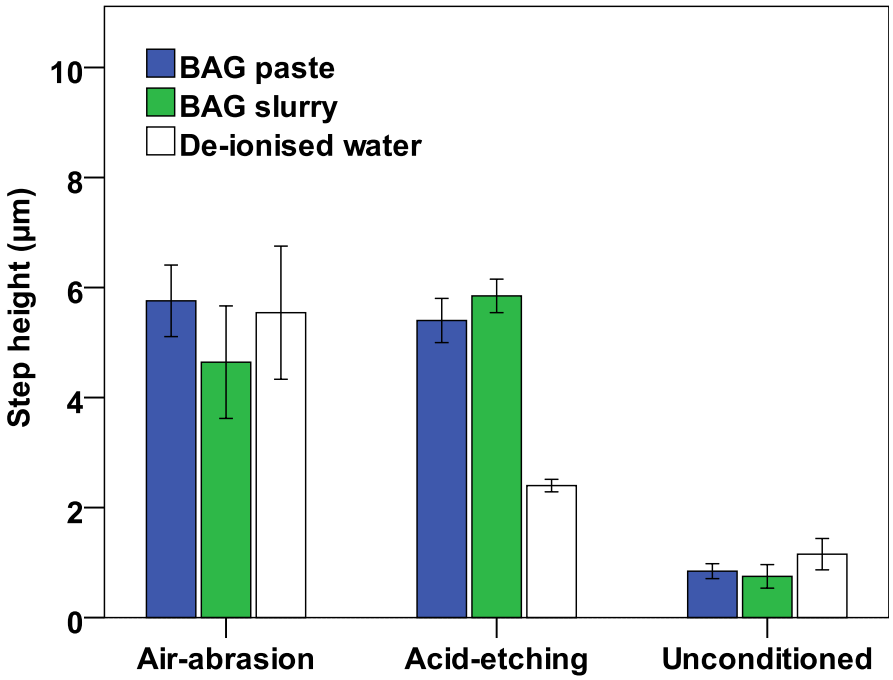

Figure 6-7: Mean±SE (µm) of step height measurements after remineralisation therapy. There were no statistically significant differences between the air-abrasion and acid-etching groups.

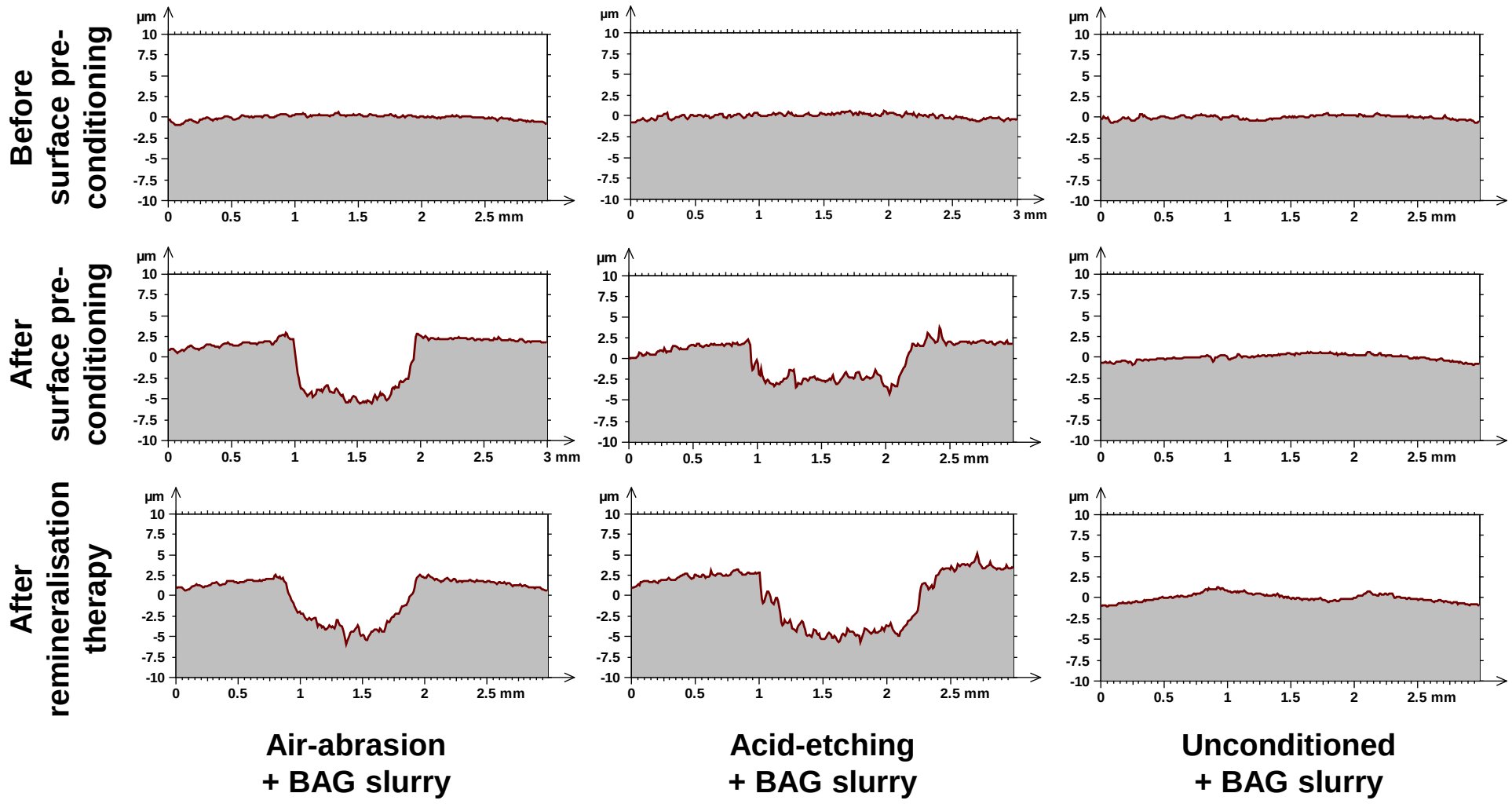

Figure 6-8: Representative profiles showing the step height differences within same samples according to the surface pre-conditioning procedures at three measurement points.

6.3.2 Results: optical coherence tomography (OCT)

Figure 6-9 represents the means and the standard errors of the reduction (%) in the subsurface light scattering in relation to the baseline scans. Pre-conditioning the lesion surface using PAA-BAG air-abrasion and acid-etching reduced significantly the subsurface light scattering of remineralised lesions when compared to unconditioned groups ($p<0.05$). BAG paste remineralisation therapy reduced significantly the light scattering compared to BAG slurry and de-ionised water ($p<0.05$). The use of BAG slurry exhibited similar subsurface light scattering to that of de-ionised water, regardless of the surface pre-conditioning procedure ($p>0.05$). Representative OCT images with their signal intensity profiles from the unconditioned + de-ionised water (negative control) and the air-abrasion + BAG paste groups are addressed in Figure 6-10. There was a reduction in the OCT signal intensity within the depth profiles following the remineralisation therapy.

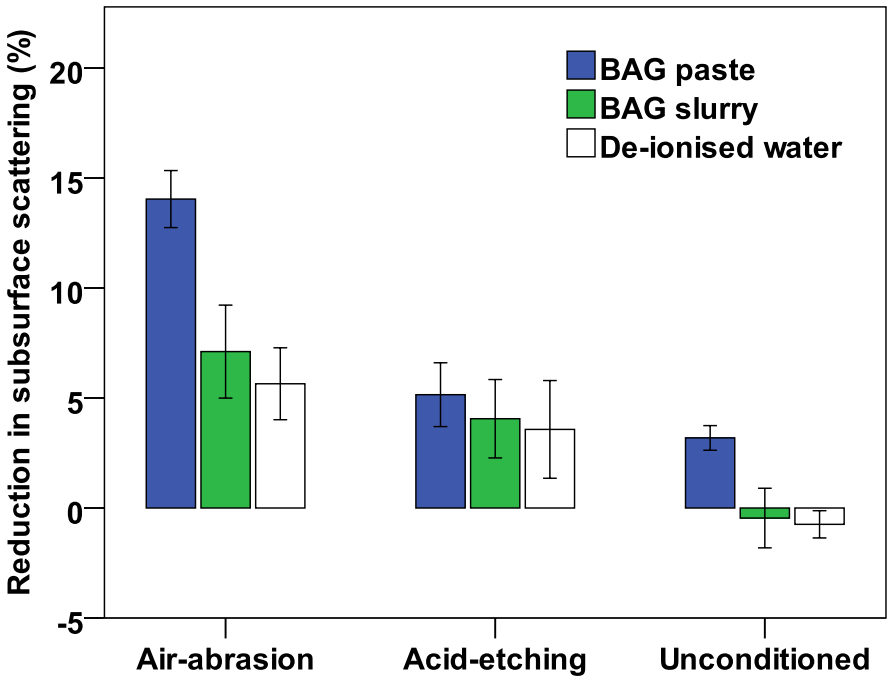

Figure 6-9: Mean±SE of the reduction (%) in the subsurface light scattering comparing to baseline scans. Air-abrasion and acid-etching significantly reduced the subsurface light scattering compared to unconditioned groups. The negative readings present an increase in the subsurface light scattering (%) after 21 days.

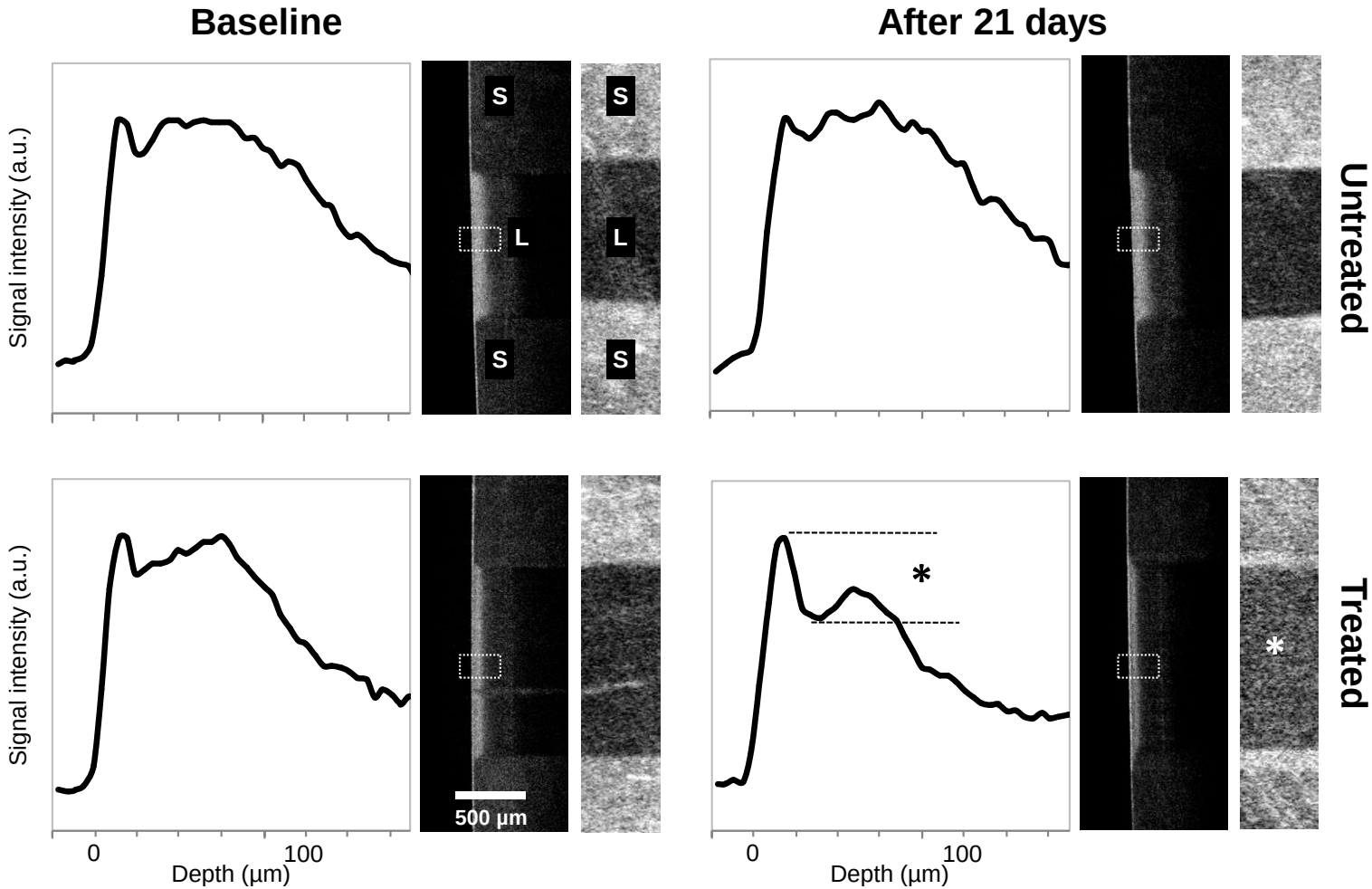

Figure 6-10: Representative OCT images of the negative control (unconditioned + de-ionised water) and the treated (air-abrasion + BAG paste) groups, before and after 21 days treatment. The depth profiles related to the OCT signal intensity within the WSL (dashed white rectangle). There was a reduction in the intensity at the subsurface level (the black star) in the treated sample when compared to the baseline intensity profile of the same sample. The TIFF analysis images (the grey-scale images) represent the reduction in the OCT signal intensity at the subsurface level measured to the surface reflection of the same sample. Note the difference in the TIFF analysis image of a treated sample after 21 day remineralisation therapy (the white star).

6.3.3 Results: Raman micro-spectroscopy

Figure 6-11 shows representative Raman spectra of scanned lesion surfaces in treated (air-abrasion + BAG slurry) and untreated (unconditioned + de-ionised water) groups. The highest peak along both spectra was that of v_1-PO_4^{3-} at 959 cm^{-1}, relating to the enamel HA. A new peak appeared within the spectra following the remineralisation therapies using BAG 45S5 at 1085 cm^{-1} assigned to $(CO_3)^{2-}$ of HCA that forms on reacted BAG 45S5 (Rehman et al., 1994).

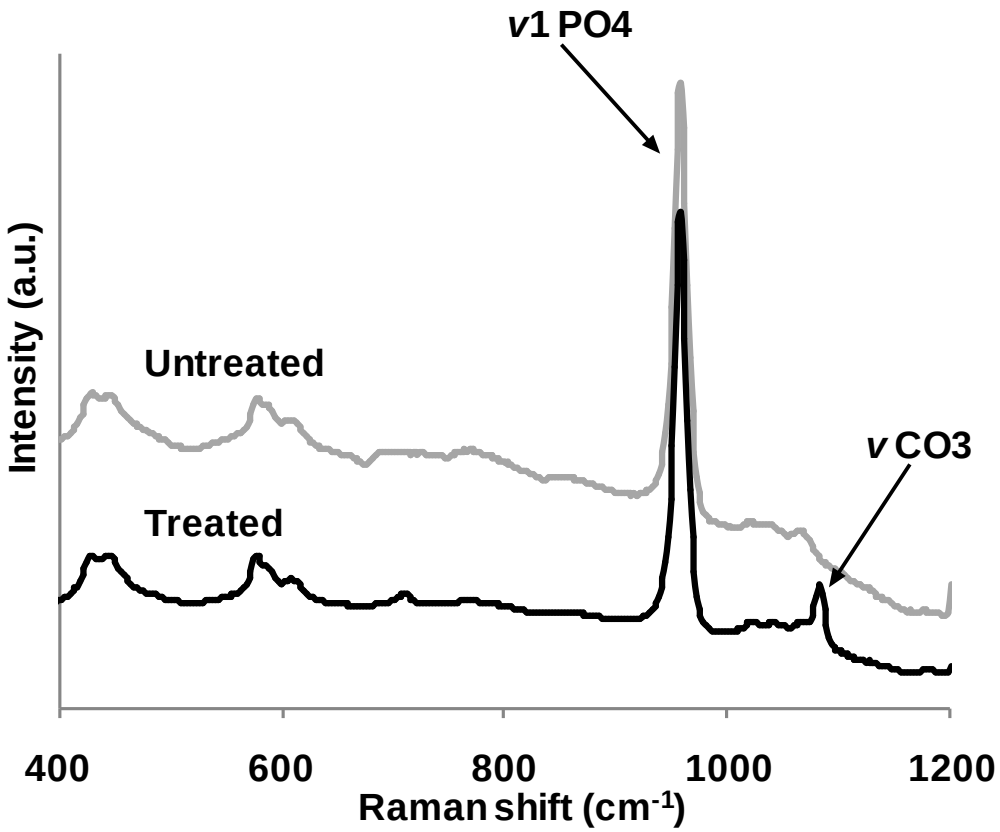

Figure 6-11: Representative Raman spectra of WSL surface in untreated (unconditioned + de-ionised water) and treated (air-abrasion + BAG slurry) samples. The arrows indicate the peaks measured in the analysis.

Pre-conditioning the lesion surface with acid-etching reduced significantly the intensity of the phosphate peak (v_1-PO_4^{3-}) at the lesion surface compared to air-abrasion and unconditioned groups (p<0.05) (Figure 6-12). The remineralisation therapy using BAG slurry increased significantly the phosphate peak intensity when compared to de-ionised water groups (p<0.05).

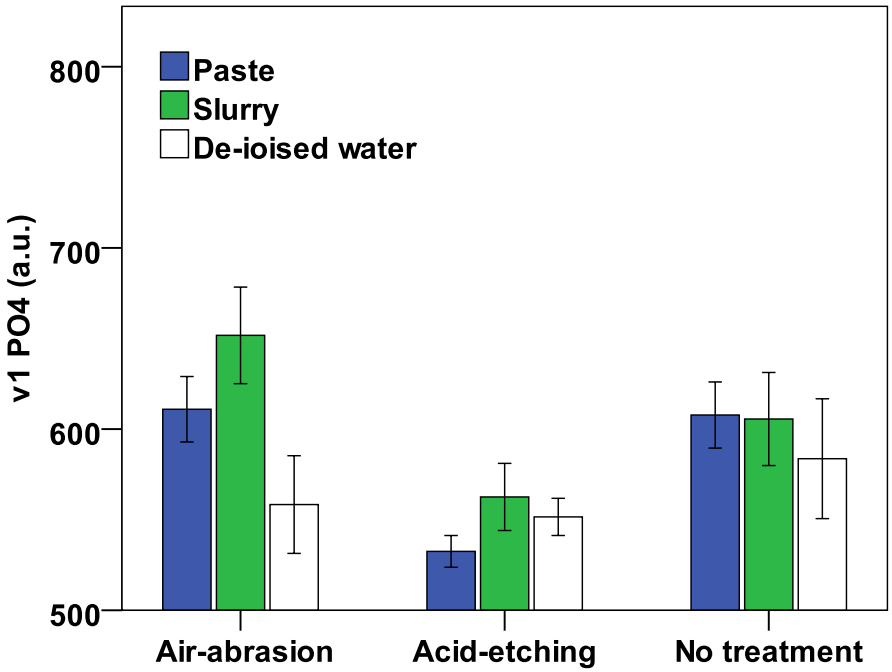

Figure 6-12: Mean±SE of *v1*-$(PO_4)^{3-}$ intensity at the lesion surfaces. Pre-conditioning the WSLs using acid-etching reduced significantly the phosphate peak intensity compared to the remaining groups.

The means and the standard errors, of the *v*-$(CO_3)^{2-}$/*v*$_1$-$(PO_4)^{3-}$ ratio are presented in Figure 6-13. The measured ratio in BAG paste and BAG slurry was significantly higher than that of de-ionised water (negative control) (p<0.05) in air-abrasion, acid-etching and unconditioned groups. The remineralisation therapy using BAG slurry increased significantly the measured ratio at the lesion surface compared to that observed using BAG paste when the surface was pre-conditioned using PAA-BAG air-abrasion (p<0.05), whilst there were no statistically significant differences between BAG slurry and BAG paste therapies when the lesions were unconditioned or pre-conditioned using acid-etch (p>0.05).

Using PAA-BAG air-abrasion to pre-condition the lesion surface increased significantly the *v*-$(CO_3)^{2-}$/*v*$_1$-$(PO_4)^{3-}$ ratio compared to the unconditioned groups when the lesions were remineralised using BAG paste or slurry (p<0.05). Pre-conditioning the lesion surface using PAA-BAG air-abrasion or acid-etching reduced significantly the measured ratio compared to the unconditioned samples when the lesions were only immersed in the de-ionised water, the negative control of the remineralisation therapy (p<0.05).

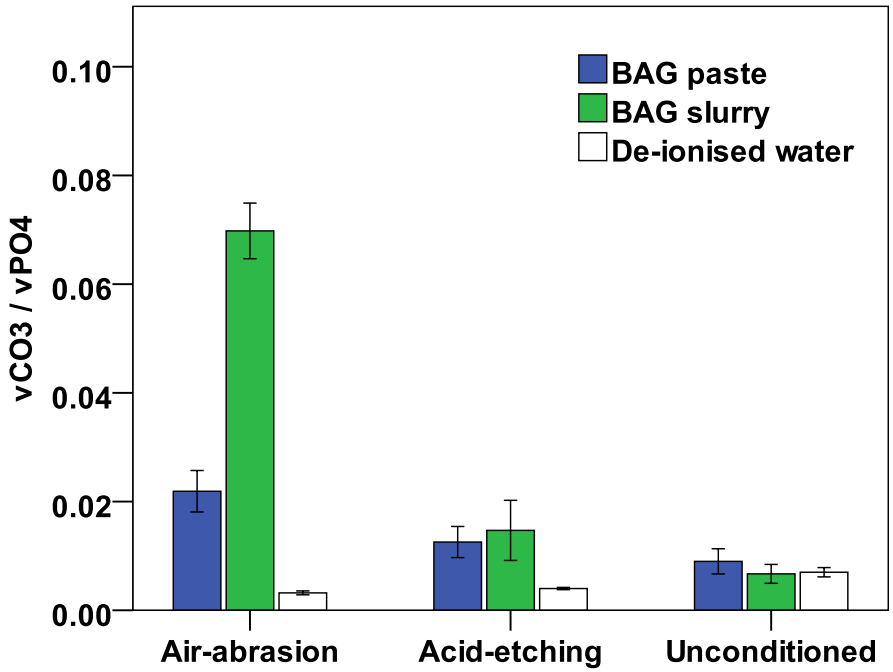

Figure 6-13: Mean±SE of v-$(CO_3)^{2-}$/$v1$-$(PO_4)^{3-}$ ratio. The use of PAA-BAG air-abrasion increased significantly the ratio value in the remineralised groups. BAG slurry increased the peak ratio when compared to BAG paste and de-ionised water.

6.3.4 Results: Knoop microhardness

The means and standard errors of lesion microhardness measurements are shown in Figure 6-14. The microhardness data were not normally distributed and hence, the analysis was carried out on the transformed data. According to the effect of pre-conditioning on the microhardness, both PAA-BAG air-abrasion and acid-etching increased the microhardness values significantly, compared to unconditioned control groups (p<0.05). No statistically significant differences were observed between the microhardness of air-abrasion and acid etching groups. As regards the remineralisation effect, both BAG paste and BAG slurry exhibited significantly higher (p<0.05) microhardness values compared to the de-ionised water groups (negative control) regardless of the surface pre-conditioned state. Within pre-conditioned groups, WSLs treated with the BAG slurry showed statistically significant higher microhardness compared to those treated with BAG paste (p<0.05).

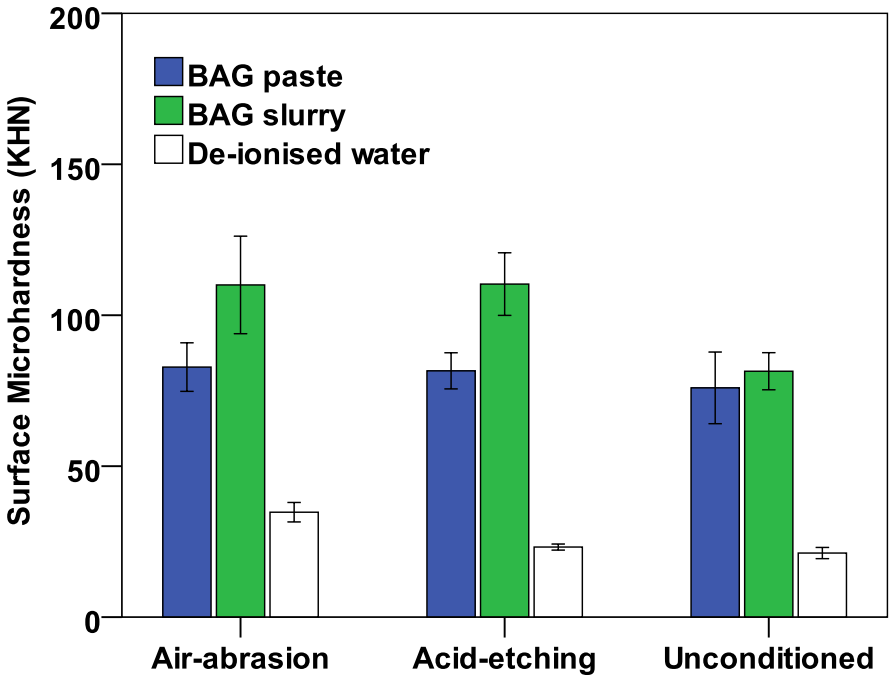

Figure 6-14: Mean±SE of lesion Knoop microhardness. There was a significant increase in the Knoop microhardness in air-abrasion and acid-etching groups compared to the unconditioned group. The remineralisation therapies using BAG 45S5 showed improved lesion microhardness values.

6.3.5 Results: microscopy imaging

Representative CLSM fluorescence images are shown in Figure 6-15 presenting the lesion depth (approximately 80-100 µm), the enamel prism outlines and the Rhodamine-B distribution. More Rhodamine-B permeation was observed within the non-treated group implying that the Rhodamine-B penetrated and was retained more within the depth of lesion. In contrast, in the CLSM-micrographs of the treated samples, less dye distribution was observed as a band-like area at the outer third of the cross-sections. No differences were observed between the BAG paste and BAG slurry experimental groups in the CLSM-micrographs.

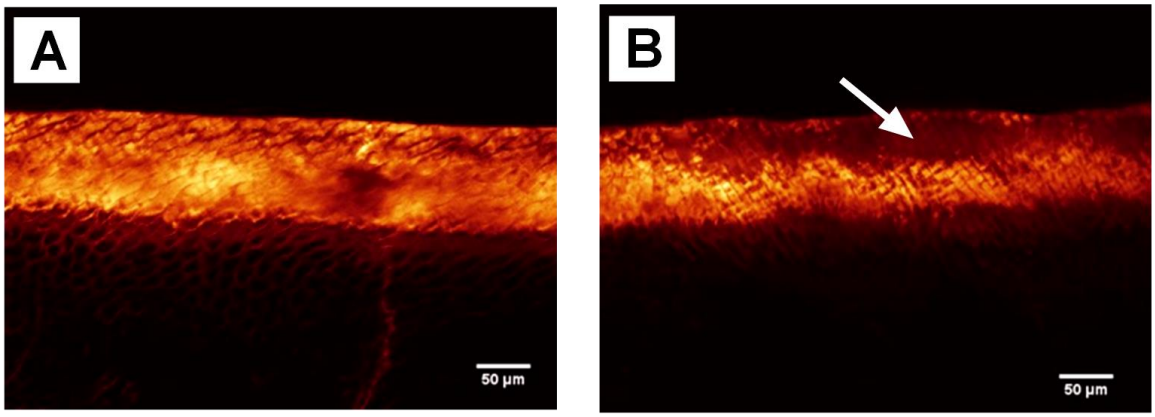

Figure 6-15: Representative CLSM images show the Rhodamine-B distribution in the cross-sectional views of the untreated WSL (A) and remineralised WSL using air-abrasion and BAG slurry (B). The enamel prism outlines can be observed along the lesion depth. A band-like area (arrow) with less Rhodamine-B permeating is observed at the outer-third of the cross-section in the treated WSL.

Representative SEM micrographs of the experimental groups are presented in Figure 6-16. The cross-sectional views of fractured non-treated lesions showed the partially demineralised enamel prisms, with no external mineral precipitation evident. In contrast, plate-like structures were observed at the lesion edge and could be differentiated from the original lesion structure (enamel prisms) in the treated groups. The external mineral precipitation was more pronounced in the BAG slurry than in the BAG paste. The lesion top surface in the non-treated group exhibited porosities resulting from the demineralisation process. This porosity was covered completely by a “newly” formed layer of mineral within the treated groups (Figure 6-16).

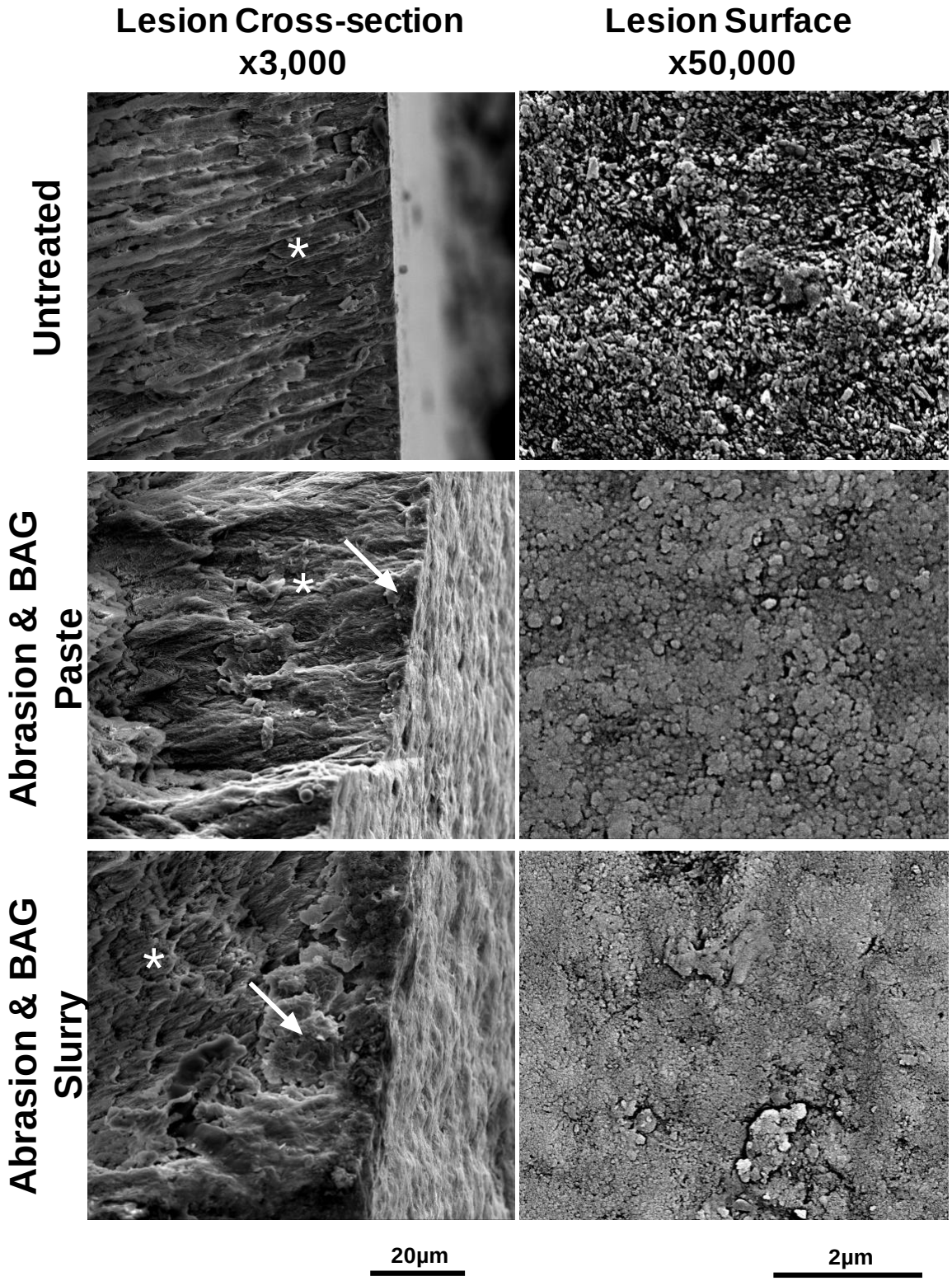

Figure 6-16: Representative SEM images of the fractured cross-sections and the lesion surface. The lesion shows the partially demineralised enamel prisms (*). The fractured cross-sections of treated samples present mineral precipitations with plate-like structures (arrow), considerably more pronounced in BAG slurry. The SEM micrographs of the top surface in non-treated sample exhibits a surface porosity resulting from the demineralisation process. The lesion surfaces in the treated group present a layer of mineral completely blocking the surface porosity.

The elemental analysis of the lesion surface using EDX mapping presented an additional peak of Si (1.73 keV) relating to the reacted BAG particles in the remineralised lesions (Figure 6-17).

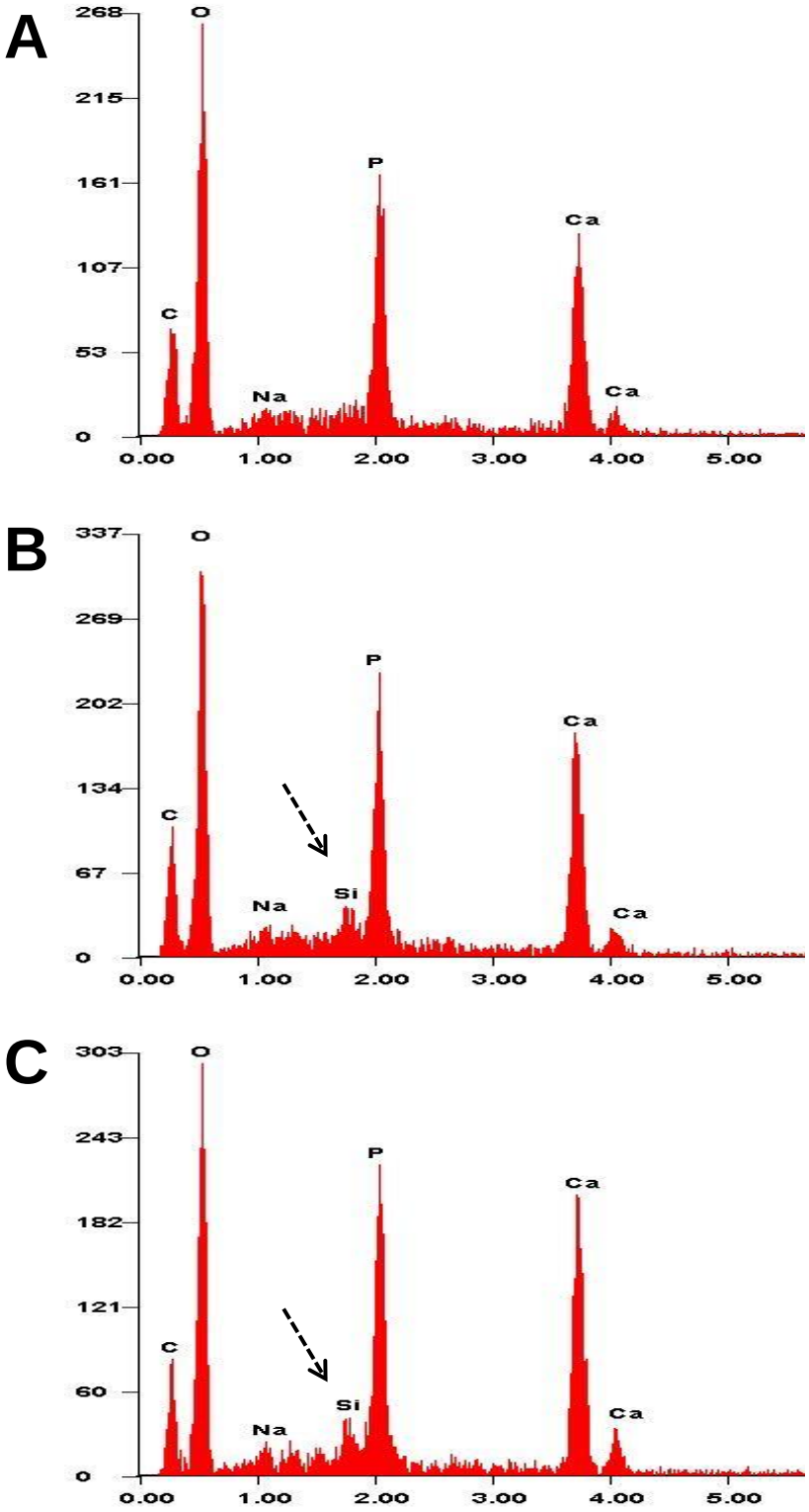

Figure 6-17: The average EDX spectra of scanned lesion surface in an untreated sample (A), remineralised WSL using air-abrasion + BAG paste (B) and remineralised WSL using air-abrasion + BAG slurry (C). Treated samples show an additional peak at (1.73 keV) related to Si of reacted BAG particles (arrow).

6.4 Discussion

6.4.1 Profilometry analysis

The use of non-contact white light profilometry in the present study permitted non-destructive assessment of the topographic changes at the lesion surface at three different experimental times. Its use introduced objectively quantitative information about the lesion surface loss and roughness. The accuracy of the profilometry used in this study for measuring step height enamel loss has been reported to be 0.042 μm (Paepegaey et al., 2013). The average surface roughness is one of the most common parameters used to report roughness in dentistry, representing the finest measurable detail of the surface geometry (Field et al., 2010). This parameter measures the profile deviations from the mean line across a profile (Eliades et al., 2004; Karan et al., 2010; Loomans et al., 2011). Pre-conditioning a WSL using PAA-BAG air-abrasion and acid-etching increased the average surface roughness and consequently the surface area providing more sites for mineral deposition (see Figure 6-6; p: 162). The rough WSL surface might offer more sites for remineralisation and show increased remineralisation (Peariasamy et al., 2001).

Using PAA-BAG air-abrasion prior to remineralisation therapy removed approximately 5 μm from the lesion surface which is insignificant clinically. PAA-BAG air-abrasion modified physically the lesion surface employing the kinetic cutting mechanism of the abrasive particles, whereby a thin superficial layer is irregularly chipped away from the lesion surface increasing the surface roughness and exposing the WSL subsurface structure. Indeed, two aspects should be considered when pre-conditioning a WSL using air-abrasion: the abrasive powder and the system's operating parameters. Here, the operating parameters used to pre-condition enamel WSLs promoted the ultraconservative application of this technology (see Chapter 3; p: 88), while PAA-BAG has been selected due to its reduced cutting efficiency when compared to BAG abrasive powder (30-60-90 μm). Assessing the cutting efficiency of PAA-BAG air-abrasion as described in Chapter 3 with the following cutting parameters: air pressure 60 psi, PFR: 3, nozzle angle: 90 degrees, nozzle-substrate distance: 2 mm and linear movement velocity: 0.5 mm/sec (n=10) revealed that using PAA-BAG air-abrasion removed only 0.05±0.01 mean±SE mm^3 from the substrate compared

to 0.97±0.01 mm^3 and 1.39±0.1 mm^3 removed using BAG (30-60-90 µm) and alumina abrasive powders respectively.

The profilometry data revealed that the remineralisation therapy using BAG paste or BAG slurry increased the step height values in the acid-etch groups. It has been shown that treating WSL with 30% phosphoric acid for 30 seconds removed 3-6 µm from the lesion surface and increased the subsurface porosity up to 21 µm, detected using polarised light microscopy when the etched surface zone exhibited higher birefringence (Hicks and Silverstone, 1984a; Lee et al., 1995). Van Drop et al. (1990) reported that when the enamel WSLs were etched with 36% phosphoric acid, the surface layer of the lesion was decalcified. The Raman analysis in this study revealed that pre-conditioning WSLs using acid-etching reduced significantly the phosphate content of enamel HA at the lesion surface. The subsurface micro-porosities and the demineralisation effect of phosphoric acid itself, may explain the slight reduction (approximately 3 µm) in the lesion surface comparing to the reference level following the physical remineralisation therapy within acid-etching groups (Figure 6-7; p: 163).

When acid-etching was conducted previously in studies to pre-condition enamel WSLs, the following remineralisation therapy included the use of remineralisation agents in solution (Flaitz and Hicks, 1993; Al-Khateeb et al., 2000). The remineralisation therapies in the present study involved a physical interaction between the slurries and etched WSL surface. Using non-contact profilometery with high vertical resolution (10 nm) permitted the detection statistically of the slight modification at the acid-etched lesion compared to those soaked in the de-ionised water implying that the delivery mode of a remineralisation agent can affect the outermost layer of WSLs and consequently the following remineralisation outcomes.

6.4.2 Optical coherence tomography (OCT)

Optical coherence tomography has been used in de- and remineralisation assessment in-vivo and in-vitro as it images non-destructively the interior structure of WSLs by differentiating between scattered and reflected photons using a near-infrared light source at a micron resolution (see Section 1.3.3.6; p: 68). In OCT, the measurement of subsurface light scattering represents the

porosity within the lesion body. This depends upon light scattering whereby the scattering increases in porous demineralised enamel (Kang et al., 2012).

The remineralisation therapy using BAG paste reduced significantly the subsurface light scattering implying that more penetration of the remineralisation agent occurred filling more subsurface micro-porosities. Pre-conditioning the lesion surface using PAA-BAG air-abrasion or acid-etching promoted this penetration. Jones and Freid (2006) reported that the remineralisation of artificial enamel WSLs reduced the optical scattering of the lesion when compared to the baseline scans. It is important to note that different factors can affect the light scattering in the remineralised WSLs such as the pores size / number, the mineral content and the natural of the enamel repair (Jones et al., 2006; Hariri et al., 2012; Kang et al., 2012).

The main differences between BAG paste and BAG slurry, which may have had an effect on remineralisation outcomes, were the concentration of BAG particles (36 wt.% in paste and 100 wt.% in slurry) and the additional chemical compositions of the paste. Raman micro-spectroscopy and microhardness detected a higher remineralisation rate within WSLs treated with the slurry as discussed later. On the other hand, the OCT subsurface data showed more reduction in subsurface light scattering within the BAG paste. The presence of glycerine in the paste might increase the penetration of the paste components into lesion depth to fill more pores.

6.4.3 Raman micro-spectroscopy

Quantitative information about the mineral concentration within a substrate can be obtained using Raman micro-spectroscopy, dependent upon the peak intensity being proportional to the number of molecules within the volume of the scanned area (Penel et al., 1998; Tramini et al., 2000). The use of the StreamLine^{TM} scanning technique in this study permitted the analysis of 2280 spectra in each sample so introducing a more representative dataset of the lesion surface. The differences between the StreamLine^{TM} and the conventional point-by-point serial scanning techniques have been discussed in Chapter 5.

The phosphate peak at 959 cm^{-1} represented the mineral content in enamel, and its intensity relates to the amount of mineral within the scanned area (Santini et al., 2008; Mohanty et al., 2012). The results in the present study suggested that the phosphate peak intensity was higher within BAG slurry samples compared to the remaining groups, in agreement with the results of the previous Chapter. This has been reported previously using other biological tissues such as cartilage, whereby, the phosphate peak at 959 cm^{-1} appeared at the early stage of its mineralisation process (Sauer et al., 1994).

The C-O Raman peak of the hydroxycarbonate apatite (HCA) layer formed on the reacted BAG particles at 1085 cm^{-1} was clearly detectable during HCA formation (Rehman et al., 1994). In the current study, the v-$(CO_3)^{2-}$/v_1-$(PO_4)^{3-}$ ratio was analysed statistically to assess the mineral content at the lesion surface. The results showed that air-abrasion pre-conditioning increased significantly the peak ratio compared to acid etching as well as the unconditioned groups. This might result from the increased lesion surface area and roughness in pre-conditioned samples which enhanced the HCA deposition within the superficial layer of lesion.

In the current study, the Raman dataset revealed that conditioning WSLs using phosphoric acid prior to remineralisation therapy exhibited similar mineral content measurements to those of the unconditioned groups. However, this pre-treatment has been described previously to promote the mineral gain of the treated lesions (DePaola et al., 1971; Al-Khateeb et al., 2000). Flaitz and Hicks (1993) reported that when the WSLs were acid-etched using 30% phosphoric acid for 30 sec before exposure to remineralisation solution, the body of the pre-conditioned lesion was approximately 25% less than that of the unconditioned lesion, measured using polarised light microscopy. Assessing the remineralisation of enamel WSLs pre-conditioned with phosphoric acid revealed that the recovery of the mineral had occurred within the lesion body, but not at the etched surface level according to the mineral profile data of contact microradiographs (CMR) (Hidaka et al., 2011). This might explain the reduced mineral content observed within the acid-etching groups using Raman micro-spectroscopy in our study since this analytical method is considered entirely a surface assessment method. In contrast, microhardness measurement showed that the etched WSLs exhibited an improved remineralisation rate compared to the equivalent unconditioned

groups. This can be considered to be a subsurface assessment method since the Knoop indenter penetrates the lesion depth by approximately 1.5 µm in depth (Schlueter et al., 2011), and the indentation is not only affected by the immediate contact areas, but also by areas at a distance of approximately 10 times the dimensions of the indenter (de Jong et al., 1987; Barbour and Rees, 2004).

6.4.4 Knoop microhardness

Previous studies reported an increase in enamel microhardness following the remineralisation therapy using BAG 45S5 (Burwell et al., 2009b; Dong et al., 2011; Guo et al., 2014). The increase in the Knoop microhardness reflects a net mineral gain and an improved crystalline structure (Featherstone et al., 1983; Kielbassa et al., 1999). Pre-conditioning the lesion surface with PAA-BAG air-abrasion and acid-etching promoted the subsequent remineralisation therapy with BAG slurry according to the microhardness testing. This might be explained since pre-conditioning WSLs increased the lesion surface roughness and thus the sites for the mineral depositions. It has been established that the hardness of enamel is a function of the degree of mineralisation and its increase reflects remineralisation (Head, 1912; Feagin et al., 1969; Gomez et al., 2014). The BAG slurry contained more BAG particles compared to the BAG paste, which can explain the improved microhardness detected for lesions treated with BAG slurry.

6.4.5 Microscopy imaging

The use of CLSM imaging in the present study was based on the fact that imbibition of a fluorescent dye into the WSL porosities decreased following remineralisation treatment (Fontana et al., 1996). It has been shown that Rhodamine-B fluorescent dye penetrates enamel micro-porosities created through the demineralisation process and that less of this dye penetrates the lesion following the remineralisation therapy (González-Cabezas et al., 1998; Zhao et al., 2014). This was observed within the treated samples in the current study where a band-like area, with a reduced Rhodamine-B permeation, was observed at the outer edge of the cross-sectional views. In the present study, the OCT and the CLSM depended on measuring the porosity of the WSLs, and both showed a reduction in lesion porosity following the remineralisation therapies.

However, the CLSM micrographs showed that the deeper part of the cross-sections exhibited a Rhodamine-B distribution similar to that observed in the untreated sample implying that the remineralisation therapy was not involved in that part of the lesion, and the complete repair had not occurred implying that more studies are still required to further enhance the penetration of BAG through the whole lesion depth. These investigations could involve the combination of (a) BAG 45S5 nanotechnology, (b) pre-conditioning the lesion surface using PAA-BAG air-abrasion, and (c) biomimetic remineralisation strategies to regulate and control the apatite crystal growth.

A layer of newly precipitated mineral was detected covering the lesion surface in the BAG paste and slurry groups. The chemical analysis of this layer using EDX analysis showed an additional silicon peak indicating that this layer consisted of HCA structures of reacted BAG 45S5. Comparing the EDX spectrum of this layer (Figure 6-17; p: 173) to that of BAG particles as received, before any use (Figure 2-3-A; p: 80) showed differences in the intensity of Ca, P and Si peaks between the two spectra implying that the layer formed following the remineralisation therapies in the present study was HCA of reacted BAG particles and was not a deposition of non-reacted BAG particles. This also was supported by the results of the Raman analysis which showed an increase in the phosphate peak v_1-$(PO_4)^{3-}$ intensity and the appearance of a new carbonate peak v-$(CO_3)^{2-}$ peak.

The SEM micrographs of fractured cross-sections permitted the direct observation of interior lesion structures and showed plate-like structures penetrating the lesion surface into the lesion body. The plate-like structures have been reported to characterise the HCA of reacted BAG 45S5, examined using SEM (Kokubo, 1990; Zhong et al., 2002). The SEM observations in this study revealed that the newly formed minerals were attached to the lesion structure since those minerals were not removed during the post-remineralisation rinsing protocol, nor were affected by fracturing or gold-coating preparation procedures for SEM analysis. Moreover, no charging was observed in the SEM micrographs of remineralised lesions implying that no loose segments were evident in the lesion structure in agreement with a previous study (Gjorgievska et al., 2013).

The use of BAG in WSL remineralisation provides an external ion source with the intention of promoting and accelerating enamel remineralisation *in vivo*. The remineralisation rate of WSLs reported in the current study is expected to be improved within the biological oral cavity due to the presence of salivary calcium / phosphate ions, and this hypothesis requires further in-situ study. An additional beneficial effect of using BAG 45S5 in WSL remineralisation is that BAG particles exhibit an antibacterial effect against certain oral bacteria, including those associated with caries and periodontal disease such as *Streptococcus sanguis*, *Streptococcus mutans* and *Actinomyces viscosus* (Allan et al., 2001; Hu et al., 2009).

Pre-conditioning WSLs using PAA-BAG air-abrasion or acid-etching exhibited similar microhardness and OCT outcomes. These analytical methods presented the subsurface changes of the remineralised WSLs. The chemical mapping of lesion surfaces using Raman micro-spectroscopy reported significantly better surface remineralisation within the air-abrasion groups presenting an advantage for air-abrasion over acid-etching in term of enhancing WSL remineralisation. Therefore, the use of PAA-BAG air-abrasion promoted the remineralisation in both the surface and subsurface WSL areas by modifying the lesion surface without any further demineralisation effect that was detected in acid-etched groups using non-contact profilometry and Raman micro-spectroscopy.

Regarding the remineralisation therapy, the use of BAG slurry resulted in significantly higher remineralisation outcomes when compared to BAG paste according to the microhardness, Raman micro-spectroscopy and SEM measurements. In fact, the BAG slurry contained more BAG particles (100 wt.%) compared to the BAG paste (36 wt.%) and therefore, it was expected to obtain better remineralisation results using the BAG slurry. However, the OCT data showed that the use of BAG paste reduced significantly the subsurface light scattering of demineralised enamel when compared to BAG slurry. As mentioned above the OCT analysis could be related to different factors such as the pores size / number, the mineral content and nature of the mineral formed. According to the results of the other analytical methods used in this study, it might appear that the OCT analysis highlighted the pores size / number within treated lesions. BAG paste contained other components such as glycerine which might have

improved the penetration of the paste components into the lesion, so reducing the pore size / number and thus the subsurface light scattering.

The clinical translation of biomimetic remineralisation strategies is still required since most in-vitro studies include the immersion of specimens in remineralisation solutions containing biomimetic analogues, which is inapplicable clinically (Niu et al., 2014). Using air-abrasion technology to seed the early carious lesion surface with bioactive particles prior to remineralisation therapy could be an appropriate clinical delivery system to apply biomimetic remineralisation strategies *in vivo*. Previous studies reported that BAG particles were retained on the treated surface after BAG air-abrasion in spite of the post-preparation cleaning regimen (Koller et al., 2007; Paolinelis et al., 2008). The methodology of this study was designed to develop the remineralisation protocol applicable clinically by pre-conditioning the lesion surface once, followed by the remineralisation therapy applied in a manner similar to current routine dental care. This approach removed an ultra-thin layer from the lesion surface, which is not clinically significant. Since the enamel surface is polluted / covered by saliva proteins and impurities in-vivo, the physical modification of a WSL surface can expose more reactive subsurface structures which in turn, may improve the seamless adhesion of a repairable layer with the lesion structure when followed directly by apatite formation (Robinson et al., 1990; Onuma et al., 2005). The adherent repairable surface layer detected in this study (Figure 6-16; p: 172) may act as a mineral reservoir for prolonged remineralisation of the lesion. Using PAA-BAG air-abrasion for this purpose also increased the lesion surface area and may seed the lesion surface with bioactive materials aiding the further remineralisation therapy.

6.5 Conclusions

The two null hypotheses investigated in this study were rejected. The results of this study leads to the following conclusions:

1. Pre-conditioning the WSL surface using PAA-BAG air-abrasion removed an ultra-thin, clinically insignificant layer from the lesion surface.
2. This pre-conditioning increased the average surface roughness of the lesion.
3. These physical modifications enhanced the subsequent remineralisation therapies using bioactive glass 45S5 assessed by (a) the increased mineral content, (b) improved mechanical properties and (c) the ultra-structural changes and therefore, may be recommended clinically to promote the mineral uptake during the remineralisation therapy.
4. Pre-conditioning the WSL using PAA-BAG air-abrasion promoted the remineralisation at the surface and subsurface WSL areas, whilst the use of acid-etching only enhanced the remineralisation at the subsurface level.
5. The use of BAG 45S5 slurry as a remineralisation agent exhibited a superior remineralisation benefit when compared to BAG paste, and therefore, might be considered for further development.

Chapter 7 General discussion, conclusions and suggestions for future work

The overall aim of the studies in this thesis was to develop the use of BAG air-abrasion as an operative technique in minimally invasive dentistry (MID) for the controlled and the selective removal of substrates and for enhancing the remineralisation of enamel white spot lesion (WSL) using BAG 45S5 technology. The overall structure of this study in terms of the relation to the MID concepts is presented in Figure 7-1. The aims and outcome summaries of the experiments conducted in this thesis are presented in Table 7-1.

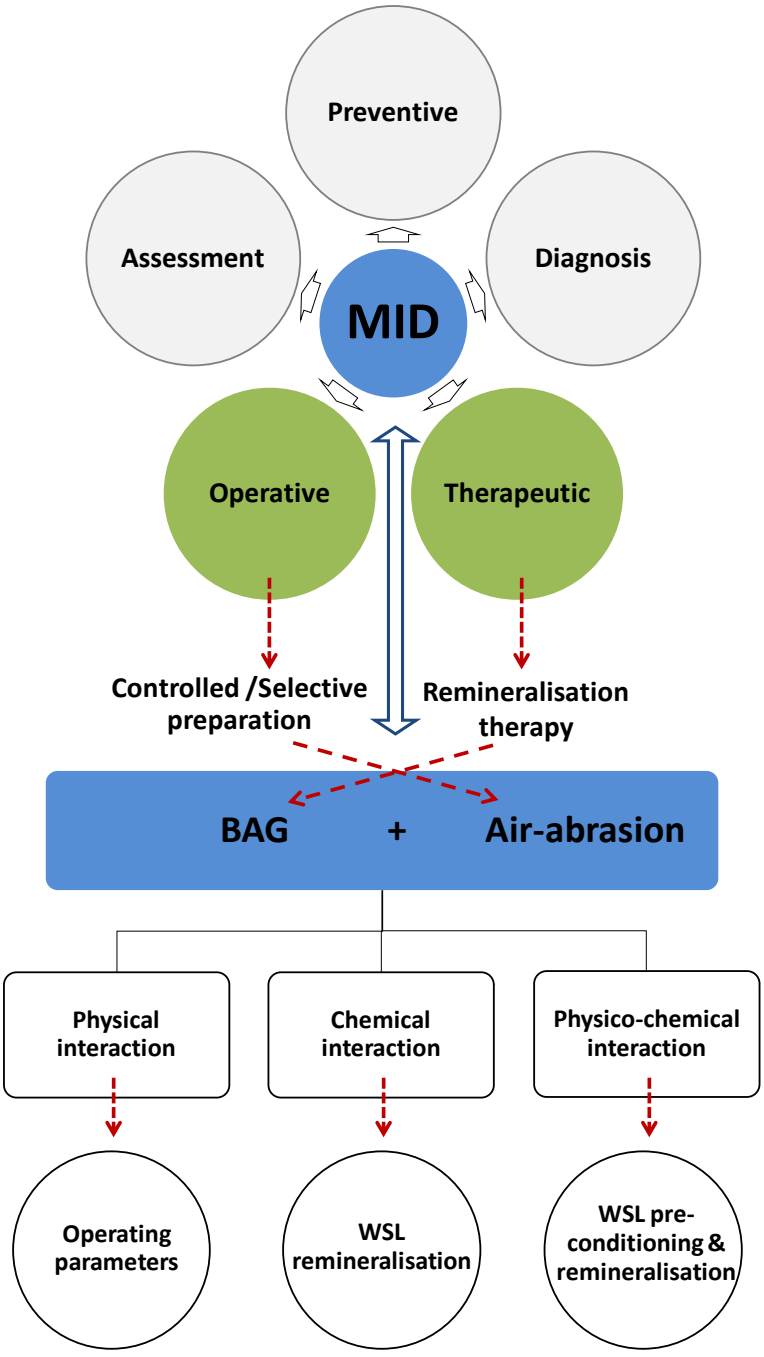

Figure 7-1: Organisational flowchart of the overall structure of this thesis in relation to minimally invasive dentistry (MID).

Table 7-1: The aims and outcome summaries of the experiments conducted in this thesis:

		Aims	Outcome summaries
Section 1 BAG air-abrasion operating parameters & cutting characteristics	**Chapter 2**	To calibrate the air-abrasion system including characterisation of the abrasive powders and the validation of the unit's operating parameters.	1. Vibration admix units exhibited a constant powder flow rate regardless of air pressure. 2. It is advisable to check the BAG powder condition within the powder chamber before the abrasion procedures to obtain a consistent powder flow rate during operation. 3. Using air-abrasion should be preceded by system calibration to identify the factors affecting the abrasive powder propulsion as they differ according to the unit's design.
	Chapter 3	To evaluate the effect of six operating parameters: air pressure, powder flow rate (PFR), nozzle-substrate distance, nozzle angle, shrouding the air stream with a curtain of water and the abrasive powder itself, on the cutting efficiency / pattern of air-abrasion.	1. All operating parameters involved in this study, except shrouding the powder stream with a curtain of water affected significantly the cutting efficiency of air-abrasion as well as its cutting pattern. 2. Alumina and BAG abrasive powders revealed statistically different cutting efficiencies. 3. Air-abrasion cutting efficiency is more conservative and controllable when BAG powder is used as an abrasive powder, encouraging its role in minimally invasive operative dentistry.
	Chapter 4	To assess the effect of three clinically adjustable air-abrasion operating parameters on the selective removal of resin composite, and to determine the required clinical time taken to carry out the procedures.	1. BAG powder is more efficient than alumina in the selective removal of resin composite. 2. The interaction effect between air pressure and PFR on resin composite removal was significant. 3. Using a moderate air pressure value with reduced PFR enhanced the selective removal of resin composite. 4. The time required for resin composite removal was deemed acceptable clinically.

Section 2 **Enamel WSL remineralisation using BAG 45S5 technology**	**Chapter 5**	To evaluate the effect of BAG 45S5 and PAA-BAG powders on artificial enamel WSL remineralisation through chemical, mechanical and ultra-structural assessments.	1. Treating enamel WSLs using BAG or PAA-BAG slurry improved the mechanical proprieties of the lesion. 2. These remineralisation therapies increased the phosphate content according to the Raman analysis. 3. Mineral depositions at the treated lesion surface were detected in SEM micrographs. 4. BAG and PAA-BAG remineralisation therapies showed similar mechanical and chemical improvements. 5. Smaller particle precipitations were detected within PAA-BAG compared to the BAG.
	Chapter 6	To assess the physical modification of WSL pre-conditioning using PAA-BAG air-abrasion and to study the impact of this modification on the overall lesion remineralisation.	1. Pre-conditioning WSL surfaces using PAA-BAG air-abrasion removed an ultra-thin, clinically insignificant layer from the lesion surface. 2. This pre-conditioning increased the average surface roughness of the lesion. 3. These physical modifications enhanced the subsequent remineralisation therapies using bioactive glass 45S5 assessed by (a) the increased mineral content, (b) improved mechanical properties and (c) the ultra-structural changes and therefore, may be recommended clinically to promote the mineral uptake during the remineralisation therapy. 4. Pre-conditioning WSLs using PAA-BAG air-abrasion promoted remineralisation both at the surface and subsurface the WSL areas, whilst the use of acid-etching only enhanced the remineralisation at the subsurface level. 5. The use of BAG 45S5 slurry as a remineralisation agent exhibited a superior remineralisation benefit when compared to BAG paste, and therefore, might be considered for further development.

Minimum intervention (MI) care is the physician's holistic team-care approach with the patient to help prevent the oral disease from occurring in the first instance (primary prevention), from becoming established (secondary prevention) and from recurring due to the failure of patients' adherence to preventive regimes and restorative treatment failure (tertiary prevention) (Featherstone and Doméjean, 2012). Minimally invasive dentistry (MID) is part of this minimum intervention care philosophy which focuses on the tooth-preserving operative techniques to restore teeth aiming to retain the maximum quantity of intact, repairable dental tissues (Peters and McLean, 2001b). Currently, there is no available operative technique with a purely "self-limiting" nature to excavate selectively the irreparable carious tissues and resin-based restorative materials (Cochrane et al., 2012b; Banerjee, 2013).

Table 1-1; p: 27 outlines the clinical operative technologies available with their main features. The hand-excavators, chemo-mechanical systems and polymeric burs might be more useful to excavate selectively the irreparable carious tissues when compared to other clinical methods. However, these techniques cannot provide adequate enamel access, essential for efficient / controlled caries excavation, implying that the use of other operative techniques is still required. Operative techniques which can be used clinically to prepare enamel include rotary instruments, ultrasonics / sono-abrasion instruments, dental lasers and air-abrasion.

The use of rotary instrumentation is ineffective in preserving the healthy sound enamel during the cutting procedure since the tactile sensation decreases with the increasing speed of this technology (Yip and Samaranayake, 1998). Undesirable tooth over-preparation may also occur using air-abrasion due to the lack of conventional tactile feedback, relied upon by dentists (Banerjee and Watson, 2002). The results of the present studies demonstrated that the ultraconservative cutting characteristics of BAG air-abrasion can be promoted by altering its operating parameters, thus enhancing its role as an operative technique in MID. The consideration of these operating parameters improved the selective removal of resin composite restorative material, one of the most common procedures in Conservative Dentistry, and permitted pre-conditioning

the softened surfaces of enamel WSLs by removing only an ultra-thin layer (approximately 5 µm) from the lesion surface.

The present studies used non-contact profilometry with a high vertical resolution (10 nm) to measure the volume (mm^3) of material removed. Measuring the substrate removal volume (3D measurement) to assess the cutting efficiency rather than measuring the depth of preparations (2D measurement) was beneficial since air-abrasion removes material unevenly. This was observed when increasing the nozzle-substrate distance or adjusting the nozzle angle to 45 degrees which promoted the cutting efficiency of the system according to the volume measurements, whilst the cutting pattern of these settings produced a reduced depth (see Figure 3-7; p: 98 and Figure 3-8; p: 99). Therefore, the 2D measurement is not the most representative method for assessing the cutting efficiency of air-abrasion.

Using ultrasonics / sono-abrasion instruments may develop cracks within the brittle enamel substrate in particular, at the stage of finishing cavity margins due to the oscillation of these instruments (Vieira et al., 2007; Tassery et al., 2013; Decup and Lasfargues, 2014). The 3D images of surfaces prepared using BAG air-abrasion in Chapters 3 and 4 revealed rounded cavo-surface margins and internal line angles with micro-roughness. Those features provide an ideal surface for dental adhesive restorative materials and might be useful to pre-condition the resin composite restoration rather than removing it when repairing defective restorations.

The effect of powder flow rate changes has been shown to be clinically and statistically significant in regard to the efficacy of the air-abrasion cutting effect (Jost-Brinkmann, 1998; Cook et al., 2001; Paolinelis et al., 2009). It is important that the manufacturers of air-abrasion technology should supply and highlight this important information for the clinical end user. Banerjee et al. (2008b) and Honda et al. (2008) showed that the powder flow rate was affected significantly by the powder reservoir volume and the air-abrasion nozzle design. The current study revealed that the emitted powder flow rate was also affected considerably by the powder-admix mechanism and the air pressure. The experiments conducted in Chapter 2 suggest a protocol to calibrate air-abrasion systems prior to any further

investigation. Clinically, a constant PFR is preferable to obtain a homogenous and efficient cutting pattern. In addition, controlling air pressure and PFR independently could be useful for specific clinical purposes such as the removal of resin composite restorations and pre-conditioning dental surfaces using bioactive materials.

The clinical use of BAG air-abrasion requires adequate training to benefit from its cutting characteristics and to avoid the undesirable over-preparation. As with other clinical operative techniques, BAG air-abrasion exhibits the lack of a pure “self-limiting” nature, when managing dentine caries (Paolinelis et al., 2008; Wang et al., 2011b). This indicates that further developments are still required to enhance the performance of this technology with regards to dentine caries. These developments might include the introduction of a self-selective air-abrasive powder for caries infected dentine. This depends on the fact that dental tissues exhibit a wide variation in their mechanical / physical properties (see Table 1-8; p: 44), which perhaps restrains the use of a single air-abrasive powder for all operative procedures in MI Conservative Dentistry. In the future, different abrasive powders might be used according to the clinical practice; BAG for enamel preparation and resin composite removal, PAA-BAG for pre-conditioning enamel WSLs to promote the remineralisation process, and probably a new abrasive powder for excavating selectively irreparable carious dentine.

The second experimental section of this thesis focused on the remineralisation of enamel white spot lesions using BAG 45S5 technology. Although the enamel WSL has been characterised histologically as early as 1918 by Hopewell-Smith and there is ample evidence to show that enamel WSLs can be remineralised in-vitro and in-vivo, the non-operative therapy of this type of early lesion is still the subject of investigation. This investigation aims to analyse the complex physico-chemical interaction between remineralisation agents and enamel structure, to promote and accelerate the remineralisation process and to translate the research findings from the laboratory to the clinic. In minimum intervention (MI) and minimally invasive dentistry, the enamel WSL should be treated non-invasively by inhibiting the demineralisation and enhancing the remineralisation process (Featherstone, 2009). Figure 7-2 outlines the different approaches to treat enamel WSL according to these MI concepts.

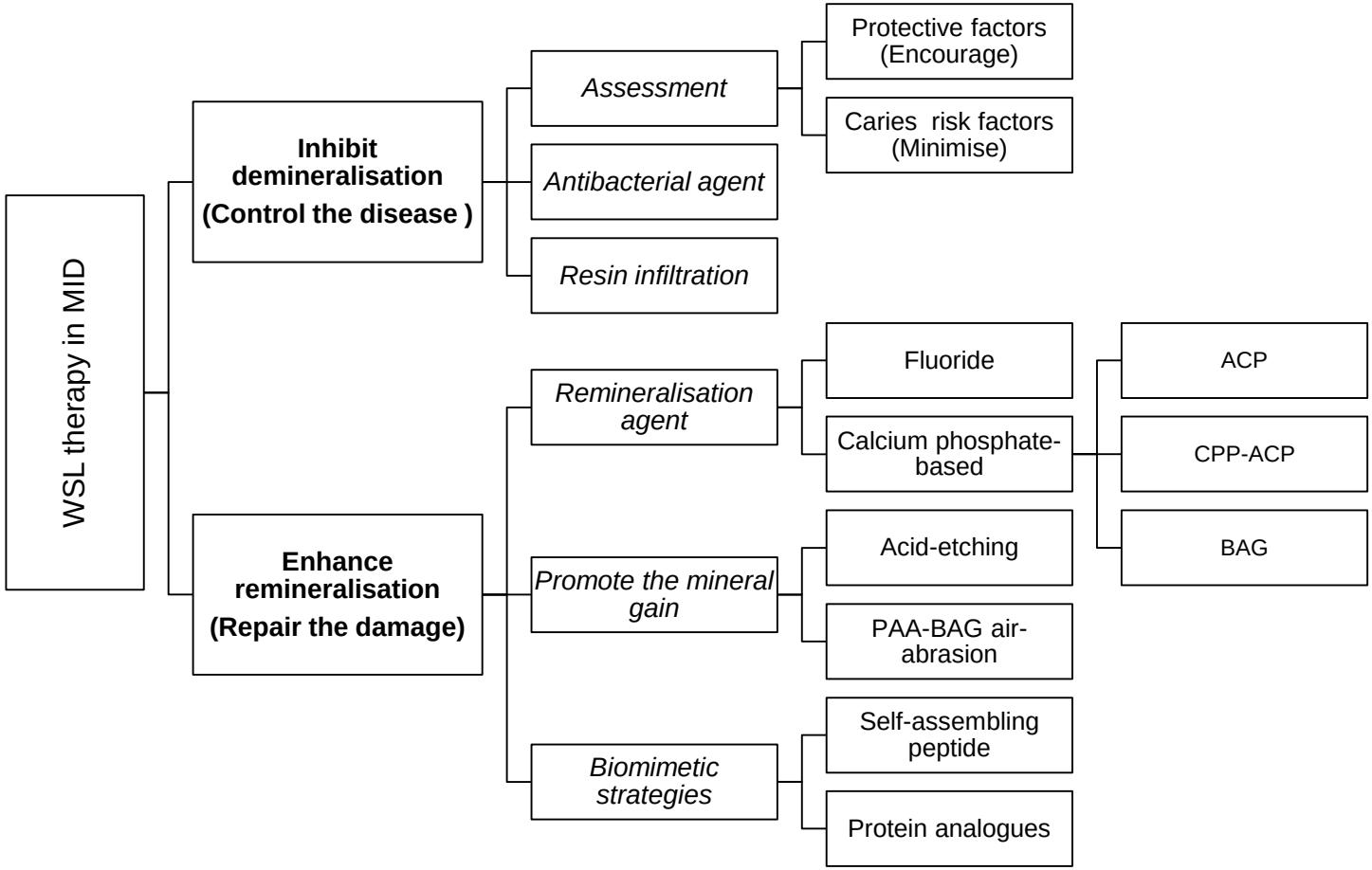

Figure 7-2: Different topical approaches to treat enamel WSLs according to the minimum intervention / minimally invasive (MI) patient care philosophies.

One of the clinical approaches to inhibit further demineralisation of an enamel WSL is to infiltrate the pore spaces with a low-viscosity light-cured resin such as Icon®-Infiltrant. This treatment aims to fill the pores of the lesion, provide mechanical support to the remaining tissue, inhibit the demineralisation process and improve the aesthetic appearance of a WSL (Robinson et al., 2001; Mueller et al., 2006). In this system, the resin application should be proceeded by pre-conditioning the lesion surfaces using 15% HCl (Paris et al., 2007; Neuhaus et al., 2012). Using HCl acid, however, removes a considerable amount of enamel that may extend up to 50 µm into the lesion, which might be equivalent to the whole lesion depth itself (Meyer-Lueckel et al., 2007). In addition, it has been demonstrated that the infiltrated resin may be degraded over time exposing the weakly demineralised body of the lesion to further caries progression (Van Landuyt et al., 2011; Neuhaus et al., 2012). This approach is time-consuming and technique sensitive and requires patients' cooperation through several procedural steps (Ekstrand et al., 2012). In addition, the potential leakage at the resin-enamel interface may cause discoloration of treated lesions and therefore, there is a need for clinical evaluation of the colour stability of lesions infiltrated with resin (Cohen-Carneiro et al., 2013; Borges et al., 2014). The main limitation of this approach is that the lesion pores are sealed by the resin preventing the potential repair of the lesion structure by the dynamic remineralisation process within the oral cavity (Brunton et al., 2013). According to current dental literature, more in-vitro studies and clinical trials are still required to ascertain the long-term success of this treatment (Yim et al., 2014).

The application of a remineralising therapy is preferable to repair the damaged lesion structure and to reduce the pores size / volume of pores within the lesion body (Walsh and Brostek, 2013). The use of fluoride in enamel de- and remineralisation is well-documented. However, repairing the incipient enamel WSL using fluoride is a slow process, limited by the bioavailability of calcium and phosphate ions (Cochrane et al., 2010). The apatite creation induced by BAG 45S5 is chemically and structurally equivalent to the mineral phase in bone and tooth (Wen et al., 2000). Therefore, BAG has the potential to remineralise enamel WSLs. The multi-analytical approach used in the present studies permitted the assessment of the mechanical, chemical, optical and ultra-structural changes within the same WSLs following the remineralisation therapy using BAG 45S5

mixtures, which has not been reported in previous studies evaluating the remineralisation of enamel WSLs using BAG 45S5; Alauddin et al. (2005) used confocal laser scanning microscopy (CLSM) in their study, Burwell et al. (2009) and Guo et al. (2014) measured the microhardness and scanned the surfaces using SEM, Rehder Neto et al. (2009) measured the surface Knoop microhardness, Gjorgievska et al. (2013) scanned the samples using SEM-EDX and finally, Ballard et al. (2013) evaluated the structural changes using a photographic camera and non-contact profilometry.

Raman micro-spectroscopy was used in the current study to characterise quantitatively the mineral content of enamel. The parameters used to acquire the Raman images lead to a high resolution of 2.7 µm which was sufficient to identify the mineral content of the treated lesion (approximately 70-100 µm deep). It has been suggested that Raman spectroscopy might be used clinically, in particular to aid in cancer diagnosis (Bakker Schut et al., 2000; Caspers et al., 2003). Developing Raman spectroscopy for the clinical dental applications using an optical fibre probe could introduce a promising diagnostic technique to assess the chemical content of carious lesions in-vivo in the future. This development might enable dental care professionals to assess the demineralisation degree within the lesion and to monitor the mineral recovery during the remineralisation therapy.

One of the fundamental requirements for an efficient remineralisation material is that it diffuses or delivers calcium and phosphate into the subsurface (Zero, 2006). The HCA crystal induced by BAG 45S5 exhibited approximately 50 nm thickness (Wen et al., 2000), and therefore these crystals could penetrate the pores of WSL surfaces which are approximately 200-300 nm wide (see Figure 6-16; p: 172). The microscopy analysis and OCT scans indicated that the mineral precipitations induced by BAG 45S5 mixtures penetrated the lesion surface through to the lesion body. The SEM analysis of the fractured sections (Figure 6-16; p: 172) permitted the direct observation of these precipitations within the lesion depth. In fact, the complete repair of WSLs had not occurred using this therapy even when the surfaces were pre-conditioned prior to remineralisation. The incomplete remineralisation of WSLs has been reported in the dental literature using other remineralisation systems *in vitro* and *in vivo* (Al-Khateeb et al., 1998; Beerens et al., 2010). This could be attributed to the fact

that surface pores might be occluded by the “newly” formed mineral precipitated reducing the access of ions to the body of the lesion and thus, restricting the remineralisation to the outermost lesion surface (Robinson et al., 1990). This might be also explained since the “new” minerals formed are not deposited and diffused in the same way as those of sound enamel crystals (Ogaard, 1989). Other factors such as the shape, the orientation and the dimensions of “new” minerals can affect the distribution of the minerals along the lesion structures (Fan et al., 2009).

One of the proposed solutions to the problem of the incomplete remineralisation of WSLs was the use of the remineralisation agent in a reduced concentration in order to promote the gradual complete recovery (O'reilly and Featherstone, 1987). However, both in-vitro and in-vivo studies demonstrated the still incomplete WSL remineralisation using this approach (Al-Khateeb et al., 1998; Zero, 2006). Another suggested technique to increase the remineralisation of a WSL is pre-conditioning the early lesion surface with phosphoric acid to increase the porosity of the lesion surface (Collys et al., 1991; Flaitz and Hicks, 1993; Al-Khateeb et al., 2000; Al-Khateeb et al., 2014). The profilometry and Raman dataset in the present study revealed that pre-conditioning the lesion surface using phosphoric acid deteriorated the integrity of the lesion structure and did not promote the mineral precipitates at the lesion surface. Therefore, the use of this technique to increase the mineral gain of a WSL is questionable since it exhibits a rather destructive nature due to the demineralisation effect of phosphoric acid as discussed earlier in this thesis. Alternatively, pre-conditioning WSL surfaces with PAA-BAG air-abrasion modified the lesion surface physically by removing an ultra-thin surface layer and increasing the lesion’s surface area. This approach enhanced the remineralisation effect using BAG 45S5 therapy, but did not achieve the optimal complete recovery.

A promising solution has been reported in the dental literature depending on using biomimetic remineralisation strategies. Non-collagenous protein analogues such as polyacrylic acid (PAA) and sodium trimetaphosphate are incorporated in the carrier vehicle to bind the calcium and phosphate ions forming nano-precursors, including amorphous calcium phosphate, small enough to penetrate the carious lesion more effectively. These nano-precursors then undergo self-

assembly and crystallographic alignment forming a crystalline structure within the lesion depth (Iijima and Moradian-Oldak, 2004; Liu et al., 2011; Qi et al., 2012; Niu et al., 2014). This approach has been recognised to remineralise dentine caries. In this study, an initial investigation was conducted to consider the impact of incorporating PAA in BAG therapy on the remineralisation of enamel WSLs. The FTIR and SEM results suggested that PAA interacted in the formation of the HCA induced by BAG 45S5, with smaller minerals formed and deposited on the superficial surfaces of treated WSLs. However, the role of PAA in the remineralisation process has not been identified in this study and therefore, the PAA-BAG composition was only considered as an air-abrasive powder at this stage. Further investigations are still required.

Another biomimetic remineralisation route has been proposed using oligometric β-sheet-forming peptides that undergo hierarchical self-assembling to provide 3D biomimetic scaffolds capable of nucleating hydroxyapatite *de novo* (Kirkham et al., 2007). It has been shown that a single treatment of self-assembling peptide (P_{11}-4) promoted WSL remineralisation in-vivo, providing a promising therapeutic option in minimally invasive dentistry (MID) (Brunton et al., 2013). The unique feature of the peptide biomimetic route is the use of an injectable bioactive material which in turn, facilitated the clinical translation of this system (Brunton et al., 2013), whilst in the non-collagenous protein analogue biomimetic route, the specimens were immersed in a remineralisation solution containing the biomimetic analogue which is inapplicable clinically (Niu et al., 2014).

In order for any remineralisation strategy to be useful clinically, it should exhibit a rapid rate of action (Featherstone et al., 1981). Therefore, using a dissolvable remineralisation agent with biomimetic strategies may accelerate the repair process when compared to the use of biomimetic strategies alone since salivary minerals can assist enamel remineralisation, but within a limited range due to pH fluctuations *in vivo* (Eisenburger et al., 2001; Huang et al., 2013). The beneficial effect of fluoride in enamel WSL remineralisation is limited by the bioavailability of fluoride in-vivo, which decreases rapidly to reach the baseline level (0.02-0.15 ppm F^-) only after 2 hours of fluoride application (Naumova et al., 2010). BAG 45S5 can act as a source of calcium and phosphate ions with a high bioactivity index (I_B = 12.5) compared to other bioactive materials such as hydroxyapatite

(I_B = 3.1) (Hench, 1988). Therefore, it has the potential to remineralise enamel white spot lesions with an increased rate of HCA formation. Referring back to Figure 7-2; p: 189, it seems that the efficient WSL remineralisation outcomes might be obtained using a combination of different techniques including (a); minimising / altering the patient caries risk factors to inhibit the demineralisation process at source, (b); pre-conditioning the lesion surface using PAA-BAG air-abrasion to increase the surface area exposing the subsurface structures, (c); the remineralisation treatment with BAG 45S5 to provide external calcium and phosphate ions with the intention of promoting and accelerating enamel remineralisation and (d): the use of biomimetic strategies to control the crystal shape / dimensions and to organise the distribution of the "new" minerals through the whole lesion depth. This suggested multi-step protocol requires further in-vitro and in-situ investigations prior to clinical introduction.

In conclusion, this thesis has demonstrated that the cutting efficiency / pattern of BAG air-abrasion can be adjusted according to the clinical application by controlling the system's operating parameters, and has showed that BAG 45S5 mixtures can remineralise enamel WSLs paving the way for further development to promote the remineralisation process. Therefore, further work is justified to assess the clinical effectiveness of BAG air-abrasion system in managing non-invasively, the carious lesion *in situ* and *in vivo*.

Suggestions for future work

1. In-situ and in-vivo studies to assess enamel WSL remineralisation using BAG 45S5 slurry, including unconditioned and pre-conditioned lesions with PAA-BAG air-abrasion.

2. Detect the mechanism(s) by which PAA modified the shape of the mineral depositions when it was incorporated into BAG 45S5.

3. Develop self-selective air-abrasive powder for caries infected dentine.

4. Translate the in-vitro measurement of enamel mineral content using Raman micro-spectroscopy into a clinical approach by developing an in-vivo Raman spectroscopic optical fibre probe system for clinical dental applications.

5. Examine the antibacterial efficacy of BAG 45S5 on dental plaque development and detect the effect of this interaction on enamel de- and remineralisation.

6. Further developing the remineralisation of enamel WSLs using BAG technology with biomimetic remineralisation strategies through the same experimental set-up conducted in this thesis.

References

Aas, J. A., Griffen, A. L., Dardis, S. R., Lee, A. M., Olsen, I., Dewhirst, F. E., Leys, E. J. & Paster, B. J. 2008. Bacteria of dental caries in primary and permanent teeth in children and young adults. *Journal of Clinical Microbiology,* 46**,** 1407-17.

Aasenden, R., Brudevold, F. & Mccann, H. G. 1968. The response of intact and experimentally altered human enamel to topical fluoride. *Archives of Oral Biology,* 13**,** 543-552

Acil, Y., Mobasseri, A. E., Warnke, P. H., Terheyden, H., Wiltfang, J. & Springer, I. 2005. Detection of mature collagen in human dental enamel. *Calcified Tissue International,* 76**,** 121-6.

Adeyemi, A. A., Jarad, F. D., Pender, N. & Higham, S. M. 2006. Comparison of quantitative light-induced fluorescence (QLF) and digital imaging applied for the detection and quantification of staining and stain removal on teeth. *Journal of Dentistry,* 34**,** 460-466.

Aina, V., Malavasi, G., Fiorio Pla, A., Munaron, L. & Morterra, C. 2009. Zinc-containing bioactive glasses: surface reactivity and behaviour towards endothelial cells. *Acta Biomaterialia,* 5**,** 1211-22.

Al-Khateeb, S., Exterkate, R., Angmar-Mansson, B. & Ten Cate, J. M. 2000. Effect of acid-etching on remineralization of enamel white spot lesions. *Acta Odontologica Scandinavica,* 58**,** 31-6.

Al-Khateeb, S., Forsberg, C.-M., De Josselin De Jong, E. & Angmar-Månsson, B. 1998. A longitudinal laser fluorescence study of white spot lesions in orthodontic patients. *American Journal of Orthodontics and Dentofacial Orthopedics,* 113**,** 595-602.

Al-Khateeb, S., Tarazi, S., Al Maaitah, E., Al-Batayneh, O. & Alhaija, E. A. 2014. Does acid etching enhance remineralisation of arrested white spot lesions? *European Archives of Paediatric Dentistry***,** 1-7.

Alammari, M. R., Smith, P. W., De Josselin De Jong, E. & Higham, S. M. 2013. Quantitative light-induced fluorescence (QLF): A tool for early occlusal dental caries detection and supporting decision making in vivo. *Journal of Dentistry,* 41**,** 127-132.

Alauddin, S., Greenspan, D., Anusavice, K. & Mecholsky, J. 2005. In vitro human enamel remineralization using bioactive glass containing dentifrice. *Journal of Dental Research,* 84**,** 2546.

Alauddin, S. S. 2004. *In vitro remineralization of human enamel with bioactive glass containing dentifrice using confocal microscopy and nanoindentation analysis for early caries defense.* University of Florida.

Allan, I., Newman, H. & Wilson, M. 2001. Antibacterial activity of particulate bioglass against supra- and subgingival bacteria. *Biomaterials,* 22**,** 1683-7.

Almahdy, A., Downey, F. C., Sauro, S., Cook, R. J., Sherriff, M., Richards, D., Watson, T. F., Banerjee, A. & Festy, F. 2012. Microbiochemical analysis of carious dentine using Raman and fluorescence spectroscopy. *Caries Research,* 46**,** 432-40.

Amaechi, B. T., Porteous, N., Ramalingam, K., Mensinkai, P. K., Ccahuana Vasquez, R. A., Sadeghpour, A. & Nakamoto, T. 2013. Remineralization of artificial enamel lesions by Theobromine. *Caries Research,* 47**,** 399-405.

Angmar-Mansson, B. & Bosch, J. J. T. 2001. Quantitative light-induced fluorescence (QLF): a method for assessment of incipient caries lesions. *Dentomaxillofacial Radiology,* 30**,** 298-307.

Angmar, B., Carlström, D. & Glas, J. E. 1963. Studies on the ultrastructure of dental enamel: IV. The mineralization of normal human enamel. *Journal of ultrastructure research,* 8**,** 12-23.

Antunes, L. A., Pedro, R. L., Vieira, A. S. & Maia, L. C. 2008. Effectiveness of high speed instrument and air abrasion on different dental substrates. *Brazilian Oral Research,* 22**,** 235-41.

Arcos, D., Greenspan, D. C. & Vallet-Regí, M. 2003. A new quantitative method to evaluate the in vitro bioactivity of melt and sol-gel-derived silicate glasses. *Journal of Biomedical Materials Research Part A,* 65**,** 344-351.

Ashmore, H., Van Abbe, N. J. & Wilson, S. J. 1972. The measurement in vitro of dentine abrasion by toothpaste. *British Dental Journal,* 133**,** 60-66.

Atmeh, A. R., Chong, E. Z., Richard, G., Festy, F. & Watson, T. F. 2012. Dentin-cement interfacial interaction: calcium silicates and polyalkenoates. *Journal of Dental Research,* 91**,** 454-9.

Attin, T. 2006. Methods for assessment of dental erosion. *Monographs in Oral Science,* 20**,** 152-72.

Austin, R. S., Rodriguez, J. M., Dunne, S., Moazzez, R. & Bartlett, D. W. 2010. The effect of increasing sodium fluoride concentrations on erosion and attrition of enamel and dentine in vitro. *Journal of Dentistry,* 38**,** 782-7.

Awonusi, A., Morris, M. D. & Tecklenburg, M. M. 2007. Carbonate assignment and calibration in the Raman spectrum of apatite. *Calcified Tissue International* 81**,** 46-52.

Azarpazhooh, A. & Limeback, H. 2008. Clinical efficacy of casein derivatives a systematic review of the literature. *The Journal of the American Dental Association,* 139**,** 915-924.

Bader, J. D., Shugars, D. A. & Bonito, A. J. 2001. A systematic review of selected caries prevention and management methods. *Community Dentistry and Oral Epidemiology,* 29**,** 399-411.

Bae, J.-H., Yi, J., Kim, S., Shim, J.-S. & Lee, K.-W. 2014. Changes in the cutting efficiency of different types of dental diamond rotary instrument with repeated cuts and disinfection. *The Journal of prosthetic dentistry,* 111**,** 64-70.

Bailey, L. R. & Phillips, R. W. 1950. Effect of certain abrasive materials on tooth enamel. *Journal of dental research,* 29**,** 740-748.

Bakker Schut, T., Witjes, M., Sterenborg, H., Speelman, O., Roodenburg, J., Marple, E., Bruining, H. & Puppels, G. 2000. In vivo detection of dysplastic tissue by Raman spectroscopy. *Analytical chemistry,* 72**,** 6010-6018.

Bakry, A. S., Marghalani, H. Y., Amin, O. A. & Tagami, J. 2014a. The effect of a bioglass paste on enamel exposed to erosive challenge. *Journal of Dentistry,* 14**,** 00158-4.

Bakry, A. S., Takahashi, H., Otsuki, M. & Tagami, J. 2014b. Evaluation of new treatment for incipient enamel demineralization using 45S5 bioglass. *Dental Materials* 30**,** 314-20.

Ballard, R. W., Hagan, J. L., Phaup, A. N., Sarkar, N., Townsend, J. A. & Armbruster, P. C. 2013. Evaluation of 3 commercially available materials for resolution of white spot lesions. *American Journal of Orthodontics and Dentofacial Orthopedics,* 143**,** S78-S84.

Banerjee, A. 2013. Minimal intervention dentistry: part 7. Minimally invasive operative caries management: rationale and techniques. *British Dental Journal,* 214**,** 107-11.

Banerjee, A. & Boyde, A. 1998. Autofluorescence and mineral content of carious dentine: scanning optical and backscattered electron microscopic studies. *Caries Research,* 32**,** 219-226.

Banerjee, A., Cook, R., Kellow, S., Shah, K., Festy, F., Sherriff, M. & Watson, T. 2010. A confocal micro-endoscopic investigation of the relationship between the microhardness of carious dentine and its autofluorescence. *European Journal of Oral Sciences,* 118**,** 75-9.

Banerjee, A., Kidd, E. & Watson, T. 2000a. Scanning electron microscopic observations of human dentine after mechanical caries excavation. *Journal of Dentistry,* 28**,** 179-186.

Banerjee, A., Pabari, H., Paolinelis, G., Thompson, I. D. & Watson, T. F. 2011a. An in vitro evaluation of selective demineralised enamel removal using bio-active glass air abrasion. *Clinical oral investigations,* 15**,** 895-900.

Banerjee, A., Paolinelis, G., Socker, M., Mcdonald, F. & Watson, T. F. 2008a. An in vitro investigation of the effectiveness of bioactive glass air-abrasion in the 'selective' removal of orthodontic resin adhesive. *European Journal of Oral Sciences,* 116**,** 488-92.

Banerjee, A., Thompson, I. D. & Watson, T. F. 2011b. Minimally invasive caries removal using bio-active glass air-abrasion. *Journal of Dentistry,* 39**,** 2-7.

Banerjee, A., Uddin, M., Paolinelis, G. & Watson, T. F. 2008b. An investigation of the effect of powder reservoir volume on the consistency of alumina powder flow rates in dental air-abrasion devices. *Journal of Dentistry,* 36**,** 224-7.

Banerjee, A. & Watson, T. F. 2002. Air abrasion: its uses and abuses. *Dental Update,* 29**,** 340-6.

Banerjee, A. & Watson, T. F. 2011. *Pickard's manual of operative dentistry 9th ed,* Oxford ; New York, Oxford University Press.

Banerjee, A., Watson, T. F. & Kidd, E. A. 2000b. Dentine caries excavation: a review of current clinical techniques. *British Dental Journal,* 188**,** 476-82.

Banerjee, A., Watson, T. F. & Kidd, E. A. 2001. Dentine caries: take it or leave it? *Journal of the South African Dental Association* 56**,** 186-92.

Barbour, M. E. & Rees, J. S. 2004. The laboratory assessment of enamel erosion: a review. *Journal of Dentistry,* 32**,** 591-602

Baumgartner, A., Dichtl, S., Hitzenberger, C. K., Sattmann, H., Robl, B., Moritz, A., Fercher, A. F. & Sperr, W. 2000. Polarization-sensitive optical coherence tomography of dental structures. *Caries Research,* 34**,** 59-69.

Beerens, M. W., Van Der Veen, M. H., Van Beek, H. & Ten Cate, J. M. 2010. Effects of casein phosphopeptide amorphous calcium fluoride phosphate paste on white spot lesions and dental plaque after orthodontic treatment: a 3-month follow-up. *European Journal of Oral Sciences,* 118**,** 610-7.

Berkovitz, B. K. B., Holland, G. R. & J., M. B. 2002. *Oral Anatomy, Histology and Embryology*, Mosby

Bertassoni, L. E., Habelitz, S., Kinney, J. H., Marshall, S. J. & Marshall, G. W., Jr. 2009. Biomechanical perspective on the remineralization of dentin. *Caries Research,* 43**,** 70-7.

Bertoluzza, A., Fagnano, C., Monti, P., Simoni, R., Tinti, A., Tosi, M. R. & Caramazza, R. 1992. Raman spectroscopy in the study of biocompatibility. *Clinical materials,* 9**,** 49-68.

Beuselinck, L., Govers, G., Poesen, J., Degraer, G. & Froyen, L. 1998. Grain-size analysis by laser diffractometry: comparison with the sieve-pipette method. *Catena,* 32**,** 193-208.

Bishara, S. E. & Ostby, A. W. 2008. White spot lesions: formation, prevention, and treatment. *Seminars in Orthodontics,* 14**,** 174-182.

Black, R. B. 1945. Technique for nonmechanical preparation of cavities and prophylaxis. *Journal of the American Dental Association,* 32**,** 955-965.

Black, R. B. 1950. Airbrasive: some fundamentals. *Journal of the American Dental Association (1939),* 41**,** 701-710.

Black, R. B. 1955. Application and revaluation of air abrasive technic. *Journal of the American Dental Association,* 50**,** 408-414.

Bonetti, G. A., Zanarini, M., Incerti Parenti, S., Lattuca, M., Marchionni, S. & Gatto, M. R. 2011. Evaluation of enamel surfaces after bracket debonding: an in-vivo study with scanning electron microscopy. *American Journal of Orthodontics and Dentofacial Orthopedics,* 140**,** 696-702.

Borges, A., Caneppele, T., Luz, M., Pucci, C. & Torres, C. 2014. Color stability of resin used for caries infiltration after exposure to different staining solutions. *Operative Dentistry,* 39**,** 433-40.

Bowen, R. L. 1962. *Dental filling material comprising vinyl silane treated fused silica and a binder consisting of the reaction product of bis phenol and glycidyl acrylate*. United States of America patent application 3,006,112.

Boyde, A. & Lester, K. S. 1967. Electron microscopy of resorbing surfaces of dental hard tissues. *Zeitschrift fuer Zellforschung und Mikroskopische Anatomie,* 83**,** 538-548.

Briner, W. W., Gray, J. A. & Francis, M. D. 1974. Significance of enamel remineralization. *Journal of dental research,* 53**,** 239-243.

Brochner, A., Christensen, C., Kristensen, B., Tranaeus, S., Karlsson, L., Sonnesen, L. & Twetman, S. 2011. Treatment of post-orthodontic white spot lesions with casein phosphopeptide-stabilised amorphous calcium phosphate. *Clinical Oral Investigations,* 15**,** 369-73.

Brunton, P., Davies, R., Burke, J., Smith, A., Aggeli, A., Brookes, S. & Kirkham, J. 2013. Treatment of early caries lesions using biomimetic self-assembling peptides–a clinical safety trial. *British dental journal,* 215**,** 1-6.

Buchalla, W., Imfeld, T., Attin, T., Swain, M. V. & Schmidlin, P. R. 2008. Relationship between nanohardness and mineral content of artificial carious enamel lesions. *Caries Research,* 42**,** 157-63.

Burke, F. J. 2003. From extension for prevention to prevention of extension:(minimal intervention dentistry). *Dental update,* 30**,** 492-8.

Burns, T., Wilson, M. & Pearson, G. J. 1995. Effect of dentine and collagen on the lethal photosensitization of Streptococcus mutans. *Caries Research,* 29**,** 192-197.

Burwell, A., Jennings, D. & Greenspan, D. 2009a. NovaMin and dentin hypersensitivity - in vitro evidence of efficacy. *The Journal of clinical dentistry,* 21**,** 66-71.

Burwell, A. K., Litkowski, L. J. & Greenspan, D. C. 2009b. Calcium sodium phosphosilicate (NovaMin): remineralization potential. *Advances in Dental Research,* 21**,** 35-9.

Can, A. M., Darling, C. L. & Fried, D. 2008. High-resolution PS-OCT of Enamel Remineralization. *Proceedings of the Society of Photo-Optical Instrumentation Engineers,* 6843**,** 68430T1-68430T7.

Canli, S. 2010. *Thickness analysis of thin films by energy dispersive X-ray spectroscopy* Middle east technical university

Carlström, D. & Glas, J. E. 1963. Studies on the ultrastructure of dental enamel: III. The birefringence of human enamel. *Journal of ultrastructure research,* 8**,** 1-11.

Carter, C. B. & Norton, M. G. 2007. *Ceramic materials*, Springer.

Caspers, P., Lucassen, G. & Puppels, G. 2003. Combined in vivo confocal Raman spectroscopy and confocal microscopy of human skin. *Biophysical journal,* 85**,** 572-580.

Celiberti, P., Francescut, P. & Lussi, A. 2006. Performance of four dentine excavation methods in deciduous teeth. *Caries Research,* 40**,** 117-123.

Cerruti, M., Greenspan, D. & Powers, K. 2005. Effect of pH and ionic strength on the reactivity of Bioglass 45S5. *Biomaterials,* 26**,** 1665-74.

Chan, K. H., Hirasuna, K. & Fried, D. 2014. Analysis of enamel surface damage after selective laser ablation of composite from tooth surfaces. *Photonics and Lasers in Medicine,* 3**,** 37-45.

Chen, F., Brown, G. M. & Song, M. 2000. Overview of three-dimensional shape measurement using optical methods. *Optical Engineering,* 39**,** 10-22.

Chen, H., Liu, X., Dai, J., Jiang, Z., Guo, T. & Ding, Y. 2013. Effect of remineralizing agents on white spot lesions after orthodontic treatment: A systematic review. *American Journal of Orthodontics and Dentofacial Orthopedics,* 143**,** 376-382 e3.

Cho, S. D., Rajitrangson, P., Matis, B. A. & Platt, J. A. 2013. Effect of Er, Cr: YSGG laser, air abrasion, and silane application on repaired shear bond strength of composites. *Operative dentistry,* 38**,** E1-E9.

Choo-Smith, L. P., Edwards, H. G. M., Endtz, H. P., Kros, J. M., Heule, F., Barr, H., Robinson, J. S., Bruining, H. A. & Puppels, G. J. 2002. Medical applications of Raman spectroscopy: from proof of principle to clinical implementation. *Biopolymers,* 67**,** 1-9.

Cochrane, N. J., Anderson, P., Davis, G. R., Adams, G. G., Stacey, M. A. & Reynolds, E. C. 2012a. An x-ray microtomographic study of natural white-spot enamel lesions. *Journal of dental research,* 91**,** 185-191.

Cochrane, N. J., Cai, F., Huq, N. L., Burrow, M. F. & Reynolds, E. C. 2010. New approaches to enhanced remineralization of tooth enamel. *Journal of Dental Research,* 89**,** 1187-97.

Cochrane, N. J., Ratneser, S. & Reynolds, E. C. 2012b. Effect of different orthodontic adhesive removal techniques on sound, demineralized and remineralized enamel. *Australian dental journal,* 57**,** 365-372.

Cohen-Carneiro, F., Pascareli, A. M., Christino, M. R. C., Vale, H. F. D. & Pontes, D. G. 2013. Color stability of carious incipient lesions located in enamel and treated with resin infiltration or remineralization. *International Journal of Paediatric Dentistry*.

Collys, K., Cleymaet, R., Coomanst, D. & Slop, D. 1991. Acid-etched enamel surfaces after 24 h exposure to calcifying media in-vitro and in-vivo. *Journal of Dentistry,* 19**,** 230-235.

Cook, R. J., Azzopardi, A., Thompson, I. D. & Watson, T. F. 2001. Real-time confocal imaging, during active air abrasion - substrate cutting. *Journal of Microscopy,* 203**,** 199-207.

Correa-Afonso, A. M., Palma-Dibb, R. G. & Pecora, J. D. 2010. Composite filling removal with erbium:yttrium-aluminum-garnet laser: morphological analyses. *Lasers in Medical Science,* 25**,** 1-7.

Craig, R. G., Peyton, F. A. & Johnson, D. W. 1961. Compressive properties of enamel, dental cements, and gold. *Journal of dental research,* 40**,** 936-945.

Cristofaro, D., Riera, R. G., Giner, L. & Mayoral, J. R. 2013. Comparative Study of the Cutting Efficiency and Working Life of Carbide Burs. *Journal of Prosthodontics,* 22**,** 391-396.

Crombie, F. A., Cochrane, N. J., Manton, D. J., Palamara, J. E. & Reynolds, E. C. 2013. Mineralisation of Developmentally Hypomineralised Human Enamel in vitro. *Caries Research,* 47**,** 259-63.

Cross, K. J., Huq, N. L., Palamara, J. E., Perich, J. W. & Reynolds, E. C. 2005. Physicochemical characterization of casein phosphopeptide-amorphous calcium phosphate nanocomplexes. *Journal of Biological Chemistry,* 280**,** 15362-9.

Damen, J. J. M., Exterkate, R. a. M. & Ten Cate, J. M. 1997. Reproducibility of TMR for the determination of longitudinal mineral changes in dental hard tissues. *Advances in Dental Research,* 11**,** 415-419.

Darling, A. I. 1961. The selective attack of caries on the dental enamel. *Annals of The Royal College of Surgeons of England,* 29**,** 354-69.

Dawes, C. 2003. What is the critical pH and why does a tooth dissolve in acid? *Journal Canadian Dental Association,* 69**,** 722-4.

De Jong, E. D. J., Van Der Linden, A. & Ten Bosch, J. J. 1987. Longitudinal microradiography: a non-destructive automated quantitative method to follow mineral changes in mineralised tissue slices. *Physics in medicine and biology,* 32**,** 1209-1220.

Decup, F. & Lasfargues, J. 2014. Minimal intervention dentistry II: part 4. Minimal intervention techniques of preparation and adhesive restorations. The contribution of the sono-abrasive techniques. *British Dental Journal,* 216**,** 393-400.

Deng, M., Wen, H. L., Dong, X. L., Li, F., Xu, X., Li, H., Li, J. Y. & Zhou, X. D. 2013. Effects of 45S5 bioglass on surface properties of dental enamel subjected to 35% hydrogen peroxide. *International Journal of Oral Science,* 5**,** 103-10.

Depaola, P. F., Aasenden, R. & Brudevold, F. 1971. The use of topically applied acidulated phosphate-fluoride preceded by mild etching of the enamel: a one-year clinical trial. *Archives of Oral Biology,* 16**,** 1155-1163.

Deyhle, H., White, S. N., Bunk, O., Beckmann, F. & Müller, B. 2014. Nanostructure of carious tooth enamel lesion. *Acta Biomaterialia,* 10**,** 355-364.

Dickinson, M. E., Wolf, K. V. & Mann, A. B. 2007. Nanomechanical and chemical characterization of incipient in-vitro carious lesions in human dental enamel. *Archives of Oral Biology,* 52**,** 753-760.

Doerner, M. F. & Nix, W. D. 1986. A method for interpreting the data from depth-sensing indentation instruments. *Journal of Materials Research,* 1**,** 601-609.

Dong, Z. H., Chang, J. A., Zhou, Y. & Lin, K. L. 2011. In vitro remineralization of human dental enamel by bioactive glasses. *Journal of Materials Science,* 46**,** 1591-1596.

Dorter, C., Yildiz, E. & Erdemir, U. 2003. Effect of operators' skills on increase in cavity volume of restorations. *Quintessence International,* 34**,** 27-30.

Dowd, F. J. 1999. Saliva and dental caries. *Dental Clinics of North America,* 43**,** 579-597.

Du Min, Q., Bian, Z., Jiang, H., Greenspan, D. C., Burwell, A. K., Zhong, J. & Tai, B. J. 2008. Clinical evaluation of a dentifrice containing calcium sodium phosphosilicate (NovaMin) for the treatment of dentin hypersensitivity. *American journal of dentistry,* 21**,** 210-214.

Edgar, W. M., Higham, S. M. & Manning, R. H. 1994. Saliva stimulation and caries prevention. *Advances in Dental Research,* 8**,** 239-45.

Efflandt, S., Magne, P., Douglas, W. & Francis, L. 2002. Interaction between bioactive glasses and human dentin. *Journal of Materials Science: Materials in Medicine,* 13**,** 557-565.

Eisenburger, M., Addy, M., Hughes, J. A. & Shellis, R. P. 2001. Effect of time on the remineralisation of enamel by synthetic saliva after citric acid erosion. *Caries Research,* 35**,** 211-215.

Ekstrand, K., Martignon, S., Bakhshandeh, A. & Ricketts, D. 2012. The non-operative resin treatment of proximal caries lesions. *Dental Update,* November**,** 614-622.

Eliades, T., Gioka, C., Eliades, G. & Makou, M. 2004. Enamel surface roughness following debonding using two resin grinding methods. *European Journal of Orthodontics,* 26**,** 333-338.

Elkassas, D. & Arafa, A. 2014. Remineralizing efficacy of different calcium-phosphate and fluoride based delivery vehicles on artificial caries like enamel lesions. *Journal of Dentistry,* 42**,** 466-474.

Elliott, J. C., Wong, F. S. L., Anderson, P., Davis, G. R. & Dowker, S. E. P. 1998. Determination of mineral concentration in dental enamel from X-ray attenuation measurements. *Connective tissue research,* 38**,** 61-72.

Epstein, S. 1951. Analysis of airbrasive procedures in dental practice. *Journal of the American Dental Association* 43**,** 578-582.

Ercoli, C., Rotella, M., Funkenbusch, P. D., Russell, S. & Feng, C. 2009. In vitro comparison of the cutting efficiency and temperature production of 10 different rotary cutting instruments. Part I: Turbine. *Journal of Prosthetic Dentistry,* 101**,** 248-61.

Ericson, D. 2003. What is minimally invasive dentistry? *Oral health & preventive dentistry,* 2**,** 287-292.

Eshel, G., Levy, G. J., Mingelgrin, U. & Singer, M. J. 2004. Critical evaluation of the use of laser diffraction for particle-size distribution analysis. *Soil Science Society of America Journal,* 68**,** 736-743.

Evans, G. 2008. Raman Analysis Speeds into Biomedicine. *Biophotonics,* February.

Fan, Y., Sun, Z. & Moradian-Oldak, J. 2009. Controlled remineralization of enamel in the presence of amelogenin and fluoride. *Biomaterials,* 30**,** 478-83.

Farah, R. A., Monk, B. C., Swain, M. V. & Drummond, B. K. 2010. Protein content of molar-incisor hypomineralisation enamel. *Journal of Dentistry,* 38**,** 591-6.

Farooq, I., Tylkowski, M., Müller, S., Janicki, T., Brauer, D. S. & Hill, R. G. 2013. Influence of sodium content on the properties of bioactive glasses for use in air abrasion. *Biomedical Materials,* 8**,** 065008(1-9).

Feagin, F., Koulourides, T. & Pigman, W. 1969. The characterization of enamel surface demineralization, remineralization, and associated hardness changes in human and bovine material. *Archives of Oral Biology,* 14**,** 1407-1417.

Featherstone, J. & Doméjean, S. 2012. Minimal intervention dentistry: part 1. From'compulsive'restorative dentistry to rational therapeutic strategies. *British Dental Journal,* 213**,** 441-445.

Featherstone, J., Rodgers, B. & Smith, M. 1981. Physicochemical requirements for rapid remineralization of early carious lesions. *Caries Research,* 15**,** 221-235.

Featherstone, J. D. 1999. Prevention and reversal of dental caries: role of low level fluoride. *Community Dent Oral Epidemiol,* 27**,** 31-40.

Featherstone, J. D. 2000. The science and practice of caries prevention. *Journal of the American Dental Association,* 131**,** 887-99.

Featherstone, J. D. 2004. The continuum of dental caries-evidence for a dynamic disease process. *Journal of Dental Research,* 83 Spec No C**,** C39-42.

Featherstone, J. D. 2009. Remineralization, the natural caries repair process--the need for new approaches. *Advances in Dental Research,* 21**,** 4-7.

Featherstone, J. D. B., Ten Cate, J. M., Shariati, M. & Arends, J. 1983. Comparison of artificial caries-like lesions by quantitative microradiography and microhardness profiles. *Caries Research,* 17**,** 385-391

Ferracane, J. L. 2011. Resin composite - state of the art. *Dental Materials,* 27**,** 29-38.

Ferrazzano, G. F., Amato, I., Cantile, T., Sangianantoni, G. & Ingenito, A. 2011. In vivo remineralising effect of GC tooth mousse on early dental enamel lesions: SEM analysis. *International Dental Journal* 61**,** 210-6.

Field, J., Waterhouse, P. & German, M. 2010. Quantifying and qualifying surface changes on dental hard tissues in vitro. *Journal of Dentistry,* 38**,** 182-90.

Finke, M., Hughes, J. A., Parker, D. M. & Jandt, K. D. 2001. Mechanical properties of in situ demineralised human enamel measured by AFM nanoindentation. *Surface science,* 491**,** 456-467.

Flaitz, C. M. & Hicks, M. J. 1993. Role of the acid-etch technique in remineralization of caries-like lesions of enamel: a polarized light and scanning electron microscopic study. *ASDC journal of dentistry for children,* 61**,** 21-28.

Flückiger, L., Waltimo, T., Stich, H. & Lussi, A. 2005. Comparison of chemomechanical caries removal using Carisolv™ or conventional hand excavation in deciduous teeth in vitro. *Journal of Dentistry,* 33**,** 87-90.

Fontana, M., Li, Y., Dunipace, A. J., Noblitt, T. W., Fischer, G., Katz, B. P. & Stookey, G. K. 1996. Measurement of enamel demineralization using microradiography and confocal microscopy - A correlational study. *Caries Research,* 30**,** 317-325.

Fujikawa, H., Matsuyama, K., Uchiyama, A., Nakashima, S. & Ujiie, T. 2007. Influence of salivary macromolecules and fluoride on enamel lesion remineralization in vitro. *Caries Research,* 42**,** 37-45.

Fure, S., Lingström, P. & Birkhed, D. 2000. Evaluation of Carisolv™ for the chemo–mechanical removal of primary root caries in vivo. *Caries Research,* 34**,** 275-280.

Ganss, C., Lussi, A. & Klimek, J. 2005. Comparison of calcium/phosphorus analysis, longitudinal microradiography and profilometry for the quantitative assessment of erosive demineralisation. *Caries Research,* 39**,** 178-184.

García, A. H., Lozano, M. a. M., Vila, J. C., Escribano, A. B. & Galve, P. F. 2006. Composite resins. A review of the materials and clinical indications. *Medicina Oral, Patología Oral y Cirugía Bucal,* 11**,** E215-220.

Geiger, A. M., Gorelick, L., Gwinnett, A. J. & Griswold, P. G. 1988. The effect of a fluoride program on white spot formation during orthodontic treatment. *American Journal of Orthodontics and Dentofacial Orthopedics,* 93**,** 29-37.

Gilchrist, F., Santini, A., Harley, K. & Deery, C. 2007. The use of micro-Raman spectroscopy to differentiate between sound and eroded primary enamel. *International Journal of Paediatric Dentistry,* 17**,** 274-280.

Gjorgievska, E. & Nicholson, J. 2011. Prevention of enamel demineralization after tooth bleaching by bioactive glass incorporated into toothpaste. *Australian dental journal,* 56**,** 193-200.

Gjorgievska, E. S. & Nicholson, J. W. 2010. A preliminary study of enamel remineralization by dentifrices based on Recalden (CPP-ACP) and Novamin (calcium-sodium-phosphosilicate). *Acta Odontol Latinoam,* 23**,** 234-9.

Gjorgievska, E. S., Nicholson, J. W., Slipper, I. J. & Stevanovic, M. M. 2013. Remineralization of demineralized enamel by toothpastes: a scanning electron microscopy, energy dispersive X-ray analysis, and three-dimensional stereo-micrographic study. *Microscopy and Microanalysis,* 19**,** 587-95.

Gomez, J., Pretty, I. A., Santarpia Iii, R. P., Cantore, B., Rege, A., Petrou, I. & Ellwood, R. P. 2014. Quantitative Light-Induced Fluorescence to Measure Enamel Remineralization in vitro. *Caries Research,* 48**,** 223-227.

Gong, J., Wu, J. & Guan, Z. 1999. Examination of the indentation size effect in low-load Vickers hardness testing of ceramics. *Journal of the European Ceramic Society,* 19**,** 2625-2631.

González-Cabezas, C., Fontana, M., Dunipace, A., Li, Y., Fischer, G., Proskin, H. & Stookey, G. 1998. Measurement of enamel remineralization using microradiography and confocal microscopy. *Caries Research,* 32**,** 385-392.

Gray, J. A. 1966. Kinetics of enamel dissolution during formation of incipient caries-like lesions. *Archives of Oral Biology,* 11**,** 397-422.

Greenspan, D. C. & Hench, L. L. 2013. Bioactive glass for tooth remineralisation and pain desensitization. *In:* HENCH, L. L. (ed.) *An Introduction to Bioceramics.* Second ed. London: Imperial College Press.

Guo, J., Fu, D., Wang, Y., Du, X. & Zhou, L. 2014. Influence of three remineralization materials on physicochemical structure of demineralized enamel. *Journal of Wuhan University of Technology - Materials Science Edition,* 29**,** 410-416.

Gureckis, K. M., Burgess, J. O. & Schwartz, R. S. 1991. Cutting effectiveness of diamond instruments subjected to cyclic sterilization methods. *The Journal of Prosthetic Dentistry,* 66**,** 721-726.

Gustafson, G. 1957. The histopathology of caries of human dental enamel with special reference to the division of the carious lesion into zones. *Acta Odontologica,* 15**,** 13-55.

Habelitz, S., Marshall, S., Marshall Jr, G. & Balooch, M. 2001. Mechanical properties of human dental enamel on the nanometre scale. *Archives of Oral Biology,* 46**,** 173-183.

Hall, A. F., Sadler, J. P., Strang, R., De Jong, E. D. J., Foye, R. H. & Creanor, S. L. 1997. Application of transverse microradiography for measurement of mineral loss by acid erosion. *Advances in Dental Research,* 11**,** 420-425.

Hariri, I., Sadr, A., Nakashima, S., Shimada, Y., Tagami, J. & Sumi, Y. 2013. Estimation of the enamel and dentin mineral content from the refractive index. *Caries Research,* 47**,** 18-26.

Hariri, I., Sadr, A., Shimada, Y., Tagami, J. & Sumi, Y. 2012. Effects of structural orientation of enamel and dentine on light attenuation and local refractive index: an optical coherence tomography study. *Journal of Dentistry,* 40**,** 387-96.

Head, J. 1912. A study of saliva and its action on tooth enamel in reference to its hardening and softening. *Journal of the American Medical Association,* 59**,** 2118-2122

Hedoux, A., Guinet, Y. & Descamps, M. 2011. The contribution of Raman spectroscopy to the analysis of phase transformations in pharmaceutical compounds. *International Journal of Pharmaceutics,* 417**,** 17-31.

Heintze, S. D., Cavalleri, A., Forjanic, M., Zellweger, G. & Rousson, V. 2006. A comparison of three different methods for the quantification of the in vitro wear of dental materials. *Dental Materials,* 22**,** 1051-62.

Hench, L. L. 1988. Bioactive ceramics. *Annals of the New York Academy of Sciences,* 523**,** 54-71.

Hench, L. L. 1991. Bioceramics: from concept to clinic. *Journal of the American Ceramic Society,* 74**,** 1487-1510

Hench, L. L. 2006. The story of Bioglass. *Journal of Materials Science: Materials in Medicine,* 17**,** 967-78.

Hench, L. L. 2010. Glass and Medicine. *International Journal of Applied Glass Science,* 1**,** 104–117.

Hench, L. L. 2013a. Chronology of Bioactive Glass Development and Clinical Applications. *New Journal of Glass and Ceramics,* 3**,** 67-73.

Hench, L. L. 2013b. An Introduction to Bioceramics. Second ed. London: Imperial College Press.

Hench, L. L., Pantano, C. G., Buscemi, P. J. & Greenspan, D. C. 1977. Analysis of bioglass fixation of hip prostheses. *Journal of Biomedical Materials Research,* 11**,** 267-282.

Hench, L. L. & Paschall, H. A. 1974. Histochemical responses at a biomaterial's interface. *Journal of Biomedical Materials Research,* 8**,** 49-64.

Hench, L. L., Splinter, R. J., Allen, W. C. & Greenlee, T. K. 1971. Bonding mechanisms at the interface of ceramic prosthetic materials. *Journal of Biomedical Materials Research,* 5**,** 117-141.

Hench, L. L. & West, J. K. 1990. The Sol-Gel Process. *Chemical Reviews,* 90**,** 33-72.

Hench, L. L. & Wilson, J. 1993. *An introduction to bioceramics*, World Scientific.

Hicks, M. J. & Silverstone, L. M. 1984a. Acid-etching of caries-like lesions of enamel: a polarized light microscopic study. *Caries Research,* 18**,** 315-26.

Hicks, M. J. & Silverstone, L. M. 1984b. Acid-etching of caries-like lesions of enamel: a scanning electron microscopic study. *Caries Research,* 18**,** 327-35.

Hidaka, K., Nishimura, K., Miyazawa, K., Miwa, H. & Goto, S. 2011. Effects of acid etchants used for bonding orthodontic brackets on the remineralization of enamel white-spot lesions. *Orthodontic Waves,* 70**,** 125-135.

Holand, W. & Beall, G. H. 2012. *Glass ceramic technology*, John Wiley & Sons.

Holly, F. J. & Gray, J. A. 1968. Mechanism for incipient carious lesion growth utilizing a physical model based on diffusion concepts. *Archives of Oral Biology,* 13**,** 319-34.

Holmen, L., Thylstrup, A., Ogaard, B. & Kragh, F. 1985. A polarized light microscopic study of progressive stages of enamel caries in vivo. *Caries Research,* 19**,** 348-54.

Honda, K., Kinoshita, N., Abe, T., Hasegawa, M. & Shimizu, A. 2008. Efficacy of a new jet nozzle for removal of carious dentin with an air abrasion system. *Dental Materials Journal,* 27**,** 835-41.

Hong, Y. H. & Lew, K. K. 1995. Quantitative and qualitative assessment of enamel surface following five composite removal methods after bracket debonding. *European Journal of Orthodontics,* 17**,** 121-8.

Hopewell-Smith, A. 1918. *The normal and pathological histology of the mouth*, P. Blakiston's Son & Company.

Horiguchi, S., Yamada, T., Inokoshi, S. & Tagami, J. 1997. Selective caries removal with air abrasion. *Operative dentistry,* 23**,** 236-243.

Hosoya, Y., Shinkawa, H. & Marshall, G. W. 2005. Influence of Carisolv on resin adhesion for two different adhesive systems to sound human primary dentin and young permanent dentin. *Journal of Dentistry,* 33**,** 283-291.

Hu, S., Chang, J., Liu, M. Q. & Ning, C. Q. 2009. Study on antibacterial effect of 45S5 Bioglass. *Journal of Materials Science: Materials in Medicine,* 20**,** 281-286.

Huang, G. J., Roloff-Chiang, B., Mills, B. E., Shalchi, S., Spiekerman, C., Korpak, A. M., Starrett, J. L., Greenlee, G. M., Drangsholt, R. J. & Matunas, J. C. 2013. Effectiveness of MI Paste Plus and PreviDent fluoride varnish for

treatment of white spot lesions: a randomized controlled trial. *American Journal of Orthodontics and Dentofacial Orthopedics,* 143**,** 31-41.

Huang, T. T. Y., He, L. H., Darendeliler, M. A. & Swain, M. V. 2010. Nano-indentation characterisation of natural carious white spot lesions. *Caries Research,* 44**,** 101-107

Huang, T. T. Y., Jones, A. S., He, L. H., Darendeliler, M. A. & Swain, M. V. 2007. Characterisation of enamel white spot lesions using X-ray micro-tomography. *Journal of Dentistry,* 35**,** 737-743.

Huang, Z. Y., Wang, B. L. & Li, H. Q. 2002. An intelligent measurement system for powder flowrate measurement in pneumatic conveying system. *Ieee Transactions on Instrumentation and Measurement,* 51**,** 700-703.

Hutchings, J., Kendall, C., Shepherd, N., Barr, H., Smith, B. & Stone, N. Rapid Raman microscopic imaging for potential histological screening. 2008. International Society for Optics and Photonics, 685305-685305-9.

Hutchings, J., Kendall, C., Smith, B., Shepherd, N., Barr, H. & Stone, N. 2009. The potential for histological screening using a combination of rapid Raman mapping and principal component analysis. *Journal of biophotonics,* 2**,** 91-103.

Iijima, M. & Moradian-Oldak, J. 2004. Control of octacalcium phosphate and apatite crystal growth by amelogenin matrices. *Journal of Materials Chemistry,* 14**,** 2189-2199.

Ingram, G. S. & Silverstone, L. M. 1981. A chemical and histological study of artificial caries in human dental enamel in vitro. *Caries Research,* 15**,** 393-8.

Ireland, A. J., Mcnamara, C., Clover, M. J., House, K., Wenger, N., Barbour, M. E., Alemzadeh, K., Zhang, L. & Sandy, J. R. 2008. 3D surface imaging in dentistry–what we are looking at. *British Dental Journal,* 205**,** 387-392.

Jegova, G., Titorenkova, R., Rashkova, M. & Mihailova, B. 2013. Raman and IR reflection micro-spectroscopic study of Er: YAG laser treated permanent and deciduous human teeth. *Journal of Raman Spectroscopy,* 44**,** 1483-1490.

Jillavenkatesa, A., Dapkunas, S. J. & Lum, L.-S. H. 2001. Particle size characterization. *National Institute of Standards and Technology,* 960-1**,** 1-165.

Jones, R. & Fried, D. 2006. Remineralization of enamel caries can decrease optical reflectivity. *Journal of dental research,* 85**,** 804-808.

Jones, R. S., Darling, C. L., Featherstone, J. D. & Fried, D. 2006. Remineralization of in vitro dental caries assessed with polarization-sensitive optical coherence tomography. *Journal of Biomedical Optics* 11**,** 014016.

Jost-Brinkmann, P. G. 1998. The influence of air polishers on tooth enamel. An in-vitro study. *Journal of Orofacial Orthopedics,* 59**,** 1-16.

Kamitakahara, M., Kawashita, M., Kokubo, T. & Nakamura, T. 2001. Effect of polyacrylic acid on the apatite formation of a bioactive ceramic in a simulated body fluid: fundamental examination of the possibility of obtaining bioactive glass-ionomer cements for orthopaedic use. *Biomaterials,* 22**,** 3191-6.

Kang, H., Darling, C. L. & Fried, D. 2012. Nondestructive monitoring of the repair of enamel artificial lesions by an acidic remineralization model using polarization-sensitive optical coherence tomography. *Dental Materials,* 28**,** 488-94.

Kang, H., Jiao, J. J., Lee, C., Le, M. H., Darling, C. L. & Fried, D. 2010. Nondestructive assessment of early tooth demineralization using cross-polarization optical coherence tomography. *IEEE Journal of Selected Topics in Quantum Electronics,* 16**,** 870-876.

Karan, S., Kircelli, B. H. & Tasdelen, B. 2010. Enamel surface roughness after debonding: comparison of two different burs. *The Angle Orthodontist,* 80**,** 1081-1088.

Karlinsey, R. & Mackey, A. 2009. Solid-state preparation and dental application of an organically modified calcium phosphate. *Journal of Materials Science,* 44**,** 346-349.

Khosravanifard, B., Nemati-Anaraki, S., Nili, S. & Rakhshan, V. 2011. Assessing the effects of three resin removal methods and bracket sandblasting on shear bond strength of metallic orthodontic brackets and enamel surface. *Orthodontic Waves,* 70**,** 27-38.

Kidd, E. A. & Fejerskov, O. 2004. What constitutes dental caries? Histopathology of carious enamel and dentin related to the action of cariogenic biofilms. *Journal of Dental Research,* 83 Spec No C**,** C35-8.

Kielbassa, A., Gillmann, L., Zantner, C., Meyer-Lueckel, H., Hellwig, E. & Schulte-Mönting, J. 2005. Profilometric and microradiographic studies on the effects of toothpaste and acidic gel abrasivity on sound and demineralized bovine dental enamel. *Caries Research,* 39**,** 380-386.

Kielbassa, A. M., Wrbas, K. T., Schulte-Mönting, J. & Hellwig, E. 1999. Correlation of transversal microradiography and microhardness on in situ-induced demineralization in irradiated and nonirradiated human dental enamel. *Archives of Oral Biology,* 44**,** 243-251.

Kim, S. S., Park, W. K., Son, W. S., Ahn, H. S., Ro, J. H. & Kim, Y. D. 2007. Enamel surface evaluation after removal of orthodontic composite remnants by intraoral sandblasting: a 3-dimensional surface profilometry study. *American Journal of Orthodontics and Dentofacial Orthopedics,* 132**,** 71-6.

Kim, Y. K., Gu, L. S., Bryan, T. E., Kim, J. R., Chen, L., Liu, Y., Yoon, J. C., Breschi, L., Pashley, D. H. & Tay, F. R. 2010. Mineralisation of reconstituted collagen using polyvinylphosphonic acid/polyacrylic acid templating matrix protein analogues in the presence of calcium, phosphate and hydroxyl ions. *Biomaterials,* 31**,** 6618-27.

Kinoshita, H., Miyoshi, N., Fukunaga, Y., Ogawa, T., Ogasawara, T. & Sano, K. 2008. Functional mapping of carious enamel in human teeth with Raman microspectroscopy. *Journal of Raman Spectroscopy,* 39**,** 655-660.

Kirkham, J., Firth, A., Vernals, D., Boden, N., Robinson, C., Shore, R., Brookes, S. & Aggeli, A. 2007. Self-assembling peptide scaffolds promote enamel remineralization. *Journal of dental research,* 86**,** 426-430.

Kissa, E. 1999. *Dispersions: characterization, testing, and measurement*, CRC Press.

Klapdohr, S. & Moszner, N. 2005. New inorganic components for dental filling composites. *Monatshefte für Chemie/Chemical Monthly,* 136**,** 21-45.

Ko, A. C., Choo-Smith, L. P., Hewko, M., Leonardi, L., Sowa, M. G., Dong, C. C., Williams, P. & Cleghorn, B. 2005. Ex vivo detection and characterization of early dental caries by optical coherence tomography and Raman spectroscopy. *Journal of Biomedical Optics* 10**,** 031118.

Koenig, K. & Schneckenburger, H. 1994. Laser-induced autofluorescence for medical diagnosis. *Journal of fluorescence,* 4**,** 17-40.

Kokubo, T. 1990. Surface chemistry of bioactive glass-ceramics. *Journal of Non-Crystalline Solids,* 120**,** 138-151.

Koller, G., Cook, R. J., Thompson, I. D., Watson, T. F. & Di Silvio, L. 2007. Surface modification of titanium implants using bioactive glasses with air abrasion technologies. *Journal of Materials Science: Materials in Medicine,* 18**,** 2291-6.

Koutsopoulos, S. 2002. Synthesis and characterization of hydroxyapatite crystals: a review study on the analytical methods. *Journal of Biomedical Materials Research,* 62**,** 600-12.

Kuptsov, A. H. & Zhizhin, G. N. 1998. *Handbook of Fourier Transform Raman and Infrared Spectra of Polymers*, Elsevier.

Lagerlöf, F. 1994. Caries-protective factors in saliva. *Advances in dental research,* 8**,** 229-238.

Larsen, M. J. & Pearce, E. I. F. 1992. Some notes on the diffusion of acidic and alkaline agents into natural human caries lesions- in-vitro. *Archives of Oral Biology,* 37**,** 411-416.

Laurell, K. A. & Hess, J. A. 1995. Scanning electron micrographic effects of air-abrasion cavity preparation on human enamel and dentin. *Quintessence international,* 26.

Leach, R. 2010. *Fundamental principles of engineering nanometrology,* Oxford; Amsterdam, William Andrew, Elsevier Science.

Lee Black, D., Mcquay, M. Q. & Bonin, M. P. 1996. Laser-based techniques for particle-size measurement: a review of sizing methods and their industrial applications. *Progress in energy and combustion science,* 22**,** 267-306

Lee, C. Q., Shey, Z. & Cobb, C. M. 1995. Microscopic appearance of enamel white-spot lesions after acid etching. *Quintessence international,* 26.

Lee, M.-S., Chen, Y.-L., Huang, P.-H., Chiang, Y.-C., Chang, H.-H., Wu, J. & Lin, C.-P. 2013. Effects of ultrasonic and high-speed air-driven devices on pulp–dentin reactions: An animal study. *Journal of Dental Sciences*.

Li, A., Wang, A. & Chen, J. 2004. Studies on poly (acrylic acid)/attapulgite superabsorbent composite. I. Synthesis and characterization. *Journal of Applied Polymer Science,* 92**,** 1596-1603.

Li, P., Nakanishi, K., Kokubo, T. & De Groot, K. 1993. Induction and morphology of hydroxyapatite, precipitated from metastable simulated body fluids on sol-gel prepared silica. *Biomaterials,* 14**,** 963-968.

Li, P., Ohtsuki, C., Kokubo, T., Nakanishi, K., Soga, N. & De Groot, K. 1994. The role of hydrated silica, titania, and alumina in inducing apatite on implants. *Journal of Biomedical Materials Research,* 28**,** 7-15.

Li, X., Wang, J., Joiner, A. & Chang, J. 2014. The remineralisation of enamel: a review of the literature. *Journal of Dentistry,* 42**,** S12-S20.

Lin, C. P., Douglas, W. H. & Erlandsen, S. L. 1993. Scanning electron microscopy of type I collagen at the dentin-enamel junction of human teeth. *J Histochem Cytochem,* 41**,** 381-8.

Lippert, F. & Lynch, R. 2014. Comparison of Knoop and Vickers surface microhardness and transverse microradiography for the study of early caries lesion formation in human and bovine enamel. *Archives of Oral Biology,* 59**,** 704-710.

Lippert, F., Parker, D. M. & Jandt, K. D. 2004. In vitro demineralization/remineralization cycles at human tooth enamel surfaces investigated by AFM and nanoindentation. *Journal of Colloid and Interface Science,* 280**,** 442-448.

Liu, Y., Li, N., Qi, Y. P., Dai, L., Bryan, T. E., Mao, J., Pashley, D. H. & Tay, F. R. 2011. Intrafibrillar collagen mineralization produced by biomimetic hierarchical nanoapatite assembly. *Advanced Materials,* 23**,** 975-980.

Lo, E. C., Zhi, Q. H. & Itthagarun, A. 2010. Comparing two quantitative methods for studying remineralization of artificial caries. *Journal of Dentistry,* 38**,** 352-9.

Loomans, B., Cardoso, M., Opdam, N., Roeters, F., De Munck, J., Huysmans, M. & Van Meerbeek, B. 2011. Surface roughness of etched composite resin in light of composite repair. *Journal of Dentistry,* 39**,** 499-505.

Los, S. & Barkmeier, W. W. 1994. Effects of dentin air abrasion with aluminum oxide and hydroxyapatite on adhesive bond strength. *Operative dentistry,* 19**,** 169

Lyman, C. E. 1990. *Scanning electron microscopy, X-ray microanalysis, and analytical electron microscopy: a laboratory workbook*, Springer.

Lynch, R. J. M., Mony, U. & Ten Cate, J. M. 2007. Effect of lesion characteristics and mineralising solution type on enamel remineralisation in vitro. *Caries Research,* 41**,** 257-262.

Magalhaes, A. C., Moron, B. M., Comar, L. P., Wiegand, A., Buchalla, W. & Buzalaf, M. A. 2009. Comparison of cross-sectional hardness and transverse microradiography of artificial carious enamel lesions induced by different demineralising solutions and gels. *Caries Research,* 43**,** 474-83.

Mahoney, E., Holt, A., Swain, M. & Kilpatrick, N. 2000. The hardness and modulus of elasticity of primary molar teeth: an ultra-micro-indentation study. *Journal of Dentistry,* 28**,** 589-594.

Mandurah, M. M., Sadr, A., Shimada, Y., Kitasako, Y., Nakashima, S., Bakhsh, T. A., Tagami, J. & Sumi, Y. 2013. Monitoring remineralization of enamel subsurface lesions by optical coherence tomography. *Journal of Biomedical Optics* 18**,** 46006.

Mangum, J. E., Crombie, F. A., Kilpatrick, N., Manton, D. J. & Hubbard, M. J. 2010. Surface integrity governs the proteome of hypomineralized enamel. *Journal of Dental Research,* 89**,** 1160-5.

Masuda, H., Higashitani, K. & Yoshida, H. 2006. *Powder technology handbook*, CRC Press.

Maupomé, G., Diez-De-Bonilla, J., Torres-Villasenor, G., Andrade-Delgado, L. D. C. & Castano, V. M. 1998. In vitro quantitative assessment of enamel microhardness after exposure to eroding immersion in a cola drink. *Caries Research,* 32**,** 148-153.

Meckel, A., Griebstein, W. & Neal, R. 1965. Structure of mature human dental enamel as observed by electron microscopy. *Archives of Oral Biology,* 10**,** 775-783.

Meredith, N., Sherriff, M., Setchell, D. J. & Swanson, S. a. V. 1996. Measurement of the microhardness and Young's modulus of human enamel and dentine using an indentation technique. *Archives of Oral Biology,* 41**,** 539-545.

Merkus, H. G. 2009. Particle size measurements: fundamentals. *Practice, Quality*.

Meyer-Lueckel, H., Paris, S. & Kielbassa, A. M. 2007. Surface layer erosion of natural caries lesions with phosphoric and hydrochloric acid gels in preparation for resin infiltration. *Caries Research,* 41**,** 223-30.

Midda, M. & Renton-Harper, P. 1991. Lasers in dentistry. *British Dental Journal,* 170**,** 343-6.

Mikli, V., Kaerdi, H., Kulu, P. & Besterci, M. 2001. Characterization of powder particle morphology. *Proceedings of the Estonian Academy of Sciences: Engineering (Estonia),* 7**,** 22-34.

Mohammed, N. R., Lynch, R. J. & Anderson, P. 2014. Effects of fluoride concentration on enamel demineralization kinetics in vitro. *Journal of Dentistry,* 42**,** 613-618.

Mohanty, B., Dadlani, D., Mahoney, D. & Mann, A. B. 2012. Characterizing and identifying incipient carious lesions in dental enamel using micro-Raman spectroscopy. *Caries Research,* 47**,** 27-33.

Molina, G. F., Cabral, R. J. & Frencken, J. E. 2009. The ART approach: clinical aspects reviewed. *Journal of Applied Oral Science,* 17**,** 89-98.

Morgan, M. V., Adams, G. G., Bailey, D. L., Tsao, C. E., Fischman, S. L. & Reynolds, E. C. 2008. The anticariogenic effect of sugar-free gum containing CPP-ACP nanocomplexes on approximal caries determined using digital bitewing radiography. *Caries Research,* 42**,** 171-184

Motisuki, C., Lima, L. M., Bronzi, E. S., Spolidorio, D. M. & Santos-Pinto, L. 2006. The effectiveness of alumina powder on carious dentin removal. *Operative dentistry,* 31**,** 371-6.

Mount, G. J. 2007. A new paradigm for operative dentistry. *Australian Dental Journal,* 52**,** 264-270.

Mueller, J., Meyer-Lueckel, H., Paris, S., Hopfenmuller, W. & Kielbassa, A. M. 2006. Inhibition of lesion progression by the penetration of resins in vitro: influence of the application procedure. *Operative dentistry,* 31**,** 338-345.

Murdoch-Kinch, C. A. & Mclean, M. E. 2003. Minimally invasive dentistry. *The Journal of the American Dental Association,* 134**,** 87-96.

Myers, G. 1954. The airbrasive technique: a report. *Brtish Dental Journal,* 7**,** 291-295.

Myers, T. D. & Myers, W. D. 1985. The use of a laser for debridement of incipient caries. *The Journal of prosthetic dentistry,* 53**,** 776-779.

Naumova, E. A., Arnold, W. H. & Gaengler, P. 2010. Fluoride bioavailability in saliva using Denttabsa compared to dentifrice. *Central European Journal of Medicine,* 5**,** 375-380.

Naumova, E. A., Niemann, N., Aretz, L. & Arnold, W. H. 2012. Effects of different amine fluoride concentrations on enamel remineralization. *Journal of Dentistry,* 40**,** 750-755.

Navarro, M. F., Rigolon, C. J., Barata, T. J., Bresciane, E., Fagundes, T. C. & Peters, M. C. 2008. Influence of occlusal access on demineralized dentin removal in the atraumatic restorative treatment (ART) approach. *American journal of dentistry,* 21**,** 251-254.

Nazari, A., Sadr, A., Campillo-Funollet, M., Nakashima, S., Shimada, Y., Tagami, J. & Sumi, Y. 2013. Effect of hydration on assessment of early enamel lesion using swept-source optical coherence tomography. *Journal of Biophotonics* 6**,** 171-7.

Neuhaus, K. W., Schlafer, S., Lussi, A. & Nyvad, B. 2012. Infiltration of natural caries lesions in relation to their activity status and acid pretreatment in vitro. *Caries Research,* 47**,** 203-210

Neves, A. D. A., Coutinho, E., De Munck, J. & Van Meerbeek, B. 2011. Caries-removal effectiveness and minimal-invasiveness potential of caries-excavation techniques: a micro-CT investigation. *Journal of Dentistry,* 39**,** 154-162.

Newbrun, E. 2001. Topical fluorides in caries prevention and management: a North American perspective. *Journal of Dental Education,* 65**,** 1078-1083.

Niu, L. N., Zhang, W., Pashley, D. H., Breschi, L., Mao, J., Chen, J. H. & Tay, F. R. 2014. Biomimetic remineralization of dentin. *Dental Materials,* 30**,** 77-96.

Notingher, I., Boccaccini, A. R., Jones, J., Maquet, V. & Hench, L. L. 2002. Application of Raman microspectroscopy to the characterisation of bioactive materials. *Materials Characterization,* 49**,** 255-260.

Notingher, I., Jones, J. R., Verrier, S., Bisson, I., Embanga, P., Edwards, P., Polak, J. M. & Hench, L. L. 2003. Application of FTIR and Raman spectroscopy to characterisation of bioactive materials and living cells. *Spectroscopy-an International Journal,* 17**,** 275-288.

O'reilly, M. & Featherstone, J. 1987. Demineralization and remineralization around orthodontic appliances: an in vivo study. *American Journal of Orthodontics and Dentofacial Orthopedics,* 92**,** 33-40.

Oesterle, L. J., Shellhart, W. C. & Belanger, G. K. 1998. The use of bovine enamel in bonding studies. *American Journal of Orthodontics and Dentofacial Orthopedics,* 114**,** 514-519.

Ogaard, B. 1989. Prevalence of white spot lesions in 19-year-olds: a study on untreated and orthodontically treated persons 5 years after treatment. *American Journal of Orthodontics and Dentofacial Orthopedics,* 96**,** 423-7.

Oman, C. R. & Applebaum, E. 1955. Ultrasonic cavity preparation. II. Progress report. *Journal of the American Dental Association,* 50**,** 414-7.

Onuma, K., Yamagishi, K. & Oyane, A. 2005. Nucleation and growth of hydroxyapatite nanocrystals for nondestructive repair of early caries lesions. *Journal of Crystal Growth,* 282**,** 199-207.

Osborn, J. W. 1981. *A Companion to Dental Studies: Dental anatomy and embryology*, Blackwell

Ozer, T., Basaran, G. & Kama, J. D. 2010. Surface roughness of the restored enamel after orthodontic treatment. *American Journal of Orthodontics and Dentofacial Orthopedics,* 137**,** 368-74.

Paepegaey, A.-M., Barker, M. L., Bartlett, D. W., Mistry, M., West, N. X., Hellin, N., Brown, L. J. & Bellamy, P. G. 2013. Measuring enamel erosion: A comparative study of contact profilometry, non-contact profilometry and confocal laser scanning microscopy. *Dental Materials,* 29**,** 1265-1272.

Paolinelis, G., Banerjee, A. & Watson, T. F. 2008. An in vitro investigation of the effect and retention of bioactive glass air-abrasive on sound and carious dentine. *Journal of Dentistry,* 36**,** 214-8.

Paolinelis, G., Banerjee, A. & Watson, T. F. 2009. An in-vitro investigation of the effects of variable operating parameters on alumina air-abrasion cutting characteristics. *Operative Dentistry,* 34**,** 87-92.

Paolinelis, G., Watson, T. F. & Banerjee, A. 2006. Microhardness as a predictor of sound and carious dentine removal using alumina air abrasion. *Caries Research,* 40**,** 292-5.

Paris, S., Meyer-Lueckel, H. & Kielbassa, A. M. 2007. Resin infiltration of natural caries lesions. *Journal of dental research,* 86**,** 662-666

Parker, A. S., Patel, A. N., Al Botros, R., Snowden, M. E., Mckelvey, K., Unwin, P. R., Ashcroft, A. T., Carvell, M., Joiner, A. & Peruffo, M. 2014. Measurement of the efficacy of calcium silicate for the protection and repair of dental enamel. *Journal of Dentistry,* 42**,** S21-S29.

Passos, S. P., Freitas, A. P., Jumaily, S., Santos, M. J., Rizkalla, A. S. & Santos Jr, G. C. 2013. Comparison of mechanical properties of five commercial dental core build-up materials. *Compendium of continuing education in dentistry* 34**,** 62-68

Peariasamy, K., Anderson, P. & Brook, A. H. 2001. A quantitative study of the effect of pumicing and etching on the remineralisation of enamel opacities. *International Journal of Paediatric Dentistry,* 11**,** 193-200.

Peitl Filho, O., Latorre, G. P. & Hench, L. L. 1996. Effect of crystallization on apatite-layer formation of bioactive glass 45S5. *Journal of Biomedical Materials Research,* 30**,** 509-14.

Peitl, O., Zanotto, E. D. & Hench, L. L. 2001. Highly bioactive P2O5-Na2O-CaO-SiO2 glass-ceramics. *Journal of Non-Crystalline Solids,* 292**,** 115-126.

Penel, G., Leroy, G., Rey, C. & Bres, E. 1998. MicroRaman spectral study of the PO_4 and CO_3 vibrational modes in synthetic and biological apatites. *Calcified Tissue International* 63**,** 475-81.

Peruchi, C., Santos-Pinto, L., Santos-Pinto, A. & Barbosa E Silva, E. 2002. Evaluation of cutting patterns produced in primary teeth by an air-abrasion system. *Quintessence international,* 33.

Peters, M. C. & Mclean, M. E. 2001a. Minimally Invasive Operative Care: I. Minimal Intervention and Concepts for Minimally Invasive Cavity Preparations. *Journal of Adhesive Dentistry,* 3**,** 7-16.

Peters, M. C. & Mclean, M. E. 2001b. Minimally Invasive Operative Care: II. Contemporary Techniques and Materials: an Overview. *Journal of Adhesive Dentistry,* 3**,** 17-31.

Petry, R., Schmitt, M. & Popp, J. 2003. Raman spectroscopy-a prospective tool in the life sciences. *ChemPhysChem,* 4**,** 14-30

Peutzfeldt, A. 1997. Resin composites in dentistry: the monomer systems. *European Journal of Oral Sciences,* 105**,** 97-116.

Pitts, N. B. & Wefel, J. S. 2009. Remineralization/desensitization: what is known? What is the future? *Advances in Dental Research,* 21**,** 83-6.

Pliska, B. T., Warner, G. A., Tantbirojn, D. & Larson, B. E. 2012. Treatment of white spot lesions with ACP paste and microabrasion. *The Angle Orthodontist,* 82**,** 765-9.

Pont, H. B., Ozcan, M., Bagis, B. & Ren, Y. 2010. Loss of surface enamel after bracket debonding: an in-vivo and ex-vivo evaluation. *American Journal of Orthodontics and Dentofacial Orthopedics,* 138**,** 387 e1-9; discussion 387-9.

Poole, D. & Brooks, A. 1961. The arrangement of crystallites in enamel prisms. *Archives of Oral Biology,* 5**,** 14-IN5.

Pradeep, A. & Sharma, A. 2010. Comparison of clinical efficacy of a dentifrice containing calcium sodium phosphosilicate to a dentifrice containing potassium nitrate and to a placebo on dentinal hypersensitivity: a randomized clinical trial. *Journal of periodontology,* 81**,** 1167-1173.

Prestes, L., Souza, B. M., Comar, L. P., Salomão, P. A., Rios, D. & Magalhães, A. C. 2013. In situ effect of chewing gum containing CPP–ACP on the mineral precipitation of eroded bovine enamel - A surface hardness analysis. *Journal of Dentistry,* 41**,** 747-751

Preston, K. P., Smith, P. W. & Higham, S. M. 2008. The influence of varying fluoride concentrations on in vitro remineralisation of artificial dentinal lesions with differing lesion morphologies. *Archives of Oral Biology,* 53**,** 20-6.

Profeta, A. C., Mannocci, F., Foxton, R. M., Thompson, I., Watson, T. F. & Sauro, S. 2012. Bioactive effects of a calcium/sodium phosphosilicate on the resin–dentine interface: a microtensile bond strength, scanning electron microscopy, and confocal microscopy study. *European Journal of Oral Sciences,* 120**,** 353-362.

Purdell-Lewis, D. J., Groeneveld, A. & Arends, J. 1976. Hardness tests on sound enamel and artificially demineralized white spot lesions. *Caries Research,* 10**,** 201-15.

Qi, Y. P., Li, N., Niu, L. N., Primus, C. M., Ling, J. Q., Pashley, D. H. & Tay, F. R. 2012. Remineralization of artificial dentinal caries lesions by

biomimetically modified mineral trioxide aggregate. *Acta Biomaterialia,* 8**,** 836-42.

Radhakrishnan, P. & Mao, J. J. 2004. Nanomechanical properties of facial sutures and sutural mineralization front. *Journal of dental research,* 83**,** 470-475.

Rafique, S., Fiske, J. & Banerjee, A. 2003. Clinical trial of an air-abrasion/chemomechanical operative procedure for the restorative treatment of dental patients. *Caries research,* 37**,** 360-364.

Rehder Neto, F. C., Maeda, F. A., Turssi, C. P. & Serra, M. C. 2009. Potential agents to control enamel caries-like lesions. *Journal of Dentistry,* 37**,** 786-90.

Rehman, I., Hench, L. L., Bonfield, W. & Smith, R. 1994. Analysis of surface layers on bioactive glasses. *Biomaterials,* 15**,** 865-70.

Ren, Y.-F., Zhao, Q., Malmstrom, H., Barnes, V. & Xu, T. 2009. Assessing fluoride treatment and resistance of dental enamel to soft drink erosion in vitro: applications of focus variation 3D scanning microscopy and stylus profilometry. *Journal of Dentistry,* 37**,** 167-176.

Reynolds, E. C. 1987. The prevention of sub-surface demineralization of bovine enamel and change in plaque composition by casein in an intra-oral model. *Journal of dental research,* 66**,** 1120-1127

Reynolds, E. C. 2008. Calcium phosphate-based remineralization systems: scientific evidence? *Australian Dental Journal,* 53**,** 268-73.

Reynolds, E. C., Cai, F., Shen, P. & Walker, G. D. 2003. Retention in plaque and remineralization of enamel lesions by various forms of calcium in a mouthrinse or sugar-free chewing gum. *Journal of Dental Research,* 82**,** 206-211.

Reynolds, E. C., Cain, C. J., Webber, E. L., Black, C. L., Riley, P. F., Johnson, I. H. & Perich, J. W. 1995. Anticariogenicity of calcium phosphate complexes of tryptic casein phosphopeptides in the rat. *Journal of dental research,* 74**,** 1272-1279.

Ring, H. C., Mogensen, M., Banzhaf, C., Themstrup, L. & Jemec, G. B. E. 2013. Optical coherence tomography imaging of telangiectasias during intense pulsed light treatment: a potential tool for rapid outcome assessment. *Archives of dermatological research,* 305**,** 299-303.

Robinson, C., Brookes, S. J., Kirkham, J., Wood, S. R. & Shore, R. C. 2001. In vitro studies of the penetration of adhesive resins into artificial caries–like lesions. *Caries Research,* 35**,** 136-141.

Robinson, C., Hallsworth, A. S., Shore, R. C. & Kirkham, J. 1990. Effect of surface zone deproteinisation on the access of mineral ions into subsurface carious lesions of human enamel. *Caries Research,* 24**,** 226-30.

Robinson, C., Kirkham, J. & Shore, R. 1995. *Dental enamel: formation to destruction.*, Boca Raton, FL: CRC Press.

Robinson, C., Shore, R. C., Brookes, S. J., Strafford, S., Wood, S. R. & Kirkham, J. 2000. The chemistry of enamel caries. *Critical Reviews in Oral Biology & Medicine,* 11**,** 481-95.

Robinson, P. 2013. Clinical applications of bioactive glasses: periodontology repair. *In:* HENCH, L. L. (ed.) *An Introduction to Bioceramics.* 2nd ed. London: Imperial College Press.

Ryf, S., Flury, S., Palaniappan, S., Lussi, A., Van Meerbeek, B. & Zimmerli, B. 2012. Enamel loss and adhesive remnants following bracket removal and various clean-up procedures in vitro. *European Journal of Orthodontics,* 34**,** 25-32.

Salehi, H., Terrer, E., Panayotov, I., Levallois, B., Jacquot, B., Tassery, H. & Cuisinier, F. 2012. Functional mapping of human sound and carious enamel and dentin with Raman spectroscopy. *Journal of Biophotonics*

San Miguel, B., Kriauciunas, R., Tosatti, S., Ehrbar, M., Ghayor, C., Textor, M. & Weber, F. E. 2010. Enhanced osteoblastic activity and bone regeneration using surface-modified porous bioactive glass scaffolds. *Journal of Biomedical Materials Research Part A,* 94**,** 1023-33.

Sano, H., Nakashima, S., Songpaisan, Y. & Phantumvanit, P. 2007. Effect of a xylitol and fluoride containing toothpaste on the remineralization of human enamel in vitro. *Journal of Oral Science,* 49**,** 67-73.

Santini, A., Pulham, C. R., Rajab, A. & Ibbetson, R. 2008. The effect of a 10% carbamide peroxide bleaching agent on the phosphate concentration of tooth enamel assessed by Raman spectroscopy. *Dental Traumatology,* 24**,** 220-3.

Santos-Pinto, L., Peruchi, C., Marker, V. A. & Cordeiro, R. 2001. Effect of handpiece tip design on the cutting efficiency of an air abrasion system. *American journal of dentistry,* 14**,** 397-401

Saravanapavan, P., Jones, J. R., Pryce, R. S. & Hench, L. L. 2003. Bioactivity of gel–glass powders in the CaO-SiO2 system: A comparison with ternary (CaO-P2P5-SiO2) and quaternary glasses (SiO2-CaO-P2O5-Na2O). *Journal of Biomedical Materials Research Part A,* 66**,** 110-119.

Sauer, G. R., Zunic, W. B., Durig, J. R. & Wuthier, R. E. 1994. Fourier transform Raman spectroscopy of synthetic and biological calcium phosphates. *Calcified Tissue International* 54**,** 414-20.

Sauro, S., Osorio, R., Watson, T. F. & Toledano, M. 2012a. Therapeutic effects of novel resin bonding systems containing bioactive glasses on mineral-depleted areas within the bonded-dentine interface. *Journal of Materials Science: Materials in Medicine,* 23**,** 1521-1532.

Sauro, S., Watson, T. F., Thompson, I. & Banerjee, A. 2012b. One-bottle self-etching adhesives applied to dentine air-abraded using bioactive glasses containing polyacrylic acid: An in-vitro microtensile bond strength and confocal microscopy study. *Journal of Dentistry,* 40**,** 896-905

Sauro, S., Watson, T. F., Thompson, I., Toledano, M., Nucci, C. & Banerjee, A. 2012c. Influence of air-abrasion executed with polyacrylic acid-Bioglass 45S5 on the bonding performance of a resin-modified glass ionomer cement. *European Journal of Oral Sciences,* 120**,** 168-177.

Schlueter, N., Ganss, C., De Sanctis, S. & Klimek, J. 2005. Evaluation of a profilometrical method for monitoring erosive tooth wear. *European Journal of Oral Sciences,* 113**,** 505-11.

Schlueter, N., Hara, A., Shellis, R. P. & Ganss, C. 2011. Methods for the measurement and characterization of erosion in enamel and dentine. *Caries Research,* 45**,** 13-23.

Schupbach, P., Neeser, J. R., Golliard, M., Rouvet, M. & Guggenheim, B. 1996. Incorporation of caseinoglycomacropeptide and caseinophosphopeptide into the salivary pellicle inhibits adherence of mutans streptococci. *Journal of Dental Research,* 75**,** 1779-88.

Sepulveda, P., Jones, J. R. & Hench, L. L. 2001. Characterization of melt-derived 45S5 and sol-gel-derived 58S bioactive glasses. *Journal of Biomedical Materials Research,* 58**,** 734-40.

Sharif, M. O., Catleugh, M., Merry, A., Tickle, M., Dunne, S. M., Brunton, P. & Aggarwal, V. R. 2010. Replacement versus repair of defective restorations in adults: resin composite. *Australian dental journal,* 55**,** 351-352.

Shimada, Y., Nakagawa, H., Sadr, A., Wada, I., Nakajima, M., Nikaido, T., Otsuki, M., Tagami, J. & Sumi, Y. 2013. Noninvasive cross-sectional imaging of proximal caries using swept-source optical coherence tomography (SS-OCT) in vivo. *Journal of Biophotonics*

Siegel, S. C. & Von Fraunhofer, J. A. 2000. Cutting efficiency of three diamond bur grit sizes. *Journal of the American Dental Association,* 131**,** 1706-10.

Silverstone, L. M. 1967. Observations on the dark zone in early enamel caries and artificial caries-like lesions. *Caries Research,* 1**,** 260-74.

Silverstone, L. M. 1973. Structure of carious enamel, including the early lesion. *Oral sciences reviews,* 3**,** 100-60.

Silverstone, L. M., Wefel, J. S., Zimmerman, B. F., Clarkson, B. H. & Featherstone, M. J. 1981. RemineraIization of natural and artificial lesions in human dental enamel in vitro. *Caries Research,* 15**,** 138-157.

Sirdeshmukh, D. B., Sirdeshmukh, L. & Subhadra, K. G. 2006. Hardness. *Micro- and Macro-Properties of Solids: Thermal, Mechanical and Dielectric Properties***,** 135-197

Skrtic, D., Antonucci, J. M., Eanes, E. D. & Brunworth, R. T. 2002. Silica-and zirconia-hybridized amorphous calcium phosphate: Effect on transformation to hydroxyapatite. *Journal of biomedical materials research,* 59**,** 597-604

Spizzirri, P. G., Cochrane, N. J., Prawer, S. & Reynolds, E. C. 2012. A Comparative study of carbonate determination in human teeth using Raman spectroscopy. *Caries Research,* 46**,** 353-360.

Stachowiak, G. W. 2000. Particle angularity and its relationship to abrasive and erosive wear. *Wear,* 241**,** 214-219

Stansbury, J. W. 2000. Curing dental resins and composites by photopolymerization. *Journal of Esthetic and Restorative Dentistry,* 12**,** 300-308.

Steiner-Oliveira, C., Nobre-Dos-Santos, M., Zero, D. T., Eckert, G. & Hara, A. T. 2010. Effect of a pulsed CO_2 laser and fluoride on the prevention of enamel and dentine erosion. *Archives of Oral Biology,* 55**,** 127-133.

Stoor, P., Soderling, E. & Salonen, J. I. 1998. Antibacterial effects of a bioactive glass paste on oral microorganisms. *Acta Odontologica Scandinavica,* 56**,** 161-5.

Strang, R., Damato, F., Creanor, S. & Stephen, K. 1987. The effect of baseline lesion mineral loss on in situ remineralization. *Journal of dental research,* 66**,** 1644-1646.

Sudjalim, T. R., Woods, M. G. & Manton, D. J. 2006. Prevention of white spot lesions in orthodontic practice: a contemporary review. *Australian Dental Journal,* 51**,** 284-9; quiz 347.

Tahmassebi, J. F., Chrysafi, N. & Duggal, M. S. 2014. The effect of ozone on progression or regression of artificial caries-like enamel lesions in-vitro. *Journal of Dentistry,* 42**,** 167-174

Taira, M., Wakasa, K., Yamaki, M. & Matsui, A. 1990. Dental cutting behaviour of mica-based and apatite-based machinable glass-ceramics. *Journal of oral rehabilitation,* 17**,** 461-472.

Tassery, H., Levallois, B., Terrer, E., Manton, D. J., Otsuki, M., Koubi, S., Gugnani, N., Panayotov, I., Jacquot, B. & Cuisinier, F. 2013. Use of new minimum intervention dentistry technologies in caries management. *Australian dental journal,* 58**,** 40-59

Tay, F. R. & Pashley, D. H. 2008. Guided tissue remineralisation of partially demineralised human dentine. *Biomaterials,* 29**,** 1127-37.

Ten Bosch, J. J. & Angmar-Månsson, B. 1991. Invited Review: A Review of Quantitative Methods for Studies of Mineral Content of Intra-oral Incipient Caries Lesions. *Journal of dental research,* 70**,** 2-14.

Ten Cate, J. 2013. Contemporary perspective on the use of fluoride products in caries prevention. *British Dental Journal,* 214**,** 161-167.

Ten Cate, J. M. 1990. In vitro studies on the effects of fluoride on de- and remineralization. *Journal of Dental Research,* 69 Spec No**,** 614-9; discussion 634-6.

Ten Cate, J. M. 2001. Remineralization of caries lesions extending into dentin. *Journal of Dental Research,* 80**,** 1407-11.

Ten Cate, J. M. 2004. Fluorides in caries prevention and control: empiricism or science. *Caries Research,* 38**,** 254-257.

Ten Cate, J. M. & Duijsters, P. P. 1982. Alternating demineralization and remineralization of artificial enamel lesions. *Caries Research,* 16**,** 201-10.

Ten Cate, J. M., Exterkate, R. A. & Buijs, M. J. 2006. The relative efficacy of fluoride toothpastes assessed with pH cycling. *Caries Research,* 40**,** 136-41.

Ten Cate, J. M., Timmer, K., Shariati, M. & Featherstone, J. D. B. 1988. Effect of timing of fluoride treatment on enamel de-and remineralization in vitro: a pH-cycling study. *Caries Research,* 22**,** 20-26.

Theuns, H. M., Shellis, R. P., Groeneveld, A., Van Dijk, J. W. E. & Poole, D. F. G. 1993. Relationships between birefringence and mineral content in artificial caries lesions of enamel. *Caries Research,* 27**,** 9-14

Thomaidis, S., Kakaboura, A., Mueller, W. D. & Zinelis, S. 2013. Mechanical properties of contemporary composite resins and their interrelations. *Dental Materials,* 29**,** 132-141

Toledano, M., Aguilera, F. S., Cabello, I. & Osorio, R. 2014. Remineralization of mechanical loaded resin–dentin interface: a transitional and synchronized multistep process. *Biomechanics and modeling in mechanobiology***,** 1-14

Tostes, M., Mucha, J. N., Coutinho, T. C. L. & Da Silva, E. M. 2013. Evaluation of the effects of the bonding agent on acid-etched human enamel demineralization: in situ study. *The European Journal of Orthodontics,* 35**,** 369-374.

Tramini, P., Pelissier, B., Valcarcel, J., Bonnet, B. & Maury, L. 2000. A Raman spectroscopic investigation of dentin and enamel structures modified by lactic acid. *Caries Research,* 34**,** 233-40.

Tranaeus, S., Al-Khateeb, S., Björkman, S., Twetman, S. & Angmar-Månsson, B. 2001. Application of quantitative light-induced fluorescence to monitor incipient lesions in caries-active children. A comparative study of remineralisation by fluoride varnish and professional cleaning. *European Journal of Oral Sciences,* 109**,** 71-75.

Tsuda, H. & Arends, J. 1997. Raman spectroscopy in dental research: a short review of recent studies. *Advances in Dental Research,* 11**,** 539-47.

Tufekci, E., Merrill, T. E., Pintado, M. R., Beyer, J. P. & Brantley, W. A. 2004. Enamel loss associated with orthodontic adhesive removal on teeth with white spot lesions: an in vitro study. *American Journal of Orthodontics and Dentofacial Orthopedics,* 125**,** 733-9.

Tung, M. S. & Eichmiller, F. C. 1998. Dental applications of amorphous calcium phosphates. *The Journal of clinical dentistry,* 10**,** 1-6

Tung, M. S. & Eichmiller, F. C. 2004. Amorphous calcium phosphates for tooth mineralization. *Compendium of Continuing Education in Dentistry,* 25**,** 9-13.

Tyas, M. J., Anusavice, K. J., Frencken, J. E. & Mount, G. J. 2000. Minimal intervention dentistry-a review. *International dental journal,* 50**,** 1-12

Umeda, A., Sugimura, J. & Yamamoto, Y. 1998. Characterization of wear particles and their relations with sliding conditions. *Wear,* 216**,** 220-228.

Van Dijk, J. W., Borggreven, J. M. & Driessens, F. C. 1979. Chemical and mathematical simulation of caries. *Caries Research,* 13**,** 169-80.

Van Dorp, C. S. E., Exterkate, R. a. M. & Ten Cate, J. M. 1990. Mineral loss during etching of enamel lesions. *Caries Research,* 24**,** 6-10

Van Houte, J. 1993. Microbiological predictors of caries risk. *Advances in Dental Research,* 7**,** 87-96

Van Landuyt, K. L., Nawrot, T., Geebelen, B., De Munck, J., Snauwaert, J., Yoshihara, K., Scheers, H., Godderis, L., Hoet, P. & Van Meerbeek, B. 2011. How much do resin-based dental materials release? A meta-analytical approach. *Dental Materials,* 27**,** 723-747

Van Meerbeek, B., Kanumilli, P., De Munck, J., Van Landuyt, K., Lambrechts, P. & Peumans, M. 2005. A randomized controlled study evaluating the effectiveness of a two-step self-etch adhesive with and without selective phosphoric-acid etching of enamel. *Dental Materials,* 21**,** 375-383.

Van Waes, H., Matter, T. & Krejci, I. 1997. Three-dimensional measurement of enamel loss caused by bonding and debonding of orthodontic brackets. *American Journal of Orthodontics and Dentofacial Orthopedics,* 112**,** 666-9.

Vieira, A., Dos Santos, M., Antunes, L., Primo, L. G. & Maia, L. C. 2007. Preparation time and sealing effect of cavities prepared by an ultrasonic device and a high-speed diamond rotary cutting system. *Journal of Oral Science,* 49**,** 207-211.

Vogel, G. L., Chow, L. C. & Carey, C. M. 2008. Calcium pre-rinse greatly increases overnight salivary fluoride after a 228 ppm fluoride rinse. *Caries Research,* 42**,** 401-404

Walsh, L. J. 2009. Contemporary technologies for remineralization therapies: A review. *International Dentistry SA,* 6**,** 6–16.

Walsh, L. J. & Brostek, A. M. 2013. Minimum intervention dentistry principles and objectives. *Australian dental journal,* 58**,** 3-16

Wang, K. X., Meekings, A., Fluhr, J. W., Mckenzie, G., Lee, D. A., Fisher, J., Markowitz, O. & Siegel, D. M. 2013. Optical coherence tomography–based optimization of Mohs micrographic surgery of basal cell carcinoma: a pilot study. *Dermatologic Surgery,* 39**,** 627-633.

Wang, X., Megert, B., Hellwig, E., Neuhaus, K. & Lussi, A. 2011a. Preventing erosion with novel agents. *Journal of Dentistry,* 39**,** 163-170.

Wang, Z., Jiang, T., Sauro, S., Wang, Y., Thompson, I., Watson, T. F., Sa, Y., Xing, W., Shen, Y. & Haapasalo, M. 2011b. Dentine remineralization induced by two bioactive glasses developed for air abrasion purposes. *Journal of Dentistry,* 39**,** 746-56.

Warren, L. D., Clark, A. E. & Hench, L. L. 1989. An investigation of Bioglass powders: quality assurance test procedure and test criteria. *Journal of Biomedical Materials Research,* 23**,** 201-9.

Watson, T. F., Cook, R. J., Festy, F., Pilecki, P., Sauro, S. & Curtis, R. V. 2008. Optical imaging techniques for dental biomaterials interfaces. *Dental Biomaterials: Imaging, Testing and Modelling. Cambridge: Woodhead Publishing***,** 37-57.

Weatherell, J. A., Robinson, C. & Hallsworth, A. S. 1972. Changes in the fluoride concentration of the labial enamel surface with age. *Caries Research,* 6**,** 312-324.

Wefel, J. 2009. Novamin®: likely clinical success. *Advances in Dental Research,* 21**,** 40-43.

Weir, M. D., Chow, L. C. & Xu, H. H. 2012. Remineralization of demineralized enamel via calcium phosphate nanocomposite. *Journal of Dental Research,* 91**,** 979-84.

Wen, H., Moradian–Oldak, J., Zhong, J., Greenspan, D. & Fincham, A. 2000. Effects of amelogenin on the transforming surface microstructures of Bioglass® in a calcifying solution. *Journal of biomedical materials research,* 52**,** 762-773.

Wen, H. B., Moradian-Oldak, J. & Fincham, A. G. 1999. Modulation of apatite crystal growth on Bioglass® by recombinant amelogenin. *Biomaterials,* 20**,** 1717-1725

White, D. J., Chen, W. C. & Nancollas, G. H. 1988. Kinetic and physical aspects of enamel remineralization--a constant composition study. *Caries Research,* 22**,** 11-9.

White, J. M. & Eakle, W. S. 2000. Rationale and treatment approach in minimally invasive dentistry. *Journal of the American Dental Association,* 131 13S-19S.

Whitehead, S. A., Shearer, A. C., Watts, D. C. & Wilson, N. H. F. 1999. Comparison of two stylus methods for measuring surface texture. *Dental Materials,* 15**,** 79-86

Whitford, G. M., Buzalaf, M. a. R., Bijella, M. F. B. & Waller, J. L. 2005. Plaque fluoride concentrations in a community without water fluoridation: effects of calcium and use of a fluoride or placebo dentifrice. *Caries Research,* 39**,** 100-107.

Wilder-Smith, C. H., Wilder-Smith, P., Kawakami-Wong, H., Voronets, J., Osann, K. & Lussi, A. 2009. Quantification of dental erosions in patients with GERD using optical coherence tomography before and after double-blind, randomized treatment with esomeprazole or placebo. *The American journal of gastroenterology,* 104**,** 2788-2795

Wilson, J., Clark, A. E., Hall, M. & Hench, L. L. 1992. Tissue response to Bioglass endosseous ridge maintenance implants. *The Journal of oral implantology,* 19**,** 295-302

Wilson, J. & Low, S. B. 1992. Bioactive ceramics for periodontal treatment: comparative studies in the Patus monkey. *Journal of Applied Biomaterials,* 3**,** 123-129

Wilson, J., Pigott, G. H., Schoen, F. J. & Hench, L. L. 1981. Toxicology and biocompatibility of bioglasses. *Journal of Biomedical Materials Research,* 15**,** 805-17.

Wilson, P. R. & Beynon, A. D. 1989. Mineralization differences between human deciduous and permanent enamel measured by quantitative microradiography. *Archives of Oral Biology,* 34**,** 85-88.

Wilwerding, T. & Aiello, A. 1990. Comparative efficiency testing 330 carbide dental burs utilizing Macor substrate. *Pediatric Dentistry,* 12**,** 170-171.

Wongkhantee, S., Patanapiradej, V., Maneenut, C. & Tantbirojn, D. 2006. Effect of acidic food and drinks on surface hardness of enamel, dentine, and tooth-coloured filling materials. *Journal of Dentistry,* 34**,** 214-20.

Yan, Y. 1996. Mass flow measurement of bulk solids in pneumatic pipelines. *Measurement Science & Technology,* 7**,** 1687-1706.

Yim, H.-K., Kwon, H.-K. & Kim, B.-I. 2014. Modification of surface pre-treatment for resin infiltration to mask natural white spot lesions. *Journal of dentistry*

Yip, H. K. & Samaranayake, L. P. 1998. Caries removal techniques and instrumentation: a review. *Clinical oral investigations,* 2**,** 148-154

Yli-Urpo, H., Narhi, M. & Narhi, T. 2005. Compound changes and tooth mineralization effects of glass ionomer cements containing bioactive glass (S53P4), an in vivo study. *Biomaterials,* 26**,** 5934-41.

Zero, D. T. 1996. Etiology of dental erosion–extrinsic factors. *European Journal of Oral Sciences,* 104**,** 1600-0722.

Zero, D. T. 2006. Dentifrices, mouthwashes, and remineralization/caries arrestment strategies. *BMC Oral Health,* 6 Suppl 1**,** S9.

Zhao, W., Xie, Q., Bedran-Russo, A. K., Pang, S., Ling, J. & Wu, C. D. 2014. The preventive effect of grape seed extract on artificial enamel caries progression in a microbial biofilm-induced caries model. *Journal of Dentistry*.

Zhong, J. P., Greenspan, D. C. & Feng, J. W. 2002. A microstructural examination of apatite induced by Bioglass in vitro. *Journal of Materials Science: Materials in Medicine,* 13**,** 321-6.

Zhou, C., Zhang, D., Bai, Y. & Li, S. 2014. Casein phosphopeptide–amorphous calcium phosphate remineralization of primary teeth early enamel lesions. *Journal of Dentistry,* 42**,** 21-29.

Publications

List of publications in international peer-reviewed journals:

- Milly, H., Austin, R. S., Thompson, I. & Banerjee, A. 2014. In Vitro Effect of Air-abrasion Operating Parameters on Dynamic Cutting Characteristics of Alumina and Bio-active Glass Powders. Operative dentistry, 39, 81-89.

- Milly, H., Andiappan, M., Thompson, I. & Banerjee, A. 2014. Bio-active glass air-abrasion has the potential to remove resin composite restorative material selectively. Applied Surface Science, 303, 272-276.

- Milly, H., Festy, F., Watson, T. F., Thompson, I. & Banerjee, A. 2014. Enamel white spot lesions can remineralise using bio-active glass and polyacrylic acid-modified bio-active glass powders. *Journal of Dentistry,* 42, 158-166.

©Operative Dentistry, 2013, 38-6, 000-000

In Vitro Effect of Air-abrasion Operating Parameters on Dynamic Cutting Characteristics of Alumina and Bio-active Glass Powders

H Milly • RS Austin • I Thompson
A Banerjee

Clinical Relevance

Bio-active glass (BAG) powder exhibits more air-abrasion conservative cutting characteristics compared to alumina powder, particularly within specific operating parameters. Clinical air-abrasion use should be preceded by studying the powder flow rate to identify the factors affecting the abrasive powder propulsion.

SUMMARY

Minimally invasive dentistry advocates the maintenance of all repairable tooth structures during operative caries management in combination with remineralization strategies. This study evaluated the effect of air-abrasion operating parameters on its cutting efficiency/pattern using bio-active glass (BAG) powder and alumina powder as a control in order to develop its use as a minimally invasive operative technique. The cutting efficiency/pattern assessment on an enamel analogue, Macor, was preceded by studying the powder flow rate (PFR) of two different commercial intraoral air-abrasion units with differing powder-air admix systems. The parameters tested included air pressure, powder flow rate, nozzle-substrate distance, nozzle angle, shrouding the air stream with a curtain of water, and the chemistry of abrasive powder. The abraded troughs were scanned and analyzed using confocal white light profilometry and MountainsMap surface analysis software. Data were analyzed statistically using one-way and repeated-measures analysis of variance tests (p=0.05). The air-abrasion unit using a vibration mechanism to admix the abrasive powder

*Hussam Milly, BDS, DipOS, MSc, Biomaterials, Biomimetics & Biophotonics Research Group, King's College London Dental Institute at Guy's Hospital, King's Health Partners, London, United Kingdom

Rupert S Austin, BDS, PhD, Unit of Prosthodontics, King's College London Dental Institute at Guy's Hospital, King's Health Partners, London, United Kingdom

Ian Thompson, B.Eng, PhD, Biomaterials, Biomimetics & Biophotonics Research Group, King's College London Dental Institute at Guy's Hospital, King's Health Partners, London, United Kingdom

Avijit Banerjee, BDS, MSc, PhD, FDS (Rest Dent) FDS RCS (Eng) FHEA, Unit of Conservative Dentistry , Biomaterials, Biomimetics & Biophotonics Research Group, King's College London Dental Institute at Guy's Hospital, King's Health Partners, London, United Kingdom

*Corresponding author: SE1 9RT, United Kingdom; e-mail: milly.hussam@kcl.ac.uk

DOI: 10.2341/12-466-L

with the air stream exhibited a constant PFR regardless of the set air pressure. Significant differences in cutting efficiency were observed according to the tested parameters ($p<0.05$). Alumina powder removed significantly more material than did BAG powder. Using low air pressure and suitable consideration of the effect of air-abrasion parameters on cutting efficiency/patterns can improve the ultraconservative cutting characteristics of BAG air-abrasion, thereby allowing an introduction of this technology for the controlled cleaning/removal of enamel, where it is indicated clinically.

INTRODUCTION

Minimally invasive dentistry (MID) encourages the preparation of the smallest cavity possible, maintaining the presence of as much repairable tissue as possible, and relying on adhesion techniques to achieve the retention and seal of the overlying restorative materials.[1-4] Air-abrasion cuts tooth tissue through the use of kinetics to blast away surface hard tissues.[5] The variables controlling air-abrasion cutting efficiency (and, therefore, its potential intrinsic ability to remove tissues selectively) can be divided into three main categories: 1) the built-in physics and mechanics of the equipment, which includes the powder-air admix mechanism, powder flow rate (PFR), powder volume reservoir, nozzle output pressure, and water shrouding the powder stream; 2) the parameters controlled by the operator, including the nozzle angle, nozzle-substrate distance, nozzle movement speed, and the targeted substrate itself; and 3) the variations found in the abrasive powder used, including the size, shape, hardness, and chemistry of the particles and their interaction with the substrate.[6-14]

There are a large number of available commercial air-abrasion units, and each can be used at various settings with different powder admix mechanisms. Therefore, in order to improve the comparability of air-abrasion studies and their clinical use, it is important to study the PFR. In addition, water shrouding the powder stream has been introduced in some units to reduce atmospheric powder scattering. The consequence of this modification on air-abrasion cutting efficiency has not been studied previously.

Using alumina powder as an abrasive can lead to undesirable clinical over-preparation of dental hard tissues.[6,13,15,16] Therefore, with the purpose of promoting air-abrasion cutting tissues selectively to meet the MID paradigm, bio-active glass (BAG) powder has been introduced with the hope that practitioners can benefit from its properties, including its antibacterial effects, remineralization potential, and its potential to remove selectively more softened diseased or damaged tooth structures.[17-21]

In order to use air-abrasion appropriately, this study assessed the effect of certain parameters on BAG air-abrasion cutting efficiency/pattern using an enamel analogue, Macor, in simulated clinical conditions, compared to conventional 27-μm alumina air-abrasion (the positive control). The abrasion assessment was preceded by a PFR study of two different intraoral air-abrasion units using different powder-air admix mechanisms.

The three null hypotheses investigated in this study were

1. There is no effect of air pressure on powder flow rate in either Aquacut or Air-Flow Master air-abrasion units.
2. Operating parameters have no effect on the cutting efficiency/pattern on an artificial enamel analogue.
3. There are no differences in the cutting efficiency between alumina and BAG powders when used under standardized clinical conditions.

MATERIALS AND METHODS

Characterization of the abrasive powders' surface topography and elemental composition were determined using scanning electron microscopy-energy dispersive x-ray spectroscopy (SEM-EDX, accelerating voltage of 25 kV, working distance of 13 mm). Particle size analysis was carried out using a laser diffraction particle analyzer (Cilas, Orleans, France), and the results were analyzed with the Particle Size Expert software package (Cilas).

The nozzle output air pressure of the air-abrasion unit was measured using a digital pressure indicator (DPI 705, Druck, UK) attached to the output nozzle. The nozzle diameter was validated using a digital measurement device (Quadra-Check 300). Periodic calibration of output pressure and the nozzle diameter was conducted throughout the experiments to ensure consistency and standardization under all experimental conditions.

PFR Evaluation

Comparing the weight of a collecting container, including a layer of sponge and a paper filter, before and after one minute of active air-abrasion permitted the study of PFR.[22] The powder reservoir was

consistently refilled with the abrasive powder to a predetermined line, and the powder was manually stirred prior to use throughout.

In order to investigate the effect of air pressure on PFR on both Aquacut (Velopex, Harlesden, UK) and Air-Flow Master (EMS, Nyon, Switzerland) air-abrasion units, the powder feed dial was fixed at the middle setting and the air pressure was adjusted into 40, 60, and 80 psi. Ten measurements were conducted within each experimental group using BAG powder.

The same method was used to calculate the PFR (g/min) for each of the powder feed dial settings—1, 3, and 5—used as a variable during cutting efficiency/pattern assessment using the Aquacut unit (nozzle output internal diameter 600 μm). This experiment was conducted by fixing the air pressure at a constant 60 psi.

Cutting Efficiency/Pattern Assessment

The dynamic abrasion procedure was performed within a plastic chamber attached to high vacuum suction using a micropositioning device to fix the nozzle and a stage to move the substrate. A Macor sheet (50×50×5 mm) was located on the stage attached to a moving coil actuator (SMAC, Crowley, UK), programmed to obtain 10-mm linear movement at a velocity of 0.5 mm/s.

The variables assessed in this study were air pressure (20, 40, and 60 psi), powder feed dial value (1, 3, and 5), nozzle angle (45° and 90°), nozzle distance (1, 2, and 5 mm), and the cutting mode (dry and wet) for both alumina and BAG powders. When each variable was investigated, the remaining parameters were fixed as follows: air pressure, 60 psi; powder feed dial, 3; nozzle angle, 90°; nozzle distance, 2 mm. Ten troughs were made in each experimental group.

Evaluation of the effect of different parameters was conducted using dry air-abrasion mode. However, to evaluate the influence of shrouding the air-powder stream with a water curtain on the cutting efficiency, a disposable plastic tip, used to mix the air stream with water, was attached to the tip of the nozzle.

Using proprietary measurement control software (STAGES, TaiCaan Technologies Ltd, Southampton, UK), a standard scan area of 5 × 2 mm was chosen over the central region of each trough. Optical white light confocal profilometry (Xyris 4000 WL, TaiCaan Technologies) was used to image the surface topography of the resulting 200 troughs. The white light sensor had a 0.01-μm resolution, a spot size of 7 μm, and a gauge range of 350 μm. The scan was performed with a 10-μm step-over distance in medium precision measurement mode.

The resulting three-dimensional (3D) topographic data sets were analyzed using MountainsMap surface analysis software (Version 6.2.6332, SARL Digital Surf, Besançon, France) to obtain the volume of the troughs (mm^3). A macro was written to read and analyze the 3D data automatically using the "measure volume of a hole" function. Air-abrasion cutting efficiency was established by comparing the volume removed with the assumption that the settings were more efficient when air-abrasion removed a greater volume of Macor. Representative 3D selected images from BAG powder groups were examined to characterize the cutting pattern.

The statistical analysis was conducted using the SPSS Statistical Package (version 19.0, SPSS Inc/IBM, Chicago, IL, USA). One-way analysis of variance (ANOVA) and Bonferroni *post hoc* testing was performed to analyze the PFR data, and repeated-measures ANOVA followed by Bonferroni *post hoc* test was used for the analysis of the cutting efficiency assessment data. The level of statistical significance was established at $p=0.05$ for both tests.

RESULTS

The alumina powder had an angular shape, while BAG powder had an aspect ratio of 1:1, with some angular edges seen on the particle surface (Figure 1). The compositions of alumina and BAG powder are shown in Figure 2. The particle size distribution percentiles (10%, 50%, and 90%) of the alumina powder were 23, 37, and 51 μm, respectively, while those of BAG powder were 23, 56, and 82 μm, respectively.

PFR Evaluation

PFR mean values (±standard deviations) regarding the effect of air pressure on PFR are shown in Figure 3. Air pressure had no effect on the PFR in the Aquacut unit, which showed constant PFR for all air pressure values. In contrast, increasing the air pressure in the Air-Flow Master® unit from 40 and 60 psi to 80 psi increased the PFR in a statistically significant manner ($p<0.001$, $p=0.01$, respectively).

PFR ranges for the Aquacut unit settings involved in this study for both powders are shown in Figure 4. The PFR increased significantly when the powder feed dial was adjusted from the minimum to the

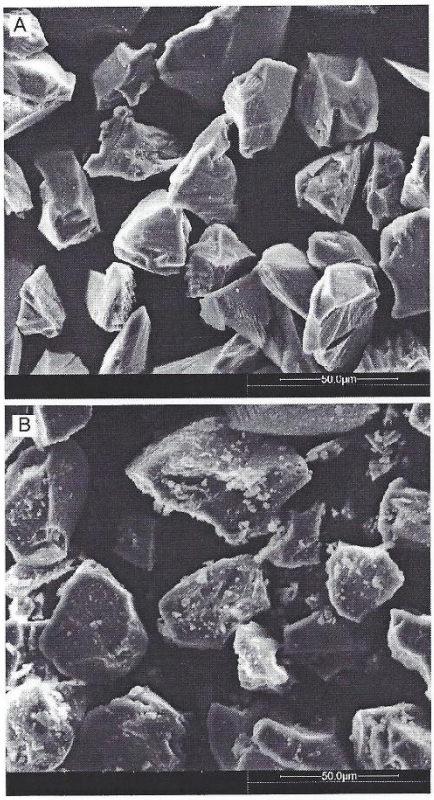

Figure 1. *(A) SEM of alumina particles; (B) SEM of BAG particles (accelerating voltage: 25 kV; working distance: 13 mm; magnification: 1500). Alumina powder exhibits an angular shape, while BAG powder has an aspect ratio of 1:1, with some angular edges seen on the particles.*

maximum value within the BAG powder groups ($p<0.001$).

Cutting Efficiency/Pattern Assessment

An increase in air pressure resulted in an increase in Macor volume removal in both powder groups. With alumina, the increase was not different statistically between the 40 and 60 psi values, while it was significant within BAG groups, which showed statistical differences among all the air pressures tested

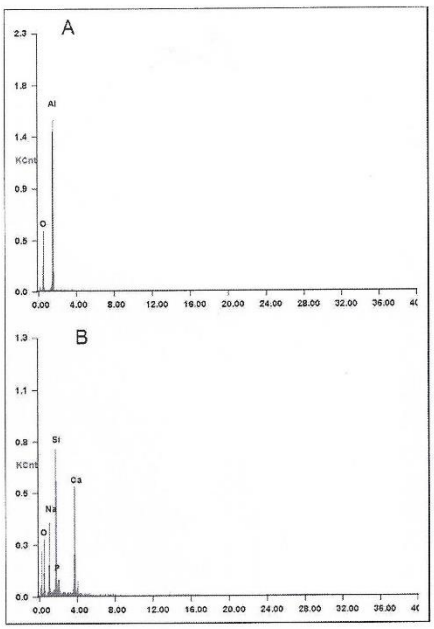

Figure 2. *(A) EDX revealed aluminium and oxygen peaks in alumina powder; (B) EDX revealed silicon, calcium, phosphorus, sodium, and oxygen peaks in BAG powder (accelerating voltage: 25 kV; working distance: 13 mm).*

($p<0.001$). The volume of material removed when the air pressure was fixed at 20 psi was 0.75 ± 0.16 mm^3 (mean ± standard deviation) in the alumina group, whereas 60%, statistically less, was removed in the BAG group (0.3 ± 0.02 mm^3; $p=0.01$). However, the difference in the Macor volume removed between the two powders was not statistically significant and declined to 30% (1.39 ± 0.33 mm^3) in the alumina group and 0.97 ± 0.04 mm^3 in the BAG group when the overall air pressure was increased to 60 psi.

Adjusting the powder feed dial to the highest value increased the volume of Macor removed ($p<0.001$, $p=0.005$ in alumina and BAG groups, respectively) (Figure 5). In addition, increasing the nozzle-substrate distance from 1 to 5 mm improved air-abrasion cutting efficiency ($p<0.001$) (Figure 6). Setting the PFR to the lowest value caused more pronounced fluctuation in the base of the trough

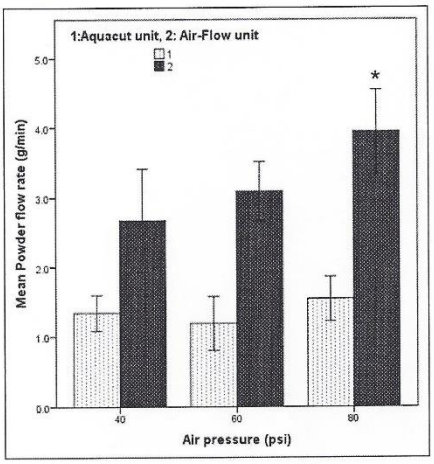

Figure 3. *PFR mean value ± standard deviation (SD) (g/min) correlated with variable air pressures (powder feed rate dial setting fixed at middle values). *Indicates statistically significant differences between air pressure at 40/60 psi and 80 psi in Air-Flow Master unit ($p<0.05$).*

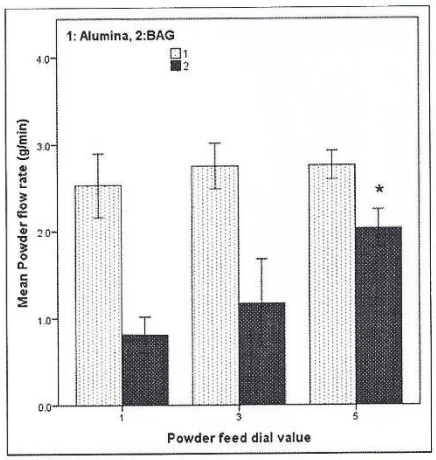

Figure 4. *PFR mean value ± standard deviation (SD) (g/min) for alumina and BAG powders correlated with variable powder feed rate settings (air pressure fixed at 60 psi). *Indicates statistically significant differences between powder feed rate dials 1 and 5 within BAG powder group ($p<0.05$).*

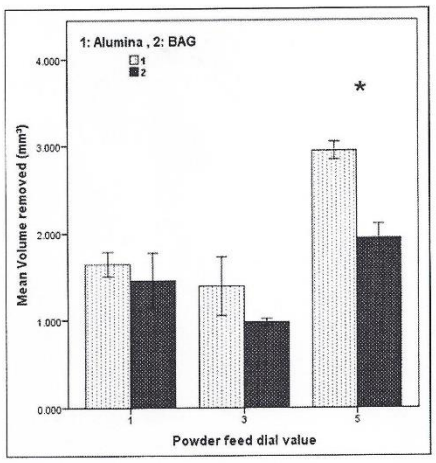

Figure 5. *Macor volume removed mean ± standard deviation (SD) for alumina and BAG groups correlated with variable powder feed rate dial settings. *Indicates statistically significant differences between powder feed rate dials 1/3 and 5 in both powder groups ($p<0.05$).*

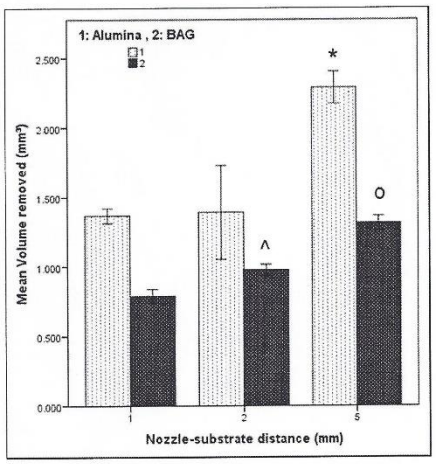

Figure 6. *Macor volume removed mean ± standard deviation (SD) for alumina and BAG groups correlated with variable nozzle-substrate distance. *Statistically significant differences between distances of 1/2 and 5 mm in alumina groups; ^Statistically significant differences between distances of 1 and 2 mm in BAG groups; °Statistically significant differences between distances of 1/2 and 5 mm in BAG groups ($p<0.05$).*

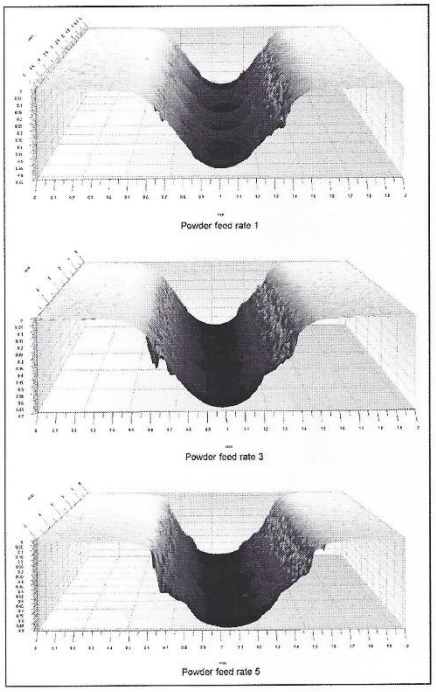

Figure 7. *3D scans of selected, representative BAG air-abrasion troughs. (A) The fluctuation in the base of the trough when powder feed dial was set at 1. (B and C) Troughs prepared using powder feed dial 3 and 5, respectively.*

along its length (Figure 7). The nozzle distance of 5 mm produced more rounded trough margins compared to those produced with shorter distances (Figure 8).

Statistically significantly more Macor was removed when the air-abrasion nozzle was fixed at 45° (2.52 ± 0.14 mm^3 and 1.76 ± 0.08 mm^3 within alumina and BAG, respectively) rather than 90° (1.39 ± 0.33 mm^3 and 0.97 ± 0.04 mm^3 within alumina and BAG, respectively) ($p<0.001$). The shape of the troughs varied according to the nozzle angle: 45° produced a trough with a "V" cross-section, while 90° presented troughs with a "U"-shaped cross section (Figure 9).

There was no significant difference in the cutting efficiency between dry and wet air-abrasion systems

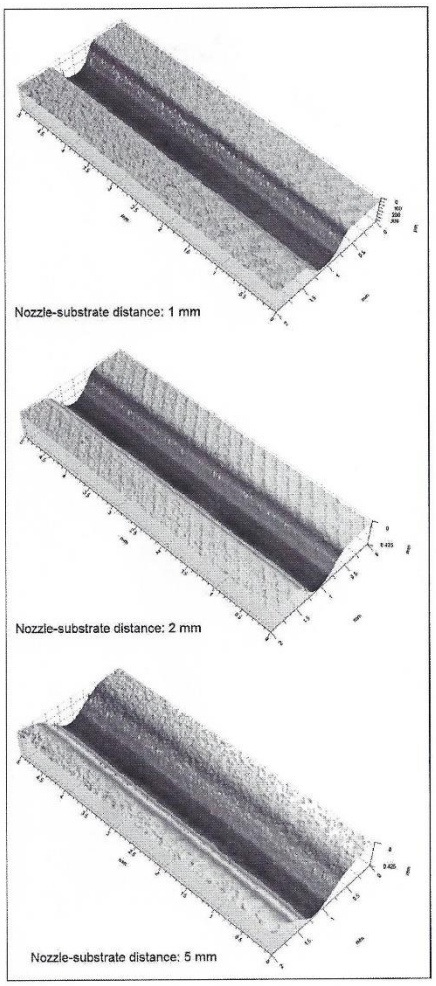

Figure 8. *Trough margin variation according to the nozzle-substrate distance within BAG powder group. Nozzle-substrate distance of 5 mm (C) results in a rounded, less well-defined trough margin compared to nozzle-substrate distances of 1 mm (A) and 2 mm (B).*

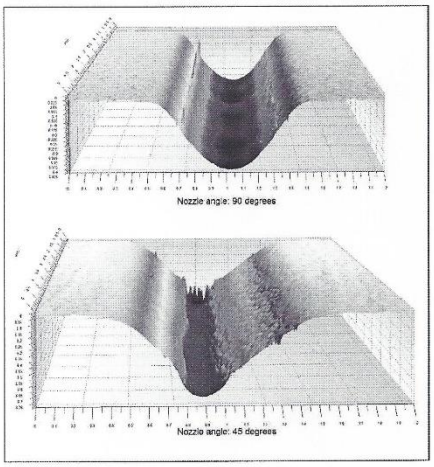

Figure 9. *Representative scans revealed the cross-sectional trough shape difference between the 90° nozzle angle (trough with "U" cross section) (A) and 45° nozzle angle (trough with "V" cross section) (B) within BAG powder groups.*

for both powders. In alumina groups, dry air-abrasion removed 3.36 ± 0.17 mm^3 and wet air-abrasion removed 3.49 ± 0.48 mm^3. The Macor volume removed in the BAG groups was 1.84 ± 0.34 mm^3 and 1.93 ± 0.61 mm^3 using dry and wet abrasion, respectively.

DISCUSSION

The two air-abrasion units employed in this study use different mechanisms to admix the abrasive powder with the air propellant stream. The Aquacut unit uses a vibration mechanism to admix the abrasive particles with the air stream, and this explains why a constant PFR was recorded regardless of the air pressure values. However, in the Airflow unit, in which an air vortex is created inside the powder chamber, air pressure not only modifies the particles velocity but it also alters the amount of expelled powder from the nozzle. PFR measurement (g/min) for the powder feed dial values during air-abrasion studies makes the results obtained using a specific air-abrasion unit comparable and reproducible using different air-abrasion units when the PFR is equilibrated to the same ranges. BAG powder exhibits different bulk density, atmospheric moisture uptake, and particle size/shape when compared to alumina, which in turn explains the variation in their flowability. Therefore, it is advised that BAG powder should be manually stirred in the reservoir prior to the abrasion procedure to help prevent the separation of the different particle sizes, which will affect the flow rate and, therefore, cutting efficiency.

Macor was used as the control substrate, as it has been used for assessing the cutting rate and efficiency of operative technologies in dentistry as a result of its consistent, uniform hardness, which is not found in human enamel, as the enamel hardness varies from person to person according to the individual's food consumption and is depth-dependent within the same tooth as a result of histological heterogeneity.[23,24] Using Macor sheets also provided a reliable, flat surface as a target for air-abrasion cutting and subsequent objective analysis using optical surface profilometry, which was used in the present study to determine the volume of material removed, as it is considered an accurate method by which to measure hard tissue loss.[25,26]

Assessing the dynamic cutting efficiency has the advantage over static cutting, as it mimics more realistically the clinical situation, in which the procedure is accomplished by moving the nozzle over the target substrate.

The findings of this study indicate that there is an increase in the air-abrasion cutting rate for both powders when air pressure increases. Since the increase in air pressure does not increase the PFR in the Aquacut unit, as proved in the PFR evaluation study, this finding may be explained based on the dependency upon the increased kinetic energy of the particles, a finding consistent with those of previous studies.[7,27] It is important to be aware that when low air pressure was applied, the difference in air-abrasion cutting efficiency between the two powders more than doubled, implying that at low air pressure settings, the cutting efficiency of air-abrasion depends mainly on the nature of the abrasive powder rather than on the physics of air-abrasion unit itself.

The finding concerning the effect of PFR on the cutting efficiency is inconsistent with the findings of a previous study,[14] which claimed that an increase in PFR without a concomitant increase in the air pressure is pointless. In the present study, employing both a dynamic cutting protocol and high vacuum suction reduced the surface choking of particles when excessive quantities of abrasive were applied. The undulating troughs resulting from using less powder may be caused by the irregular distribution of particles within the air stream. Most

of the particles are concentrated into a small portion of the stream's cross-sectional area.[28]

Previous studies[9,29] indicated an inverse relationship between the distance and the cutting efficiency. In those studies, the researchers used the cross-sectional views of the cut surfaces to assess the cutting efficiency, whereas in this experiment the whole volume removed was calculated using the 3D measurement methodology.

When the nozzle was fixed at 45°, the percentage of the air stream's peripheral portion, which presents a reduced concentration of particles with reduced velocity,[10] increased, and that in turn produced cross-sectional "V"-shaped troughs.

The air-abrasion operating parameters controlling the nozzle position affected significantly the cutting efficiency observed in both powder groups. This can be explained by the fact that increasing the distance and fixing the nozzle at 45° reduced the surface choking of particles, which is assumed to disturb negatively the propellant stream.

One of the objectives in this study was to determine the difference in cutting efficiency between alumina and BAG powders. It was noticeable that alumina powder removed considerably more material than did BAG powder. In addition, the cutting efficiency was more controllable within BAG powder groups since only slight differences in operating parameters altered the cutting efficiency, while alumina powder groups demanded considerable alterations in the parameters to exhibit statistical differences in the cutting rate. The abrasive powders consisted of different shapes, particle size distributions, and hardnesses,[13,30] which may explain the variations observed in this study of cutting efficiency and sensitivity to the operating parameters.

CONCLUSIONS

The three null hypotheses investigated were rejected. Using air-abrasion should be preceded by system calibration to identify the factors affecting the abrasive powder propulsion, as they differ according to the unit's design. Vibration admix units exhibited a constant powder flow rate regardless of air pressure. However, it is advocated that practitioners check the BAG powder condition within the powder chamber before the abrasion procedures to obtain a sufficient powder flow rate. Manufacturers need to take note and provide this information clearly to clinicians. Air-abrasion cutting efficiency is more conservative and controllable when BAG powder is used as an abrasive powder, encouraging its role in minimally invasive operative dentistry.

Acknowledgments

The authors acknowledge the Comprehensive Biomedical Research Centre at Guy's & St Thomas' Trust and the support from the Centre of Excellence in Medical Engineering funded by the Wellcome Trust. The authors also acknowledge Mr Peter Pilecki and Mr Richard Mallett for their laboratory support and Mr Manoharan Andiappan for the statistical advice.

Conflict of Interest

The authors of this manuscript certify that they have no proprietary, financial, or other personal interest of any nature or kind in any product, service, and/or company that is presented in this article.

(Accepted 23 January 2013)

REFERENCES

1. Banerjee A, Watson TF, & Kidd EA (2000) Dentine caries excavation: A review of current clinical techniques *British Dental Journal* **188(9)** 476-482.
2. tenCate JM (2008) Remineralization of deep enamel dentine caries lesions *Australian Dental Journal* **53(3)** 281-285.
3. Mount GJ (2007) A new paradigm for operative dentistry *Australian Dental Journal* **52(4)** 264-270.
4. Mickenautsch S, Yengopal V, & Banerjee A (2010) A traumatic restorative treatment versus amalgam restoration longevity: A systematic review *Clinical Oral Investigations* **14(3)** 233-240.
5. Black RB (1950) Airbrasive—Some fundamentals *Journal of the American Dental Association* **41(6)** 701-710.
6. Horiguchi S, Yamada T, Inokoshi S, & Tagami J (1998) Selective caries removal with air abrasion *Operative Dentistry* **23(5)** 236-243.
7. White JM, & Eakle WS (2000) Rationale and treatment approach in minimally invasive dentistry *Journal of the American Dental Association* **131(Supplement)** 13S-19S.
8. Banerjee A, Pabari H, Paolinelis G, Thompson ID, & Watson TF (2011) An in vitro evaluation of selective demineralised enamel removal using bio-active glass air abrasion *Clinical Oral Investigations* **15(6)** 895-900.
9. Bailey LR, & Phillips RW (1950) Effect of certain abrasive materials on tooth enamel *Journal of Dental Research* **29(6)** 740-748.
10. Laurell KA, & Hess JA (1995) Scanning electron micrographic effects of air-abrasion cavity preparation on human enamel and dentin *Quintessence International* **26(2)** 139-144.
11. Jost-Brinkmann PG (1998) The influence of air polishers on tooth enamel. An in-vitro study *Journal of Orofacial Orthopedics* **59(1)** 1-16.
12. Santos-Pinto L, Peruchi C, Marker VA, & Cordeiro R (2001) Effect of handpiece tip design on the cutting

efficiency of an air abrasion system *American Journal of Dentistry* **14(6)** 397-401.

13. Paolinelis G, Banerjee A, & Watson TF (2008) An in vitro investigation of the effect and retention of bioactive glass air-abrasive on sound and carious dentine *Journal of Dentistry* **36(3)** 214-218.
14. Paolinelis G, Banerjee A, & Watson TF (2009) An in-vitro investigation of the effects of variable operating parameters on alumina air-abrasion cutting characteristics *Operative Dentistry* **34(1)** 87-92.
15. Banerjee A, Paolinelis G, Socker M, McDonald F, & Watson TF (2008) An in vitro investigation of the effectiveness of bioactive glass air-abrasion in the 'selective' removal of orthodontic resin adhesive *European Journal of Oral Sciences* **116(5)** 488-492.
16. Motisuki C, Lima LM, Bronzi ES, Spolidorio DM, & Santos-Pinto L (2006) The effectiveness of alumina powder on carious dentin removal *Operative Dentistry* **31(3)** 371-376.
17. Banerjee A (2013) Minimal intervention dentistry: part 7. Minimally invasive operative caries management: rationale and techniques *British Dental Journal* **214(3)** 107-111.
18. Allan I, Newman H, & Wilson M (2001) Antibacterial activity of particulate bioglass against supra- and subgingival bacteria *Biomaterials* **22(12)** 1683-1687.
19. Hu S, Chang J, Liu M, & Ning C (2009) Study on antibacterial effect of 45S5 bioglass *Journal of Materials Science Materials in Medicine* **20(1)** 281-286.
20. Banerjee A, Thompson ID, & Watson TF (2011) Minimally invasive caries removal using bio-active glass air-abrasion *Journal of Dentistry* **39(1)** 2-7.
21. Gjorgievska E, & Nicholson J (2011) Prevention of enamel demineralization after tooth bleaching by bioactive glass incorporated into toothpaste *Australian Dental Journal* **56(2)** 193-200.
22. Banerjee A, Uddin M, Paolinelis G, & Watson TF (2008) An investigation of the effect of powder reservoir volume on the consistency of alumina powder flow rates in dental air-abrasion devices *Journal of Dentistry* **36(3)** 224-227.
23. Wongkhantee S, Patanapiradej V, Maneenut C, & Tantbirojn D (2006) Effect of acidic food and drinks on surface hardness of enamel, dentine, and tooth-coloured filling materials *Journal of Dentistry* **34(3)** 214-220.
24. Ercoli C, Rotella M, Funkenbusch PD, Russell S, & Feng C (2009) In vitro comparison of the cutting efficiency and temperature production of 10 different rotary cutting instruments. Part I: Turbine *Journal of Prosthetic Dentistry* **101(4)** 248-261.
25. Austin RS, Rodriguez JM, Dunne S, Moazzez R, & Bartlett DW (2010) The effect of increasing sodium fluoride concentrations on erosion and attrition of enamel and dentine in vitro *Journal of Dentistry* **38(10)** 782-787.
26. Schlueter N, Hara A, Shellis RP, & Ganss C (2011) Methods for the measurement and characterization of erosion in enamel and dentine *Caries Research* **45(Supplement 1)** 13-23.
27. Cook RJ, Azzopardi A, Thompson ID, & Watson TF (2001) Real-time confocal imaging, during active air abrasion-substrate cutting *Journal of Microscopy* **203(Supplement 2)** 199-207.
28. Yan Y (1996) Mass flow measurement of bulk solids in pneumatic pipelines *Measurement Science and Technology* **7(12)** 1687-1706.
29. Peruchi C, Santos-Pinto L, Santos-Pinto A, Barbosa E, & Silva E (2002) Evaluation of cutting patterns produced in primary teeth by an air-abrasion system *Quintessence International* **33(4)** 279-283.
30. Thompson ID, & Hench LL (1998) Mechanical properties of bioactive glasses, glass-ceramics and composites *Proceedings of the Institution of Medical Engineers* **212(2)** 127-136.

Applied Surface Science 303 (2014) 272–276

Contents lists available at ScienceDirect

Applied Surface Science

journal homepage: www.elsevier.com/locate/apsusc

Bio-active glass air-abrasion has the potential to remove resin composite restorative material selectively

Hussam Milly[a], Manoharan Andiappan[b], Ian Thompson[a], Avijit Banerjee[a,c,*]

[a] Biomaterials, Biomimetics & Biophotonics Research Group, Kings College London Dental Institute at Guy's Hospital, King's Health Partners, London, UK
[b] Unit of Dental Public Health, Kings College London Dental Institute at Guy's Hospital, King's Health Partners, London, UK
[c] Unit of Conservative Dentistry, King's College London Dental Institute at Guy's Hospital, King's Health Partners, London, UK

ARTICLE INFO

Article history:
Received 17 January 2014
Received in revised form 25 February 2014
Accepted 26 February 2014
Available online 12 March 2014

Keywords:
Air-abrasion
Alumina
Bio-active glass (BAG)
Operating parameters
Resin composite

ABSTRACT

The aims of this study were to assess: (a) the chemistry, morphology and bioactivity of bio-active glass (BAG) air-abrasive powder, (b) the effect of three air-abrasion operating parameters: air pressure, powder flow rate (PFR) and the abrasive powder itself, on the selective removal of resin composite and (c) the required "time taken". BAG abrasive particles were characterised using scanning electron microscopy-energy dispersive X-ray spectrometry (SEM-EDX) and Fourier-transform infrared spectroscopy (FTIR). Standardised resin composite restorations created within an enamel analogue block (Macor™) in vitro, were removed using air-abrasion undersimulated clinical conditions. 90 standardised cavities were scanned before and after resin composite removal using laser profilometry and the volume of the resulting 3D images calculated. Multilevel linear model was used to identify the significant factors affecting Macor™ removal. BAG powder removed resin composite more selectively than conventional air-abrasion alumina powder using the same operating parameters ($p < 0.001$) and the effect of altering the unit's operating parameters was significant ($p < 0.001$). In conclusion, BAG powder is more efficient than alumina in the selective removal of resin composite particularly under specific operating parameters, and therefore may be recommended clinically as a method of preserving sound enamel structure when repairing and removing defective resin composite restorations.

1. Introduction

Using rotary instruments to remove or repair aesthetically and biologically unsatisfactory resin composite restorations or resin luting cement remnants on tooth surfaces after de-bonding fixed orthodontic appliances, alters tooth surface topography resulting in enamel cracks, scarring and scratches [1,2]. Air-abrasion tooth cutting technology may be a useful alternative, utilising the abrasive particulate kinetic energy to produce small, rounded cavity margins, ideal internal line angle contours and a surface finish optimised for the adhesion of contemporary dental materials [3,4].

Bio-active glass (BAG) was discovered by Hench and colleagues in 1969 with numerous applications in the repair and reconstruction of damaged tissues [5]. BAG 45S5 powder contains 45 wt% SiO_2, 24.5 wt% NaO, 24.4 wt% CaO and 6 wt% P_2O_5 [5]. This powder has been used as a clinical abrasive powder benefitting from its remineralisation ability and its potential to remove selectively more softened, diseased or weakened tooth structure [6–8]. A previous study showed that using BAG air-abrasion for orthodontic adhesive cement remnant removal in vitro caused significantly less enamel surface damage/loss compared to that caused by using conventional 27 μm alumina air-abrasion [9].

In the light of results from a previous study evaluating BAG air-abrasion cutting efficiency/patterns [10], it would seem logical to expect that altering the air-abrasion operating parameters may affect its capacity to remove selectively resin composite and consequently preserve more sound, intact enamel. Therefore, the objectives of this study were to assess: (a) the chemistry, morphology and bioactivity of BAG powder, (b) the effect of three clinically adjustable air-abrasion operating parameters: air pressure, powder flow rate (PFR) and the abrasive powder itself, on the selective removal of resin composite and (c) the required clinical time taken to carry out the procedures.

The characteristics of BAG powder were determined using scanning electron microscopy-energy dispersive X-ray spectrometry (SEM-EDX) and laser diffraction particle analysis, whilst

* Corresponding author at: Unit of Conservative Dentistry, King's College London Dental Institute, Floor 26, Tower Wing, Guy's Dental Hospital, London SE1 9RT, UK. Tel.: +44 0207 188 1577/7486; fax: +44 0207 188 1577/7486.
E-mail address: avijit.banerjee@kcl.ac.uk (A. Banerjee).

http://dx.doi.org/10.1016/j.apsusc.2014.02.165
0169-4332/

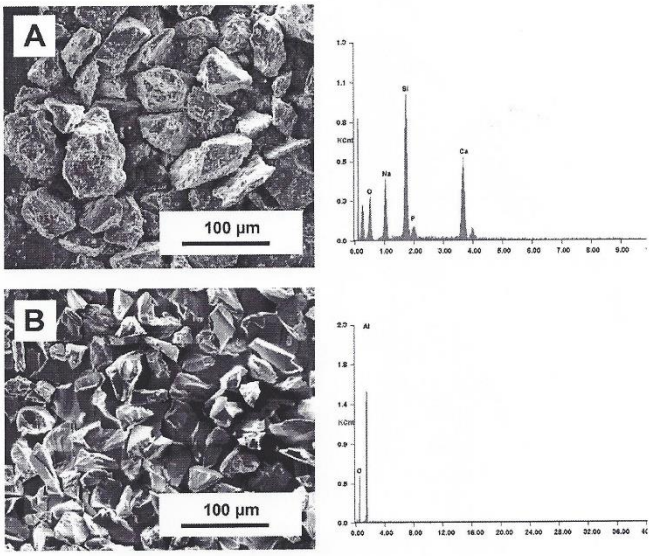

Fig. 1. SEM-EDX (accelerating voltage: 10 kV, working distance: 10 mm) for BAG (A) reveals the particles' aspect ratio of 1:1, with angular edges and surrounded by a submicron dust. They contained calcium, phosphorus, sodium and oxygen. The particles within the alumina powder (B) exhibit an angular shape and consist of aluminium and oxygen.

the powder bioactivity was inspected using Fourier-transform infrared spectroscopy (FTIR). The selective removal measurement was accomplished by comparing the volume of standardised cavities created within an enamel analogue (Macor™) permitting an experimental standardisation of hardness and thermal properties, both similar to those of human dental enamel [11]. The three null hypotheses investigated in this study were: (a) using BAG as an alternative to conventional 27 µm alumina powder shows no difference in resin composite removal selectivity; (b) there is no effect of air pressure and PFR setting on resin composite removal selectivity within both abrasive powder groups, and (c) the required clinical time taken is no different between alumina and BAG powders.

2. Materials and methods

2.1. Characterisation of abrasive powders

BAG 45S5 abrasive powder (Sylc, OSspray, London, UK) and alumina powder (Aquacut, Velopex, Horesham, UK) particles' surface topography and elemental composition were determined using SEM-EDX (FEI Co. Ltd., Cambridge, UK) (accelerating voltage: 10 kV, working distance: 10 mm). Particle size analysis was carried out using a laser diffraction particle analyser (1180, CILAS, Orleans, France).

The bioactivity of BAG powder was validated by adding 0.3 g of BAG powder to 200 ml Tris (tris-hydroxymethyl amino methane) buffer solution adjusted to pH 7.25 with hydrochloride acid. The bioactivity test was conducted dynamically, permitting a uniform exposure of the particles to the buffer solution in a water bath at 175 rpm and 37 °C for 20 h. The powder was then filtered, acetone-washed, air-dried and scanned using a FTIR Spectrometer (Perkin-Elmer, Beaconsfield, UK). The FTIR spectrum was collated by averaging 8 scans with a 4 cm^{-1} resolution and 400–1400 cm^{-1} spectral range. The bioactivity test procedures using Tris buffer was repeated three times.

2.2. Resin composite removal assessment

An Aquacut™ air-abrasion unit (Velopex, Harlesden, UK) with a circular cross-section nozzle (internal diameter 600 µm) was used throughout the study. This unit utilises a mechanical vibration mechanism to admix the abrasive powder with the propellant air stream and thus enables the operator to control both air pressure and PFR independently using pre-set dials on the unit's fascia [10].

Rounded cavities with standard dimensions (diameter; 3 mm, depth; 0.7 mm) were prepared within a Macor™ sheet using a standardised drill bit. The reference Macor™ area around each cavity was protected by placing tape with a standard 7 mm round hole, onto the Macor™ surface over the cavity. Thus, each cavity was surrounded by a peripheral ring of flat Macor™ exposed to the air-abrasion stream and a taped, covered area which acted as a reference level from which to analyse the scanning outputs. All cavities were filled with Filtek™ Supreme Ultra (3 M ESPE, St. Paul, MN, USA) resin composite restorative material, and light cured (Optilux 501, Kerr, Orange, CA, USA) for 40 s according to the manufacturer's instructions. For each clinically adjustable air pressure value (40, 60 and 80 psi) three PFR dial settings (1, 3 and 5 representing the lowest, the middle and the highest values respectively on the unit) were tested, establishing nine experimental groups for each abrasive powder. The resin composite was removed according to the conditions of each group ($n = 5$). The powder reservoir was refilled to a pre-determined line consistently throughout the experiment. Complete resin composite removal was confirmed after rinsing and drying the cavity, by visual inspection using 2.5× magnification

loupes (OrascopticHiRes; Sybron Dental Specialties, Orange, CA, USA). The resin composite shade (B2B) was selected to present a different opacity to the white Macor™ background allowing the complete restoration to be visualised more easily and checked for complete "clinical" removal. The total time for complete clinical removal of the resin composite was recorded in seconds. The recorded time did not include the examination time of the cavity throughout the experiment.

Non-contact laser profilometry (Xyris™ 4000 TL, TaiCaan™ Technologies Ltd., Southampton, UK) was used to scan the 90 cavities including the surrounding reference areas prior to placing the resin composite and then again after completed air-abrasion procedure. The scan was performed with a 30 μm step-over distance and 0.25 μm vertical resolution. The resulting 3D cavity profiles were analysed after levelling the reference areas of the 3D image to a "zero" plane. The amount of intact, undesirable Macor™ volume loss was determined by comparing the volume of each cavity before and after resin composite removal. The less the Macor™ volume loss, the more optimal were considered the air-abrasion settings in as much as they led to an improved selectivity for resin composite removal.

2.3. Statistical analysis

Multilevel linear modelling was performed to analyse the data statistically using Stata 11.2 (Stata-CorpLP, College Station, TX, USA) at 5% level of significance.

3. Results

3.1. Characterisation of abrasive powders

The alumina particles had an angular shape, while BAG powder exhibited a more rounded, cubic shape surrounded by a submicron dust, according to SEM image (Fig. 1). The chemical compositions of the tested powder were determined as peaks within EDX spectrum (Fig. 1). The particle size distribution percentiles (10, 50 and 90%) of alumina were 23, 37 and 51 μm, and of BAG powder were 23, 56 and 82 μm respectively.

FTIR baseline spectrum of BAG (Fig. 2A) presented a prominent peak assigned to Si—O—Si stretching mode at 1030 cm^{-1} with a clear shoulder at 920 cm^{-1} related to the non-bridging oxygen Si—O—NBO [12]. A shift in the main peak from 1030 cm^{-1} to 1070 cm^{-1} was monitored in the reacted powder spectrum as a result of growing phosphate component (Fig. 2B) [13]. Double peaks at 570 and 600 cm^{-1} related to P—O bending vibrational mode within hydroxyapatite appeared within the reacted powder [5,14].

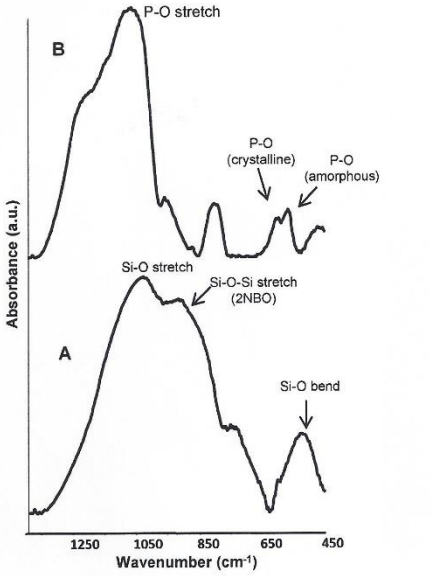

Fig. 2. FTIR spectra of BAG powder before (A) and after treated with Tris buffer solution (B). The baseline spectrum presented a prominent peak assigned to Si—O—Si, whilst the spectrum of reacted powder presents a double peak related to P—O within hydroxyapatite.

3.2. Resin composite removal

Representative 3D views and cross-sectional profiles of a cavity treated with BAG air-abrasion are shown in Fig. 3. The means and standard deviations of Macor™ volume loss are presented in Fig. 4. BAG powder removed significantly less Macor™ volume compared to alumina ($p < 0.001$). The interaction between air pressure and PFR setting on Macor™ volume loss was statistically significant ($p < 0.001$). In addition, this interaction affected the variance range between the tested powders in removal selectivity. PFR setting 1 and an air pressure of 60 psi removed 3.5 ± 1.2 mm^3 and 3.0 ± 1.1 mm^3 (mean ± SD) Macor™ volume within alumina and BAG groups respectively. Higher air pressure (80 psi) for the same PFR setting 1 abraded 5.3 ± 1.5 mm^3 Macor™ with alumina and 3.7 ± 0.7 mm^3 (mean ± SD) for BAG.

Further analysis of the interaction between PFR setting and air pressure revealed that the Macor™ volume removed within PFR setting groups differed significantly within the alumina groups at air pressure of 60 psi and within BAG at air pressure of 60 and 80 psi ($p < 0.001$), whilst no statistical differences were observed at an air pressure 40 psi for both abrasive powders. More Macor™ material was removed unnecessarily when the air pressure was raised to 80 psi at PFR setting 3 and 5 for both powders ($p < 0.001$). The parameters removing the largest and most undesirable Macor™ volume within the alumina groups were 80 psi air pressure and PFR setting 3: 7.1 ± 2 mm^3, whilst for BAG, these were 80 psi air pressure and PFR setting 5: 6.7 ± 1.2 mm^3 (mean ± SD). Alumina removed resin composite the fastest ($p = 0.001$), but data showed wide standard deviations (Table 1).

4. Discussion

BAG air-abrasion was significantly more selective than alumina air-abrasion in removing resin composite supporting its clinical use in minimally invasive, tooth preserving reparative dentistry. BAG particles have a rounded, cubic shape, while alumina particles have sharper, angular edges so increasing its physical abrasiveness. The submicron dust surrounding the BAG particles may inhibit the flow of the glass powder and therefore help to reduce its relative clinical abrasion effect. Another limiting factor is that BAG particles' have a reduced Vicker's hardness (VHN 458) compared to that of alumina powder (VHN 2300) [15]. A previous study stated that BAG powder was better than alumina powder in removing orthodontic resin adhesive selectively after fixed orthodontic bracket de-bonding procedures [9]. The current study added the effect of two additional variables, air pressure and PFR, on resin composite removal, anticipating the capability of this technology to preserve the maximum amount of intact enamel to meet the

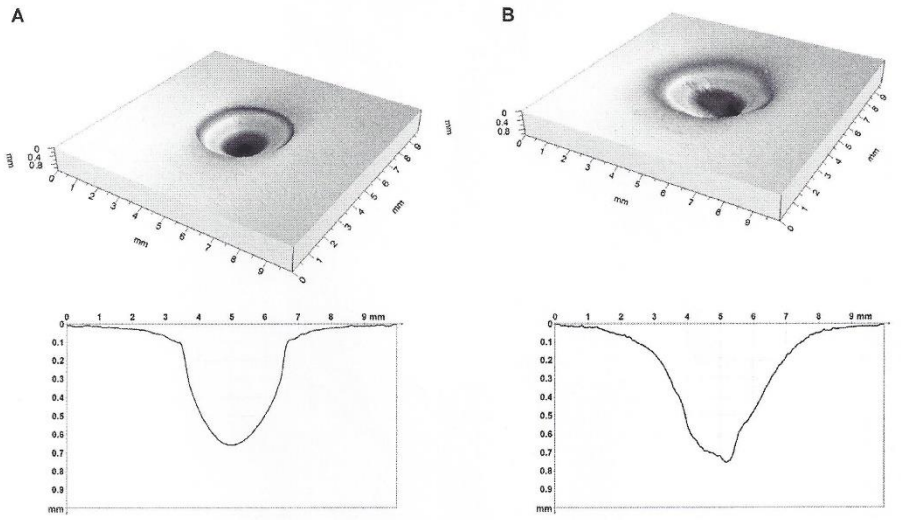

Fig. 3. 3D and cross-sectional profiles of selected, representative images of a cavity treated using BAG air-abrasion. (A) The cavity prior to restoring with resin composite which was then removed using BAG air-abrasion (B).

contemporary minimally invasive operative dentistry paradigm that faces restorative dentistry today.

The resin composite was placed in the prepared cavity without any adhesive to avoid resin composite remnants being retained on the surface. Previous studies revealed that even though the tooth surface appeared to be resin-free after removing resin remnants, many retained resin islands were observed using SEM [2,16]. Some of the air-abrasion operating parameters, including; nozzle-substrate distance, nozzle angle and nozzle-movement speed, were not fixed in order to mimic the variable clinical situation where these parameters would and could not be controlled effectively and are fully operator-dependent.

The clinical performance of dental resin composite is correlated positively to its mechanical properties, which in turn, are determined primarily by the filler content within the structure. The resin composite restorative material, used in the current study, contained 78.5 wt% fillers (the particle size; 0.6–10 μm) and exhibited high Knoop hardness (69.87 MPa) and flexural modulus (12 MPa) values. These are deemed clinically suitable to permit its use as a restorative dental material for both anterior and posterior teeth [17].

The findings of this study suggest that there was an increase in the Macor™ substrate removal when air pressure was increased. The rise in propellant pressure increases the velocity and the kinetic energy of the carried particles making them more destructive to the substrate. Adjusting the PFR setting to its highest value removed significantly more of the Macor™ substrate, indicating that using excessive amounts of either powder type is not advised. However, when reduced quantities of both powders were used with a low air pressure, increased Macor™ substrate removal was observed. This could be explained as the operator felt compelled to reduce the relative movement of the air-abrasion nozzle over a specific area of the

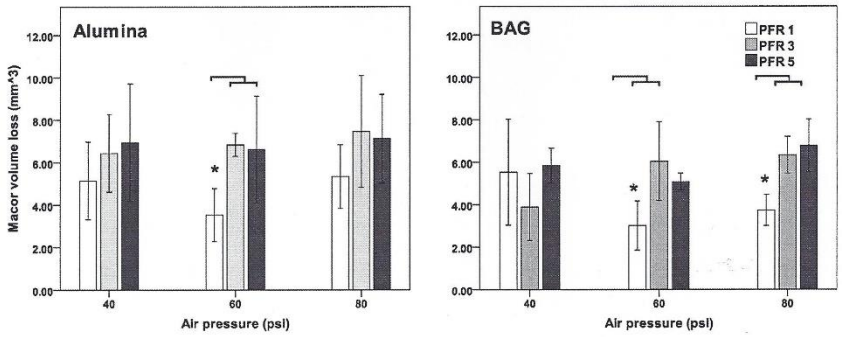

Fig. 4. Mean ± SD (mm^3) of Macor™ volume loss according to the conditions of each group. (*) indicates statistically significant differences ($p < 0.05$).

Table 1
Mean ± SD (s) of the time required for rein composite removal according to conditions of each group, and the statistically significant differences between the tested powders using equivalent parameters.

Group	Powder	PFR	Air pressure (psi)	Clinical removal time (mean ± SD (s))
1	Alumina	1	40	93 ± 21.1
2			60	73.4 ± 22.9
3			80	90.4 ± 25.1
4		3	40	129 ± 41.7
5			60	66.4 ± 8.1
6			80	49.4 ± 7.4
7		5	40	96.6 ± 17.9
8			60	66.8 ± 8.2
9			80	54.6 ± 7
10	BAG	1	40	172 ± 55.3
11			60	95.6 ± 21.7
12			80	94.4 ± 43.1
13		3	40	160.8 ± 31.1
14			60	111.8 ± 23.7
15			80	74.2 ± 5
16		5	40	103.8 ± 28.6
17			60	74.6 ± 12.4
18			80	64.6 ± 30.5

Significance: (1) vs. (10): $p = 0.001$; (5) vs. (14): $p = 0.005$; (6) vs. (15): $p = 0.003$.

restoration surface to compensate for the reduction of both powder flow rate and particle speed. This would have the ultimate clinical effect of increasing the risk of operator-induced "over-preparation" at particular sites as the nozzle may be held stationary over specific areas of the cavity for longer periods. Therefore, an extreme reduction in the volume of the abrasive stream to avoid cavity over-preparation, is not recommended as the apparent benefit is nullified by the clinical variation of the operator.

BAG powder has a potential advantage over alumina powder in minimally invasive reparative dentistry as it interacts with an aqueous solution to form hydroxycarbonate apatite (HCA) layer [18], validated in the present study using FTIR spectrometry. Therefore, BAG particles retained on the tooth surface treated using BAG air-abrasion technology has the potential to aid the remineralisation.

Comparing the Macor™ volume removed and the required removal time between both abrasive powders suggested that using higher air pressure or excessive amounts of both powders produced similar air-abrasion cutting performances in contrast to those produced using reduced settings. This implies that within the parameters of low air pressure and PFR settings, the cutting efficiency of clinical air-abrasion depends primarily on the nature of the abrasive powder rather than on the operating physics of the unit itself. Cavity shape/size standardisation throughout the experimental groups allowed time evaluation due to the similarity of resin composite restoration volume within all samples. BAG powder required statistically significantly more time than alumina powder to remove the restoration fully. However, this time difference was deemed acceptable clinically, particularly if more healthy intact tissues could be preserved as an outcome.

5. Conclusions

The three null hypotheses were rejected. Using a moderate air pressure with reduced PFR, enhanced the selective removal of resin composite. The utilisation of Macor™ as an enamel analogue in the current study reduced the variability reported in biological enamel samples, but at the same time presented a limitation in due to the variety between the two substrates at microstructure level. Within the limitation of this in vitro study, it can be concluded that BAG air-abrasion removed resin composite, included within an enamel analogue, Macor™, more selectively than alumina air-abrasion, and therefore maybe recommended clinically for the purpose of repairing defective resin composite restoration margins and removing composite remnants on enamel after de-bonding orthodontic appliances under the auspices of minimally invasive operative/reparative tooth preserving dentistry.

References

[1] G.A. Bonetti, M. Zanarini, S. Incerti Parenti, M. Lattuca, S. Marchionni, M.R. Gatto, Evaluation of enamel surfaces after bracket debonding: an in-vivo study with scanning electron microscopy, American Journal of Orthodontics and Dentofacial Orthopedics 140 (2011) 696–702.
[2] H.B. Pont, M. Ozcan, B. Bagis, Y. Ren, Loss of surface enamel after bracket debonding: an in-vivo and ex-vivo evaluation, American Journal of Orthodontics and Dentofacial Orthopedics 138 (2010) 387–389.
[3] G. Myers, The airbrasive technique: a report, British Dental Journal 7 (1954) 291–295.
[4] A. Banerjee, T.F. Watson, Air abrasion: its uses and abuses, Dental Update 29 (2002) 340–346.
[5] L.L. Hench, in: An Introduction to Bioceramics, Imperial College Press, London, 2013.
[6] A. Banerjee, I.D. Thompson, T.F. Watson, Minimally invasive caries removal using bio-active glass air-abrasion, Journal of Dentistry 39 (2011) 2–7.
[7] E.S. Gjorgievska, J.W. Nicholson, I.J. Slipper, M.M. Stevanovic, Remineralization of demineralized enamel by toothpastes: a scanning electron microscopy, energy dispersive X-ray analysis, and three-dimensional stereo-micrographic study, Microscopy and Microanalysis 19 (2013) 587–595.
[8] G. Paolinelis, A. Banerjee, T.F. Watson, An in vitro investigation of the effect and retention of bioactive glass air-abrasive on sound and carious dentine, Journal of Dentistry 36 (2008) 214–218.
[9] A. Banerjee, G. Paolinelis, M. Socker, F. McDonald, T.F. Watson, An in vitro investigation of the effectiveness of bioactive glass air-abrasion in the 'selective' removal of orthodontic resin adhesive, European Journal of Oral Sciences 116 (2008) 488–492.
[10] H. Milly, R. Austin, I. Thompson, A. Banerjee, In-vitro effect of air-abrasion operating parameters on dynamic cutting characteristics of alumina and bio-active glass powders, Operative Dentistry 39 (2014) 81–89.
[11] C. Ercoli, M. Rotella, P.D. Funkenbusch, S. Russell, C. Feng, In vitro comparison of the cutting efficiency and temperature production of 10 different rotary cutting instruments. Part I: Turbine, Journal of Prosthetic Dentistry 101 (2009) 248–261.
[12] M. Cerruti, D. Greenspan, K. Powers, Effect of pH and ionic strength on the reactivity of Bioglass 4555, Biomaterials 26 (2005) 1665–1674.
[13] O. Peitl Filho, G.P. LaTorre, L.L. Hench, Effect of crystallization on apatite-layer formation of bioactive glass 4555, Journal of Biomedical Materials Research 30 (1996) 509–514.
[14] J.P. Zhong, D.C. Greenspan, J.W. Feng, A microstructural examination of apatite induced by Bioglass in vitro, Journal of Materials Science Materials in Medicine 13 (2002) 321–326.
[15] I.D. Thompson, L.L. Hench, Mechanical properties of bioactive glasses, glass-ceramics and composites, Proceedings of the Institution of Mechanical Engineers, Part H 212 (1998) 127–136.
[16] Y.H. Hong, K.K. Lew, Quantitative and qualitative assessment of enamel surface following five composite removal methods after bracket debonding, European Journal of Orthodontics 17 (1995) 121–128.
[17] S. Thomaidis, A. Kakaboura, W.D. Mueller, S. Zinelis, Mechanical properties of contemporary composite resins and their interrelations, Dental Materials 29 (2013) e 132–e 141.
[18] E. Kontonasaki, T. Zorba, L. Papadopoulou, E. Pavlidou, X. Chatzistavrou, K. Paraskevopoulos, et al., Hydroxy carbonate apatite formation on particulate bioglass in vitro as a function of time, Crystal Research and Technology 37 (2002) 1165–1171.

JOURNAL OF DENTISTRY 42 (2014) 158–166

Available online at www.sciencedirect.com

ScienceDirect

journal homepage: www.intl.elsevierhealth.com/journals/jden

Enamel white spot lesions can remineralise using bio-active glass and polyacrylic acid-modified bio-active glass powders

Hussam Milly [a], *Frederic Festy* [a], *Timothy F. Watson* [a,b], *Ian Thompson* [a], *Avijit Banerjee* [a,b,*]

[a] *Biomaterials, Biomimetics & Biophotonics Research Group, King's College London Dental Institute at Guy's Hospital, King's Health Partners, London, UK*

[b] *Unit of Conservative Dentistry, King's College London Dental Institute at Guy's Hospital, King's Health Partners, London, UK*

ARTICLE INFO

Article history:
Received 16 September 2013
Received in revised form
11 November 2013
Accepted 18 November 2013

Keywords:
Bio-active glass (BAG)
Polyacrylic acid (PAA)
Enamel white spot lesion (WSL)
Remineralisation
Microhardness
Micro-Raman spectroscopy

ABSTRACT

Objective: To evaluate the potential of bio-active glass (BAG) powder and BAG containing polyacrylic acid (PAA-BAG) to remineralise enamel white spot lesions (WSL).

Methods: 32 human enamel samples with artificial WSLs were assigned to 4 experimental groups ($n = 8$); (a) BAG slurry, (b) PAA-BAG slurry, (c) "standardised" remineralisation solution (positive control) and (d) de-ionised water (negative control). Mechanical properties of enamel were assessed using surface and cross-section Knoop microhardness. Micro-Raman spectroscopy in StreamLine™ scan mode was used to scan lesion cross-sections. The intensity of the Raman phosphate peak at 959 cm^{-1} was fitted and measured producing depth profiles analysed using a double-step fitting function. A further 20 samples ($n = 5$) were used to obtain 3D images of surfaces using non-contact white light profilometry permitting measurement of lesion step height in relation to the sound enamel reference level, and to scan the lesion surface using scanning electron microscopy (SEM). Data were analysed statistically using one-way ANOVA with Tukey's HSD post-hoc tests.

Results: BAG, PAA-BAG and the remineralisation solution exhibited statistically significantly higher surface and cross-section Knoop microhardness compared to the negative control. Micro-Raman spectroscopy detected significantly higher phosphate content within the treated groups compared to the negative control group. Lesions' depth was not significantly reduced. SEM images revealed mineral depositions, with different sizes and shapes, within BAG, PAA-BAG and the positive control groups.

Conclusion: BAG and PAA-BAG surface treatments enhance enamel WSL remineralisation, assessed by the resultant improved mechanical properties, higher phosphate content and morphological changes within the artificial lesions.

* *Corresponding author at*: Unit of Conservative Dentistry, King's College London Dental Institute, Floor 26, Tower Wing, Guy's Dental Hospital, London. SE1 9RT, UK. Tel.: +44 207 188 1577 / 7486; fax: +44 207 188 1577 / 7486.
E-mail address: avijit.banerjee@kcl.ac.uk (A. Banerjee).

0300-5712/$ – see front matter © 2013 Elsevier Ltd. All rights reserved.
http://dx.doi.org/10.1016/j.jdent.2013.11.012

1. Introduction

Minimally invasive dentistry encompasses the philosophy of preservation of the maximum quantity of repairable dental tissues and utilising preventive, remineralisation approaches in incipient carious lesion management.[1,2] The enamel white spot lesion (WSL) is the earliest clinically evident manifestation of the caries process, exhibiting subsurface porosity caused by an imbalance between the biological dynamic processes of de- and remineralisation.[3,4] In the minimally invasive reparative dentistry paradigm, incipient enamel carious lesions should not be managed with surgical intervention, but with non-invasive remineralisation strategies wherever possible.[2]

Bio-active glass (BAG) can act as a source of a large amount of CaO and P_2O_5 in a Na_2O–SiO_2 matrix with a rapid dissolution rate and high ionic concentration.[5] The bioactivity index determines the rate at which a bio-active material produces a chemical bond with a natural tissue.[6] BAG 45S5 exhibits a high bioactivity index ($I_B = 12.5$) compared to other bio-active materials such as hydroxyapatite ($I_B = 3$),[6] and therefore it has the potentila to remineralise enamel white spot lesions with an increased rate of HA formation. BAG has been introduced clinically as an air-abrasion abrasive powder to be used under the auspices of minimally invasive dentistry and has showed promising results for the controlled, selective removal of an enamel analogue substrate, demineralised enamel and resin composite restoration/cements, particularly using specific operating parameters.[7–10] Polyacrylic acid (PAA) has been added to bio-active materials in order to mimic the functional role of non-collagenous proteins in binding the calcium and phosphate ions to form nano-precursors, including amorphous calcium phosphate, small enough to penetrate the carious lesion more effectively.[11,12] Using BAG powder containing 40 wt% PAA to treat the dentine using air-abrasion technology reduced the micropermeability between the dentine and the adhesive layer in vitro, and might be a suitable strategy to enhance bond durability.[13] To the authors' knowledge, there is no information published to ascertain the potential role of using PAA-BAG on enamel white spot lesion remineralisation.

Micro-Raman spectroscopy is used as a quantitative chemical assessment methodology for biological samples in conjunction with the fact that the Raman peak intensity is proportional to the number of molecules within the volume of scanned area.[14] The Raman phosphate peak at 959 cm^{-1} characterises tetrahedral PO_4 group (P–O bond) within HA.[15] Monitoring the intensity of this peak has been used to assess the degree of demineralisation within enamel caries.[16,17] The present study utilised this measurement to assess the potential increase in phosphate content within the lesion as a result of remineralisation treatments. Depth profiles of phosphate peak intensity along the cross-sections of the samples were created and fitted using a double-step function. To date, the use of Raman phosphate peak intensity measurement and high-speed line scanning to detect a potential increase in the phosphate content within the incipient lesion as a result of a remineralisation treatment has not been reported in the dental literature.

Hardness measurements provide information about the mineral density and mechanical properties of hard tissue surfaces,[18] and are a reliable, objective method to study demineralised enamel and dentine lesions.[19] The aim of the present study was to evaluate the effect of BAG and PAA-BAG powders on artificial enamel WSL remineralisation through morphological, mechanical and chemical assessments using a "standard" remineralisation solution as a positive control and de-ionised water as a negative control. The morphological changes of the lesion surface were assessed using optical white light confocal profilometry and scanning electron microscopy (SEM). The null hypothesis investigated was that treating enamel WSL with BAG or PAA-BAG slurries has no beneficial effect on enamel WSL remineralisation when compared to the controls.

2. Materials and methods

2.1. *Samples preparation and remineralisation treatment*

Fifty-two enamel slabs (4 mm × 4 mm × 2 mm) were cut from the buccal surfaces of caries-free human extracted lower molars, collected using an ethics protocol reviewed and approved by the East Central London Research Ethics Committee (Reference 10/H0721/55). The teeth were refrigerated during storage, used within a month from the extraction and sectioned using a diamond wafering blade (XL 12205, Benetec Ltd., London, UK) obtaining one specimen from each tooth. The slabs' surface integrity was inspected using microscopy at 40× magnification and the samples were then included face down in acrylic resin using a hard-anodised aluminium and brass sample former (Syndicad Ingenieurbüro, München, Germany). The superficial enamel layer was removed using a water-cooled rotating polishing machine (Meta-Serv 3000 Grinder-Polisher, Buehler, Lake Bluff, IL, USA) using a sequential polishing protocol; 600-grit silica carbide disc for 10 s, 1200-grit for 20 s, 2400-grit for 30 and 4000-grit for 45 s, followed by 3 min of ultrasonication. This created more consistent, reproducible artificial enamel lesions,[20] and improved the reliability of the profilometry assessment.[21]

Melted dental wax was applied to protect part of the enamel leaving an exposed window of 3 mm × 1 mm in the central area. WSLs were created using a previously reported bi-layer demineralisation protocol of 8% methylcellulose gel buffered with a lactic acid layer (0.1 mol/L, pH 4.6) for 14 days at 37 °C.[22,23]

The ultra-morphology of enamel surface was checked after polishing procedures and after producing artificial WSLs using a confocal tandem scanning microscope (TSM) (Noran Instruments, Middleton, WI, USA), with a ×100/1.4 NA oil-immersion objective in reflection scanning mode, to ascertain the presence of cross-sectional enamel prisms in the intact and demineralised enamel surfaces. Samples were assigned randomly into four experimental groups, with the composition of the applied materials detailed in Table 1. Microhardness measurements of intact sound enamel in each sample were recorded to calculate any statistical differences between specimens in each group prior to any remineralisation treatment. BAG and PAA-BAG were prepared as slurries (L/P

Table 1 – Represents experimental groups and composition of applied materials.

Group	Treatment	Composition
a	BAG slurry prepared with de-ionised water (L/P ratio of 1 g/m)	Bio active glass 45S5 powder[a]: particle size distribution: (2–6–12 μm). SiO_2: 45%, CaO: 24.4%, Na_2O: 24.6% and P_2O_5: 6%
b	PAA-BAG slurry prepared with de-ionised water (L/P ratio of 1 g/m)	60 wt% bio active glass 45S5 powder: particle size distribution: (2–6–12 μm). SiO_2: 45%, CaO: 24.4%, Na_2O: 24.6% and P_2O_5: 6% 40 wt% polyacrylic acid (PAA) powder[b]: particle size distribution: (1–10–19 μm) MW: 1800.
c	Positive control	Remineralisation solution[23]: 20 mMHepes, 130 mMKCl, 1.5 mM $CaCl_2$ and 0.9 mM KH_2PO_4 (adjusted to pH 7.0 with KOH)
d	Negative control	De-ionised water

[a] Sylc (OSspray, London, UK).
[b] Sigma Chemicals (Gillingham, Dorset, UK).

ratio of 1 g/m), and applied without any mechanical agitation. The surface remineralisation treatments were conducted for 7 days at 37 °C and refreshed daily. Samples within each of the four test groups ($n = 13$) were rinsed thoroughly after treatment with de-ionised water and assigned for profilometric and scanning electron microscopic (SEM) assessments ($n = 5$), and for microhardness and Raman analyses ($n = 8$).

2.2. *SEM scanning*

A scanning electron microscope (FEI Co., Ltd., Cambridge, UK) was utilised to examine the ultra-structure of the lesion surface (accelerating voltage of 10 kV, working distance of 10 mm). The samples were gold sputter-coated before SEM analysis (Emitech K550, UK). Further two samples from PAA-BAG and negative control groups were sectioned, gold sputter-coated and scanned using the same parameters. The scan area included both the lesion cross-section and part of its surface.

2.2.1. *Surface and cross-sectional microhardness measurements*

A Struers Duramin microhardness tester (Struers Ltd., Denmark) with a Knoop diamond indenter was used. A pilot study was conducted to figure out the proper parameters to assess the microhardness of the lesion; 50 g load for 10 s. The indentations were imaged with a 40/0.65 NA objective and the Knoop values were calculated using the manufacturer's software supplied. Five measurements, 200 μm apart, were recorded and then averaged to measure the lesion surface microhardness of each sample. The samples were then hemi-sectioned using a diamond wafering blade. Each cross-sectioned surface was hand-polished up to 1200 grit to produce a flat surface. The integrity of the lesion and the flatness of the cross-sections were examined using a 40/0.65 NA objective prior to any further experimental analyses. For cross-sectional microhardness testing, three measurements, 100 μm apart and 30 μm away from the outer lesion surface were recorded and averaged within each sample.

2.3. *Micro-Raman spectroscopy*

A Renishaw inVia Raman microscope (Renishaw Plc, Wotton-under-Edge, UK) running in Streamline™ scanning mode was used to scan the cross-sectioned surfaces using a 785-nm diode laser (100% laser power) focused using a 20/0.45 air objective. The signal was acquired using a 600 lines/mm diffraction grating centred at 800 cm^{-1} and a CCD exposure time of 2 s. The microscope was calibrated using an internal silicon sample with a characteristic band at 520 cm^{-1}. For each sample, a Raman map of the air/lesion/enamel interface was recorded at the middle part of the lesion. The Raman map was started at 125 μm on the outer side of the lesion (air) and extended to approximately 400 μm within the sound enamel, covering an area of 525 × 350 μm^2 and containing 1740 spectra acquired with a 2.7 μm resolution across the air/lesion/enamel interface. Raman maps were exported into in-house curve-fitting software to fit the spectra and to generate grey-scale images (Fig. 1A) and depth profiles of phosphate peak intensity at 959 cm^{-1} ($PO_4^{-3}\nu 1$). The demineralised enamel produced a small amount of autofluorescence, as do most biological samples (Fig. 1B). To take this slowly varying background into consideration, the PO peak was fitted with a linear combination of a Gaussian function and a first order polynomial, as it is routinely done in Raman analysis. The fitting function was therefore the following:

$$F(X) = AX + B + C\ \exp\left\{\frac{-(X-D)^2}{2E^2}\right\}$$

The intensity of the PO peak was given by the fitting parameter C from the above equation. The Raman analysis in the current study was based on peak ratio analysis, namely the ratio between the mineral peak within the lesion and the mineral peak within healthy enamel. This ratio was analysed by fitting the depth profiles of phosphate peak intensity objectively using a double-step function, by the means of written software (Fig. 1C), to obtain: the phosphate peak intensity percentage within the lesion to that of the deeper sound enamel (the distance between lesion and sound steps in the vertical direction), and the lesion depth (the distance between lesion and sound enamel steps in the horizontal direction).

2.4. *Profilometric analysis*

A standard scan area of 3 mm × 2 mm was chosen over the WSL to include the lesion in the centre (1 mm) surrounded by flat sound enamel on each side (1 mm), acting as a reference area. The sample surface was scanned before and after treatment using optical white light confocal profilometry

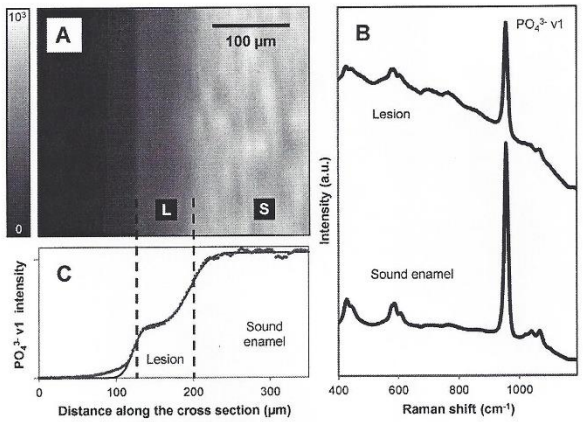

Fig. 1 – (A) Representative grey-scale image of Raman phosphate peak intensity at 959 cm^{-1} including the demineralised (L) and sound enamel (S) areas of the scanned map. (B) Raman spectra of demineralised and deep sound enamel areas within the same sample. (C) Depth profile of phosphate peak intensity (broken line) fitted using double-step function (solid line).

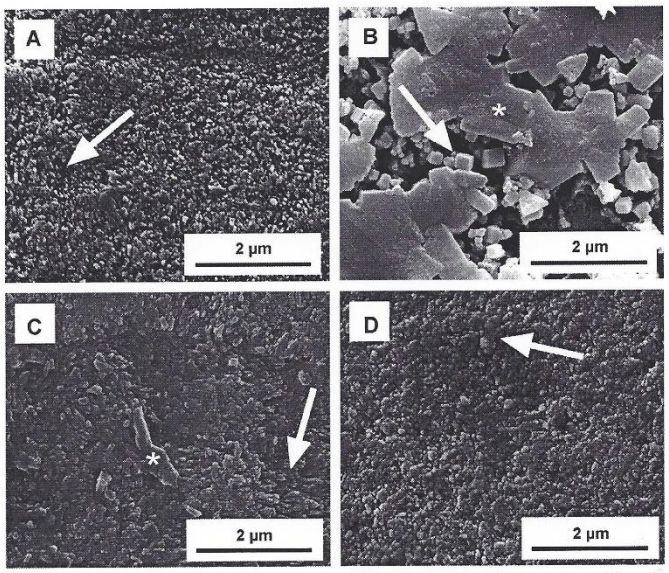

Fig. 2 – Representative SEM images of lesion surface according to the treatment (at 50,000× magnification). (A) Lesion surface within the negative control group exhibits porosity (arrow) with no mineral depositions. (B) Mineral precipitations with large plate-shape (star) and small cubic-shape (arrow) structures in BAG group. (C) Small plate- (star) and flake-like (arrow) structure covers and blocked the surface porosity in PAA-BAG group. (D) Small rounded-shaped particles (arrow) within the positive control group.

(Xyris™ 4000 WL, TaiCaan™, Southampton, UK) with a 10 μm step-over distance and a 10 nm vertical resolution. The resulting 3D images were analysed by levelling the sound enamel areas to a best-fit (zero plane). The step height measurement of the lesion surface in relation to the sound enamel level, which was protected by a tape throughout the treatment, was obtained by averaging five measurements within each sample.

2.5. *Statistical analysis*

Statistical analysis was conducted using SPSS statistical package (version 20; SPSS Inc., IBM, Chicago, IL, USA). Data were tested for normality using Q–Q plots and Shapiro–Wilk tests, and using one-way analysis of variance (ANOVA) and Tukey's HSD post hoc tests to calculate the significant factors at $p = 0.05$.

3. Results

3.1. *SEM analysis*

Representative SEM images of samples from each of the four experimental groups are shown in Fig. 2. Variance was detected between the negative control and the remaining experimental groups. The lesion surface in the negative control exhibited porosity resulting from the demineralisation process, with no evidence of mineral deposition (Fig. 2A). SEM images of BAG exhibited mineral depositions with large two-dimensional, plate-like structures and small three-dimensional, cubic structures (Fig. 2B). The plate-like structures were smaller within the PAA-BAG compared to BAG group with small flake-like structures blocking completely the porous lesion surface (Fig. 2C). Small rounded particles covering the lesion surface were observed in the remineralisation solution group (Fig. 2D). The cross-sectional views of PAA-BAG (Fig. 3B) showed a layer of mineral covering the lesion surface, whilst no evidence of remineralisation was detected within the negative control group (Fig. 3A). The high magnification images of the cross-sections showed mineral structures firmly attached and embedded to the lesion surface within PAA-BAG group (Fig. 3B).

3.1.1. *Surface and cross-sectional microhardness measurements*

Knoop microhardness measurements of sound enamel showed consistent values within the experimental groups prior to commencing the remineralisation treatments. The sound enamel Knoop microhardness was 329.5 ± 23.1 KHN (mean ± SE) within the BAG group, 307.5 ± 20.9 KHN in the PAA-BAG group, 299.9 ± 22.0 KHN in remineralisation solution group and 326.1 ± 21.4 KHN for the negative control group.

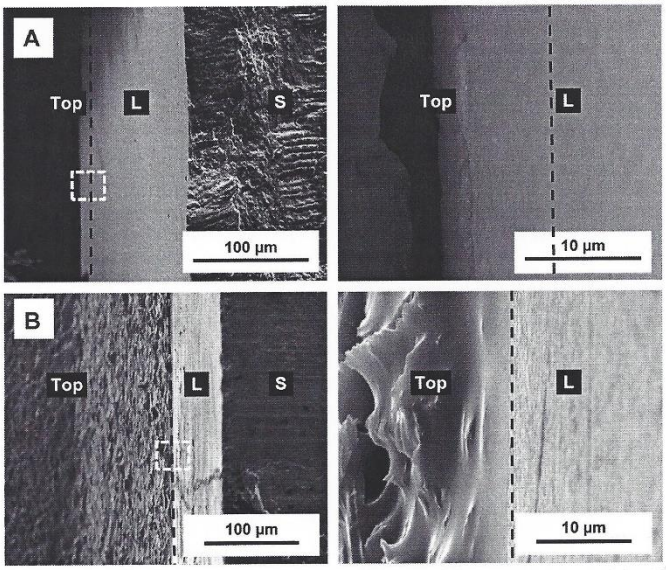

Fig. 3 – SEM images of cross-sections within the negative control and PAA-BAG groups at 800× (left) and 10,000× (right) magnifications. The broken line determines the border between the cross-sectional view and the lesion surface (top). The lesion surface within PAA-BAG (B) covered with a layer of minerals in contrast to that of the negative control which showed no mineral precipitations (A). Higher magnification of the outer edge of lesion showed the mineral structures firmly attached to the lesion surface within PAA-BAG.

Fig. 5. The phosphate peak intensity percentage within the lesion compared to that of the deeper sound enamel in the negative control group was 38.18 ± 1.7% (mean ± SE), statistically significantly less than that of BAG group (48.93 ± 2.7%) ($p = 0.04$), PAA-BAG (49.1 ± 2.6%) ($p = 0.04$) and remineralisation solution (50.19 ± 3.5%) ($p = 0.02$). However, the treatment did not reduce the lesion depth statistically compared to that of the negative control group. The lesion depth was (81.4 ± 3.2 μm) (mean ± SE) within the negative control group, (66.7 ± 3 μm) in the BAG group, (74.1 ± 7.1 μm) in PAA-BAG group and (67.6 ± 4.8 μm) for remineralisation group. Representative grey-scale images and depth profiles of PO_4^{3-} υ_1 peak intensity are presented in Fig. 5. Overall, there was a considerable drop in the depth profile in all groups within the lesion area (125–200 μm) compared to the deep sound enamel area (≥200 μm), which, in turn, presented similar intensity profiles within all the samples tested. The depth profiles within the negative control group exhibited larger distances between the lesion and deeper enamel steps, in the vertical direction, compared to the other groups implying that less phosphate content was present within the lesion. The depth profiles of BAG and remineralisation solution showed a sharp peak within the lesion step, whilst within PAA-BAG depth profiles the phosphate peak intensity increased along the whole lesion depth.

3.3. *Profilometric analysis*

Using BAG and PAA-BAG as a slurry did not damage the surface layer of the lesion as the profilometry step height difference measurement of lesion surface before and after treatment showed no statistically significant difference within all experimental groups; (0.64 ± 0.29 μm) (mean ± SE) within the BAG group, (0.78 ± 0.24 μm) for the PAA-BAG group, (0.56 ± 0.24 μm) or within remineralisation solution group and (0.46 ± 0.20 μm) in the control group.

4. Discussion

The key approach in enamel WSL remineralisation is to utilise dissolvable materials containing ions required to deposit minerals similar to those of enamel and at the same time which can diffuse through the lesion.[24] Biomimetic remineralisation of carious lesions has been reported using bio-active materials in the presence of protein analogues such as PAA to promote remineralisation through the lesion depth.[25] BAG may enhance the remineralisation of demineralised dentine and inhibit the demineralisation of enamel.[26–29] In the current study, PAA was not included in the BAG processing procedure, and therefore it was not released from BAG particles, but interacted with reacted BAG agglomerates. The concentration of PAA was selected to reduce the abrasiveness of BAG particles for further utilisation with air-abrasion technology in future studies, as well as to benefit from the potential role of PAA in regulating mineral growth.[11,25]

Even though the lesion surface was thoroughly rinsed prior SEM analysis, mineral deposits were readily detected within BAG and PAA-BAG groups implying that the observed structures firmly attached to lesion surface, and this attachment was detected in the cross-sectional SEM images. The plate- and cubic-like structures observed in the SEM images of BAG and PAA-BAG groups are comparable to the apatite crystals shapes of reacted BAG described in the literature.[30,31] Mineral precipitations formed using PAA-BAG slurry were significantly smaller than those of BAG group and completely blocked the porosity of the lesion surface concurring with a previous study which revealed smaller structures could be monitored when PAA was used with Portland cement.[11] These smaller mineral structures have a potential to penetrate the lesion surface and enhance the remineralisation along the whole lesion depth. The formation of the small structures within PAA-BAG group may be explained depending on non-classical crystallisation pathway concepts where Ca and P ions are sequestered by biomimetic analogues such as PAA to form amorphous calcium phosphate nano-precursors which in turn transform into small crystalline apatite minerals.[32]

Lesion surface microhardness was considerably higher than the equivalent cross-sectional measurement implying that much of the new mineral was formed and deposited in the superficial part of the lesion rather than the lesion body.[33] BAG, PAA-BAG and the positive control groups exhibited higher surface and cross-sectional Knoop microhardness compared to the negative control group. Previous studies reported an increase in the mechanical properties of acid-etched enamel and demineralised dentine treated by BAG paste.[26,34] This mechanical improvement could be caused as a result of "new" mineral deposition within the lesion,[18] resulting from BAG 45S5 bioactivity process that forms HA layers at the interface level.

The StreamLine™ Raman scanning is a high-speed line scanning system that allows faster and better excitation intensity distribution across the sample surface as it utilises the Raman microscope optics to illuminate a moving line across the sample and to read the data continuously.[35] The phosphate Raman peaks were observed within Raman spectra at the same positions detected in the literature.[14,36] Peak intensity evaluation has been reported as a suitable parameter to detect a difference between sound and demineralised enamel regions.[37] In the present study, the phosphate peak intensity within the demineralised enamel was compared to that of the deeper sound enamel within the same sample, acting as a reference area. The lesion presented 40% phosphate peak intensity compared to the deeper sound enamel in the control group. This drop in the depth profile extended to approximately 80 μm depth. These depth profile features, of phosphate peak intensity within artificial enamel white spot lesions, are consistent with those described in a previous study.[17]

BAG and PAA-BAG were applied as slurry, without mechanical agitation, to avoid any damage to the lesion structure, and this was confirmed by profilometric analysis. The profilometric results imply that the improvement in the mechanical and chemical measurements of the treated lesions occurred within the structure of the lesion and not as a result of damaging histologically, the lesion morphology and exposing the deeper intact tissue. Using BAG, PAA-BAG and remineralisation solution in the present study did not reduce the lesion depth. This result may be explained as the

calcium and phosphate ions' diffusion/precipitation may be restricted to the superficial area of the lesion inhibiting whole lesion remineralisation. This feature has been reported in the literature when different remineralisation agents were applied to treat enamel carious lesions.[38–40] To overcome this limitation, altering/modifying the lesion surface to improve mineral diffusion may still be required or even desirable.[41–43]

Treating BAG particles with an aqueous solution such as saliva causes a leaching and exchanging of BAG ions with those in the solution and that in turn increases the interfacial pH followed by breaking Si–O–Si–O–Si–O bridges and forming a $Si(OH)_4$ layer. Calcium and phosphate ions are released from BAG, at this stage, to form an amorphous CaP layer, which is crystallised to a mixed hydroxyl-carbonate apatite layer.[44] Rama phosphate peak intensity percentages were significantly higher within BAG, PAA-BAG groups compared to that of the negative control group implying that more phosphate ions were presented as a result of remineralisation treatment. The bioactive process of BAG and the precipitation of minerals at the lesion surface, observed within SEM images, may explain the higher Raman phosphate peak intensity monitored in the present study.

The beneficial effect of utilising bio-active glass and polyacrylic acid-modified bio-active glass powders in enamel white spot remineralisation paves the way for further investigation into the clinical application of such materials in the remineralisation of enamel in vivo under the auspices of minimally invasive reparative dentistry which advocates the preservation of repairable enamel structure and the use of remineralisation strategies to "heal" early lesions.[1]

5. Conclusions

The original null hypothesis was rejected as enamel WSLs treated with BAG and PAA-BAG exhibited improved mechanical proprieties and higher phosphate content compared to the negative control and presented mineral depositions formed at the lesion surface. Smaller particle precipitations were detected within PAA-BAG compared to the BAG, and therefore this modification has a potential to promote entire mineral gain of treated lesions.

REFERENCES

1. Banerjee A. Minimal intervention dentistry: Part 7. Minimally invasive operative caries management: rationale and techniques. *British Dental Journal* 2013;**214**:107–11.
2. Mount GJ. A new paradigm for operative dentistry. *Australian Dental Journal* 2007;**52**:264–70.
3. Featherstone JD. The science and practice of caries prevention. *Journal of the American Dental Association* 2000;**131**:887–99.
4. Kidd EA, Fejerskov O. What constitutes dental caries? Histopathology of carious enamel and dentin related to the action of cariogenic biofilms. *Journal of Dental Research* 2004;**83**:C35–8.
5. Hench LL. The story of bioglass. *Journal of Materials Science Materials in Medicine* 2006;**17**:967–78.
6. Thompson ID, Hench LL. Mechanical properties of bioactive glasses, glass-ceramics and composites. *Proceedings of the Institution of Mechanical Engineers* 1998;**212**:127–36.
7. Banerjee A, Thompson ID, Watson TF. Minimally invasive caries removal using bio-active glass air-abrasion. *Journal of Dentistry* 2011;**39**:2–7.
8. Paolinelis G, Banerjee A, Watson TF. An in vitro investigation of the effect and retention of bioactive glass air-abrasive on sound and carious dentine. *Journal of Dentistry* 2008;**36**:214–8.
9. Banerjee A, Paolinelis G, Socker M, Mcdonald F, Watson TF. An in vitro investigation of the effectiveness of bioactive glass air-abrasion in the 'selective' removal of orthodontic resin adhesive. *European Journal of Oral Sciences* 2008;**116**:488–92.
10. **Milly H, Austin R, Thompson I, Banerjee A. In-vitro effect of air-abrasion operating parameters on dynamic cutting characteristics of alumina and bio-active glass powders. *Operative Dentistry* 2013. in-press.**
11. Tay FR, Pashley DH. Guided tissue remineralisation of partially demineralised human dentine. *Biomaterials* 2008;**29**:1127–37.
12. Kamitakahara M, Kawashita M, Kokubo T, Nakamura T. Effect of polyacrylic acid on the apatite formation of a bioactive ceramic in a simulated body fluid: fundamental examination of the possibility of obtaining bioactive glass-ionomer cements for orthopaedic use. *Biomaterials* 2001;**22**:3191–6.
13. Sauro S, Watson TF, Thompson I, Banerjee A. One-bottle self-etching adhesives applied to dentine air-abraded using bioactive glasses containing polyacrylic acid: an in vitro microtensile bond strength and confocal microscopy study. *Journal of Dentistry* 2012;**40**:896–905.
14. Tsuda H, Arends J. Raman spectroscopy in dental research: a short review of recent studies. *Advances in Dental Research* 1997;**11**:539–47.
15. Koutsopoulos S. Synthesis and characterization of hydroxyapatite crystals: a review study on the analytical methods. *Journal of Biomedical Materials Research* 2002;**62**:600–12.
16. Kinoshita H, Miyoshi N, Fukunaga Y, Ogawa T, Ogasawara T, Sano K. Functional mapping of carious enamel in human teeth with Raman microspectroscopy. *Journal of Raman Spectroscopy* 2008;**39**:655–60.
17. Mohanty B, Dadlani D, Mahoney D, Mann AB. Characterizing and identifying incipient carious lesions in dental enamel using micro-Raman spectroscopy. *Caries Research* 2012;**47**:27–33.
18. Buchalla W, Imfeld T, Attin T, Swain MV, Schmidlin PR. Relationship between nanohardness and mineral content of artificial carious enamel lesions. *Caries Research* 2008;**42**:157–63.
19. Banerjee A, Cook R, Kellow S, Shah K, Festy F, Sherriff M, *et al.* A confocal micro-endoscopic investigation of the relationship between the microhardness of carious dentine and its autofluorescence. *European Journal of Oral Sciences* 2010;**118**:75–9.
20. ten Cate JM, Duijsters PP. Alternating demineralization and remineralization of artificial enamel lesions. *Caries Research* 1982;**16**:201–10.
21. Austin RS, Rodriguez JM, Dunne S, Moazzez R, Bartlett DW. The effect of increasing sodium fluoride concentrations on erosion and attrition of enamel and dentine in vitro. *Journal of Dentistry* 2010;**38**:782–7.
22. Ingram GS, Silverstone LM. A chemical and histological study of artificial caries in human dental enamel in vitro. *Caries Research* 1981;**15**:393–8.

23. ten Cate JM, Exterkate RA, Buijs MJ. The relative efficacy of fluoride toothpastes assessed with pH cycling. *Caries Research* 2006;**40**:136–41.
24. Cochrane NJ, Cai F, Huq NL, Burrow MF, Reynolds EC. New approaches to enhanced remineralization of tooth enamel. *Journal of Dental Research* 2010;**89**:1187–97.
25. Qi YP, Li N, Niu LN, Primus CM, Ling JQ, Pashley DH, *et al.* Remineralization of artificial dentinal caries lesions by biomimetically modified mineral trioxide aggregate. *Acta Biomaterialia* 2012;**8**:836–42.
26. Dong ZH, Chang JA, Zhou Y, Lin KL. In vitro remineralization of human dental enamel by bioactive glasses. *Journal of Materials Science* 2011;**46**:1591–6.
27. Wang Z, Jiang T, Sauro S, Wang Y, Thompson I, Watson TF, *et al.* Dentine remineralization induced by two bioactive glasses developed for air abrasion purposes. *Journal of Dentistry* 2011;**39**:746–56.
28. Sauro S, Thompson I, Watson TF. Effects of common dental materials used in preventive or operative dentistry on dentin permeability and remineralization. *Operative Dentistry* 2011;**36**:222–30.
29. Vollenweider M, Brunner TJ, Knecht S, Grass RN, Zehnder M, Imfeld T, *et al.* Remineralization of human dentin using ultrafine bioactive glass particles. *Acta Biomaterialia* 2007;**3**:936–43.
30. Zhong JP, Greenspan DC, Feng JW. A microstructural examination of apatite induced by Bioglass in vitro. *Journal of Materials Science Materials in Medicine* 2002;**13**:321–6.
31. Ohtsuki P, Li C, Kokubo T, Nakanishi K, Soga N, Nakamura T, *et al.* Apatite formation induced by silica gel in a simulated body fluid. *Journal of the American Ceramic Society* 1992;**75**:2094–7.
32. Niu LN, Zhang W, Pashley DH, Breschi L, Mao J, Chen JH, *et al.* Biomimetic remineralization of dentin. *Dental Materials* 2013. pii: S0109-5641(13)00175-9.
33. Robinson C, Shore RC, Brookes SJ, Strafford S, Wood SR, Kirkham J. The chemistry of enamel caries. *Critical Reviews in Oral Biology and Medicine* 2000;**11**:481–95.
34. Burwell AK, Litkowski LJ, Greenspan DC. Calcium sodium phosphosilicate (NovaMin): remineralization potential. *Advances in Dental Research* 2009;**21**:35–9.
35. Hedoux A, Guinet Y, Descamps M. The contribution of Raman spectroscopy to the analysis of phase transformations in pharmaceutical compounds. *International Journal of Pharmaceutics* 2011;**417**:17–31.
36. Awonusi A, Morris MD, Tecklenburg MM. Carbonate assignment and calibration in the Raman spectrum of apatite. *Calcified Tissue International* 2007;**81**:46–52.
37. Ko AC, Choo-Smith LP, Hewko M, Leonardi L, Sowa MG, Dong CC, *et al.* Ex vivo detection and characterization of early dental caries by optical coherence tomography and Raman spectroscopy. *Journal of Biomedical Optics* 2005;**10**:031118.
38. Pliska BT, Warner GA, Tantbirojn D, Larson BE. Treatment of white spot lesions with ACP paste and microabrasion. *Angle Orthodontist* 2012;**82**:765–9.
39. Ferrazzano GF, Amato I, Cantile T, Sangianantoni G, Ingenito A. In vivo remineralising effect of GC tooth mousse on early dental enamel lesions: SEM analysis. *International Dentistry Journal* 2011;**61**:210–6.
40. Beerens MW, Van Der Veen MH, Van Beek H, ten Cate JM. Effects of casein phosphopeptide amorphous calcium fluoride phosphate paste on white spot lesions and dental plaque after orthodontic treatment: a 3-month follow-up. *European Journal of Oral Sciences* 2010;**118**:610–7.
41. Crombie FA, Cochrane NJ, Manton DJ, Palamara JE, Reynolds EC. Mineralisation of developmentally hypomineralised human enamel in vitro. *Caries Research* 2013;**47**:259–63.
42. Robinson C, Hallsworth AS, Shore RC, Kirkham J. Effect of surface zone deproteinisation on the access of mineral ions into subsurface carious lesions of human enamel. *Caries Research* 1990;**24**:226–30.
43. Al-Khateeb S, Exterkate R, Angmar-Mansson B, ten Cate JM. Effect of acid-etching on remineralization of enamel white spot lesions. *Acta Odontologica Scandinavica* 2000;**58**:31–6.
44. Hench LL. An introduction to bioceramics. London: Imperial College Press; 2013.